THE UNIVERSITY OF CHICAGO

NOISE AND FLUCTUATIONS FOR QUANTUM INFORMATION PROCESSING

A DISSERTATION SUBMITTED TO
THE FACULTY OF THE PRITZKER SCHOOL OF MOLECULAR ENGINEERING
IN CANDIDACY FOR THE DEGREE OF
DOCTOR OF PHILOSOPHY

BY
YUXIN WANG

CHICAGO, ILLINOIS
AUGUST 2023

CONTENTS

LIST OF FIGURES

LIST OF TABLES

ACKNOWLEDGMENTS

Firstly, I would like to thank my advisor, Prof. Aashish Clerk, for his mentorship and support throughout my PhD. Aash has shown me how to perform research by actually doing it on a daily basis. Whenever I have questions, technical or otherwise, Aash is always a great resource to go to for inspiration and guidance. I would always appreciate the opportunity to work in his group.

I also want to thank my thesis committee members, Profs. David Awschalom and Liang Jiang, and my candidacy committee members, Profs. Vincenzo Vitelli and Tian Zhong. The questions and comments they offered regarding my research and presentation are invaluable and have helped me improve greatly.

My PhD journey would not be complete without all the amazing collaborators that I have the pleasure to work with. I owe special thanks to Alireza Seif and F. Joseph Heremans, who have both been great mentors and friends. Hopefully the collaborations could continue after my time at Chicago. I am also grateful for the opportunity to work closely with (former) members in the group: Andrew Pocklington, Yariv Yanay, Gideon Lee, Tony Jin, Andrew Lingenfelter, and Mingxing (Jeffrey) Yao. While my participation in those collaborations may not necessarily help speed up the completion of the projects, I have greatly enjoyed the times when we brainstormed together new ideas and possible solutions to all the theoretical mysteries that come along the way. I also wish to thank the noise spec team: Paul Jerger, Jonathan Marcks, Benjamin Soloway, Michael Solomon, Chris Egerstrom, Masaya Fukami, Nazar Delegan on the experimental side, and Nikita Onizhuk on the simulation side. I have grown used to looking forward to our meeting every Thursday for the exciting discussions that are a combination of consistent wonder (from a theorist's perspective) and excitement, as well as occasional frustration. I want to thank Paul Jerger especially; without his dedication and marvelous work ethic, the experimental paper on quench phase sensing might never have come into existence. For the nonreciprocity project, I also want to thank Yingying Wang,

Sean van Geldern, and Prof. Chen Wang. I have learned a lot about superconducting circuit systems from them, and it was quite rewarding to work with experimentalists who are also greatly interested in the theoretical description of their system. Last but certainly not least, I would like to thank Qian Xu and Guo (Jerry) Zheng for the squeezed cat project. It was really fun to work on a problem where one's ideas could be directly put to use.

I feel very fortunate to work alongside a group of knowledgeable and friendly people, including Luke, Kero, Alexander, David, Peter, Setiawan, Ryo, Martin, and Antoine. As each of us works on different topics (and some of us even come from diverse backgrounds in physics), every conversation we have had has been a learning experience for me. It has been a unique experience to work in a group with such diverse yet connected research themes.

I would also like to thank all the folks who are working or used to work in the theory office: Chang, Changchun, Mengzhen, Senrui, Pei, Ming, Kevin, Nam, Mona, Junyu, Debayan, Yat, Bikun, Zhaoyou, Sisi, Chiao-Hsuan, and Filip. I have greatly enjoyed all the spontaneous research discussions we had and the free food opportunities shared. Speaking of free food, I am very much obliged to the organizers of the superconducting journal club: Etienne, Joel, Haoxiong, and Jeffrey. The journal club has offered me a place to learn about the most recent experimental progress in superconducting circuits, and the food was always top-notch.

Finally, I hope to thank my family and friends. Obtaining a PhD is no easy task, and I am grateful for their unconditional support. Additionally, realizing that this acknowledgment is far from a comprehensive list, I want to thank all who have helped me get to where I am now.

ABSTRACT

Noise and fluctuations play a crucial role in quantum physics. They are not only important from a fundamental perspective—noise is ubiquitous in the quantum regime due to the Heisenberg uncertainty principle—but also interesting for practical purposes, as understanding and suppression of unwanted noise are key to constructing quantum information processors. While they are commonly treated as adversarial elements for quantum information processing, it is interesting to ask if noise and fluctuations can be exploited to make quantum-based technologies more powerful. An answer to this question can lead to applications that are directly compatible with state-of-the-art experimental platforms, where system decoherence is small but non-negligible. Further, it can also shed light on how quantum fluctuations are uniquely different from their classical counterparts.

In this thesis, we present a variety of theoretical advances in this direction. We start by examining how fundamental limits on quantum noise impose constraints on dynamics of open quantum systems. We consider the microscopic origin of Markovian dissipation, one of the most common types of quantum decoherence, and show that the Heisenberg uncertainty principle, and the resulting quantum noise inequalities, directly manifest as restrictions on the dissipative dynamics. Based on this insight, we propose a general recipe for designing non-Hermitian quantum dynamics without using any dissipation. Next, we turn to the question of distinguishing quantum versus classical noises. We study this in two scenarios: characterization of non-Gaussian quantum noise, and identifying genuinely quantum Markovian dephasing processes. For the former problem, we present a general characterization method based on quantum noise bispectra, and find a surprising quantum fluctuation-induced breaking of detailed balance in the case of driven photon shot noise. For the second question, we adopt an experimentally motivated approach, and define quantum dephasing environments as the ones having entangling power over the systems to which they are coupled. Focusing on purely dephasing environments, we identify necessary and suffi-

cient conditions for entanglement generation, which have implications for, e.g., dissipative generation of entanglement.

Finally, we discuss applications inspired by the aforementioned insights. First, we consider quantum sensing protocols that exploit qubit dephasing to probe noise properties of an unknown environment. We show a general sensing modality that uses inadvertent quenches imparted by the probe to its environment, which allows one to measure the environmental spectral function. Our method unlocks a new class of quantum sensors beyond standard dephasing-based sensing protocols, which is directly compatible with numerous quantum platforms ranging from defect-based solid-state spin qubits to superconducting circuits. Second, we present a general strategy, based on inherent dissipative gauge symmetries of continuous Markovian processes, to design fully nonreciprocal dynamics in generic bipartite quantum systems. Intriguingly, this new mechanism for obtaining nonreciprocal interactions also leads to a general method for dissipative, deterministic realizations of unitary quantum gates.

CHAPTER 1

INTRODUCTION

Since the birth of quantum mechanics, the question of to what extent quantum and classical laws of physics are distinct from each other has attracted immense interest from physicists. On one hand, this study underlies the understanding of the foundation of quantum theory [1–4]. On the other hand, the idea that classical and quantum theories could differ in a fundamental manner suggests that the quantum theory may enable states and processes with no counterpart in the classical world, generating potential resources for novel applications [5–9]. These two complementary lines of research both motivate the study of quantum information processing, and tremendous progress has been made in the past decades in terms of both the theoretical understanding and experimental realizations of quantum processors [10–13]. However, the pursuit of scalable implementation of quantum information processors with practically relevant applications is still ongoing and remains an area of active research [14]. Towards this goal, an outstanding challenge is the extreme sensitivity of quantum systems to external perturbations, making a physical qubit hyper susceptible to environmental noise and fluctuations [15–18]. This fragility of quantum information provides both a difficulty and an opportunity: as noise represents one of the most fundamental distinctions between quantum and classical mechanics through the Heisenberg uncertainty principle, having an accurate characterization of the noise properties in quantum system could lead to discoveries of novel physical phenomena. Alternatively, such knowledge could also inform the design of quantum information hardware, and eventually help achieve quantum advantage in applications.

This thesis presents a collection of works that are motivated by the similar unifying theme: finding physically meaningful ways to distinguish between quantum and classical systems, particularly through the lens of noise and fluctuations. We address this question via various approaches, including deriving fundamental bounds on quantum dynamical processes as imposed by the Heisenberg uncertainty principle (Chapters 2 and 3), characterizing noise

properties in a generic quantum system (Chapters 4 and 5), as well as designing dissipative dynamics (Chapter 6), such as nonreciprocal processes, that can be used as a resource for quantum information processing. The ultimate goal of this thesis is two-fold: provide a theoretical understandings of noise, fluctuations and dissipative dynamics to shed more light on the connections and boundary between quantum and classical phenomena, and form a toolbox of characterization techniques and engineered quantum interactions that would allow quantum information processing applications. Often these two goals are complementary: as shown in the following chapters, new understanding in the fundamental limits of noise in quantum systems could inform the design of quantum dynamics.

The rest of this thesis is organized as follows. As a warm-up exercise and to introduce some of the technical language, we start in Chapter 2 by considering one of the most common and featureless models of environmental noise, i.e., Markovian dephasing bath, where the system dynamics can be described by Lindblad master equations. For this model, we show in Section 2.3 that the physical constraints imposed by the fact that the dissipative dynamics should generate completely positive trace preserving (CPTP) maps on the master equation parameters are mathematically equivalent to a form of quantum noise inequalities. The latter corresponds to the application of Heisenberg uncertainty relations to the Fourier components of environmental operators. Next, in Chapter 3, we consider the implications of quantum noise properties on coherent dynamics, and show that a generic non-Hermitian Hamiltonian can be mapped to the dynamical matrix of a dissipation-free quantum system. Crucially, we make use of particle-non-conserving bosonic quadratic Hamiltonians, whose dynamical matrices are naturally non-Hermitian. We present general strategies that can implement non-Hermitian setup ranging from $\mathcal{PT}$-symmetric dimers to general multimode systems. We also discuss applications of this general mapping to quantum sensing, entanglement dynamics and topology.

We then turn to the problem of identifying features of genuinely quantum environments.

We investigate this problem in two different contexts: spectrally resolving properties of quantum noise, and distinguishing between quantum and classical Markovian dephasing processes. First, Chapter 4 is concerned with the theoretical techniques for describing noise properties of non-Gaussian quantum environments. Making use of a Keldysh field-theory-based approach, we provide a general method for computing the quantum noise polyspectra (i.e. frequency-resolved higher cumulants) of a generic quantum bath. Focusing on the case of photon shot noise generated by a driven damped harmonic oscillator, we further calculate the quantum noise bispectra of the noise process, which reveals an intriguing quantum breaking of detailed balance conditions. Second, Section 2.4 deals with the problem of distinguishing between quantum or classical Markovian dephasing environments. To answer this question, we adopt an operationally motivated criterion based on whether the dissipative dynamics can create entanglement, something that in principle can be directly tested in experiments. Invoking the Peres-Heredecki (i.e., positive partial transpose) criterion, we derive necessary and sufficient conditions for when Markovian dephasing environments exhibit nontrivial entangling power, or equivalently, when they can be unambiguously distinguished from local or correlated classical noise processes.

Shifting attention now to applications, in the last part of this thesis, we discuss ways to utilize dissipative dynamics as a resource. Two concrete examples are provided for this purpose. Chapter 5 studies a novel sensing modality in the context of quantum sensing and quantum noise spectroscopy protocols, which exploit the dephasing of a sensor qubit to probe properties of its surrounding, unknown environment. In this case, we show how the very presence of the qubit sensor in the standard sensing and noise spectroscopy pulse sequences would give rise to an inadvertent quench on the sensing target, i.e. a sudden change in the environmental Hamiltonian. These quenches encode information about the initial environmental state, and because of the qubit-environment coupling, would also lead to observable changes in the qubit dynamics. Based on this insight, we propose simple and general strate-

gies that can enhance standard dephasing-based sensing protocols. Specifically, we present sensing protocols that allow a model-independent extraction of environmental temperature, detection of the bath in non-thermal states, and application of those general ideas to the paradigmatic examples of $1/f$ quantum noise sources and Ohmic baths. We further develop a general protocol to modulate the quenches, which enables spectral reconstruction of the bath density of states function. We also discuss how our approach can be directly implemented using a variety of state-of-the-art quantum platforms including solid-state defect spin qubits, circuit QED systems, and quantum dots.

Finally, in Chapter 6, we discuss a general recipe for designing a novel form of nonreciprocal quantum interactions. This is achieved via a universal and inherent class of dissipative gauge symmetries of a generic Lindblad master equation, where the dynamics stay invariant under a phase shift of the jump operators. As an interesting application, our method enables a completely dissipative realization of an arbitrary unitary quantum operation. We also introduce a general metric for quantifying the amount of nonreciprocity of a generic quantum map, whose applicability is fully general and extends beyond the standard scattering-matrix-based picture.

Chapters 2 to 6 are written as self-contained chapters, each of which can be read independently. We end with a discussion on open questions in Chapter 7.

CHAPTER 2

WARM-UP EXAMPLE: MARKOVIAN DEPHASING QUANTUM MASTER EQUATIONS

2.1 Overview of results

This chapter provides both an introduction to some of the basic theoretical techniques, as well as new results following up a previous work [19], where we proposed an operational criterion to distinguish between quantum and classical dissipative environments, based on whether the said dissipation could generate entanglement in the system. In Sections 2.2 and 2.3, we first introduce the basic theory method of quantum master equations, and provide intuitions for understanding the physical parameter constraints on such equations, with a focus on the paradigmatic example of pure-dephasing Markovian environments. In Section 2.4, we then derive sufficient condition for a generic Markovian dephasing environment to have entangling power on multipartite quantum systems, which generalizes the results in Ref. [19] (that focuses on multiqubit Markovian dephasing environments). For the case with a single dissipator, we further derive necessary and sufficient conditions for the dissipation to generate entanglement, and apply this result to the example of harmonic oscillator systems whose dynamics are due to completely dissipative forces.

2.2 Setup: Markovian dephasing quantum master equations

Consider a generic multi-partite quantum system, consisting of N subsystems, coupled to a stationary environment. While our approach applies to general types of dissipation, in this chapter we focus on pure-dephasing environments. More specifically, we assume that the system frequencies are sufficiently off-resonant from environmental transitions, and we further restrict the system and environment to have at most 2-body interactions. Thus, in

the rotating frame with respect to the internal system (S) and environment (E) Hamiltonians, $\hat{H}_{\mathrm{S}}$ and $\hat{H}_{\mathrm{E}}$, one can approximate the system-environment interaction with a pure-dephasing-type coupling, as

$$\hat{H}_{\mathrm{int}}(t) = \sum_{j=1}^{N} \hat{M}_j \otimes \hat{B}_j(t). \tag{2.1}$$

Here, $\hat{M}_j$ are local Hermitian operators acting on susystem j, and $\hat{B}_j(t) \equiv e^{i\hat{H}_{\mathrm{E}}t}\hat{B}_j e^{-i\hat{H}_{\mathrm{E}}t}$ denote Hermitian environmental operators in the rotating frame. Note that the spectra of the local system operators $\hat{M}_j$ can be completely distinct.

In the regime where the environment can be treated effectively as Markovian, and making use of Born-Markovian approximation (see, e.g., [20]), we can integrate out environmental degrees of freedom and describe system dynamics via a Lindblad master equation $\frac{d\hat{\rho}}{dt} = \mathcal{L}\hat{\rho}$ [21], with the Liouvillian given by

$$\mathcal{L}\hat{\rho} = -i\sum_{j,k} h_{jk}\left[\hat{M}_j\hat{M}_k, \hat{\rho}\right] + \sum_{j,k=1}^{N} \gamma_{jk}\left(\hat{M}_k\hat{\rho}\hat{M}_j - \frac{1}{2}\left\{\hat{M}_j\hat{M}_k, \hat{\rho}\right\}\right), \tag{2.2}$$

where the coefficient matrices h and γ can be written in terms of appropriate correlation functions of the bath, as

$$h_{\ell m} = \frac{1}{4i}\int_0^\infty d\tau \langle[\hat{B}_\ell(\tau) - \hat{B}_\ell(-\tau), \hat{B}_m(0)]\rangle, \tag{2.3}$$

$$\gamma_{\ell m} = \int_{-\infty}^{\infty} d\tau \langle \hat{B}_\ell(\tau)\hat{B}_m(0)\rangle. \tag{2.4}$$

Note that h is real and symmetric by construction; the corresponding Hamiltonian term in Eq. (2.2) is also known as the Lamb shift term. For Eq. (2.2) to describe a Lindblad master equation, i.e., in order for the time evolution described by this equation to generate completely-positive trace-preserving (CPTP) maps [22], we require that the coefficient matrix

γ of the dissipative dynamics to be Hermitian and positive semidefinite, as

$$\gamma = \gamma^{\dagger}, \quad \gamma \geq 0. \tag{2.5}$$

The real part of this dissipator matrix Reγ can be conveniently understood as dephasing due to classical, correlated noise. In contrast, while the imaginary part of Imγ is known to be allowed in a general quantum master equation (see, e.g., Ref. [20]), the physical origin of this term is somewhat obscure.

To obtain a physical understanding of the coefficient matrices in Eqs. (2.3) and (2.4), it is useful to relate the Hamiltonian and dephasing parameters to the quantum noise spectrum and response susceptibility of the bath. More specifically, the real part of the dephasing coefficient matrix Reγ corresponds to a zero-frequency symmetrized quantum noise spectrum $\overline{S}_{\ell m}[\omega] \equiv \frac{1}{2}\int_{-\infty}^{\infty} ds e^{i\omega s}\langle\{\hat{B}_{\ell}(s), \hat{B}_{m}(0)\}\rangle$ [23]

$$\mathrm{Re}\gamma_{\ell m} = \frac{1}{2}\int_{-\infty}^{\infty} d\tau \langle\{\hat{B}_{\ell}(\tau), \hat{B}_{m}(0)\}\rangle = \mathrm{Re}\overline{S}_{\ell m}[\omega = 0]. \tag{2.6}$$

Interestingly, the imaginary parts of the dissipator coefficients Imγ can be directly related to the (Green-Kubo) linear response susceptibility function $G^{R}_{\ell m}[\omega]$ (see, e.g., [24] for a pedagogical introduction)

$$G^{R}_{\ell m}[\omega] \equiv -i\int_{0}^{\infty} ds e^{i\omega s}\langle[\hat{B}_{\ell}(s), \hat{B}_{m}(0)]\rangle. \tag{2.7}$$

These response functions capture how the system responds to a weak perturbation oscillating at frequency ω. Comparing above equation to the general dephasing coefficients in Eq. (2.4),

we thus obtain

$$h_{\ell m} = \frac{1}{4}\left(\mathrm{Re}G^R_{\ell m}\left[\omega=0\right]+\mathrm{Re}G^R_{m\ell}\left[\omega=0\right]\right), \tag{2.8}$$

$$\begin{aligned}\mathrm{Im}\gamma_{\ell m} =& -\frac{i}{2}\int_{-\infty}^{\infty} d\tau\langle[\hat{B}_\ell\left(\tau\right),\hat{B}_m\left(0\right)]\rangle \\ =& -\frac{i}{2}\int_{0}^{\infty} d\tau\langle[\hat{B}_\ell\left(\tau\right),\hat{B}_m\left(0\right)]\rangle+\frac{i}{2}\int_{0}^{\infty} d\tau\langle[\hat{B}_m\left(\tau\right),\hat{B}_\ell\left(0\right)]\rangle \\ =& \frac{1}{2}\left(\mathrm{Re}G^R_{\ell m}\left[\omega=0\right]-\mathrm{Re}G^R_{m\ell}\left[\omega=0\right]\right).\end{aligned} \tag{2.9}$$

2.3 Physical intuition for the positivity constraint on pure-dephasing dynamics via quantum noise inequalities

Consider a generic Lindblad master equation of the form in Eq. (2.2), which is given by

$$\frac{d}{dt}\hat{\rho}(t) = -i\sum_{j,k}h_{jk}\left[\hat{M}_j\hat{M}_k,\hat{\rho}\right]+\sum_{j,k=1}^{N}\gamma_{jk}\left(\hat{M}_k\hat{\rho}\hat{M}_j-\frac{1}{2}\left\{\hat{M}_j\hat{M}_k,\hat{\rho}\right\}\right). \tag{2.10}$$

As mentioned, for this master equation be physical, the dissipator coefficient matrix is required to be a positive semidefinite (PSD) matrix, i.e.

$$\gamma \geq 0. \tag{2.11}$$

On the other hand, we have shown that starting from a general microscopic quantum bath model, the real and imaginary parts of dissipator coefficients $\gamma_{\ell m}$ are given by zero-frequency components of symmetrized quantum noise spectrum $\overline{S}_{\ell m}\left[\omega=0\right]$ and the asymmetric susceptibility function $\mathcal{S}^{-}_{\ell m}\left[\omega=0\right]$, respectively, as

$$\mathrm{Re}\gamma_{\ell m} = \overline{S}_{\ell m}\left[\omega=0\right], \tag{2.12a}$$

$$\mathrm{Im}\gamma_{\ell m} = \mathcal{S}^{-}_{\ell m}\left[\omega=0\right] \equiv \frac{G^R_{\ell m}\left[0\right]-G^R_{m\ell}\left[0\right]}{2}. \tag{2.12b}$$

The PSD condition $\gamma \geq 0$ thus impose collective constraints on the symmetrized bath noise spectra and the susceptibility functions. At first glance, this might seem surprising, as classical physics would allow noiseless response. In contrast, the PSD condition requires that the quantum bath response is limited by noise correlators as

$$\overline{S}_{\ell\ell}\left[\omega=0\right]\overline{S}_{mm}\left[\omega=0\right]-\left|\overline{S}_{\ell m}\left[\omega=0\right]\right|^{2}\geq\left|\mathcal{S}_{\ell m}^{-}\left[\omega=0\right]\right|^{2}. \tag{2.13}$$

These constraints, also known as quantum noise inequalities, are frequency-domain versions of the Heisenberg uncertainty relations. Physically, they describe quantum backaction that necessarily accompany weak measurements on the quantum bath [23].

We now show that the PSD constraint on the quantum bath correlators is also necessary for the quantum noise inequalities to hold. Given a generic dissipator coefficient matrix, we can diagonalize it as

$$\gamma=U^{\dagger}\Gamma U, \tag{2.14}$$

so that we can express the quantum bath correlators as

$$\hat{D}_{\alpha}=\sum_{m}U_{\alpha m}\hat{B}_{m}, \tag{2.15}$$

$$\int_{-\infty}^{\infty}d\tau\langle\hat{D}_{\alpha}\left(\tau\right)\hat{D}_{\beta}^{\dagger}\left(0\right)\rangle=\delta_{\alpha\beta}\Gamma_{\alpha}. \tag{2.16}$$

Defining the Hermitian and anti-Hermitian contributions to the new bath operators as $\hat{D}_{\alpha}=\hat{I}_{\alpha}+i\hat{F}_{\alpha}$, we can rewrite the eigenvalues of the dissipator matrix as

$$\begin{aligned}\Gamma_{\alpha}&=\overline{S}_{I_{\alpha}I_{\alpha}}\left[0\right]+\overline{S}_{F_{\alpha}F_{\alpha}}\left[0\right]+G_{I_{\alpha}F_{\alpha}}^{R}\left[0\right]-G_{F_{\alpha}I_{\alpha}}^{R}\left[0\right]\\&=\overline{S}_{I_{\alpha}I_{\alpha}}\left[0\right]+\overline{S}_{F_{\alpha}F_{\alpha}}\left[0\right]+2\mathcal{S}_{I_{\alpha}F_{\alpha}}^{-}\left[0\right].\end{aligned} \tag{2.17}$$

Applying the quantum noise inequality to the pair of operators $\hat{I}_\alpha$ and $\hat{F}_\alpha$, we can prove that the eigenvalues must be nonnegative as

$$\Gamma_\alpha \geq 2\sqrt{\overline{S}_{I_\alpha I_\alpha}[0]\,\overline{S}_{F_\alpha F_\alpha}[0]} + 2\mathcal{S}^{-}_{I_\alpha F_\alpha}[0] \geq 0. \tag{2.18}$$

Thus, we have shown that the quantum noise inequalities between all possible pairs of zero-frequency component of bath operators are necessary and sufficient conditions for the dissipative coefficient matrix γ to be positive semidefinite.

2.4 Sufficient and necessary conditions for Markovian dephasing environments to have entangling power

2.4.1 Translating the positive partial transpose criterion to constraints on the dephasing coefficient matrix

Let us again consider a generic multi-partite quantum system, consisting of N subsystems, coupled to a Markovian pure-dephasing environment. The system dynamics can be described by Lindblad master equation given by Eq. 2.2, which we rewrite as

$$\mathcal{L}(\hat{\rho}) = -i\left[\hat{H}_{\mathrm{LS}}, \hat{\rho}\right] + \sum_{j,k=1}^{N} c_{jk}\left(\hat{M}_k\hat{\rho}\hat{M}_j - \frac{1}{2}\left\{\hat{M}_j\hat{M}_k, \hat{\rho}\right\}\right). \tag{2.19}$$

The dephasing matrix $C = (c_{ij})$ must be positive semi-definite (PSD) for any physical baths. We will focus on the dissipative part of dynamics (and ignore the Lamb-shift Hamiltonian $\hat{H}_{\mathrm{LS}}$) henceforth. While there are multiple (possibly inequivalent) approaches to distinguishing a truly quantum environment from its classical counterparts, here we apply an operational definition: the dissipation is quantum if and only if it can generate entanglement during the time evolution [19]. Note that we do not require nonzero steady state entanglement.

We now use the Peres-Horodecki criterion [25, 26] to explicitly derive a sufficient condition for the dissipative part of Eq. (2.19) to have entanglement power. We consider a generic bipartition into subsystems A and B, so that the dynamics of the partial transposed state of the system with respect to A, i.e. $\hat{\rho}^{T_A} = (\mathcal{T}_A \otimes 1)(\hat{\rho})$, can be written as $\frac{d}{dt}\hat{\rho}^{T_A} = \tilde{\mathcal{L}}\left(\hat{\rho}^{T_A}\right)$. The new superoperator $\tilde{\mathcal{L}}$ is given by

$$\tilde{\mathcal{L}}(\hat{\rho}^{T_A}) = -i\left[\hat{H}_{\mathrm{PT}}, \hat{\rho}^{T_A}\right] + \tilde{\mathcal{L}}_{\mathrm{diss}}\left(\hat{\rho}^{T_A}\right). \tag{2.20}$$

The equation of motion of the partial transposed state $\hat{\rho}^{T_A}$ takes a similar form as the standard master equation in Eq. (2.19), but may generate non-positive maps. The Hamiltonian term is again given by $\hat{H}_{\mathrm{PT}} = \frac{1}{2}\sum_{ij}\tilde{h}_{ij}\hat{M}_i\hat{M}_j$ with real coefficient matrix $\tilde{H}$. The superoperator $\tilde{\mathcal{L}}_{\mathrm{diss}}$ can be written compactly in terms of a new coefficient matrix $\tilde{C}$ as

$$\tilde{\mathcal{L}}_{\mathrm{diss}}(\hat{\rho}^{T_A}) = \sum_{j,k=1}^{N}\tilde{c}_{jk}\left(\hat{M}_k\hat{\rho}\hat{M}_j - \frac{1}{2}\left\{\hat{M}_j\hat{M}_k, \hat{\rho}\right\}\right). \tag{2.21}$$

The coefficient matrices $\tilde{H}$ and $\tilde{C}$ can be obtained from explicitly performing the partial transpose operation on the original master equation, Eq. (2.19). For convenience, we rewrite all coefficient matrices in terms of block matrices defined on A and B degrees of freedom, as

$$M = \begin{pmatrix} M_{AA} & M_{AB} \\ M_{BA} & M_{BB} \end{pmatrix}, \quad (M = H, C, \tilde{H}, \tilde{C}). \tag{2.22}$$

One can thus show that

$$\tilde{H}_{AA} = -H_{AA}, \quad \tilde{H}_{AB} = \mathrm{Im}C_{AB}, \quad \tilde{H}_{BB} = H_{BB}, \tag{2.23}$$

$$\tilde{C}_{AA} = C_{AA}^T, \quad \tilde{C}_{AB} = -\mathrm{Re}C_{AB} + iH_{AB}, \quad \tilde{C}_{BB} = C_{BB}. \tag{2.24}$$

The remaining blocks can be obtained using the symmetry relations $\tilde{H}_{BA} = \tilde{H}_{AB}^T$ and

$\tilde{C}_{BA} = \tilde{C}^{\dagger}_{AB}$.

Reference [19] has shown that for multiqubit systems, the dissipation can generate entanglement if the corresponding $\tilde{C}$ has one or more negative eigenvalue. Here, we show that similar sufficient condition holds for Eq. (2.19), which describes general quantum systems. To prove this, we can restrict to only two sublevels of each subsystem, and we refer to the new effective qubits formed by these levels as pseudospins on site j with Pauli operators $\hat{Z}_j$. It is straightforward to see that if the dissipation restricted to these sublevels can generate entanglement between pseudospins, then the dissipation in Eq. (2.19) can also generate entanglement in the orginial system. We can thus consider (lack of) entanglement generation in the effective N-qubit system.

The Hermitian system operators $\hat{M}_j$ reduce to qubit operators $m_j + d_j\hat{Z}_j$, where $\hat{Z}_j$ are Pauli operators acting on pseudospin j, and m_j and d_j are real coefficients. For subsystems that are not trivial dark modes of the dissipation, we can choose the pseudospins such that $d_j > 0$. The corresponding dephasing coefficient matrix C' in the pseudospin basis can be expressed in terms of the original C matrix, and a rescaling matrix D as

$$C' = DCD, \tag{2.25}$$

where we define D as $D = \mathrm{diag}(d_1, \ldots, d_N)$. One can show that $\tilde{C}'$ corresponding to equation of motion of the partial transposed pseudospin state can be obtained in a similar way, as

$$\tilde{C}' = D\tilde{C}D. \tag{2.26}$$

As a result, $\tilde{C}'$ is positive semidefinite if and only if $\tilde{C}$ is PSD. Thus, the reduction of Eq. (2.19) into the pseudospin basis can generate entanglement if $\tilde{C}$ is not PSD. We have now shown that for generic commuting local operators $\hat{M}_j$, the dissipative dynamics in Eq. (2.19) can create entanglement as long as the corresponding $\tilde{C}$ has a negative eigenvalue.

2.4.2 *Sufficient condition for no entangling power: local-measurement-and-feedforward protocols*

We first focus on the question of what types of dissipative dynamics *cannot* generate entanglement. As we show in the next subsection, this discussion is also helpful for understanding the sufficient condition for pure dephasing processes to generate entanglement.

We start by considering a dissipative process generated by continuously monitoring the Hermitian operator $\hat{A}$, and applying a conditional feedback or feedforward force to the Hermitian operator $\hat{B}$ whose strength depends linearly on the measurement signal. As shown in Ref. [27], in the limit where delay time is negligible, this measurement-and-feedforward (MF) process can be described by the master equation $\frac{d\hat{\rho}}{dt} = \mathcal{L}_{\text{m.f.}}\{\hat{A}, \hat{B}\}\hat{\rho}$, with Liouvillian $\mathcal{L}_{\text{m.f.}}\{\hat{A}, \hat{B}\}$ given by

$$\mathcal{L}_{\text{m.f.}}\{\hat{A}, \hat{B}\}\hat{\rho} \equiv -i\Gamma[\hat{A}\hat{B}, \hat{\rho}] + \Gamma\mathcal{D}[\hat{B} + i\hat{A}]\hat{\rho}, \tag{2.27}$$

where the dissipative coupling strength Γ is set by the geometric mean of measurement rate and feedforward force strength.

While above discussion is valid for generic operators $\hat{A}$ and $\hat{B}$, for the specific case where they are local operators acting on two different subsystems, we can use the connection to the MF process to rigorously show that dynamics generated by $\mathcal{L}_{\text{m.f.}}\{\hat{A}, \hat{B}\}$ has no entangling power. It is thus straightforward to prove that the dissipator $\mathcal{D}[\hat{A} + i\hat{B}]$ also can never generate entanglement, since we have the following decomposition

$$\mathcal{D}[\hat{A} + i\hat{B}]\hat{\rho} = \frac{1}{2}\left(\mathcal{L}_{\text{m.f.}}\{\hat{B}, \hat{A}\} + \mathcal{L}_{\text{m.f.}}\{\hat{A}, -\hat{B}\}\right)\hat{\rho}. \tag{2.28}$$

It is interesting to consider the dissipative process where one measures local operator $\hat{A}$ and applies a corresponding feedback force on a linear combination of local operetors $\alpha\hat{A}+\hat{B}$,

with a real coefficient α. The system dynamics is now given by master equation

$$\begin{aligned}&\mathcal{L}_{\text{m.f.}}\{\hat{A}, \alpha\hat{A}+\hat{B}\}\hat{\rho}\\ =&-i\Gamma[\hat{A}(\alpha\hat{A}+\hat{B}), \hat{\rho}]+\Gamma\mathcal{D}[\alpha\hat{A}+\hat{B}+i\hat{A}]\hat{\rho}.\end{aligned} \tag{2.29}$$

If both $\hat{A}$ and $\hat{B}$ are local operators, one can again use the MF realization to show that the Lindbladian $\mathcal{L}_{\text{m.f.}}\{\hat{A}, \alpha\hat{A}+\hat{B}\}$ cannot generate entanglement. For convenience, we will call such dissipative processes local MF processes. This further allows us to show that dynamics generated by dissipator $\mathcal{D}[\hat{A}+e^{ie^{i\varphi}}\hat{B}]$ does not have entangling power, as we can decompose the dissipative process into sum of contributions from local MF processes and local unitary transformations, as

$$\mathcal{D}[\hat{A}+e^{i\varphi}\hat{B}]=\frac{1}{2}\mathcal{D}[\hat{A}+e^{i\varphi}\hat{B}]\hat{\rho}+\frac{1}{2}\mathcal{D}[\hat{B}+e^{-i\varphi}\hat{A}]\hat{\rho} \tag{2.30}$$

$$\begin{aligned}=&\frac{1}{2}\mathcal{L}_{\text{m.f.}}\{\hat{B}\sin\theta, \hat{A}+\hat{B}\cos\theta\}\hat{\rho}+\frac{1}{2}\mathcal{L}_{\text{m.f.}}\{\hat{A}\sin\theta, -\hat{B}-\hat{A}\cos\theta\}\hat{\rho}\\ &-\frac{i}{2}[(\hat{A}^2-\hat{B}^2)\sin\theta\cos\theta, \hat{\rho}].\end{aligned} \tag{2.31}$$

2.4.3 Sufficient condition for a single dissipator to have entangling power

We have presented sufficient condition for master equation in Eq. (2.19) to be able to generate entanglement in transient dynamics. It is worth asking if we could also derive the necessary and sufficient condition for the dissipative dynamics to be able to create entanglement. While this is challenging for the most general C matrix, here we provide a first step towards answering the question, i.e. we consider Lindbladians with a single dissipator. For a generic bipatition into A and B, we could rewrite the dissipator as $\mathcal{D}[\hat{A}_1+i\hat{A}_2+\hat{B}_1+i\hat{B}_2]$, where $\hat{A}_j$, $\hat{B}_j$ $(j=1,2)$ are traceless Hermitian operators. Note that the dynamics is invariant up to a global gauge transformation $e^{i\theta}(\hat{A}_1+i\hat{A}_2+\hat{B}_1+i\hat{B}_2)$ with phase θ, we choose the phase such that either $\hat{A}_1$, $\hat{A}_2$ are linearly independent or $\hat{A}_2=0$.

Let us first consider the case with $\hat{A}_2 = 0$, so that the dissipator can be written as $\mathcal{D}[\hat{A}_1 + \hat{B}_1 + i\hat{B}_2]$. If $\hat{B}_1$ and $\hat{B}_2$ are linearly dependent, then from Eq. (2.31) we can show that the dissipator does not generate entanglement. Conversely if $\hat{B}_1$ and $\hat{B}_2$ are linearly independent, the dissipator $\mathcal{D}[\hat{A}_1+\hat{B}_1+i\hat{B}_2]$ can always generate entanglement. To show this, we consider the dephasing coefficient matrix $\tilde{C}$ describing dynamics of the partial transposed state $\hat{\rho}^{T_A}$. For purposes that will become clear, it is useful to consider transformation of C under local orthogonal transformation O

$$C' = OCO^T, \tag{2.32}$$

where O has a block diagonal form as

$$O = \begin{pmatrix} O_A & 0 \\ 0 & O_B \end{pmatrix}, \quad O^T O = \mathbb{I}_{AB}. \tag{2.33}$$

One can show that the corresponding $\tilde{C}'$, define via Eq. (2.24) acting on C', can be related to $\tilde{C}$ as

$$\tilde{C}' = O^T \tilde{C} O. \tag{2.34}$$

Noting that the PSD condition for $\tilde{C}$ is invariant under any local orthogonal transformation O, we can check the entangling power $\mathcal{D}[\hat{A}_1 + \hat{B}_1 + i\hat{B}_2]$ by projecting the dissipator onto basis operators. For example, we could rewrite $\hat{B}_2$ using basis operator determined by $\hat{B}_1$ as $\hat{B}_2 = b_1\hat{B}_1 + b_\perp \hat{B}_\perp$, so that the new coefficient matrix is

$$C_{\text{eff}} = \begin{pmatrix} 1 & 1 - ib_1 & -ib_\perp \\ 1 + ib_1 & 1 + b_1^2 & -ib_\perp(1 + ib_1) \\ ib_\perp & ib_\perp(1 - ib_1) & b_\perp^2 \end{pmatrix}. \tag{2.35}$$

One can easily verify that in this effective basis, the corresponding $\tilde{C}_{\text{eff}}$ matrix is not PSD. We have thus shown that the dissipator $\mathcal{D}[\hat{A}_1 + \hat{B}_1 + i\hat{B}_2]$ can generate entanglement.

For the scenario where we have a nontrivial $\hat{A}_2$, if $\hat{B}_1$ or $\hat{B}_2$ vanishes then we could permute A and B subsystems, and the reasoning above still apply. If both $\hat{B}_1$ and $\hat{B}_2$ are nonzero, we could also reduce the problem to the form of $\mathcal{D}[\hat{A}_1 + \hat{B}_1 + i\hat{B}_2]$ by restricting to two eigenstates of $\hat{A}_1 + i\hat{A}_2$ with distinct eigenvalues, so that similar arguments would apply to this case as well.

2.4.4 Case study: harmonic oscillators experiencing dissipative forces

In this section, we focus on the scenario where the total system consists of N harmonic oscillator modes c_j $(j = 1, 2, \ldots, N)$, and dissipators only involve commuting quadrature operators of each modes. In this case, we can define the local operators in Eq. (2.19) as

$$\hat{M}_j = \hat{x}_j, \quad \hat{x}_j \equiv (\hat{c}_j + \hat{c}_j^\dagger)/\sqrt{2}. \tag{2.36}$$

Because the Liouvillian in this case is quadratic, the dynamics it generates is completely linear, i.e. if the system starts in an initial Gaussian state, it will stay Gaussian throughout the time evolution. We can then straightforwardly characterize the time evolution using the equations of motion of the first two moments. This noninteracting bosonic setup thus provides a simple model system for understanding entanglement generation via purely dephasing dynamics.

For simplicity, we consider Lindbladian with a single dissipator, as

$$\mathcal{L}_{\text{sing}} = \Gamma\mathcal{D}[\hat{L}_0], \quad \hat{L}_0 = \sum_{j=1}^{N} \alpha_j \hat{x}_j, \tag{2.37}$$

where α_j are complex coefficients. Without loss of generality, we assume $\alpha_1 = 1$ and the system starts in the vacuum state, which is a product state and has no initial entanglement.

We now focus on entanglement between the first mode and the other $N-1$ modes. For this bipartition, it is straightforward to see that dynamics of entanglement generated by Eq. (2.37) is fully equivalent to an effective 3-mode model with corresponding quadrature operators $\hat{x}_1$, $\hat{x}_r$, and $\hat{x}_\perp$, which satisfy the following condition

$$\hat{L}_0 = \hat{x}_1 + (|\mathrm{Re}\boldsymbol{\alpha}_{\backslash\{1\}}| + iv_r)\hat{x}_r + iv_\perp \hat{x}_\perp. \tag{2.38}$$

The $\hat{x}_r$ quadrature involves the real part of coefficients α_j acting on the $2, 3, \ldots, N$ modes, which can be defined as

$$\hat{x}_r = \frac{1}{|\mathrm{Re}\boldsymbol{\alpha}_{\backslash\{1\}}|}\sum_{j=2}^{N} \mathrm{Re}\alpha_j \hat{x}_j, \quad |\mathrm{Re}\boldsymbol{\alpha}_{\backslash\{1\}}| \equiv \sqrt{\sum_{j=2}^{N} (\mathrm{Re}\alpha_j)^2}. \tag{2.39}$$

The third quadrature operator $\hat{x}_\perp$ can be uniquely determined, by requiring that its coefficients are set by the component of vector $\mathrm{Im}\boldsymbol{\alpha}$ that is orthogonal with respect to $\mathrm{Re}\boldsymbol{\alpha}_{\backslash\{1\}}$. We can obtain $\hat{x}_\perp$ explicitly as

$$\hat{x}_\perp = \frac{1}{v_\perp}\sum_{j=2}^{N} v_{\perp,j}\hat{x}_j, \quad v_\perp = \sqrt{\sum_{j=2}^{N} v_{\perp,j}^2}, \tag{2.40}$$

$$v_{\perp,j} = \mathrm{Im}\alpha_j - \mathrm{Re}\alpha_j \frac{\mathrm{Re}\boldsymbol{\alpha}_{\backslash\{1\}} \cdot \mathrm{Im}\boldsymbol{\alpha}}{|\mathrm{Re}\boldsymbol{\alpha}_{\backslash\{1\}}|^2}. \tag{2.41}$$

From the discussion in Sec. 2.4.3, we see that if $|\mathrm{Re}\boldsymbol{\alpha}_{\backslash\{1\}}| = 0$ or $v_\perp = 0$, then the Lindbladian in Eq. (2.37) cannot generate any entanglement between mode 1 and the rest of the system. We thus assume $|\mathrm{Re}\boldsymbol{\alpha}_{\backslash\{1\}}| v_\perp > 0$ hereafter. Because one can always use local unitary operations to transform the original quadrature basis $\{\hat{x}_1, \ldots, \hat{x}_N\}$ into a new basis set including $\{\hat{x}_1, \hat{x}_r, \hat{x}_\perp\}$ without affecting entanglement between mode 1 and the rest of the system, we restrict to the 3-mode setup in Eq. (2.38) henceforth. For convenience, we

relabel our mode basis and rewrite the general jump operator in Eq. (2.38) as

$$\hat{L}_0 = \hat{x}_1 + (u_2 + iv_2)\hat{x}_2 + iv_3\hat{x}_3, \tag{2.42}$$

where u_2, v_2, v_3 are real-valued coefficients, $u_2 > 0$ and $v_3 > 0$. Again invoking the resultsin Sec. 2.4.3, one can show that in this case, the dissipator corresponding to Eq. (2.42) can generate entanglement. Otherwise, if $u_2 = 0$ or $v_3 = 0$, then the dissipative dynamics can be realized via local measurement-and-feedforward processes, and hence cannot create entanglement.

2.5 Conclusions

In this chapter, we provide an introduction to the basic methods of quantum master equation and quantum noise spectrum, concepts that will reappear multiple times in this thesis. We also generalize the results in Ref. [19], proving sufficient condition for entanglement generation in generic multipartite systems with pure-dephasing dynamics, as well as the necessary and sufficient conditions for a single dephasing dissipator to have nontrivial entangling power. One need not stop here: a natural question to ask is whether one can prove necessary and sufficient conditions for entanglement generation due to more complex dephasing Lindbladians. In the more general case, a technical challenge is whether the pure-dephasing dynamics could ever generate bound entanglement [28–30], which would not be detectable with our approach based on the Peres-Horodecki criterion. We are not aware of an example of purely dephasing dephasing dynamcis creating nonzero bound entanglement, although to the best of our knowledge, we also do not know of a rigorous proof that excludes the case of bound entanglement. Another interesting problem is about entanglement generation power for dissipative dynamics beyond the pure-dephasing scenario. Last but not least, an important issue that we did not touch on in this chapter is to what extent the dissipative mechanism of

entanglement generation discussed here is relevant to current experimental implementations. While one could imagine using reservoir engineering techniques to build quantum devices with the desired dissipative dynamics [31], it would be interesting to explore whether or not similar dynamics could ever be found in naturally occurring dissipative processes.

CHAPTER 3

NON-HERMITIAN DYNAMICS WITHOUT DISSIPATION IN QUANTUM SYSTEMS

3.1 Overview of results

Models based on non-Hermitian Hamiltonians can exhibit a range of surprising and potentially useful phenomena. Physical realizations typically involve couplings to sources of incoherent gain and loss; this is problematic in quantum settings, because of the unavoidable fluctuations associated with this dissipation. In this chapter, we present several routes for obtaining unconditional non-Hermitian dynamics in non-dissipative quantum systems. We exploit the fact that quadratic bosonic Hamiltonians that do not conserve particle number give rise to non-Hermitian dynamical matrices. We discuss the nature of these mappings from non-Hermitian to Hermitian Hamiltonians, and explore applications to quantum sensing, entanglement dynamics and topological band theory. The systems we discuss could be realized in a variety of photonic and phononic platforms using the ubiquitous resource of parametric driving.

3.2 Introduction

Systems whose dynamics are governed by a non-Hermitian Hamiltonian exhibit a wealth of unique phenomena, and have been the subject of considerable recent theoretical and experimental interest [33]. Non-Hermitian dynamics is typically realized by the structured introduction of both loss and gain, and is usually studied in the context of coupled-mode systems or tight-binding lattices with linear dynamics. Such systems can exhibit the spontaneous

breaking of parity-time ($\mathcal{PT}$) symmetry, as well as exceptional points in parameter space, where Hamiltonian eigenvalues coalesce. A variety of phenomena in such non-Hermitian systems have been studied, including quasi-adiabatic evolution and chiral mode switching [34–45], directional invisibility [46], the possibility of enhanced parameter sensing [47–51], and even applications to robust wireless power transfer [52].

While the majority of work on non-Hermitian $\mathcal{PT}$-symmetric systems has been in classical settings, it is natural to ask whether their rich properties can also be exploited in quantum systems. A natural stumbling block is that in the quantum context, the gain and loss typically used to implement non-Hermitian dynamics invariably introduces noise into the system; as explored in several studies [43, 50, 51], this limits the utility of many non-Hermitian effects in quantum systems. While in principle such bath-induced noise effects could be avoided using measurement and postselection [53, 54], this is difficult if not infeasible in many setups.

In this chapter, we present and analyze an alternative method for realizing effective non-Hermitian dynamics in a quantum setting that requires *no* couplings to external dissipative baths, and requires no measurement-induced conditioning. The basic idea is to exploit the unitary physics of squeezing (and anti-squeezing) in parametrically-driven quantum bosonic systems. As is well known, this coherent form of driving can lead to dynamics that exhibits exponential growth and/or decay in time. We show that in a wide range of contexts, this can be made to parallel the exponential growth and decay associated with incoherent gain/loss processes, allowing a route for the noiseless implementation of non-Hermitian dynamics. At a formal level, we utilize the unitary correspondence between the non-Hermitian dynamical coupled mode equations of interest, and the Heisenberg equations of motion in our Hermitian bosonic system. We provide a detailed analysis of how this idea can be implemented both in simple two-mode systems (with and without $\mathcal{PT}$ symmetry), as well as in more complicated multi-mode lattice systems. We also use this general mapping to explore a va-

Mapping scheme	DPA	NDPA	QMFS
Section	Section 3.3.2	Sections 3.4.1-3.4.2	Section 3.3.4, Section 3.4.3
Target non-Hermitian system	$\mathcal{PT}$ dimer	multimode $\mathcal{PT}$ system	generic non-Hermitian system
Hamiltonians	$\mathcal{H}_{\mathcal{PT}} \to \hat{H}_{\mathrm{DPA}}$	$\mathcal{H}_{\mathrm{tb}} \to \hat{H}_{\mathrm{NDPA}}$	$\mathcal{H}_N \to \hat{H}_{\mathrm{QMFS,multi.}}$
Number of modes in non-Hermitian setup / in corresponding paramp system	$2\,/\,1$	$2N\,/\,2N$	$N\,/\,2N$
Advantages	only requires a single bosonic mode	do not need doubling of the number of modes	mapping exists for generic non-Hermitian Hamiltonians
Constraints	mapping requires a constraint on the form of the initial state	mapping exists for only a subset of $\mathcal{PT}$-symmetric $\mathcal{H}_{\mathrm{tb}}$	always realizes two copies of the target non-Hermitian dynamics ($\mathcal{H}_N$ and $\mathcal{H}_N^\dagger$)

Table 3.1: Summary of three different strategies for mapping non-Hermitian Hamiltonians to Hermitian quantum parametric amplifier setups. See corresponding sections for details.

riety of non-Hermitian phenomena (e.g. chiral mode switching, exceptional-point sensing) in a dissipation-free quantum setting. We close by showing how these mappings can also be useful when considering topological band structure in non-Hermitian systems.

We stress that the non-Hermitian nature of dynamical matrices in quadratic bosonic systems has long been realized. Recent work has utilized this to establish mappings between specific 1D models [55, 56], as well as a means for applying non-Hermitian symmetry classes to bosonic problems [56, 57]. Recent work has also pointed out that a simple model of two coupled non-dissipative modes can exhibit an exceptional point [58–60]. Our focus is quite different: we discuss *general* methods that enable one to realize a given non-Hermitian

Hamiltonian of interest without dissipation using a parametrically-driven (but Hermitian) bosonic system, paying special attention to $\mathcal{PT}$-symmetric systems and multi-mode lattice models. A brief summary of the three different approaches we develop to construct the mapped system is given in Table 3.1 for convenience.

3.3 Dissipationless non-Hermitian two-mode dynamics

We start by reviewing the basic dynamics of a non-Hermitian two-mode $\mathcal{PT}$-symmetric dimer, and show how this can be directly mapped to the *unitary* squeezing dynamics generated by a dissipation-free parametric amplifier model. We then extend this discussion to two-mode non-Hermitian systems where $\mathcal{PT}$ symmetry is broken, and show that a similar mapping to a quantum system is still possible.

3.3.1 Review: $\mathcal{PT}$ Dimer

A standard two-mode $\mathcal{PT}$ dimer consists of two tunnel-coupled modes (amplitudes $\alpha_1(t), \alpha_2(t)$) where mode 1 (2) is subject to gain (loss), with the gain and loss rates set equal to γ (see Fig. 3.1). The equations of motion are

$$i\frac{d}{dt}\begin{pmatrix} \alpha_1(t) \\ \alpha_2(t) \end{pmatrix} = \mathcal{H}_{\mathcal{PT}}\begin{pmatrix} \alpha_1(t) \\ \alpha_2(t) \end{pmatrix}, \tag{3.1}$$

where the 2×2 effective non-Hermitian Hamiltonian is

$$\mathcal{H}_{\mathcal{PT}} = \begin{pmatrix} +i\frac{\gamma}{2} & g \\ g & -i\frac{\gamma}{2} \end{pmatrix} = i\frac{\gamma}{2}\sigma_z + g\sigma_x. \tag{3.2}$$

g is the tunneling amplitude (which we take without loss of generality to be real and positive), and σ_z, σ_x are standard Pauli matrices. We will use the calligraphic symbol $\mathcal{H}$ throughout

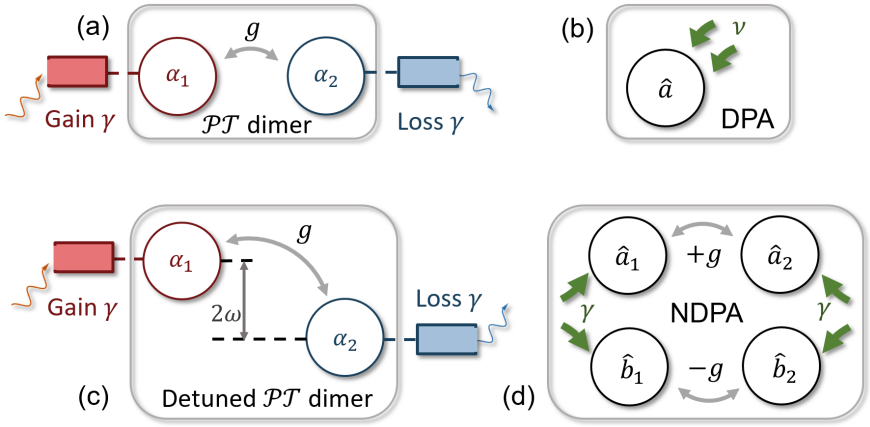

Fig. 3.1: Schematics depicting non-Hermitian two mode systems and equivalent Hermitian driven bosonic setups. (a) Standard two-mode $\mathcal{PT}$ dimer with balanced gain and loss. This system is unitarily equivalent to the system in (b): a single-mode bosonic degenerate parametric amplifier (DPA) with drive amplitude $\nu = \gamma$. (c) Detuned gain-loss dimer, where an energy detuning between modes breaks $\mathcal{PT}$ symmetry; this is equivalent to the system in (d), a four-mode non-degenerate parametric amplifier setup. As discussed in the text, these mappings can be extended to multi-mode and lattice systems.

to denote non-Hermitian Hamiltonians. Defining the time-reversal operation $\mathcal{T}$ as complex conjugation, and defining parity $\mathcal{P}$ as the interchange of the two modes, we see that $\mathcal{H}_{\mathcal{PT}}$ is invariant under $\mathcal{PT}$.

The eigenvalues of $\mathcal{H}_{\mathcal{PT}}$ are given by

$$\lambda_{\pm} = \pm\sqrt{g^2 - \left(\frac{\gamma}{2}\right)^2}. \tag{3.3}$$

At the critical point $g = \gamma/2 \equiv g_c$, the $\mathcal{PT}$-symmetric Hamiltonian $\mathcal{H}_{\mathcal{PT}}$ is defective, corresponding to a (second order) exceptional point in parameter space. For $g < g_c$, the mode eigenvalues become complex, implying exponential growth and decay in the time domain; this transition is often referred to as the "spontaneous breaking of $\mathcal{PT}$ symmetry".

Consider next a more general non-Hermitian 2 mode problem, where the dynamics are again given by Eq. (3.1) with $\mathcal{H}_{\mathcal{PT}}$ replaced by a more general effective Hamiltonian:

$$\mathcal{H} = \left(\vec{c} + i\vec{d}\right) \cdot \vec{\sigma}. \tag{3.4}$$

Here $\vec{c}$, $\vec{d}$ are real vectors, and we have ignored any constant-matrix part of $\mathcal{H}$ (as this has a trivial effect on dynamics). This general non-Hermitian Hamiltonian is unitarily equivalent to $\mathcal{H}_{\mathcal{PT}}$ (and has eigenvalues of the form in Eq. (3.3)) whenever its Hermitian and anti-Hermitian parts are orthogonal, i.e.

$$\vec{c} \cdot \vec{d} = 0. \tag{3.5}$$

While the preceding discussion is all classical, one might think that the extension to a quantum setting is trivial: just replace mode amplitudes $\alpha_1(t), \alpha_2(t)$ in Eq. (3.1) by canonical bosonic Heisenberg-picture annihilation operators $\hat{a}_1(t), \hat{a}_2(t)$, and interpret the result as a set of coupled Heisenberg equations of motion. This in general is not a valid evolution, as the dynamics will not preserve canonical commutation relations, i.e. at all times $[\hat{a}_j(t), \hat{a}^\dagger_{j'}(t)] = \delta_{jj'}$. This is perhaps most evident in the simple case where $g = 0$, and one has simple exponential growth (decay) of mode 1 (2).

At a physical level, this inconsistency arises because the gain/loss terms that give rise to the non-Hermitian part of $\mathcal{H}$ arise from couplings to dissipative environments. In addition to providing gain/loss, these baths will also drive the system with noise, and this noise cannot be neglected in the quantum case. By adding appropriate inhomogeneous quantum noise terms to the RHS of Eq. (3.1), one can then obtain an allowed quantum evolution (i.e. commutation relations are preserved in time). A systematic procedure for constructing quantum noise terms consistent with a given non-Hermitian Hamiltonian was presented recently in Ref. [50].

3.3.2 Mapping to a degenerate parametric amplifier

Our goal is to realize the effective non-Hermitian dynamics of Eq. (3.1) in a quantum system *without* having dissipation and the corresponding driving noise. To that end, we consider the quantum Hamiltonian of a single bosonic mode $\hat{a}$ that is parametrically driven (i.e. subject

to two-photon driving). In an appropriate rotating frame, the Hamiltonian is:

$$\hat{H}_{\mathrm{DPA}} = \delta \hat{a}^\dagger \hat{a} + \frac{\nu}{2}\left(i\hat{a}^{\dagger 2} + h.c.\right), \tag{3.6}$$

where δ represents a detuning term, and ν is the magnitude of the parametric drive. This is the standard Hamiltonian of a degenerate parametric amplifier, a system that is extremely well-studied in quantum optics (see, e.g., [61, 62]), and that can be realized in a wide range of settings. It generates a unitary time evolution, which for $\delta = 0$ reduces to a single-mode squeezing transformation. Without loss of generality, we work in a gauge where ν is real and positive in what follows.

Despite having only a single mode, the dynamics has a 2 component structure, as the parametric drive couples $\hat{a}$ and $\hat{a}^\dagger$. Defining a vector of operators

$$|\hat{a}\rangle = (\hat{a}, \hat{a}^\dagger)^T, \tag{3.7}$$

the Heisenberg equations of motions can be written as

$$i\partial_t |\hat{a}\rangle = \mathcal{M}_{\mathrm{DPA}} |\hat{a}\rangle, \tag{3.8}$$

where the dynamical matrix $\mathcal{M}_{\mathrm{DPA}}$ is

$$\mathcal{M}_{\mathrm{DPA}} = \begin{pmatrix} \delta & i\nu \\ i\nu & -\delta \end{pmatrix} = \delta\sigma_z + i\nu\sigma_x. \tag{3.9}$$

We see immediately that the structure of the Heisenberg EOM for this Hermitian problem mirrors that of the effective non-Hermitian dimer system in Eq. (3.1), with the dynamical matrix $\mathcal{M}_{\mathrm{DPA}}$ playing the role of an effective non-Hermitian Hamiltonian $\mathcal{H}$. Further, $\mathcal{M}_{\mathrm{DPA}}$ satisfies the condition in Eq. (3.4), implying that it is unitarily equivalent to $\mathcal{H}_{\mathcal{PT}}$ in Eq. (3.2)

(with $\delta = g$ and $\nu = \gamma/2$). This effective $\mathcal{PT}$ symmetry cannot be broken in our single mode problem (as Eq. (3.6) is the most general single-mode, quadratic, Hermitian and bosonic Hamiltonian).

Not surprisingly, the eigenvalues of $\mathcal{M}_{\rm DPA}$ have exactly the same structure as the $\mathcal{PT}$ dimer:

$$\lambda_{\rm DPA,\pm} = \pm\sqrt{\delta^2 - \nu^2}. \tag{3.10}$$

It follows that the parametric drive ν plays the role of the incoherent gain/loss in $\mathcal{H}_{\mathcal{PT}}$, whereas the detuning δ plays the role of the tunnel coupling. As we show in the next subsection, this allows us to directly map the physics of the threshold transition in our DPA system to the "spontaneous" breaking of $\mathcal{PT}$-symmetry that occurs in $\mathcal{H}_{\mathcal{PT}}$ when $\gamma/2$ is made larger than g. In particular, the DPA dynamical matrix exhibits an exceptional point when $\nu = \delta$, i.e. at the parametric oscillation threshold.

Before exploring this connection, we return to the problem of commutation relations: why doesn't the non-Hermitian nature of the dynamical matrix (and the possibility of exponential growth / decay) in time cause issues in our DPA system? The easiest way of seeing this is to explicitly make the unitary transformation that maps the dynamical matrix $\mathcal{M}_{\rm DPA}$ in Eq. (3.9) to the gain-loss form of $\mathcal{H}_{\mathcal{PT}}$ in Eq. (3.2). With this transformation, the Heisenberg equations of motion in Eq. (3.8) now take the form:

$$i\partial_t \begin{pmatrix} \hat{q} \\ i\hat{p} \end{pmatrix} = \begin{pmatrix} i\nu & \delta \\ \delta & -i\nu \end{pmatrix} \begin{pmatrix} \hat{q} \\ i\hat{p} \end{pmatrix} \tag{3.11}$$

where $\hat{q} \equiv (\hat{a} + \hat{a}^\dagger)/\sqrt{2}$, $\hat{p} \equiv i(\hat{a}^\dagger - \hat{a})/\sqrt{2}$ are canonical (Hermitian) quadrature operators. With this transformation, we see that the dynamical matrix for the DPA in the quadrature basis has explicitly the same form as the non-Hermitian Hamiltonian $\mathcal{H}_{\mathcal{PT}}$ in Eq. (3.2) describing the gain-loss $\mathcal{PT}$ dimer. We can also see why there is no longer any issue with

commutation relations: the exponential growth that occurs when $|\delta| < \nu$ causes $\hat{q}$ to grow exponentially in time, and $\hat{p}$ to decay exponential in time, *at the same rate*. This is just standard, unitary squeezing dynamics. This exponential growth preserves the canonical $[\hat{q}, \hat{p}] = i$ commutation relation at all times.

We thus see that by exploiting the squeezing / anti-squeezing, we can replicate the dynamics of the non-Hermitian $\mathcal{PT}$ dimer in Eq. (3.1). Of course, in this mapping we have just a single mode, and hence only a single complex degree of freedom (whereas in Eq. (3.1), there are two complex degrees of freedom). In Eq. (3.11), this manifests itself in the fact that the relative phase between the two amplitudes *must* be i. By using a two-mode, non-degenerate parametric amplifier system, this phase constraint can be lifted; this will be discussed in Section 3.4.1. Section 3.3.4 presents yet another approach allowing even more flexibility.

Before proceeding, we briefly pause to note another connection between the $\mathcal{PT}$ dimer Hamiltonian $\mathcal{H}_{\mathcal{PT}}$ and the DPA dynamical matrix $\mathcal{M}_{\text{DPA}}$: they are are both pseudo-Hermitian matrices. By definition, a pseudo-Hermitian matrix is isospectral with its Hermitian conjugate, so that

$$\mathcal{H}^\dagger = \eta \mathcal{H} \eta^{-1}, \tag{3.12}$$

where η is Hermitian and invertible [63]. It is easy to see that the dynamical matrix of a generic multi-mode bosonic parametric amplifier system is pseudo-Hermitian; this was recently explicitly pointed out by Lieu [56] (see also Appendix 3.7.1). This connection is however of limited use for our problem: while a given $\mathcal{PT}$-symmetric Hamiltonian is always pseudo-Hermitian, it is not necessarily unitarily equivalent to the dynamical matrix of some quantum bosonic system having the same number of modes (see Appendix 3.7.5).

3.3.3 "Phase transitions", exceptional points and conserved quantities

A consequence of the above mapping is that the so-called $\mathcal{PT}$ symmetry breaking phase transition in $\mathcal{H}_{\mathcal{PT}}$ is equivalent to the threshold transition in a parametric amplifier. Recall that $\mathcal{H}_{\mathcal{PT}}$ exhibits a transition in the eigenvectors and eigenvalues as a function of g; this is referred to as the "spontaneous breaking of $\mathcal{PT}$ symmetry" [64]. The transition occurs at $g = \gamma/2 \equiv g_c$, i.e. the point at which $\mathcal{H}_{\mathcal{PT}}$ has an exceptional point. When $g > g_c$, one is in the $\mathcal{PT}$-unbroken phase. $\mathcal{H}_{\mathcal{PT}}$ has purely real eigenvalues, and its right eigenvectors $\vec{r}_\pm$ are delocalized (i.e. their amplitudes in each mode are equal) as

$$\vec{r}_\pm = \frac{1}{\sqrt{2}} \left(1, -ie^{\pm i\alpha}\right)^T, \tag{3.13}$$

with $\alpha = \arccos(\gamma/2g)$. In contrast, when g is reduced below g_c, one is in the $\mathcal{PT}$-broken phase. $\mathcal{H}_{\mathcal{PT}}$ has purely imaginary eigenvalues, and the eigenvectors now exhibit localization.

The above behaviour is equivalent to the threshold behaviour of a detuned DPA. For $|\delta| > \nu$, the parametric drive is too non-resonant to cause any instability, and the system has purely oscillatory dynamics (as it would if $\nu = 0$). In contrast, when $|\delta|$ is reduced below ν, one crosses the threshold for parametric instability. One now has exponential decay and growth, which (as discussed) corresponds to the squeezing / anti-squeezing of canonically conjugate quadratures. The effective localization of the eigenvectors in this regime corresponds to the fact that the amplified quadrature is predominantly $\hat{q}$, while the squeezed quadrature is predominantly $\hat{p}$.

Finally, consider the case where one tunes $\delta = \nu$ and is thus exactly at the EP. The DPA Hamiltonian in this case is:

$$\hat{H}_{\text{DPA}} = \frac{\nu}{2} \left(e^{-i\pi/4}\hat{a} + e^{i\pi/4}\hat{a}^\dagger\right)^2 \equiv \nu\hat{Q}^2. \tag{3.14}$$

The Hermitian quadrature operator $\hat{Q}$ is a conserved quantity, and thus $\hat{H}_{\text{DPA}}$ is said to

possess a quantum non-demolition (QND) structure. This structure is directly responsible for the lack of any oscillatory dynamics. The co-existence of exceptional points and conserved QND quadrature operators is not just limited to this simple example: it is a generic feature in particle non-conserving bosonic Hamiltonians. For example, in Appendix 3.7.6, we discuss a 3-mode system that can be tuned to a third-order EP; this coincides with it having two conserved QND quadrature operators.

3.3.4 Mapping for more general two mode non-Hermitian Hamiltonian

We now discuss a more general approach for realizing non-Hermitian two-mode dynamics in dissipation-free quantum systems. Unlike the mapping to a DPA discussed in Section 3.3.2, this alternate method does not require a $\mathcal{PT}$-symmetric non-Hermitian Hamiltonian $\mathcal{H}$, and does not place restrictions on the phases of mode amplitudes. Our approach adapts the concept of quantum-mechanics free subsystems (QMFS) introduced by Tsang and Caves [65]: by introducing extra bosonic modes, one can have a *commuting* set of operators with arbitrary (possibly non-Hermitian) dynamics. As all relevant operators commute, there is no need to add noise terms. While QMFS are conventionally discussed and utilized for quantum back-action evasion [65–69], we show here that they are also a powerful tool for realizing effective non-Hermitian quantum dynamics in a dissipationless setting.

Consider a two-mode non-Hermitian system where $\mathcal{PT}$ is explicitly broken by the addition of a detuning term ω:

$$\mathcal{H}_\omega = \left(\omega + i\frac{\gamma}{2}\right)\sigma_z + g\sigma_x. \tag{3.15}$$

This Hamiltonian is not unitarily equivalent to a $\mathcal{PT}$ system (c.f. Eq. (3.5)), and thus its dynamics cannot be realized by a DPA using the mapping of Section 3.3.2.

As usual, the goal is to have a quantum system whose Heisenberg equations of motion

are governed by $\mathcal{H}_\omega$ without any extra added quantum noise terms, i.e.

$$i\frac{d}{dt}\begin{pmatrix}\hat{z}_1(t)\\ \hat{z}_2(t)\end{pmatrix} = \mathcal{H}_\omega \begin{pmatrix}\hat{z}_1(t)\\ \hat{z}_2(t)\end{pmatrix}. \tag{3.16}$$

The operators $\hat{z}_j$ should play the analogous role of the mode amplitudes in the classical coupled-mode equations Eq. (3.2), and hence should encode two complex degrees of freedom. As discussed, the obvious choice where $\hat{z}_j$ represent canonical annihilation operators of two bosonic modes does not work: the resulting dynamics would not in general preserve canonical commutation relations.

Clearly, a simple solution would be to use operators $\hat{z}_j$ where for all j, j'

$$[\hat{z}_j, \hat{z}_{j'}^\dagger] = [\hat{z}_j, \hat{z}_{j'}] = 0. \tag{3.17}$$

As all operators commute, there would be no additional quantum constraints on Eq. (3.16). Throughout this chapter, we will use the term *pseudo-modes* to denote a set of fully commuting operators $\hat{z}_j, \hat{z}_j^\dagger$ that obey some desired non-Hermitian dynamics. While these pseudo-mode operators are not canonical bosonic annihilation / creation operators, they can play the role of mode amplitudes in the classical coupled mode theory.

For our two-mode problem, we can construct appropriate pseudo-modes by considering a system of *four* canonical bosonic modes, with annihilation operators $\hat{a}_1, \hat{a}_2, \hat{b}_1, \hat{b}_2$. Each mode can be written in terms of Hermitian quadrature operators ($j = 1, 2$):

$$\hat{a}_j = \tfrac{1}{\sqrt{2}}\left(\hat{x}_{a,j} + i\hat{p}_{a,j}\right), \tag{3.18}$$

$$\hat{b}_j = \tfrac{1}{\sqrt{2}}\left(\hat{x}_{b,j} + i\hat{p}_{b,j}\right). \tag{3.19}$$

One could now also define collective quadrature operators in the standard manner:

$$\hat{x}_{\pm,j} = \frac{1}{\sqrt{2}}\left(\hat{x}_{a,j} \pm \hat{x}_{b,j}\right), \tag{3.20a}$$

$$\hat{p}_{\pm,j} = \frac{1}{\sqrt{2}}\left(\hat{p}_{a,j} \pm \hat{p}_{b,j}\right). \tag{3.20b}$$

These satisfy standard canonical commutation relations, namely $\left[\hat{x}_{\pm,j}, \hat{p}_{\pm,j'}\right] = i\delta_{jj'}$, $\left[\hat{x}_{\pm,j}, \hat{x}_{\mp,j'}\right] = \left[\hat{p}_{\pm,j}, \hat{p}_{\mp,j'}\right] = \left[\hat{x}_{\pm,j}, \hat{p}_{\mp,j'}\right] = 0$. Note that all + collective quadrature operators commute with all − operators.

We can now construct non-Hermitian pseudo-mode operators $\hat{z}_j$ with the desired properties by building them out of a fully commuting set of four collective quadrature operators. While there are many possible choices, we will use:

$$\hat{z}_j = \hat{x}_{+,j} + i\hat{p}_{-,j} = \hat{a}_j + \hat{b}_j^\dagger. \tag{3.21}$$

Eq. (3.17) is thus satisfied: we have two complex degrees of freedom where there are no constraints from commutation relations.

All that remains is to construct a physical (Hermitian) Hamiltonian where the four collective quadratures of interest are dynamically coupled as per Eq. (3.16). This can be accomplished using

$$\begin{aligned}\hat{H}_{\omega\mathrm{PA}} &= \omega\left(\hat{a}_1^\dagger\hat{a}_1 - \hat{a}_2^\dagger\hat{a}_2 + \hat{b}_2^\dagger\hat{b}_2 - \hat{b}_1^\dagger\hat{b}_1\right) \\ &+ \left[g\left(\hat{a}_1^\dagger\hat{a}_2 - \hat{b}_1^\dagger\hat{b}_2\right) + i\frac{\gamma}{2}\left(\hat{a}_1^\dagger\hat{b}_1^\dagger - \hat{a}_2^\dagger\hat{b}_2^\dagger\right) + h.c.\right].\end{aligned} \tag{3.22}$$

This represents a system of two tunnel-coupled non-degenerate parametric amplifiers. One can verify that the Heisenberg equations of motion for collective quadratures generated by the *Hermitian* Hamiltonian $\hat{H}_{\omega\mathrm{PA}}$ correspond to Eq. (3.16), with the pseudo-modes defined in Eq. (3.21). We thus have our desired mapping.

Note that with this choice, the collective quadratures that do not appear in the definition of $\hat{z}_j$ can be used to construct another pair of pseudo-modes:

$$\hat{\tilde{z}}_j = \hat{x}_{-,j} + i\hat{p}_{+,j}. \tag{3.23}$$

The dynamics does not couple $\hat{z}$ and $\hat{\tilde{z}}$ operators; using Eq. (3.22), the latter satisfy:

$$i\frac{d}{dt}\begin{pmatrix} \hat{\tilde{z}}_1(t) \\ \hat{\tilde{z}}_2(t) \end{pmatrix} = \mathcal{H}_\omega^\dagger \begin{pmatrix} \hat{\tilde{z}}_1(t) \\ \hat{\tilde{z}}_2(t) \end{pmatrix}. \tag{3.24}$$

Thus, in doubling the degrees of freedom, we have constructed two sets of commuting "pseudo-mode" operators; the first set evolves according to $\mathcal{H}_\omega$, the second to $\mathcal{H}_\omega^\dagger$.

It is instructive to also consider the structure of the Heisenberg equations of motion when written in terms of the true canonical mode annihilation operators; the desired non-Hermitian structure is present there as well. Letting $|\hat{v}_2\rangle$ denote the four-vector of operators $(\hat{a}_1, \hat{a}_2, \hat{b}_1^\dagger, \hat{b}_2^\dagger)^T$, the Heisenberg equations of motion generated by $\hat{H}_{\omega\mathrm{PA}}$ have the general form

$$i\frac{d}{dt}|\hat{v}_2\rangle = \mathcal{M}_{\omega\mathrm{PA}}|\hat{v}_2\rangle. \tag{3.25}$$

Here $\mathcal{M}_{\omega\mathrm{PA}}$ is the system's mode-basis dynamical matrix; it is unitarily equivalent to a $\mathcal{PT}$-symmetric matrix:

$$\mathcal{H}_{\omega\mathcal{PT}} = \begin{pmatrix} \mathcal{H}_\omega & 0 \\ 0 & \mathcal{H}_\omega^* \end{pmatrix} = \mathcal{U}_4 \mathcal{M}_{\omega\mathrm{PA}} \mathcal{U}_4^\dagger, \tag{3.26}$$

$$\mathcal{U}_4 = \frac{1}{\sqrt{2}}\begin{pmatrix} \mathbb{I}_2 & -\mathbb{I}_2 \\ \mathbb{I}_2 & \mathbb{I}_2 \end{pmatrix}. \tag{3.27}$$

This provides another way to interpret our mapping: by doubling the degrees of freedom and

introducing a mirror system of the detuned $\mathcal{PT}$ dimer $\mathcal{H}_\omega$ in Eq. (3.15) which evolves under $\mathcal{H}_\omega^* = \mathcal{H}_\omega^\dagger$, we effectively restore $\mathcal{PT}$ symmetry for the entire, composite system, allowing a mapping to a parametrically-driven bosonic Hamiltonian.

We end this section by stressing that our construction using four modes is not limited to the particular non-Hermitian Hamiltonian $\mathcal{H}_\omega$, but can be used to realize the dynamics of *any* non-Hermitian two-mode Hamiltonian $\mathcal{H}$. One again represents the quasi-mode operators $\hat{z}_1$ and $\hat{z}_2$ using Eqs. (3.21). One obtains the desired dynamics in Eq. (3.16) (with $\mathcal{H}_\omega$ replaced by $\mathcal{H}$) if the Hermitian Hamiltonian describing the four mode system is taken to be:

$$\hat{H}_{\rm QMFS} = \frac{1}{2}\sum_{j,j'=1}^{2}\Big[\Big(\mathcal{H}+\mathcal{H}^\dagger\Big)_{jj'}\Big(\hat{a}_j^\dagger\hat{a}_{j'}-\hat{b}_j\hat{b}_{j'}^\dagger\Big) + \Big(\mathcal{H}-\mathcal{H}^\dagger\Big)_{jj'}\Big(\hat{a}_j^\dagger\hat{b}_{j'}^\dagger-\hat{a}_{j'}\hat{b}_j\Big)\Big]. \tag{3.28}$$

We see that the particle-number conserving terms are associated with the Hermitian part of $\mathcal{H}$, whereas the non-Hermitian parts of $\mathcal{H}$ are associated with particle-nonconserving two-photon driving terms.

3.4 Dissipationless non-Hermitian lattice dynamics

We now show that the approaches in the previous section for realizing effective non-Hermitian dynamics in driven, dissipation-free quantum bosonic systems can be generalized to a multi-mode lattice setting. We will focus on approach where the number of modes in the original non-Hermtian system and the bosonic system are identical; this will be accomplished by using non-degenerate parametric driving (where pairs of photons are added to distinct modes).

3.4.1 Standard non-Hermitian $\mathcal{PT}$-symmetric tight-binding chain

We start with a simple, but paradigmatic case: a one-dimensional, nearest-neighbour tight-binding chain with on-site gain/loss terms that respects $\mathcal{PT}$ symmetry. We refer to this as a "standard" $\mathcal{PT}$ tight-binding chain. Non-Hermitian lattice models of this form have been the subject of many recent studies (see, e.g., [46, 47, 49, 56, 70–72]). We show that it is possible to realize identical dynamics in a Hermitian driven bosonic system, without any need to introduce dissipation *or* double the number of degrees of freedom. We also show that this approach can be generalized to a wider class of models.

We consider a 1D lattice of coupled modes having $2N$ sites, labelled (from left to right) by $j \in \{-N, -N+1, ..., -1, 1, ..., N-1, N\}$. We will also (as is common) describe our non-Hermitian Hamiltonian using second-quantized notation, with $\hat{c}_j$ being the mode annihilation operator on site j. The non-Hermitian lattice Hamiltonian then has the form:

$$\begin{aligned}\hat{\mathcal{H}}_{\text{tb}} = &\sum_{j=-N+1}^{-1} \left(t_j \hat{c}_j^\dagger \hat{c}_{j-1} + h.c. \right) + \left(t_0 \hat{c}_1^\dagger \hat{c}_{-1} + h.c. \right) \\ &+ \sum_{j=1}^{N-1} \left(t_j \hat{c}_{j+1}^\dagger \hat{c}_j + h.c. \right) + i \sum_j \frac{\gamma_j}{2} \hat{c}_j^\dagger \hat{c}_j . \end{aligned} \tag{3.29}$$

The first three terms represents Hermitian hopping on the lattice, with hopping strength t_j on each bond (which we take to be real without loss of generality). The last, non-Hermitian term describes on-site gain/loss on each site, with a corresponding rate $\gamma_j/2$.

We now constrain this model by insisting that it be $\mathcal{PT}$-symmetric. $\mathcal{P}$ is defined as the real-space operation which maps $\hat{c}_j$ to $\hat{c}_{-j}$, and $\mathcal{T}$ is defined as before as simple complex conjugation of the Hamiltonian matrix. $\mathcal{PT}$ symmetry thus requires:

$$t_j = t_{-j}, \tag{3.30a}$$

$$-\gamma_j = \gamma_{-j}. \tag{3.30b}$$

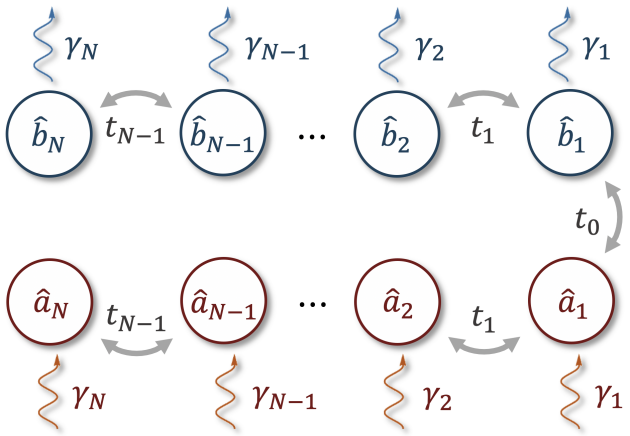

Fig. 3.2: Illustration of a $2N$-mode nearest-neighbor tight-binding $\mathcal{PT}$-symmetric system, whose Hamiltonian $\hat{\mathcal{H}}_{\rm tb}$ is given in Eq. (3.32). Insisting on $\mathcal{PT}$ symmetry, and relabelling $\hat{a}_j \to \hat{c}_{-j}$ and $\hat{b}_j \to \hat{c}_j$, the figure also represents the tight-binding Hamiltonian $\hat{\mathcal{H}}_{\rm tb}$ in Eq. (3.29). There always exists unitary correspondence between a system of this form and a Hermitian parametrically-driven bosonic system having an identical number of modes (see discussion in main text).

Note that the class of models of this form includes the widely-studied non-Hermitian $\mathcal{PT}$-symmetric Su-Schrieffer-Heeger (SSH) model [70, 71, 73, 74]. This would correspond to a dimerized structure for the hoppings and loss: $t_j = t + (-)^j t'$ and $\gamma_j = (-)^j \gamma_0$.

It will be useful to re-write the Hamiltonian in a more structured form by relabelling the mode operators via

$$\hat{c}_{-j} \to \hat{a}_j, \quad \hat{c}_j \to \hat{b}_j \quad (j = 1, 2, \cdots, N). \tag{3.31}$$

As depicted in Fig. 3.2, the Hamiltonian becomes

$$\begin{aligned}\hat{\mathcal{H}}_{\rm tb} = \sum_{j,j'=1}^{N} \Big[& \Omega_{jj'} \left(\hat{a}_j^\dagger \hat{a}_{j'} + \hat{b}_j^\dagger \hat{b}_{j'} \right) \\ & + i\Gamma_{jj'} \left(\hat{a}_j^\dagger \hat{a}_{j'} - \hat{b}_j^\dagger \hat{b}_{j'} \right) + J_{jj'} \hat{a}_j^\dagger \hat{b}_{j'} + \tilde{J}_{jj'}\, \hat{b}_j^\dagger \hat{a}_{j'} \Big],\end{aligned} \tag{3.32}$$

where Ω, Γ, J and $\tilde{J}$ are all $N \times N$ coefficient matrices with entries given by

$$\Omega_{ll'} = t_l \delta_{l',l+1} + t_{l'} \delta_{l',l-1}, \tag{3.33a}$$

$$\Gamma_{ll'} = \gamma_l \delta_{l,l'}/2, \tag{3.33b}$$

$$J_{ll'} = t_0 \delta_{l,1} \delta_{l',1} = \tilde{J}_{ll'}. \tag{3.33c}$$

In this new basis, $\mathcal{P}$ is simply the operation which interchanges a_j and b_j ($j = 1, 2, \cdots, N$).

We now proceed in analogy to our treatment of the $\mathcal{PT}$ dimer in Section 3.3.2. We first obtain the equations of motion for the a_j and b_j modes amplitudes α_j and β_j, generated by $\hat{\mathcal{H}}_{\rm tb}$ as

$$i\partial_t \begin{pmatrix} \vec{\alpha} \\ \vec{\beta} \end{pmatrix} = \mathcal{H}_{\rm tb} \begin{pmatrix} \vec{\alpha} \\ \vec{\beta} \end{pmatrix}, \tag{3.34}$$

with the resulting non-Hermitian dynamical matrix given by

$$\mathcal{H}_{\rm tb} = \begin{pmatrix} \Omega + i\Gamma & J \\ \tilde{J} & \Omega - i\Gamma \end{pmatrix}, \tag{3.35}$$

with $\tilde{J} = J$.

The block structure of the matrix $\mathcal{H}_{\rm tb}$ (corresponding to a_j/b_j modes) allows us to make a simple rotation $\mathcal{U}_{\rm tb}$ which moves the non-Hermitian gain/loss terms to the off-diagonal blocks:

$$\mathcal{M}_{\rm tb} = \mathcal{U}_{\rm tb} \mathcal{H}_{\rm tb} \mathcal{U}_{\rm tb}^\dagger = \begin{pmatrix} \Omega + J & i\Gamma \\ i\Gamma & \Omega - J \end{pmatrix}, \tag{3.36}$$

$$\mathcal{U}_{\rm tb} = \frac{1}{\sqrt{2}} \begin{pmatrix} \mathbb{I}_N & \mathbb{I}_N \\ \mathbb{I}_N & -\mathbb{I}_N \end{pmatrix}. \tag{3.37}$$

In analogy to the two-mode problem in Section 3.3.2, the rotated matrix $\mathcal{M}_{\rm tb}$ now has the

form of a dynamical matrix of a parametrically driven bosonic system with $2N$ sites. However, unlike the mapping in Section 3.3.2, the relevant system here involves non-degenerate parametric drives (i.e. two-photon driving terms that involve distinct modes). The dynamical matrix $\mathcal{M}_{\rm tb}$ above corresponds to the *Hermitian* bosonic Hamiltonian

$$\begin{aligned}\hat{H}_{\rm NDPA} = \sum_{j,j'}^{N} \Big[& \Omega_{jj'} \left(\hat{a}_j^\dagger \hat{a}_{j'} - \hat{b}_j^\dagger \hat{b}_{j'} \right) \\ & + J_{jj'} \left(\hat{a}_j^\dagger \hat{a}_{j'} + \hat{b}_j^\dagger \hat{b}_{j'} \right) + i\Gamma_{jj'} \left(\hat{a}_j^\dagger \hat{b}_{j'}^\dagger - \hat{b}_j \hat{a}_{j'} \right) \Big] . \end{aligned} \tag{3.38}$$

To be explicit, the Heisenberg equations of motion corresponding to this Hermitian Hamiltonian can be compactly written as

$$i\partial_t \left| \hat{v}_N \right\rangle = \mathcal{M}_{\rm tb} \left| \hat{v}_N \right\rangle , \tag{3.39a}$$

where $\left| \hat{v}_N \right\rangle = (\hat{a}_1, \hat{a}_2, \cdots, \hat{a}_N, \hat{b}_1^\dagger, \hat{b}_2^\dagger, \cdots, \hat{b}_N^\dagger)^T$. Thus, we see that the dynamics of the general $\mathcal{PT}$-symmetric non-Hermitian gain-loss lattice model in Eq. (3.32) can be realized by the non-dissipative, Hermitian quantum Hamiltonian in Eq. (3.38). As before, the exponential growth and decay that could result from the gain and loss terms are mapped onto a unitary squeezing operations in the driven quantum model (in this case two-mode squeezing operations).

With this explicit non-degenerate parametric-amplifier (NDPA) Hamiltonian $\hat{H}_{\rm NDPA}$ in hand, it is interesting to return to the simple $\mathcal{PT}$ dimer discussed in Section 3.3.2. This corresponds to the case $N = 1$ of the 1D $\mathcal{PT}$ chain considered in this section. In this case, the matrix Ω becomes an overall constant in the non-Hermtian Hamiltonian $\hat{\mathcal{H}}_{\rm tb}$ and can be ignored, and our mapping shows that the dynamics is equivalent to a simple two-mode NDPA in Eq. (3.38). We stress that this is a distinct mapping from that in Section 3.3.2, which involves a single-mode DPA. By having two modes here, there is no constraint on the

phases of mode amplitudes, as the number of complex degrees of freedom is the same as the original non-Hermitian coupled-mode problem. As we will show in the next section, this lack of constraints remains the same in the general multi-mode version of the problem as well.

3.4.2 Generalized non-Hermitian $\mathcal{PT}$-symmetric tight-binding chain

We now consider more general $\mathcal{PT}$-symmetric non-Hermitian lattice models, which could be in higher dimensions, have long range hopping terms, and have non-local non-Hermitian terms. The unitary mapping $\mathcal{U}_{\text{tb}}$ derived above is also valid for a wide class of these generalized models. Note first that a generic $\mathcal{PT}$-symmetric non-Hermitian Hamiltonian (in arbitrary dimensions, with $2N$ sites) can always be written in the form given in Eq. (3.32), where $\mathcal{PT}$ symmetry requires that the coefficient matrices Ω, Γ are real, as well as $\tilde{J} = J^*$. Our mapping to a Hermitian parametric amplifier problem (as per Eq. (3.38)) remains valid as long as the coefficient matrices Ω, Γ and J are all real, symmetric matrices. This encompasses a much broader class of models than the 1D nearest neighbour, imaginary potential model described by Eqs. (3.33).

Among the extra kinds of terms that can be accommodated in the starting non-Hermitian $\mathcal{PT}$ lattice model are:

- real detunings of a_j and b_j modes, given by real, diagonal matrix elements of Ω;
- real, coherent (i.e. Hermitian) coupling between any two a_j and $a_{j'}$ (or b_j and $b_{j'}$) modes with a completely real coupling strength, represented by off-diagonal matrix elements of Ω;
- real, coherent coupling between any two a_j and $b_{j'}$ modes with a completely real coupling strength, represented by corresponding matrix elements of J;
- imaginary, dissipative (i.e. non-Hermitian) couplings between any two different modes, represented by off-diagonal matrix elements of Γ.

As an example, our mapping to a NDPA system remains valid for a 2D tight-binding $\mathcal{PT}$ lattice, as long as the coherent couplings are purely real, and the dissipative couplings are purely imaginary. Conversely, for non-Hermitian tight-binding models where hopping phases encode non-trivial fluxes, we may construct an example where the mapping does not work. Necessary conditions for such a mapping to exist are presented in Appendix 3.7.3, while simple four mode systems where the correspondence fails are discussed in Appendix 3.7.5.

3.4.3 Mapping for arbitrary multi-mode non-Hermitian Hamiltonians

In Sections 3.4.1 and 3.4.2, we described a general mapping between a wide class of non-Hermitian, $\mathcal{PT}$ symmetric lattice models and the dynamical matrix of a Hermitian, parametrically driven bosonic system. Crucially, this mapping preserved the number of modes. As discussed, it cannot be applied to *all* possible $\mathcal{PT}$ lattice models, nor can it be used for systems with broken $\mathcal{PT}$.

In this section, we show how the general QMFS strategy introduced in Section 3.3.4 can be generalized to map an arbitrary non-Hermitian lattice model to a Hermitian, parametrically-driven bosonic problem. While more general, this strategy comes with a price: the driven bosonic system will have twice the number of modes as in the original non-Hermitian Hamiltonian.

The approach is to generalize the construction presented in Eq. (3.28) of Section 3.3.4 to a general N-mode non-Hermitian Hamiltonian $\mathcal{H}_N$. We will use a $2N$-mode bosonic system, with canonical quadrature operators $\hat{x}_{\pm,j}$ and $\hat{p}_{\pm,j}$ for $j = 1, 2, \ldots, N$. The only nonzero commutators between the quadratures are

$$\left[\hat{x}_{\pm,j}, \hat{p}_{\pm,j'}\right] = i\delta_{jj'}, \tag{3.40}$$

for $j, j' = 1, 2, \ldots, N$.

To implement the general QMFS strategy, we wish to construct a Hamiltonian where a set of fully commuting collective quadratures has a linear dynamics corresponding to $\mathcal{H}_N$. Following the convention for the two-mode case in Eqs. (3.21,3.23), we first introduce two sets of pseudo-modes $\hat{z}_{\pm,j}$ $(j = 1, 2, \ldots, N)$ as

$$\hat{z}_{\pm,j} = \hat{x}_{\pm,j} + i\hat{p}_{\mp,j}. \tag{3.41}$$

Mirroring the strategy of Section 3.3.4, we want a Hermitian bosonic Hamiltonian that yields the equations of motion:

$$i\partial_t \vec{\hat{z}}_+ = \mathcal{H}_N \vec{\hat{z}}_+, \tag{3.42a}$$

$$i\partial_t \vec{\hat{z}}_- = \mathcal{H}_N^\dagger \vec{\hat{z}}_-, \tag{3.42b}$$

where we define N-vectors $\vec{\hat{z}}_\pm$ consisting of the pseudo-mode operators $\hat{z}_{\pm,j}$, respectively, for notational convenience. As before, the desired dynamics will only couple mutually commuting quadratures. It is straightforward to prove that the two equations above generate a dynamics that preserve all canonical commutation relations, i.e. they generate a symplectic transformation of the bosonic system (see Appendix 3.7.7 for details). Further, one can show that this dynamics is generated by the Hermitian $2N$-mode Hamiltonian

$$\begin{aligned}\hat{H}_{\text{QMFS,multi.}} = \frac{1}{2}\sum_{j,j'=1}^{N} \Big[&\Big(\mathcal{H}_N + \mathcal{H}_N^\dagger\Big)_{jj'} \Big(\hat{a}_j^\dagger \hat{a}_{j'} - \hat{b}_j \hat{b}_{j'}^\dagger\Big) \\ &+ \Big(\mathcal{H}_N - \mathcal{H}_N^\dagger\Big)_{jj'} \Big(\hat{a}_j^\dagger \hat{b}_{j'}^\dagger - \hat{a}_{j'} \hat{b}_j\Big)\Big],\end{aligned} \tag{3.43}$$

where we define the bosonic mode operators in parallel to Eq. (3.21) as

$$\hat{a}_j \pm \hat{b}_j^\dagger = \hat{x}_{\pm,j} + i\hat{p}_{\mp,j} = \hat{z}_{\pm,j}. \tag{3.44}$$

The approach here is of course directly applicable to the case where the non-Hermitian $\mathcal{H}_N$ describes a lattice model in real space. Our mapping doubles the number of modes: for every lattice site in the original model, there are now two bosonic modes $\hat{a}_j, \hat{b}_j$. Note however from Eq. (3.43) that our mapping is fully local. For every band $E_n(\vec{k})$ of $\mathcal{H}_N$, the closed-form dynamics of the $\hat{a}_j$ and $\hat{b}_j^\dagger$ operators will correspondingly contribute two independent bands $E_n(\vec{k})$ and $E_n^*(\vec{k})$ in the bosonic problem; this follows directly from Eqs. (3.42a)-(3.42b). We stress that this doubled band structure only solves half of the entire BdG problem of the bosonic Hamiltonian; the full band structure will also include contributions from dynamics of the $\hat{b}_j$ and $\hat{a}_j^\dagger$ operators, which can also be obtained from Eqs. (3.42a)-(3.42b) as the $-E_n(\vec{k})$ and $-E_n^*(\vec{k})$ bands.

3.5 Applications

In this section, we discuss how the mappings introduced in the previous sections can be used to realize various well-known non-Hermitian effects in dissipation-free, quantum settings.

3.5.1 Exceptional point sensing

We first consider sensing methods that exploit the strong sensitivity of mode eigenvalues of a $\mathcal{PT}$-symmetric non-Hermitian system that is tuned to the vicinity of an exceptional point (EP) [47, 49]. The most common version of this scheme involves a simple gain-loss $\mathcal{PT}$ dimer (c.f. Section 3.3.1) with an effective non-Hermitian Hamiltonian

$$\mathcal{H}[\epsilon] = \mathcal{H}_{\mathcal{PT}} = i\frac{\gamma}{2}\sigma_z + (g_0 + \epsilon)\sigma_x. \tag{3.45}$$

The goal is to estimate the small parameter ϵ. If the unperturbed Hamiltonian $\mathcal{H}[0]$ is tuned to the EP by choosing $g_0 = \gamma/2 = g_c$, then the perturbation ϵ induces an eigenvalue splitting

that scales as $\sqrt{\epsilon}$, i.e. from Eq. (3.3), we have:

$$|\lambda_+ - \lambda_-| \simeq 2\sqrt{2g_0\epsilon}. \tag{3.46}$$

For small $\epsilon \ll g_0$, this is parametrically larger than a conventional mode splitting in a Hermitian system, which would be proportional to ϵ.

To exploit this eigenvalue sensitivity for measurement, it was suggested in Refs. [47, 49] to look at the reflection of a probe tone applied to the system at frequency $\omega_{\rm p}$. The frequency-dependent reflection coefficient $R[\omega_{\rm p}]$ would then reflect the parametric mode-splitting of the eigenvalues. While the advantage of this approach seems obvious, recent studies have shown that the unavoidable noise associated with incoherent gain and loss in the quantum regime can limit any enhancement of signal-to-noise ratio [50, 51].

Here, we show an analogous EP sensing scheme can be implemented in a parametric amplifier setup, without having to introduce any incoherent gain and loss, and corresponding noise. While there are many ways to proceed, the simplest is to use the unitary mapping introduced in Section 3.3.2 that maps the $\mathcal{PT}$ dimer in Eq. (3.45) to a single-mode, degenerate parametric amplifier (DPA). Letting $\delta = g_0$ and $\nu = \gamma/2$, the Hermitian DPA Hamiltonian corresponding to $\mathcal{H}[\epsilon]$ is then given by:

$$\hat{H}_{\rm DPA}\left[\epsilon\right] = \left(\delta + \epsilon\right)\hat{a}^\dagger\hat{a} + \frac{\nu}{2}\left(i\hat{a}^{\dagger 2} + h.c.\right). \tag{3.47}$$

As usual, the tunneling in $\mathcal{H}[\epsilon]$ becomes a detuning term, and the gain/loss terms in $\mathcal{H}[\epsilon]$ become a two-photon drive. We stress that the dynamical matrix of this Hermitian Hamiltonian is unitarily equivalent to $\mathcal{H}[\epsilon]$, and has the same eigenvalues. Note that the perturbation ϵ is now a standard dispersive coupling, something that arises in many measurement contexts. In the case where ϵ corresponds to the state of a qubit, this exact setup was realized in a recent superconducting quantum circuit experiment (though operated in a different regime) [75].

We now mimic the EP sensing protocol, by first tuning $\delta = \nu$ so that the unperturbed system is at the EP. To probe the ϵ-induced mode splitting, we will again look at the reflection of a probe tone applied at frequency ω_p. We couple the cavity $\hat{a}$ to an input-output waveguide (or transmission line), with a coupling rate κ_{ext}. The total decay rate of the cavity is given by

$$\kappa = \kappa_{\text{ext}} + \kappa_i, \tag{3.48}$$

where κ_i denotes intrinsic damping rate of the cavity. Here we assume the cavity is in the over-coupled regime, and the cavity linewdith is just given by the external coupling rate $\kappa = \kappa_{\text{ext}}$. As we will show later, the sensing signal is robust to unwanted loss (namely intrinsic damping of the cavity) for practical parameters. Using standard input-output theory [76], the Heisenberg equation of motion of $\hat{a}$ is

$$\frac{d}{dt}\hat{a} = -i\delta\hat{a} + \nu\hat{a}^\dagger - \frac{\kappa}{2}\hat{a} - \sqrt{\kappa}\Big(\alpha_{\text{in}}e^{-i\omega_p t} + \hat{\zeta}_{\text{in}}(t)\Big), \tag{3.49a}$$

where α_{in} is the amplitude of the probe tone, and $\hat{\zeta}_{\text{in}}(t)$ describes vacuum noise entering through the waveguide. Note that we are working in a rotating frame determined by the frequency of the pump field used to realize the parametric interaction.

The introduction of the waveguide shifts the eigenvalues of the dynamical matrix by a constant, but the system still possesses an EP. We pick the pump detuning $\delta = \nu \equiv \delta_c$ so that the unperturbed system is tuned to this EP. We then calculate the total output flux $P_{\text{out}}\left(\omega_p\right)$ (including both the reflected signal and idler beams), as a function of the probe frequency ω_p, to see how the ϵ-induced mode splitting impacts the light leaving the cavity. Using the standard input-output relation $\hat{a}_{\text{out}} = \hat{a}_{\text{in}} + \sqrt{\kappa}\hat{a}$ [76], the output flux is

$$\frac{P_{\text{out}}\left(\omega_p\right)}{\left|\alpha_{\text{in}}\right|^2} = 1 + \frac{2\kappa^2\nu^2}{\left(f\left[\omega_p\right]\right)^2 + \kappa^2\left(\delta^2 - \nu^2\right)}, \tag{3.50}$$

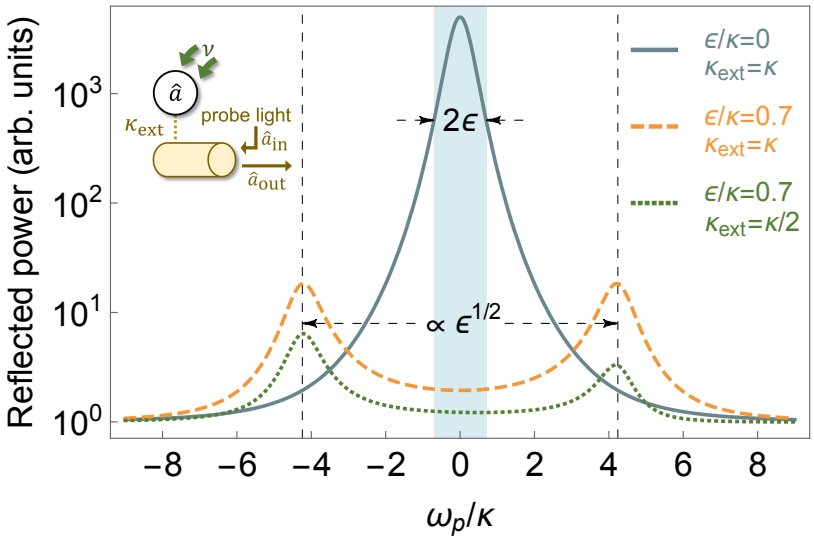

Fig. 3.3: Exceptional-point sensing with a degenerate parametric amplifier (DPA). A detuned DPA is tuned to an EP by matching the pump detuning and parametric drive amplitudes. Probe light of frequency ω_p (in the rotating frame) is sent into the cavity via waveguide (coupling rate $\kappa_{\rm ext}$). Plotted is the frequency-dependent reflected flux of the probe tone. Unless stated differently below, we consider the overcoupled cavity regime so that the cavity linewidth, given by $\kappa = \kappa_{\rm ext} + \kappa_i$, can be taken as $\kappa = \kappa_{\rm ext}$. Dark cyan solid line: reflected flux for the unperturbed system, showing a single peak. Orange dashed line: reflected flux where the system is perturbed by shifting the cavity frequency an amount $\epsilon = 0.7\kappa$ (c.f. Eq. (3.47)). One now has two distinct peaks, with a splitting that scales as $\sqrt{\epsilon}$. Green dotted line: same conditions as the orange dashed curve except for nonzero intrinsic cavity loss $\kappa_i = \kappa_{\rm ext}$, so that the cavity operates in the critical coupling regime $\kappa_{\rm ext} = \kappa/2$. Note that peak splitting is robust in the presence of unwanted cavity loss. Parameters correspond to a parametric drive amplitude $\nu/\kappa = 12.5$, and pump detuning $\delta = \nu$ originally set to the EP.

where $f\left[\omega_p\right] = \omega_p^2 + (\kappa/2)^2 - \delta^2 + \nu^2$. Note that we do not include the contribution from amplified vacuum fluctuations here, as this yields a background that is independent of both ω_p and $\alpha_{\rm in}$. In the limit of a weak coupling to the waveguide, we will observe narrow peak(s) in $P_{\rm out}$ that correspond to the dynamical matrix eigenvalues $\lambda_\pm$, see Fig. 3.3. For $\epsilon = 0$, there is just a single peak, whereas for non-zero ϵ there are two peaks, with the expected splitting $|\lambda_+ - \lambda_-| \simeq 2\sqrt{2\epsilon\delta_c} \gg \epsilon$ (see also Eq. (3.46)). In the presence of intrinsic cavity loss, as shown in Fig. 3.3 the peak structure still survives, although the reflected power becomes weaker.

We thus see that the EP sensing scheme of Refs. [47, 49] can be directly implemented in a parametric-amplifier setup, without any need for incoherent gain and loss. We leave a full analysis of the noise properties and ultimate sensitivity of this scheme (both in the linear and nonlinear response regimes) to a future work. Note that the general analysis in Ref. [50] of linear-response EP sensing assumed a Hamiltonian that conserves particle number, and thus does not apply directly to the DPA setup described here. Also note that higher-order exceptional points have been discussed in the context of sensing; these too can be realized without dissipation using parametrically-driven bosonic modes (see Appendix 3.7.6).

3.5.2 Quasi-adiabatic evolution and chiral mode switching

Another striking effect associated with exceptional points involves the chirality of non-adiabatic effects in non-Hermitian systems whose parameters are cyclically varied [34–42]. The paradigmatic system is the detuned gain-loss dimer $\mathcal{H}_\omega$ in Eq. (3.15), where now the tunneling g and detuning ω are made time-dependent:

$$\mathcal{H}_\omega(t) = \left(\omega(t) + i\frac{\gamma}{2}\right)\sigma_z + g(t)\sigma_x. \tag{3.51}$$

Consider a cyclic time-variation of parameters, where $(g(t), \omega(t))$ follow a closed path in parameter space that encloses one of the two EPs at $(g_c = \pm\gamma/2, \omega = 0)$ (see inset in Fig.3.4a). Non-adiabatic effects in such a setup depend crucially on the direction one traverses the path in parameter space: for one direction, there is no switching between adiabatic eigenmodes, whereas for the other direction, there is appreciable switching. Section 3.7.8 gives a basic introduction to this phenomena; see Ref. [40] for a more comprehensive discussion.

Recent experiments have probed this EP encircling physics in classical settings [41, 42], and it has been suggested that such effects could be useful in quantum settings [36]. As usual though, the unavoidable noise associated with incoherent gain and loss in quantum systems

would be problematic. We show here how the mapping introduced in Section 3.3.4 to a dissipation-free driven bosonic system allows one to realize this chiral switching behaviour without any dissipation or noise. As a concrete quantum application of our mapping, we show how the chiral switching behaviour impacts the evolution of entanglement in our system.

As discussed in Section 3.3.4, we can realize the dynamics of $\mathcal{H}_\omega(t)$ in Eq. (3.51) without dissipation using a four-mode, parametrically-driven bosonic system with a Hamiltonian $\hat{H}_{\omega\mathrm{PA}}(t)$ given by Eq. (3.22). First, consider the non-Hermitian system described by $\mathcal{H}_\omega(t)$. The time-evolution matrix $\mathcal{U}_\omega(t)$ corresponding to this Hamiltonian relates final and initial mode amplitudes, and is determined by

$$i\partial_t \mathcal{U}_\omega(t) = \mathcal{H}_\omega(t)\,\mathcal{U}_\omega(t), \quad \mathcal{U}_\omega(t=0) = 1. \tag{3.52}$$

Our Hermitian, bosonic four mode system has been constructed so that the quasi-mode operators $\hat{z}_1, \hat{z}_2$ defined in Eq. (3.21) evolve exactly like amplitudes in the non-Hermitian system. This implies that

$$\begin{pmatrix} \hat{z}_1(t) \\ \hat{z}_2(t) \end{pmatrix} = \mathcal{U}_\omega(t) \cdot \begin{pmatrix} \hat{z}_1(0) \\ \hat{z}_2(0) \end{pmatrix}, \tag{3.53}$$

where we stress that these are operator equations. Thus, the chiral switching behaviour encoded in $\mathcal{U}_\omega(t)$ will directly manifest itself in the quantum bosonic system, without any need to inject noise to preserve commutation relations.

The chiral switching behaviour is best understood by analyzing the dynamics in terms of the instantaneous eigemodes $\vec{r}_\pm(t)$ of $\mathcal{H}_\omega(t)$. These are defined via

$$\mathcal{H}_\omega(t)\,\vec{r}_\pm(t) = \lambda_\pm(t)\,\vec{r}_\pm(t), \tag{3.54}$$

where explicit forms for the eigenmodes and eigenvalues $\lambda_\pm(t)$ are given Eq. (3.134) of

Appendix 3.7.8. Classically, we could describe the instantaneous state of our system in terms of the amplitudes $c_{\pm}(t)$ of the two eigenmodes. In our quantum parametric amplifier analogue, these amplitudes become operators:

$$\hat{c}_{\pm}(t) = \vec{r}_{\pm}^{T}(t) \cdot \vec{\hat{z}}(t), \tag{3.55}$$

Not surprisingly, the average values of these operators behave exactly as the corresponding amplitudes in the classical setup. Preparing a particular initial condition would involve displacing the four bosonic modes appropriately. In Fig. 3.4, we show the evolution of the average instantaneous mode amplitudes $|\langle \hat{c}_{\pm}(t) \rangle|$, for evolution along a circular path in the (g, ω) parameter space that encircles an EP. In both cases, the initial state is chosen so that only the + eigenmode is initially excited, i.e. $\langle\, \vec{\hat{z}}(t=0)\, \rangle = \vec{r}_{+}(t=0)$. As can be seen from the figure, for evolution corresponding to a counter-clockwise (CCW) encircling, the amplitudes of the pseudo-modes correspond to predominantly exciting the instantaneous + eigenmode. In contrast, for a clockwise encircling, one sees that there is a switching: at the final time T, the pseudo-mode amplitudes correspond to predominantly exciting the − instantaneous eigenmode. Note that because of the EP structure in our system, the instantaneous eigenmodes at the final time $t = T$ are flipped versions of those at $t = 0$, i.e. $\vec{r}_{\pm}(t=T) = \vec{r}_{\mp}(t=0)$ [40].

A more interesting situation is to consider the evolution of a general quantum state for either a CW or CCW parameter evolution. In Appendix 3.7.9, we derive the quantum unitary transformations describing both these cases, and discuss them using the Bloch-Messiah decomposition [77]. This allows us to view each transformation as the product of two beam-splitter operations, interspersed with a squeezing operation. Interestingly, we find that both the CW and CCW complete encirclings are described by the same squeezing operation; the chirality only appears in the initial and final beam-splitter operations.

To see a direct consequence of this, imagine a quantum state with non-zero photon num-

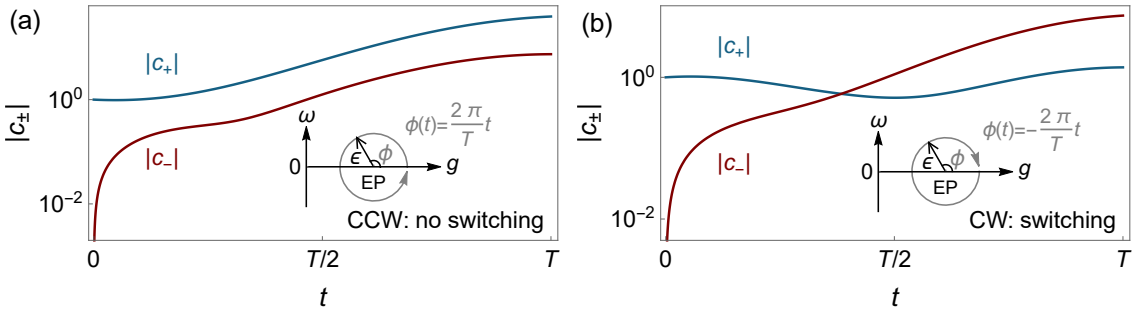

Fig. 3.4: Chiral nature of quasi-adiabatic dynamics in a four-mode Hermitian bosonic system (c.f. Eq. (3.22)) whose dynamics mimics the gain-loss dimer in Eq. (3.51). In each plot, $g(t)$ and $\omega(t)$ are varied along a circle in parameter space (see insets). (a) Evolution of instantaneous eigenmode amplitudes $|\langle \hat{c}_\pm(t)\rangle|$ (c.f. Eq. (3.55)), for a counter-clockwise (CCW) parameter variation. (b) Same, but now for a clockwise (CW) variation. In both cases, the initial state is a coherent state with $\langle \hat{c}_+(0)\rangle = 1$, $\langle \hat{c}_-(0)\rangle = 0$. For the CCW evolution, one sees an adiabatic evolution (the + mode remains dominant), whereas for CW evolution, there is a non-adiabatic switching, and the − mode is dominant at the end of the protocol. For both plots $\gamma T = 20$ and $\epsilon/\gamma = 0.1$.

ber, but where $\langle \hat{z}_1\rangle = \langle \hat{z}_2\rangle = 0$. Classically, we could imagine at $t = 0$ stochastically preparing the system in the + eigenmode with a random phase; the simplest choice would be to take $c_+(0)$ to be a Gaussian random variable (while $c_-(0)$ is set to zero). Using our equivalent quantum parametric amplifier setup $\hat{H}_{\omega\mathrm{PA}}(t)$, we could consider an analogous initial condition. In particular, we start the quantum four-mode system in a zero-mean Gaussian pure state whose covariance matrix at $t = 0$ predominantly populates the + eigenmode. By this, we mean an initial state where $\langle \hat{c}_+^\dagger \hat{c}_+\rangle \gg \langle \hat{c}_-^\dagger \hat{c}_-\rangle$. This state will necessarily have entanglement correlations between the 1 subsystem (formed by modes a_1, b_1) and the 2 subsystem (formed by modes a_2, b_2). We can now ask how this entanglement evolves in time as we cyclically vary g and ω as before. We stress that we are always comparing the final values of the entanglement (i.e. at $t = T$) for the CW versus CCW encirclings. This parallels what is done in the classical case, when one compares the mode occupancies at the end of the two protocols.

In Fig. 3.5, we show the evolution of the 1-2 subsystem entanglement (as quantified by the logarithmic negativity [78, 79]), for various circular parameter variations. In each case,

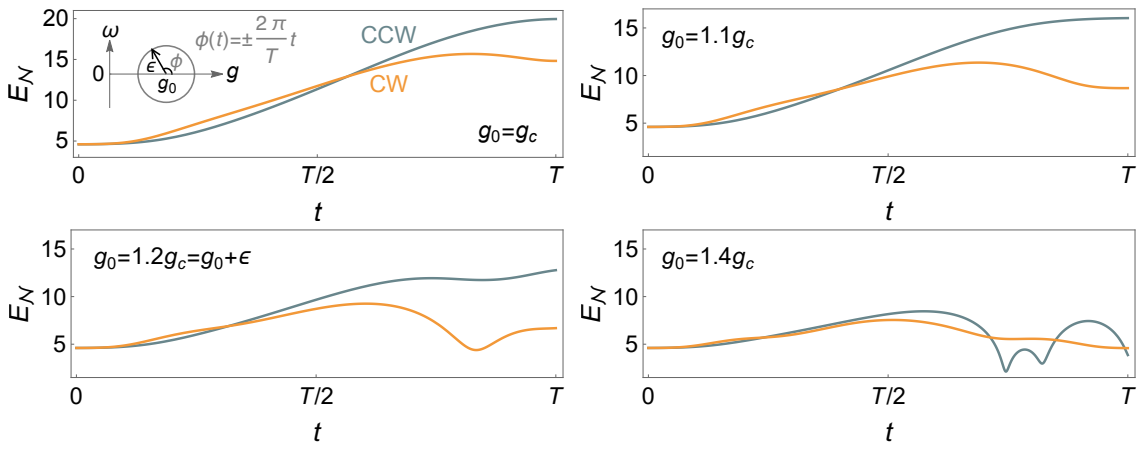

Fig. 3.5: Entanglement evolution during EP encircling. We consider bipartite entanglement in a Hermitian four-mode bosonic system whose dynamics corresponds to the detuned gain-loss dimer described by $\mathcal{H}_\omega(t)$ (c.f. Eq. (3.51)). The parameters (g, ω) follow a complete circle in parameter space. Entanglement (as quantified by the logarithmic negativity E_N) between the a_1, b_1 modes and a_2, b_2 modes is plotted as a function of time; the two curves in each panel are for a clockwise (CW) versus counterclockwise (CCW) parameter variation. The center of the circular trajectory $(g = g_0, \omega)$ is different for each panel (as indicated). The top left panel corresponds to a trajectory centered on the exceptional point at $g_0 = g_c \equiv \gamma/2$, whereas in the other panels, the trajectory is displaced to the right. One sees that entanglement generation at $t = T$ after a full cycle is manifestly chiral when the trajectory encircles the EP, while this is lost when the trajectory is far from the EP. The initial state is chosen to asymmetrically populate the + eigenmode (see main text), and $\gamma T = 20$, $\epsilon/\gamma = 0.1$.

we start with zero-mean Gaussian states of our four bosonic modes with the same amount of initial entanglement. This initial state is chosen to have an average total photon number of approximately 8, and an asymmetry quantified by

$$\frac{\langle \hat{c}_+^\dagger \hat{c}_+ \rangle}{\langle \hat{c}_-^\dagger \hat{c}_- \rangle} \simeq \frac{10^2}{|\vec{r}_+(t=0)|^2 \cdot |\vec{r}_-(t=0)|^2} \gg 1. \tag{3.56}$$

Further details and motivation for this choice are given in Appendix 3.7.9; our chosen state corresponds to $e^{2\lambda_0} = 10$ in Eq. (3.155). The two curves in each panel correspond to CW and CCW traversal of the same circular path in the (g, ω) parameter space. The first panel corresponds to the same path as in Fig. 3.4; in the remaining panels, we displace the path so that it eventually no longer encloses the EP. For paths enclosing the EP, we see that the

entanglement by the end of time evolution exhibits a marked chiral behaviour: the amount of entanglement at $t = T$ depends crucially on the direction that the path is traversed. This asymmetry gradually becomes negligible as we displace the circular path away from the EP. The results here show that the chirality associated with EP encircling can indeed have impliciations for quantum dynamics (e.g. in determining the generation of entanglement).

3.5.3 Connecting topology in non-Hermitian systems to Hermitian driven bosonic systems

As a final application, we discuss how our mappings can be applied to non-Hermitian lattice models with topologically non-trivial bands. There has been considerable recent interest in studying such models, see e.g. [56, 57, 70–72, 80–83]. Our mappings provide a route for realizing these topological bands in fully Hermitian bosonic systems, without any need to couple to external dissipation. More specifically, in Ref. [84], a non-Hermitian Chern number was introduced to characterize bands in 2D non-Hermitian systems. Using our mapping, it is straightforward to show that these Chern numbers are equivalent to topological invariants that were introduced earlier to characterize bands in Hermitian bosonic systems with pairing terms [85, 86]; this is demonstrated in Appendix 3.7.10. Our discussion here complements recent studies showing that the symmetry-based classification of non-Hermitian Hamiltonians can also be applied to anomalous bosonic systems [56, 82].

Despite the immense interest in non-Hermitian topology, most work has focused on models that are topological even if the non-Hermitian terms are set to zero (i.e. in the absence of gain and loss). As discussed below, our approach allows us to construct a model where this is no longer true: non-trivial band topology *only* emerges in the presence of non-zero gain and loss. We accomplish this by constructing the non-Hermitian equivalent of a recently-studied bosonic model where parametric driving induces topology [86].

We consider a 2D Kagome lattice, where on each lattice site we have a two-cavity $\mathcal{PT}$-

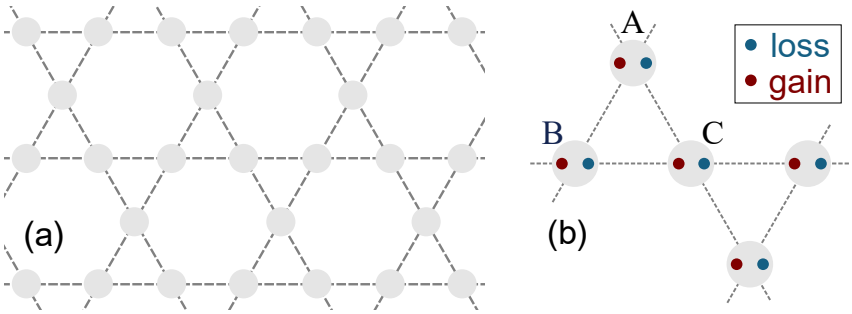

Fig. 3.6: Schematic of the $\mathcal{PT}$ Kagome model (c.f. Eq. (3.57)), where the system is topologically non-trivial only with the introduction of non-zero gain and loss. (a) Kagome lattice, where each site (grey circle) is a gain-loss dimer. (b) Unit cell.

symmetric gain-loss dimer (see Fig. 3.6). The system Hamiltonian will consist of a purely Hermitian hopping terms coupling nearest neighbour lattices, and purely local term which includes non-Hermitian effects:

$$\hat{\mathcal{H}}_{\text{Kagome}} = \hat{\mathcal{H}}_{\text{hopping}} + \hat{\mathcal{H}}_{\text{local}}. \tag{3.57}$$

We will use the composite index $\mathrm{j} = (\mathbf{j}, s) = (j_1, j_2, s)$ to label both the unit cell (j_1, j_2) and basis element $s = A, B, C$ of each lattice site. Further, we will use a pseudospin $\uparrow, \downarrow$ to index each element of the cavity dimer located at a given lattice site.

Letting $\hat{\psi}_{\mathrm{j}} = \begin{pmatrix} \hat{a}_{\mathrm{j},\uparrow} & \hat{a}_{\mathrm{j},\downarrow} \end{pmatrix}^T$ the onsite terms are

$$\hat{\mathcal{H}}_{\text{local}} = \sum_{\mathrm{j}} \hat{\psi}_{\mathrm{j}}^{\dagger} \left(i\nu\sigma_z + \omega_0\sigma_x \right) \hat{\psi}_{\mathrm{j}}. \tag{3.58}$$

These local terms describe a $\mathcal{PT}$ dimer at each lattice site, with tunneling amplitude ω_0 and gain/loss rate ν.

The tunneling terms between cavities on nearest neighbour lattice sites is described by

the Hermitian Hamiltonian

$$\hat{\mathcal{H}}_{\text{hopping}} = \sum_{\langle \mathrm{j},\mathrm{j}' \rangle} \psi_{\mathrm{j}}^{\dagger} \mathcal{J}\left[ss'\right] \psi_{\mathrm{j}'}, \tag{3.59}$$

where the hopping matrix elements depend on both sublattice index and pseudo-spin:

$$\mathcal{J}\left[ss'\right] = \frac{J}{2}\left(e^{i\varphi_{ss'}}\sqrt{3}\sigma_0 + \sigma_x\right), \tag{3.60}$$

$$\varphi_{ss'} = \begin{cases} +\frac{\pi}{2}, & ss' = AB, BC, CA, \\ -\frac{\pi}{2}, & ss' = BA, CB, AC, \end{cases} \tag{3.61}$$

J is the overall hopping amplitude. We see that there are hopping terms that both preserve and flip the pseudo spin (i.e. a gain cavity on a given site can tunnel to either a gain or loss cavity on a neighbouring site). Further, the spin-conserving tunneling is complex, and thus encodes a synthetic gauge field. The tunneling here can be viewed as a generalized kind of synthetic spin-orbit coupling.

Consider first the properties of our system in the case where there are no gain/loss terms (i.e. $\nu = 0$), and the Hamiltonian is Hermitian. In this case, the system has no topologically non-trivial bands, as it is possible to completely gauge away the hopping phases. To see this, note that in this case σ_x on each lattice site commutes with the Hamiltonian. It thus useful to use a local basis of σ_x eigenstates:

$$\hat{a}_{\mathrm{j},\pm} = \frac{1}{\sqrt{2}}\left(\hat{a}_{\mathrm{j},\uparrow} \pm \hat{a}_{\mathrm{j},\downarrow}\right), \tag{3.62}$$

In this basis, the Hamiltonian decouples into two independent tight-binding models

$$\mathcal{H}_{\text{Kagome},\pm} = \pm\left(\sum_{\mathrm{j}} \omega_0 \hat{a}_{\mathrm{j},\pm}^{\dagger}\hat{a}_{\mathrm{j},\pm} + \sum_{\langle \mathrm{j},\mathrm{j}' \rangle} J e^{\pm i\frac{2\varphi_{ss'}}{3}} \hat{a}_{\mathrm{j},\pm}^{\dagger}\hat{a}_{\mathrm{j}',\pm}\right), \tag{3.63}$$

with uniform onsite energies $\pm\omega_0$ and nearest-neighbor couplings $\pm J \exp(\mp i 2\varphi_{ss'}/3)$. We thus have two decoupled Kagome lattices, with the $+$ $(-)$ lattice have a synthetic Aharonov-Bohm flux π $(-\pi)$ in each triangular plaquette. These fluxes do not break time-reversal symmetry, and can be eliminated by a local gauge transformation:

$$\hat{a}_{\mathbf{j},B,\pm} \to \hat{a}'_{\mathbf{j},B,\pm} = e^{\mp i \frac{2\pi}{3}} \hat{a}_{\mathbf{j},B,\pm}, \tag{3.64a}$$

$$\hat{a}_{\mathbf{j},C,\pm} \to \hat{a}'_{\mathbf{j},C,\pm} = e^{\mp i \frac{4\pi}{3}} \hat{a}_{\mathbf{j},C,\pm}. \tag{3.64b}$$

This results in a decoupled pair of time-reversal invariant, topologically trivial Kagome models

$$\hat{H}'_{\text{Kagome},\pm} = \pm \left(\sum_{\mathrm{j}} \omega_0 \hat{a}^\dagger_{\mathrm{j},\pm} \hat{a}_{\mathrm{j},\pm} - \sum_{\langle \mathrm{j}\mathrm{j}' \rangle} J \hat{a}^\dagger_{\mathrm{j},\pm} \hat{a}_{\mathrm{j}',\pm} \right). \tag{3.65}$$

If we now turn on the gain/loss parts of the Hamiltonian (i.e. make ν non-zero in Eq. (3.58)), it is no longer possible to gauge away the hopping phases. At an intuitive level, the non-Hermitian terms are off-diagonal in the $+/-$ basis used to write Eq. (3.65), and hence can enable hopping processes that pick up non-trivial fluxes.

The topological properties of the resulting model can be completely understood by mapping the system to a Hermitian, parametrically-driven bosonic model having a single bosonic mode on each lattice site (see Appendix 3.7.11). As usual, the non-Hermitian gain/loss terms are mapped to parametric driving terms, and the dimer structure is mapped to the particle-hole structure of the bosonic theory. The resulting bosonic theory is equivalent to the parametrically driven Kagome lattice mode studied by Peano et al in Ref. [86]. The model exhibits topological bands and protected edge states whenever ν is non-zero. Since the mapping is fully local in real space (two bosonic modes, with balanced gain and loss, per lattice site), it thus follows that our non-Hermitian $\mathcal{PT}$ model exhibits topological bands (with non-zero Chern number) and edge states if and only if there is non-zero gain loss. We thus have, as desired, a model where topology is induced by gain/loss.

3.6 Conclusions

In this chapter we have given a thorough discussion of how one can realize non-Hermitian dynamics without the need to couple to external dissipation. We make use of a simple but surprising fact: a Hermitian, quadratic bosonic Hamiltonian that breaks particle number conservation necessarily gives rise to a non-Hermitian dynamical matrix. We have discussed three generic strategies for using this correspondence to realize a given non-Hermitian (linear) Hamiltonian using a quadratic bosonic system. Given an initial N mode non-Hermitian problem, one can always accomplish this mapping using a $2N$ mode bosonic system and the quantum-mechanics free subsystem (QMFS) approach discussed in Sections 3.3.4 and 3.4.3. In other more constrained cases, it is possible to mimic the desired dynamics using N modes (Section 3.4) or even $N/2$ modes (Section 3.3.2). We summarize advantages and constraints of these three strategies in Table 3.1 for reference.

Our work has considered just a few possible applications and implications of this mapping. In future work, it will be interesting to use this mapping to explore a wider class of non-Hermitian dynamical phenomena (such as the recently observed non-Hermitian analogue of Fermi arcs [87]), and to develop new kinds of quantum control protocols in parametrically driven systems. It will also be extremely interesting to extend our approach to describe systems with true nonlinearities.

3.7 Appendices

3.7.1 A note on pseudo-Hermiticity

In general, the $2N \times 2N$ dynamical matrix $\mathcal{H}_{\text{eff},N}$ of a N-mode bosonic parametrically-driven system is related to a Hermitian Bogoliubov de Gennes Hamiltonian H_{BdG} by

$$\mathcal{H}_{\text{eff},N} = \sigma_{N,z} H_{\text{BdG}}, \tag{3.66}$$

where $\sigma_{N,z} = \mathrm{diag}\,(\mathbb{I}_N, -\mathbb{I}_N)$ is the diagonal matrix incorporating bosonic commutation relations, so that $\mathcal{H}_{\mathrm{eff},N}$ is always $\sigma_{N,z}$-pseudo-Hermitian as [56, 63]

$$\mathcal{H}_{\mathrm{eff},N}^{\dagger} = \sigma_{N,z}\mathcal{H}_{\mathrm{eff},N}\sigma_{N,z}. \tag{3.67}$$

Previous works have shown that $\mathcal{PT}$-symmetric Hamiltonians are always η-pseudo-Hermitian, where η is an invertible Hermitian operator [63, 88, 89]. However, two pseudo-Hermitian matrices need not be unitarily equivalent, even though they may be isospectral. Hence, the fact that $\mathcal{PT}$-symmetric Hamiltonians are pseudo-Hermitian does not guarantee that they are unitarily equivalent to the dynamical matrix of some Hermitian, bosonic problem.

3.7.2 Canonical form for a general class of $\mathcal{PT}$-symmetric non-Hermitian Hamiltonian

Consider the most general $2N$-mode $\mathcal{PT}$-symmetric non-Hermitian Hamiltonian. Using the same conventions as Section 3.4.1, the Hamiltonian has the form

$$\mathcal{H}_{\mathcal{PT}} = \begin{pmatrix} \mathcal{E} & \mathcal{F} \\ \mathcal{F}^* & \mathcal{E}^* \end{pmatrix}, \tag{3.68}$$

where $\mathcal{E}$ and $\mathcal{F}$ are arbitrary $N \times N$ matrices. As always, we define time reversal operation as complex conjugation, and the parity operation is an exchange of modes described by

$$\sigma_{N,x} = \begin{pmatrix} 0 & \mathbb{I}_N \\ \mathbb{I}_N & 0 \end{pmatrix}. \tag{3.69}$$

We will show that as long as the anti-Hermitian part of $\mathcal{H}_{\mathcal{PT}}$ is full rank, it is always possible to unitarily transform $\mathcal{H}_{\mathcal{PT}}$ to a form $\mathcal{H}_2$ where the non-Hermitian part of $\mathcal{H}$ is

diagonal, namely:

$$\mathcal{H}_2 = \begin{pmatrix} \tilde{\Sigma} + i\Gamma_N & \tilde{J} \\ \tilde{J}^* & \tilde{\Sigma}^* - i\Gamma_N \end{pmatrix}. \tag{3.70}$$

Here $\tilde{\Sigma}$ is a Hermitian $N \times N$ matrix, Γ_N is a real, diagonal, non-negative $N \times N$ matrix, and the $N \times N$ matrix $\tilde{J}$ is symmetric. Note that $\mathcal{H}_2$ still explicitly retains $\mathcal{PT}$ symmetry as defined before, as $\mathcal{H}_2^* = \sigma_{N,x}\mathcal{H}_2\sigma_{N,x}$.

We can always write $\mathcal{H}_{\mathcal{PT}}$ in terms of its Hermitian and anti-Hermitian parts as $\mathcal{H}_{\mathcal{PT}} = H_{\mathcal{PT}} + i\Gamma_{\mathcal{PT}}$. The $\mathcal{PT}$ symmetry of $\mathcal{H}_{\mathcal{PT}}$ then implies

$$H^*_{\mathcal{PT}} = \sigma_{N,x} H_{\mathcal{PT}} \sigma_{N,x}, \tag{3.71a}$$

$$\Gamma^*_{\mathcal{PT}} = -\sigma_{N,x} \Gamma_{\mathcal{PT}} \sigma_{N,x}. \tag{3.71b}$$

Eq. (3.71b) implies that the eigenvalues of $\Gamma_{\mathcal{PT}}$ are real and come in pairs of opposite signs. It can thus be diagonalized as

$$\mathcal{U}_\Gamma \Gamma_{\mathcal{PT}} \mathcal{U}_\Gamma^\dagger = \Gamma_D, \tag{3.72}$$

where $\Gamma_D = \mathrm{diag}\,(\Gamma_N, -\Gamma_N)$, and Γ_N is a diagonal $N \times N$ matrix with non-negative entries.

Using $\mathcal{U}_\Gamma$ to transform $\mathcal{H}_{\mathcal{PT}}$, i.e. $\mathcal{H}_1 = \mathcal{U}_\Gamma \mathcal{H}_{\mathcal{PT}} \mathcal{U}_\Gamma^\dagger$, we obtain

$$\mathcal{H}_1 = H_1 + i\Gamma_D = \begin{pmatrix} \Sigma_1 + i\Gamma_N & J \\ J^\dagger & \Sigma_2 - i\Gamma_N \end{pmatrix}, \tag{3.73}$$

$\mathcal{PT}$ symmetry implies that the Hermitian matrix H_1 and the non-negative matrix Γ_D must

satisfy

$$H_1 = \tilde{\mathcal{U}}_\Gamma H_1^* \tilde{\mathcal{U}}_\Gamma^\dagger, \tag{3.74a}$$

$$\Gamma_D = -\tilde{\mathcal{U}}_\Gamma \Gamma_D \tilde{\mathcal{U}}_\Gamma^\dagger, \tag{3.74b}$$

where we have introduced the symmetric unitary matrix $\tilde{\mathcal{U}}_\Gamma = \mathcal{U}_\Gamma \sigma_{N,x} \mathcal{U}_\Gamma^T$.

Eq. (3.74b) can be written explicitly as

$$\begin{pmatrix} +\Gamma_N & 0 \\ 0 & -\Gamma_N \end{pmatrix} \tilde{\mathcal{U}}_\Gamma + \tilde{\mathcal{U}}_\Gamma \begin{pmatrix} +\Gamma_N & 0 \\ 0 & -\Gamma_N \end{pmatrix} = 0, \tag{3.75}$$

In what follows, we assume that $\Gamma_{\mathcal{PT}}$ is full rank; physically, this implies that all modes in the system are coupled to the dissipation. As a consequence, Γ_N has no zeros on the diagonal. The above equation then provides a constraint on the form of $\tilde{\mathcal{U}}_\Gamma$: its diagonal blocks must be identically zero. We can thus write it as

$$\tilde{\mathcal{U}}_\Gamma = \begin{pmatrix} 0 & \tilde{u}_{12} \\ \tilde{u}_{12}^T & 0 \end{pmatrix}, \tag{3.76}$$

with $[\tilde{u}_{12}, \Gamma_N] = 0$.

The remaining $\mathcal{PT}$ condition on H_1 in Eq. (3.74a) now reads

$$\begin{pmatrix} \Sigma_1 & J \\ J^\dagger & \Sigma_2 \end{pmatrix} \begin{pmatrix} 0 & \tilde{u}_{12} \\ \tilde{u}_{12}^T & 0 \end{pmatrix} = \begin{pmatrix} 0 & \tilde{u}_{12} \\ \tilde{u}_{12}^T & 0 \end{pmatrix} \begin{pmatrix} \Sigma_1^* & J^* \\ J^T & \Sigma_2^* \end{pmatrix}, \tag{3.77}$$

or equivalently

$$J^\dagger \tilde{u}_{12} = \tilde{u}_{12}^T J^* \Leftrightarrow J\tilde{u}_{12}^T = \tilde{u}_{12} J^T, \tag{3.78a}$$

$$\Sigma_1 \tilde{u}_{12} = \tilde{u}_{12}\Sigma_2^* \Leftrightarrow \Sigma_2 \tilde{u}_{12}^T = \tilde{u}_{12}^T \Sigma_1^*. \tag{3.78b}$$

It follows that there exists a unitary matrix $\tilde{u}_{12}$ that commutes with Γ_N and satisfy the equalities

$$\Sigma_1^* = \tilde{u}_{12}^* \Sigma_2 \tilde{u}_{12}^T, \tag{3.79a}$$

$$J\tilde{u}_{12}^T = \tilde{u}_{12} J^T = \left(J\tilde{u}_{12}^T\right)^T = \left(\tilde{u}_{12}^* J^\dagger\right)^*. \tag{3.79b}$$

We can now finally use this unitary matrix to transform our non-Hermitian $\mathcal{PT}$ Hamiltonian into a simpler, final form $\mathcal{H}_2$:

$$\begin{aligned}\mathcal{H}_2 &\equiv \begin{pmatrix} \mathbb{I}_N & 0 \\ 0 & \tilde{u}_{12}^* \end{pmatrix} \begin{pmatrix} \Sigma_1 + i\Gamma_N & J \\ J^\dagger & \Sigma_2 - i\Gamma_N \end{pmatrix} \begin{pmatrix} \mathbb{I}_N & 0 \\ 0 & \tilde{u}_{12}^T \end{pmatrix} \\ &= \begin{pmatrix} \Sigma_1 + i\Gamma_N & J\tilde{u}_{12}^T \\ \left(J\tilde{u}_{12}^T\right)^* & \Sigma_1^* - i\Gamma_N \end{pmatrix},\end{aligned} \tag{3.80}$$

Defining $\tilde{\Sigma} = \Sigma_1$ and $\tilde{J} = J\tilde{u}_{12}^\dagger$ and $\tilde{J} = J\tilde{u}_{12}^T$, this is exactly the form given in Eq. (3.70).

3.7.3 Constraints on representing $\mathcal{PT}$ non-Hermitian Hamiltonians with Hermitian bosonic Hamiltonians

In this subsection we will derive necessary and sufficient conditions for determining whether a given $2N$-mode $\mathcal{PT}$-symmetric non-Hermitian Hamiltonian is unitarily equivalent to the dynamical matrix of a Hermitian, $2N$ mode parametric amplifier system. The most general $2N$ mode $\mathcal{PT}$-symmetric non-Hermitian Hamiltonian $\mathcal{H}_{\mathcal{PT}}$ was given in Eq. (3.68). As

shown above, as long as its non-Hermitian part is full rank, it can be transformed to the canonical form $\mathcal{H}_2$ in Eq. (3.70), where the anti-Hermitian terms are diagonal. We will work with this form in what follows.

The question now is whether it is possible to find a unitary matrix $\mathcal{U}$ that transforms the generic $\mathcal{PT}$ Hamiltonian $\mathcal{H}_2$ in Eq. (3.70) to a physical bosonic dynamical matrix $\mathcal{M}_N$, i.e.

$$\mathcal{U}\mathcal{H}_2\mathcal{U}^\dagger = \mathcal{M}_N. \tag{3.81}$$

We will consider the least constrained mapping, where $\mathcal{M}_N$ is a $2N \times 2N$ matrix describing *non-degenerate* parametric driving. This is the same situation as in Section 3.4: the bosonic theory has N "a" modes and N "b" modes, and the parametric driving conserves the total number of a minus b bosons. As discussed in the main text (c.f. Eq. (3.159)), in this case the dynamical matrix will take the form

$$\mathcal{M}_N = \begin{pmatrix} \mu_a & \nu \\ -\nu^\dagger & -\mu_b^T \end{pmatrix}, \tag{3.82}$$

where $\mu_{a,b}$ are arbitrary Hermitian $N \times N$ matrices, and ν can be any $N \times N$ matrix.

For a given $\mathcal{PT}$ Hamiltonian $\mathcal{H}_2$, it is not always possible to find a $\mathcal{U}$ and $\mathcal{M}_N$ satisfying Eq. (3.81). This is because the bosonic dynamical matrix $\mathcal{M}_N$ is pseudo-Hermitian in a constrained fashion. Recall (see Appendix 3.7.1) that any physical $\mathcal{M}_N$ must satisfy:

$$\mathcal{M}_N^\dagger = \sigma_{N,z}\, \mathcal{M}_N\, \sigma_{N,z}, \tag{3.83}$$

where as always, $\sigma_{N,z}$ is a z Pauli matrix in particle-hole space.

It thus follows that *any* $\mathcal{PT}$ Hamiltonian that is unitarily equivalent to a bosonic dy-

namical matrix $\mathcal{M}_N$ must satisfy

$$\mathcal{H}_2^\dagger = \mathcal{W}\mathcal{H}_2\mathcal{W}^\dagger, \tag{3.84}$$

for some $2N \times 2N$ matrix $\mathcal{W}$ satisfying

$$\mathcal{W} = \mathcal{W}^\dagger = \mathcal{W}^{-1}, \tag{3.85a}$$

$$\operatorname{Tr}\mathcal{W} = 0, \tag{3.85b}$$

(i.e. a Hermitian unitary matrix with N eigenvalues $+1$ and N eigenvalues -1). If a unitary equivalence existed as per Eq. (3.81), we could explicitly construct $\mathcal{W}$ as $\mathcal{W} = \mathcal{U}\sigma_{N,z}\mathcal{U}^\dagger$. Eqs. (3.84) and (3.85) thus represent a necessary condition for the existence of a $\mathcal{M}_N$ that is unitarily equivalent to a given $\mathcal{H}_2$. Note this is a tighter constraint than simply requiring $\mathcal{H}_2$ to be pseudo-Hermitian (something that is always true).

To show that this is also a *sufficient* condition, suppose one can find a $\mathcal{W}$ satisfying Eqs. (3.84) and (3.85). $\mathcal{W}$ could be then diagonalized as $\mathcal{W} = \mathcal{U}_\mathcal{W}\sigma_{N,z}\mathcal{U}_\mathcal{W}^\dagger$ for some unitary $\mathcal{U}_\mathcal{W}$. It then easily follows that the matrix $\tilde{\mathcal{M}} \equiv \mathcal{U}_\mathcal{W}^\dagger\mathcal{H}_2\mathcal{U}_\mathcal{W}$ satisfies the pseudo-Hermiticity condition in Eq. (3.83), and thus represents a valid bosonic dynamical matrix.

We can derive more explicit conditions in the case where the anti-Hermitian part of $\mathcal{H}_2$ is full-rank (i.e. Γ_N is positive). In this case, Eq. (3.84) can only be satisfied if $\mathcal{W}$ has the form

$$\mathcal{W} = \begin{pmatrix} 0 & w_{12} \\ w_{12}^\dagger & 0 \end{pmatrix}, \tag{3.86}$$

where the unitary matrix w_{12} commutes with Γ_N. This form of $\mathcal{W}$ is explicitly Hermitian, unitary and traceless, so it fulfills all the conditions in Eq. (3.85).

From Eq. (3.85), we can now derive:

$$\begin{pmatrix} 0 & w_{12} \\ w_{12}^\dagger & 0 \end{pmatrix} \begin{pmatrix} \tilde{\Sigma} & \tilde{J} \\ \tilde{J}^* & \tilde{\Sigma}^* \end{pmatrix} = \begin{pmatrix} \tilde{\Sigma} & \tilde{J} \\ \tilde{J}^* & \tilde{\Sigma}^* \end{pmatrix} \begin{pmatrix} 0 & w_{12} \\ w_{12}^\dagger & 0 \end{pmatrix}. \tag{3.87}$$

Hence, a necesary condition for $\mathcal{H}_2$ to be unitarily equivalent to a bosonic dynamical matrix is the existence of an $N \times N$ unitary matrix w_{12} that satisfies the equations

$$w_{12}\tilde{J}^* = \tilde{J}w_{12}^\dagger, \tag{3.88a}$$

$$w_{12}\tilde{\Sigma}^* = \tilde{\Sigma}w_{12}. \tag{3.88b}$$

3.7.4 Constraints on representing Hermitian bosonic Hamiltonians with $\mathcal{PT}$ non-Hermitian Hamiltonians

We now ask the converse of the question discussed in the previous subsection. Given a generic $2N$-mode non-degenerate parametric amplifier (NDPA) with Hermitian Hamiltonian $\hat{H}_{\text{NDPA,multi.}}$, whose non-Hermitian dynamical matrix $\mathcal{M}_N$ takes the form (see Eq. (3.82))

$$\mathcal{M}_N = \begin{pmatrix} \mu_a & \nu \\ -\nu^\dagger & -\mu_b^T \end{pmatrix}, \tag{3.89}$$

we would like to know if there exists unitary matrix $\mathcal{U}_{\mathcal{M}}^\dagger$ that transforms $\mathcal{M}_N$ to an effective non-Hermitian Hamiltonian matrix $\mathcal{H}_{\mathcal{PT}}$ with explicit $\mathcal{PT}$ symmetry

$$\mathcal{U}_{\mathcal{M}}\mathcal{M}_N\mathcal{U}_{\mathcal{M}}^\dagger = \sigma_{N,x}\Big(\mathcal{U}_{\mathcal{M}}\mathcal{M}_N\mathcal{U}_{\mathcal{M}}^\dagger\Big)^*\sigma_{N,x}, \tag{3.90}$$

or equivalently

$$\mathcal{M}_N = \mathcal{U}_{\mathcal{M}}^{\dagger}\sigma_{N,x}\mathcal{U}_{\mathcal{M}}^{*}\mathcal{M}_N^{*}\mathcal{U}_{\mathcal{M}}^{T}\sigma_{N,x}\mathcal{U}_{\mathcal{M}}, \tag{3.91}$$

$$\Rightarrow \mathcal{M}_N = \mathcal{W}_{\mathcal{M}}\mathcal{M}_N^{*}\mathcal{W}_{\mathcal{M}}^{\dagger}, \tag{3.92}$$

where $\mathcal{W}_{\mathcal{M}} = \mathcal{U}_{\mathcal{M}}^{\dagger}\sigma_{N,x}\mathcal{U}_{\mathcal{M}}^{*}$. Thus to determine the existence of a unitarily equivalent $\mathcal{H}_{\mathcal{PT}}$ for dynamical matrix $\mathcal{M}_N$, we can equivalently ask if there exists a symmetric, unitary matrix $\mathcal{W}_{\mathcal{M}}$ that can be written in the form

$$\mathcal{W}_{\mathcal{M}} = \mathcal{U}_{\mathcal{M}}^{\dagger}\sigma_{N,x}\mathcal{U}_{\mathcal{M}}^{*}, \tag{3.93}$$

such that Eq. (3.92) is satisfied. Physically, being unitarily equivalent to any $\mathcal{PT}$-symmetric Hamiltonian can thus be viewed as a generalized $\mathcal{W}_{\mathcal{M}}$-anti-unitary symmetry for the dynamical matrix considered, with specific constraints imposed on the unitary matrix $\mathcal{W}_{\mathcal{M}}$.

In analogy to the derivation of canonical form for $\mathcal{PT}$-symmetric Hamiltonians $\mathcal{H}_{\mathcal{PT}}$, we now transform $\mathcal{M}_N$ to a more tractable form. Noting that the $N \times N$ off-diagonal block matrix ν can be written as singular value decomposition $\nu = \mathcal{V}_a^{\dagger} D_\nu \mathcal{V}_b$, or equivalently

$$\mathcal{V}_a \nu \mathcal{V}_b^{\dagger} = D_\nu = \mathcal{V}_b \nu^{\dagger} \mathcal{V}_a^{\dagger}, \tag{3.94}$$

we can transform the off-diagonal blocks into non-negative diagonal matrix D_ν

$$\begin{aligned}\mathcal{H}_1 &= \begin{pmatrix} \mathcal{V}_a & 0 \\ 0 & \mathcal{V}_b \end{pmatrix} \begin{pmatrix} \mu_a & \nu \\ -\nu^{\dagger} & -\mu_b^{T} \end{pmatrix} \begin{pmatrix} \mathcal{V}_a^{\dagger} & 0 \\ 0 & \mathcal{V}_b^{\dagger} \end{pmatrix} \\ &= \begin{pmatrix} \mathcal{V}_a \mu_a \mathcal{V}_a^{\dagger} & D_\nu \\ -D_\nu & -\mathcal{V}_b \mu_b^{T} \mathcal{V}_b^{\dagger} \end{pmatrix},\end{aligned} \tag{3.95}$$

which can be rewritten in terms of $N \times N$ Hermitian matrices Σ, Δ as

$$\mathcal{H}_1 = \begin{pmatrix} \Sigma + \Delta & D_\nu \\ -D_\nu & \Delta - \Sigma \end{pmatrix}. \tag{3.96}$$

The next step is to rotate the anti-Hermitian part to diagonal blocks via a unitary transformation, where we obtain

$$\mathcal{H}_2 = \begin{pmatrix} \Delta + iD_\nu & \Sigma \\ \Sigma & \Delta - iD_\nu \end{pmatrix} = H_1 + i\Gamma_\nu, \tag{3.97}$$

so that the equality in Eq. (3.92) can be equivalently written as the conditions on the $2N \times 2N$ Hermitian matrix H_1 and the $2N \times 2N$ non-negative diagonal matrix Γ_ν

$$H_1 = \tilde{\mathcal{W}}_{\mathcal{M}} H_1^* \tilde{\mathcal{W}}_{\mathcal{M}}^\dagger, \tag{3.98a}$$

$$\Gamma_\nu = -\tilde{\mathcal{W}}_{\mathcal{M}} \Gamma_\nu^* \tilde{\mathcal{W}}_{\mathcal{M}}^\dagger, \tag{3.98b}$$

where $\tilde{\mathcal{W}}_{\mathcal{M}} = \tilde{\mathcal{U}}_{\mathcal{M}}^\dagger \sigma_{N,x} \tilde{\mathcal{U}}_{\mathcal{M}}^*$ should again be symmetric and unitary for the unitary equivalence between $\mathcal{M}_N$ and any $\mathcal{PT}$-symmetric Hamiltonian matrix $\mathcal{H}_{\mathcal{PT}}$ to exist. To proceed and obtain necessary and sufficient conditions for the existence of such unitary equivalence, we now assume that D_ν is positive definite, so that Eq. (3.98b) requires that $\tilde{\mathcal{W}}_{\mathcal{M}}$ must take the form

$$\tilde{\mathcal{W}}_{\mathcal{M}} = \begin{pmatrix} 0 & w_{12} \\ w_{12}^T & 0 \end{pmatrix}, \tag{3.99}$$

where the off-diagonal blocks must be unitary and commute with the diagonal matrix $[w_{12}, D_\nu] = 0$. We note that the criterion $\tilde{\mathcal{W}}_{\mathcal{M}} = \tilde{\mathcal{U}}_{\mathcal{M}}^\dagger \sigma_{N,x} \tilde{\mathcal{U}}_{\mathcal{M}}^*$ is automatically satisfied

as

$$\tilde{\mathcal{W}}_{\mathcal{M}} = \begin{pmatrix} \mathbb{I}_N & 0 \\ 0 & w_{12}^T \end{pmatrix} \begin{pmatrix} 0 & \mathbb{I}_N \\ \mathbb{I}_N & 0 \end{pmatrix} \begin{pmatrix} \mathbb{I}_N & 0 \\ 0 & w_{12} \end{pmatrix}. \tag{3.100}$$

Substituting the form of $\tilde{\mathcal{W}}_{\mathcal{M}}$ into Eq. (3.98a), we obtain

$$\begin{pmatrix} \Delta & \Sigma \\ \Sigma & \Delta \end{pmatrix} \begin{pmatrix} 0 & w_{12} \\ w_{12}^T & 0 \end{pmatrix} = \begin{pmatrix} 0 & w_{12} \\ w_{12}^T & 0 \end{pmatrix} \begin{pmatrix} \Delta^* & \Sigma^* \\ \Sigma^* & \Delta^* \end{pmatrix}. \tag{3.101}$$

We thus obtain a set of sufficient conditions for a given dynamical matrix $\mathcal{M}_N$ to be unitarily equivalent to a $\mathcal{PT}$-symmetric Hamiltonian $\mathcal{H}_{\mathcal{PT}}$, which is the existence of a unitary matrix w_{12} such that

$$w_{12}\Sigma = \Sigma^* w_{12}^T, \tag{3.102a}$$

$$w_{12}\Delta = \Delta^* w_{12}, \tag{3.102b}$$

which also commutes with the diagonal matrix $[w_{12}, D_\nu] = 0$. For a positive definite diagonal matrix D_ν corresponding to the parametric drivings, the conditions above will also be necessary conditions.

3.7.5 Examples of four-mode $\mathcal{PT}$ and PA models where the correspondence fails

In this subsection, we will present a four-mode $\mathcal{PT}$-symmetric non-Hermitian Hamiltonian $\hat{\mathcal{H}}_{\mathcal{PT},4}$, for which there does not exist any unitarily equivalent Hermitian parametric Hamiltonian of four (or less) modes. According to results in Appendix 3.7.2, it suffices to only consider $\mathcal{PT}$-symmetric Hamiltonians in the canonical form of $\mathcal{H}_2$ in Eq. (3.70). We start

with a tight-binding four-mode Hamiltonian in the canonical form

$$\begin{aligned}\hat{\mathcal{H}}_{\mathrm{tb},4} = i\frac{\gamma}{2}\left(\hat{a}_1^\dagger\hat{a}_1 + \hat{a}_2^\dagger\hat{a}_2 - \hat{b}_1^\dagger\hat{b}_1 - \hat{b}_2^\dagger\hat{b}_2\right) \\ + g\left(\hat{a}_1^\dagger\hat{a}_2 + \hat{b}_1^\dagger\hat{b}_2 + \hat{a}_1^\dagger\hat{b}_1 + \hat{a}_2^\dagger\hat{b}_2 + h.c.\right),\end{aligned} \tag{3.103}$$

where the coefficients γ and g are both real, so that it takes the form of $\hat{\mathcal{H}}_{\mathrm{tb}}$ in Eq. (3.29) the main text. Now we add a Hermitian perturbation $\hat{V}_1$ as

$$\hat{V}_1 = \delta\left(i\hat{a}_2^\dagger\hat{b}_2 + h.c.\right), \tag{3.104}$$

so that the total Hamiltonian is now given by $\hat{\mathcal{H}}'_{\mathrm{tb},4} = \hat{\mathcal{H}}_{\mathrm{tb},4} + \hat{V}_1$. We note that the perturbation ($\delta > 0$) breaks time reversal symmetry of the coherent part in the Hamiltonian $\hat{\mathcal{H}}'_{\mathrm{tb},4}$, which still takes the canonical form in Eq. (3.70) with component coefficient 2×2 matrices now given by

$$\tilde{\Sigma} = g\sigma_x, \tag{3.105a}$$

$$\tilde{J} = \left(t + \frac{i\delta}{2}\right)\sigma_0 - \frac{i\delta}{2}\sigma_z, \tag{3.105b}$$

$$\Gamma_N = \frac{\gamma}{2}\sigma_0, \tag{3.105c}$$

for which we can check the conditions in Eqs. (3.88) algebraically. It is straightforward but tedious to check these conditins for all possible 2×2 unitary matrices w_{12}. We find that it is impossible to construct a unitary w_{12} such that all the conditions are satisfied. Thus, we have constructed a four-mode $\mathcal{PT}$-symmetric to which there does not exist any unitarily equivalent PA system having four or less modes.

Conversely, there also exists parametric model whose dynamical matrix is not unitarily equivalent to any $\mathcal{PT}$-symmetric system with equal number of modes. If we have a

parametric model that (up to a local gauge transformation) fits the form in Eq. (3.38)

$$\hat{H}_{\text{p.a.},4} = g\left(\hat{a}_1^\dagger \hat{a}_2 - \hat{b}_1^\dagger \hat{b}_2\right) + \nu_1 \hat{a}_1^\dagger \hat{b}_1^\dagger + \nu_2 \hat{a}_2^\dagger \hat{b}_2^\dagger + h.c., \tag{3.106}$$

where g and $\nu_1 \neq \nu_2$ are real positive parameters, then the correspondence can be broken by adding a Hermitian perturbation as beam-splitter interactions with completely imaginary phase $\hat{V}_2 = \delta\left(i\hat{a}_1^\dagger \hat{a}_2 - i\hat{b}_1^\dagger \hat{b}_2 + h.c.\right)$, where we assume $\delta > 0$ without lack of generality. We note that the perturbation introduces a nontrivial phase into the parametric Hamiltonian, and the dynamics of the system can still be described by a 4×4 non-Hermitian dynamical matrix, which is automatically in the form in Eq. (3.96). The corresponding canonical form in Eq. (3.96) now has coefficient 2×2 matrices as

$$\Delta = g\sigma_x, \tag{3.107a}$$

$$\Sigma = -\delta\sigma_y, \tag{3.107b}$$

$$D_\nu = \frac{\nu_1 + \nu_2}{2}\sigma_0 + \frac{\nu_1 - \nu_2}{2}\sigma_z, \tag{3.107c}$$

but now the dynamics is not unitarily equivalent to any four-mode $\mathcal{PT}$-symmetric Hamiltonian.

3.7.6 Higher-order exceptional point in PA systems

In Section 3.5.1, we have presented EP enhanced mode splitting based on the $\sqrt{\epsilon}$ scaling of the splitting of eigenvalues in a $\mathcal{PT}$-symmetric non-Hermitian system. With some minor twists on the multimode mapping in Section 3.4.2, unitary mappings from $\mathcal{PT}$-symmetric system with odd number of modes to non-degenerate parametric amplifiers with equal number of modes could also be constructed. The idea is to leave the single $\mathcal{PT}$-symmetric mode unchanged, perform mapping for the rest of the modes as before, and assign coherent, particle-number conserving interaction terms to realize dynamics of the remaining bosonic

mode. As proposed in Refs. [90–92], such NDPA could exhibit higher order exceptional point, with mode splitting scaling as $\epsilon^{1/3}$.

We first describe the basics ingredients of higher order exceptional point and the corresponding enhanced mode splitting in a $\mathcal{PT}$-symmetric three-mode system. Although the higher order exceptional points can also be found in systems with more number of modes, we focus on the $\mathcal{PT}$ trimer setup for demonstrating purpose. The sensing scheme now consists of an unperturbed three-mode system with the Hamiltonian given by

$$\mathcal{H}_{\mathrm{HOEP}}\left[0\right]=\begin{pmatrix} +i\frac{\gamma}{2} & g & 0 \\ g & 0 & g \\ 0 & g & -i\frac{\gamma}{2} \end{pmatrix}, \tag{3.108}$$

and we intend to estimate the small parameter ϵ by probing the output power spectrum of the perturbed Hamiltonian

$$\mathcal{H}\left[\epsilon\right]=\begin{pmatrix} +i\frac{\gamma}{2} & g & 0 \\ g & \epsilon & g \\ 0 & g & -i\frac{\gamma}{2} \end{pmatrix}. \tag{3.109}$$

If the unperturbed Hamiltonian $\mathcal{H}\left[0\right]$ is set to the third-order EP ($g_c=\sqrt{2}\gamma/4$), then the power spectrum has a single resonance peak. In this case, the small perturbation ϵ in the mode detuning will induce mode splitting in the output spectrum, which scales as $\epsilon^{1/3}$ and may be even more sensitive than the splitting scaled as $\sqrt{\epsilon}$ in $\mathcal{PT}$ dimer settings. The $\epsilon^{1/3}$ scaling of mode splitting with respect to small ϵ perturbations close to the third-order exceptional point has recently been verified in optical experiments [93].

Again we aim to achieve the same $\epsilon^{1/3}$ scaling of mode splitting in a PA setup, without having to introduce any external bath (i.e., noise source). Applying the unitary mapping in Section 3.3.2 to the two-mode subsystem with gain and loss, the corresponding ϵ-dependent

NDPA Hamiltonian can be obtained as

$$\hat{H}_{\text{NDPA},3}\left[\epsilon\right] = \epsilon\hat{b}^\dagger\hat{b} + \left(\sqrt{2}g\hat{a}_2^\dagger\hat{b} + i\frac{\nu}{2}\hat{a}_1^\dagger\hat{a}_2^\dagger + h.c.\right), \tag{3.110}$$

where the detuning term ϵ becomes the detuning term of the third bosonic mode b, and the gain and loss at rate γ are transformed into the parametric drive with strength $\nu = \gamma$. Note that this bosonic Hamiltonian has the general structure of a driven three-mode optomechanical system, where a mechanical resonator $\hat{a}_2$ interacts with two electromagnetic modes $\hat{b}, \hat{a}_1$ via radiation-pressure interactions. This setup has been previously studied for entanglement generation [94–97].

It is also interesting to consider the form of the Hamiltonian when $\epsilon = 0$, $g = \sqrt{2}\gamma/4$ and we are exactly tuned to the EP. As discussed in Section 3.3.3, EP's in bosonic Hamiltonians coincide with conserved Hermitian quadrature variables. The same is true in our system. Making the gauge change $\hat{b} \to \hat{b}' = -i\hat{b}$, the Hamiltonian at the exceptional point can be written

$$\hat{H}_{\text{NDPA},3} = \frac{\gamma}{2}\left(\hat{X}_2(\hat{P}_1 - \hat{P}_{b'}) + \hat{P}_2(\hat{X}_1 + \hat{X}_{b'})\right), \tag{3.111}$$

where we have introduced standard quadrature operators for each mode. It follows immediately that there are two conserved quadratures $\hat{Q}_\pm$ in this system:

$$\hat{Q}_- = \frac{1}{\sqrt{2}}\left(\hat{P}_1 - \hat{P}_{b'}\right), \tag{3.112}$$

$$\hat{Q}_+ = \frac{1}{\sqrt{2}}\left(\hat{X}_1 + \hat{X}_{b'}\right). \tag{3.113}$$

3.7.7 QMFS for multi-mode systems: construction and corresponding symplectic transformations

In Section 3.4.3, we discussed how the dynamics of an arbitrary N mode non-Hermitian Hamiltonian could be realized using a QMFS embedded in a $2N$ mode bosonic system. We provide more details here as to how one constructs such multi-mode QMFS, and also discuss properties of the corresponding symplectic transformation generated by this dynamics.

Constraints on a general QMFS

Consider an N mode linear and Hermitian bosonic system where the dynamics does not couple canonically conjugate quadratures. We can write the equations of motion as

$$\partial_t \vec{\hat{q}}\,(t) = \mathcal{A}\,(t)\,\vec{\hat{q}}\,(t)\,, \tag{3.114a}$$

$$\partial_t \vec{\hat{\pi}}\,(t) = \mathcal{B}\,(t)\,\vec{\hat{\pi}}\,(t)\,, \tag{3.114b}$$

where $\mathcal{A}\,(t)$ and $\mathcal{B}\,(t)$ are generic real dynamical matrices, and $\vec{\hat{q}}$ and $\vec{\hat{\pi}}$ are both column vectors formed by N quadrature operatures satisfying the canonical commutation relations as

$$\left[\hat{q}_j, \hat{\pi}_{j'}\right] = i\delta_{jj'}, \tag{3.115}$$

with all other commutators between the quadratures vanishing $\left[\hat{q}_j, \hat{q}_{j'}\right] = \left[\hat{\pi}_j, \hat{\pi}_{j'}\right] = 0$.

We require the dynamics to preserve the canonical commutation relations at all times. It is straightforward to show that a necessary and sufficient condition to ensure this is that at all times:

$$\mathcal{B}\,(t) = -\mathcal{A}^T\,(t)\,. \tag{3.116}$$

for all time t.

Similarly, if integration of the equations of motion yields

$$\vec{\hat{q}}\,(t) = \mathcal{U}_{\mathcal{A}}\,(t)\,\vec{\hat{q}}\,(0)\,, \tag{3.117a}$$

$$\vec{\hat{\pi}}\,(t) = \mathcal{U}_{\mathcal{B}}\,(t)\,\vec{\hat{\pi}}\,(0)\,, \tag{3.117b}$$

then the preservation of canonical commutation relations holds if and only if

$$\mathcal{U}_{\mathcal{A}}\,(t)\,\mathcal{U}_{\mathcal{B}}^{T}\,(t) = \mathbb{I}_N. \tag{3.118}$$

QMFS for realizing arbitrary multi-mode non-Hermtian dynamics

We can use the results above to verify the QMFS dynamics presented in Section 3.4.3 does indeed correspond to a Hermitian bosonic Hamiltonian. in Section 3.4.3, an arbitrary non-Hermitian Hamiltonian $\mathcal{H}_N$ was encoded in a QMFS via Eq. (3.42a), i.e.

$$i\partial_t \vec{\hat{z}}_+ = \mathcal{H}_N \vec{\hat{z}}_+, \tag{3.119}$$

with pseudo-modes $\vec{z}_\pm$ defined in Eq. (3.41).

In terms of the column vectors formed by quadrature operators $\vec{\hat{x}}_+$ and $\vec{\hat{p}}_-$, we have

$$\partial_t \begin{pmatrix} \vec{\hat{x}}_+ \\ \vec{\hat{p}}_- \end{pmatrix} = \begin{pmatrix} \mathrm{Im}\,\mathcal{H}_N & \mathrm{Re}\,\mathcal{H}_N \\ -\mathrm{Re}\,\mathcal{H}_N & \mathrm{Im}\,\mathcal{H}_N \end{pmatrix} \begin{pmatrix} \vec{\hat{x}}_+ \\ \vec{\hat{p}}_- \end{pmatrix}. \tag{3.120}$$

Now, using Eq. (3.116) to ensure conjugate quadratures evolve appropriately, we obtain

$$\partial_t \begin{pmatrix} \vec{\hat{p}}_+ \\ -\vec{\hat{x}}_- \end{pmatrix} = \begin{pmatrix} -\mathrm{Im}\,\mathcal{H}_N^T & \mathrm{Re}\,\mathcal{H}_N^T \\ -\mathrm{Re}\,\mathcal{H}_N^T & -\mathrm{Im}\,\mathcal{H}_N^T \end{pmatrix} \begin{pmatrix} \vec{\hat{p}}_+ \\ -\vec{\hat{x}}_- \end{pmatrix}. \tag{3.121}$$

The above equation is equivalent to

$$i\partial_t \vec{\hat{z}}_- = \mathcal{H}_N^\dagger \vec{\hat{z}}_-, \tag{3.122}$$

as given in Section 3.4.3. It thus follows that the QMFS dynamics given in Section 3.4.3 does indeed preserve canonical commutation relations.

The above approach is also valid for an arbitrary time-dependent non-Hermitian dynamical matrix $\mathcal{H}_N(t)$. Note first that the classical amplitude evolution is controlled by the $N \times N$ complex matrix $\mathcal{U}_N(t)$. It satisfies:

$$i\partial_t \mathcal{U}_N(t) = \mathcal{H}_N(t)\,\mathcal{U}_N(t)\,. \tag{3.123}$$

In terms of the quadratures $\hat{x}_{\pm,j}$ and $\hat{p}_{\pm,j}$, we have

$$\begin{pmatrix} \vec{\hat{x}}_+(t) \\ \vec{\hat{p}}_-(t) \end{pmatrix} = \begin{pmatrix} \mathrm{Re}\,\mathcal{U}_N(t) & -\mathrm{Im}\,\mathcal{U}_N(t) \\ \mathrm{Im}\,\mathcal{U}_N(t) & \mathrm{Re}\,\mathcal{U}_N(t) \end{pmatrix} \begin{pmatrix} \vec{\hat{x}}_+(0) \\ \vec{\hat{p}}_-(0) \end{pmatrix}, \tag{3.124a}$$

$$\begin{pmatrix} \vec{\hat{p}}_+(t) \\ -\vec{\hat{x}}_-(t) \end{pmatrix} = \begin{pmatrix} \mathrm{Re}\,\mathcal{V}_N(t) & \mathrm{Im}\,\mathcal{V}_N(t) \\ -\mathrm{Im}\,\mathcal{V}_N(t) & \mathrm{Re}\,\mathcal{V}_N(t) \end{pmatrix} \begin{pmatrix} \vec{\hat{p}}_+(0) \\ -\vec{\hat{x}}_-(0) \end{pmatrix}, \tag{3.124b}$$

where the coefficient matrix $\mathcal{V}_N(t)$ is defined as

$$\mathcal{V}_N(t) \equiv \left[\mathcal{U}_N^T(t)\right]^{-1}. \tag{3.125}$$

It follows immediately that the constraint in Eq. (3.118) is obeyed.

Finally, the above transformation can be equivalently described in terms of the bosonic

annihilation and creation operators as

$$\begin{pmatrix} \vec{\hat{a}}(t) \\ \vec{\hat{b}}(t) \end{pmatrix} = A(t) \cdot \begin{pmatrix} \vec{\hat{a}}(0) \\ \vec{\hat{b}}(0) \end{pmatrix} + B(t) \cdot \begin{pmatrix} \vec{\hat{a}}^{\dagger}(0) \\ \vec{\hat{b}}^{\dagger}(0) \end{pmatrix}, \tag{3.126}$$

where

$$A(t) = \frac{1}{2} \begin{pmatrix} \mathcal{U}_N(t) + \left[\mathcal{U}_N^{\dagger}(t)\right]^{-1} & 0 \\ 0 & \mathcal{U}_N^{*}(t) + \left[\mathcal{U}_N^{T}(t)\right]^{-1} \end{pmatrix}, \tag{3.127a}$$

$$B(t) = \frac{1}{2} \begin{pmatrix} 0 & \mathcal{U}_N(t) - \left[\mathcal{U}_N^{\dagger}(t)\right]^{-1} \\ \mathcal{U}_N^{*}(t) - \left[\mathcal{U}_N^{T}(t)\right]^{-1} & 0 \end{pmatrix}. \tag{3.127b}$$

Bloch-Messiah representation of the multi-mode QMFS evolution

As discussed above, the non-Hermitian Hamiltonian $\mathcal{H}_N(t)$ induces a symplectic (i.e. unitary) transformation in the corresponding bosonic QMFS system. To understand its nature better, it is helpful to use the Bloch-Messiah (BM) decomposition [77]. This reduces an arbitrary Gaussian unitary to a sequence of three simple operations: a beam-splitter operation, a product of single-mode squeezing operations, then another beam-splitter operation.

In terms of Eq. (3.126), the Bloch-Messiah decomposition corresponds to

$$A = U_{\mathrm{BM}} D_A V_{\mathrm{BM}}^{\dagger}, \tag{3.128a}$$

$$B = U_{\mathrm{BM}} D_B V_{\mathrm{BM}}^{T}, \tag{3.128b}$$

where U_{BM} and V_{BM} are unitary, and D_A, D_B are non-negative diagonal matrices with the constraint $D_A^2 = D_B^2 + \mathbb{I}_{2N}$.

The Bloch-Messiah matrices can be explicitly computed. We first write a singular value

decomposition for the time evolution matrix $\mathcal{U}_N(t)$ in Eq. (3.123):

$$\mathcal{U}_N(t) = W_1 D_{\mathcal{U}} W_2^{\dagger}, \tag{3.129}$$

and then use this to define the diagonal unitary matrix $W_{\mathcal{U}}$:

$$W_{\mathcal{U}} = \sqrt{\left(D_{\mathcal{U}} - D_{\mathcal{U}}^{-1}\right) \cdot \left|D_{\mathcal{U}} - D_{\mathcal{U}}^{-1}\right|^{-1}}. \tag{3.130}$$

With these definitions, the unitary matrices in the BM decomposition (describing initial and final beam-splitter operations) are given by:

$$U_{\mathrm{BM}} = \begin{pmatrix} W_1 & 0 \\ 0 & W_1^* \end{pmatrix} \cdot \frac{1}{\sqrt{2}} \begin{pmatrix} 1 & -1 \\ 1 & 1 \end{pmatrix} \cdot \begin{pmatrix} W_{\mathcal{U}} & 0 \\ 0 & W_{\mathcal{U}}^* \end{pmatrix}, \tag{3.131a}$$

$$V_{\mathrm{BM}}^{\dagger} = \begin{pmatrix} W_{\mathcal{U}}^* & 0 \\ 0 & W_{\mathcal{U}} \end{pmatrix} \cdot \frac{1}{\sqrt{2}} \begin{pmatrix} 1 & 1 \\ -1 & 1 \end{pmatrix} \cdot \begin{pmatrix} W_2^{\dagger} & 0 \\ 0 & W_2^T \end{pmatrix}. \tag{3.131b}$$

Correspondingly, the diagonal matrices describing the squeezing operations in the BM decomposition can be computed as:

$$D_A = \begin{pmatrix} \frac{D_{\mathcal{U}} + D_{\mathcal{U}}^{-1}}{2} & 0 \\ 0 & \frac{D_{\mathcal{U}} + D_{\mathcal{U}}^{-1}}{2} \end{pmatrix}, \tag{3.132a}$$

$$D_B = \begin{pmatrix} \frac{\left|D_{\mathcal{U}}^{-1} - D_{\mathcal{U}}\right|}{2} & 0 \\ 0 & \frac{\left|D_{\mathcal{U}}^{-1} - D_{\mathcal{U}}\right|}{2} \end{pmatrix}. \tag{3.132b}$$

3.7.8 Review of the EP encircling

Here, we briefly review the quasi-adiabatic dynamical phenomena by encircling an EP in two-mode non-Hermitian systems. We use the convention in Ref. [40] for clarity. We consider a

system evolving according to the time-dependent non-Hermitian Hamiltonian $\mathcal{H}_\omega(t)$ given in Eq. (3.51) whose instantaneous eigenvalues are given by

$$\lambda_\pm(t) = \pm\sqrt{(\omega(t) + i\gamma/2)^2 + g(t)^2}. \tag{3.133}$$

We assume that the parameters are varied at a rate much slower than the eigenvalue gap $|\lambda_+ - \lambda_-|$. We choose the left (right) instantaneous eigenvectors $\vec{l}_\pm(t)$ ($\vec{r}_\pm(t)$) of $\mathcal{H}_\omega(t)$ to be biorthonormal and satisfy $\vec{l}_\pm = \vec{r}_\pm$, implying:

$$\vec{r}_\pm = \left(1 + \rho_\pm^2\right)^{-\frac{1}{2}} \cdot \begin{pmatrix} \rho_\pm \\ 1 \end{pmatrix}, \tag{3.134a}$$

$$\rho_\pm = \frac{\omega + i\gamma/2 + \lambda_\pm}{g}. \tag{3.134b}$$

We consider varying parameters $g(t)$ and $\omega(t)$ along a circle that encloses the EP:

$$g(t) = g_0 + \epsilon\cos\phi(t), \tag{3.135a}$$

$$\omega(t) = \epsilon\sin\phi(t), \tag{3.135b}$$

where the center of the circle is taken to be the exceptional point $g_0 = \gamma/2$, and $\epsilon < \gamma/2$ is a small positive parameter characterizing the encircling radius. The circling phase is chosen such that EP is encircled once, with $\phi(t_i) = \phi\left(t_f\right)$ during the time duration that we consider, and the evolution time is chosen such that $t_f - t_i = T \gg 1/|\lambda_+ - \lambda_-|$.

The system is prepared in one of the instantaneous eigenmodes (e.g. the λ_+ branch) $\vec{z}(t_i) = \vec{r}_+(t_i)$ at the beginning time t_i, and we consider solution to the equation of motion $i\partial_t\vec{z} = \mathcal{H}_\omega\vec{z}$. For the Hamiltonian matrix $\mathcal{H}_\omega(t)$ at given time t, we expand the state vector

$\vec{z}(t)$ at time t in terms of instantaneous eigenvectors as

$$\vec{z}(t) = c_+(t)\,\vec{r}_+(t) + c_-(t)\,\vec{r}_-(t)\,. \tag{3.136}$$

If the dynamics were adiabatic, we would expect the amplitude $c_-(t)$ to be negligible for the entire protocol. Note that as the EP is encircled once during the time evolution, the instantaneous eigenmodes undergo a switch by the end of the evolution, i.e. $\lambda_\pm(t_f) = \lambda_\mp(t_i)$. Surprisingly, for the path that encircles the EP once, the adiabatic prediction holds for parametric encircling path along only one direction, whereas a non-adiabatic transition will occur in the opposite direction, as depicted in Fig. 3.4 in the main text. This chiral mode switching phenomenon could be interpreted physically as a consequence of stability loss delay [40].

3.7.9 Exceptional point encircling: details

We present here additional details for the quasi-adiabatic exceptional point encircling dynamics presented in Section 3.5.2; the focus is on how the dynamics of the non-Hermitian gain-loss dimer Hamiltonian $\mathcal{H}_\omega(t)$ (c.f. Eq. (3.51)) directly determines the quantum evolution in our Hermitian, four-mode bosonic system (Hamiltonian $\hat{H}_{\omega\mathrm{PA}}(t)$, c.f. Eq. (3.22)). We will make explicit use of the Bloch-Messiah (BM) reduction of the symplectic transformation generated by $\mathcal{H}_\omega(t)$ (as introduced in Appendix 3.7.7).

Symmetry constraints

Note first that, by construction, $\mathcal{H}_\omega(t)$ is a symmetric matrix, and satisfies the chiral symmetry condition $\{\mathcal{H}_\omega(t), \sigma_y\} = 0$. As a result, the amplitude-evolution matrix $\mathcal{U}_\omega(t)$ generated

by $\mathcal{H}_\omega(t)$ (c.f. Eq. (3.52)) obeys the constraint

$$\left[\mathcal{U}_\omega^T(t)\right]^{-1} = \sigma_y \mathcal{U}_\omega(t)\,\sigma_y. \tag{3.137}$$

It also follows that $\det \mathcal{U}_\omega(t) = 1$.

These conditions can be used to constrain the form of the unitary operator $\hat{U}_\omega(t)$ which describes evolution in the four-mode Hermitian bosonic system corresponding to $\mathcal{H}_\omega(t)$ (constructed using the QMFS approach). One finds that the diagonal matrices $D_A(t)$ and $D_B(t)$ in the BM reduction of $\hat{U}_\omega(t)$ (c.f. Eqs. (3.126) and (3.128)) are both proportional to the unit matrix, i.e.

$$D_A(t) = \cosh\lambda_s(t)\cdot\mathbb{I}_4, \tag{3.138a}$$

$$D_B(t) = \sinh\lambda_s(t)\cdot\mathbb{I}_4, \tag{3.138b}$$

with the squeezing parameter $\lambda_s(t)$ given by

$$\cosh\lambda_s(t) = \frac{1}{2}\sqrt{\mathrm{tr}\left[\mathcal{U}_\omega^\dagger(t)\,\mathcal{U}_\omega(t)\right]+2}. \tag{3.139}$$

It follows that the squeezing part of the BM decomposition necessarily corresponds to four identical single-mode squeezing operations.

Symplectic transformation for the four-mode QMFS Hermitian bosonic system

We now derive the explicit form of the symplectic transformation for the collective quadratures $\hat{x}_{\pm,j}$ and $\hat{q}_{\pm,j}$ $(j = 1, 2)$ under the time evolution generated by the time-dependent

parametric Hamiltonian $\hat{H}_{\omega\mathrm{PA}}(t)$ (c.f. Eq. (3.22)). Using Eq. (3.124), we immediately have

$$\begin{pmatrix} \hat{x}_{1,+}(t) \\ \hat{x}_{2,+}(t) \\ \hat{p}_{1,-}(t) \\ \hat{p}_{2,-}(t) \end{pmatrix} = \begin{pmatrix} \mathrm{Re}\,\mathcal{U}_\omega(t) & -\mathrm{Im}\,\mathcal{U}_\omega(t) \\ \mathrm{Im}\,\mathcal{U}_\omega(t) & \mathrm{Re}\,\mathcal{U}_\omega(t) \end{pmatrix} \begin{pmatrix} \hat{x}_{1,+}(0) \\ \hat{x}_{2,+}(0) \\ \hat{p}_{1,-}(0) \\ \hat{p}_{2,-}(0) \end{pmatrix}, \tag{3.140a}$$

$$\begin{pmatrix} \hat{p}_{1,+}(t) \\ \hat{p}_{2,+}(t) \\ -\hat{x}_{1,-}(t) \\ -\hat{x}_{2,-}(t) \end{pmatrix} = \begin{pmatrix} \mathrm{Re}\,\mathcal{V}_\omega(t) & \mathrm{Im}\,\mathcal{V}_\omega(t) \\ -\mathrm{Im}\,\mathcal{V}_\omega(t) & \mathrm{Re}\,\mathcal{V}_\omega(t) \end{pmatrix} \begin{pmatrix} \hat{p}_{1,+}(0) \\ \hat{p}_{2,+}(0) \\ -\hat{x}_{1,-}(0) \\ -\hat{x}_{2,-}(0) \end{pmatrix}, \tag{3.140b}$$

where $\mathcal{V}_\omega(t) \equiv \left[\mathcal{U}_\omega^T(t)\right]^{-1}$ (see Eq. (3.125)).

As derived in Eq. (3.137), the chiral symmetry of $\mathcal{H}_\omega(t)$ ensures the equality $\mathcal{V}_\omega(t) = \sigma_y \mathcal{U}_\omega(t)\,\sigma_y$, so that the equation of motion Eq. (3.140b) can be equivalently rewritten in terms of the matrix $\mathcal{U}_\omega(t)$ as

$$\begin{pmatrix} \hat{x}_{2,-}(t) \\ -\hat{x}_{1,-}(t) \\ \hat{p}_{2,+}(t) \\ -\hat{p}_{1,+}(t) \end{pmatrix} = \begin{pmatrix} \mathrm{Re}\,\mathcal{U}_\omega(t) & \mathrm{Im}\,\mathcal{U}_\omega(t) \\ -\mathrm{Im}\,\mathcal{U}_\omega(t) & \mathrm{Re}\,\mathcal{U}_\omega(t) \end{pmatrix} \begin{pmatrix} \hat{x}_{2,-}(0) \\ -\hat{x}_{1,-}(0) \\ \hat{p}_{2,+}(0) \\ -\hat{p}_{1,+}(0) \end{pmatrix}. \tag{3.141}$$

Note that the symplectic transform presented here in terms of the collective quadratures $\hat{x}_{\pm,j}$ and $\hat{p}_{\pm,j}$ is equivalent to the one discussed in Eq. (3.53) in the main text, which can

be compactly written using the pseudo-modes $\hat{z}_j$ and $\hat{\tilde{z}}_j$ (c.f. Eqs. (3.21) and (3.23)) as

$$\begin{pmatrix} \hat{z}_1(t) \\ \hat{z}_2(t) \end{pmatrix} = \mathcal{U}_\omega(t) \cdot \begin{pmatrix} \hat{z}_1(0) \\ \hat{z}_2(0) \end{pmatrix}, \tag{3.142a}$$

$$\begin{pmatrix} \hat{\tilde{z}}_1(t) \\ \hat{\tilde{z}}_2(t) \end{pmatrix} = \left[\mathcal{U}_\omega^\dagger(t)\right]^{-1} \cdot \begin{pmatrix} \hat{\tilde{z}}_1(0) \\ \hat{\tilde{z}}_2(0) \end{pmatrix}. \tag{3.142b}$$

Comparing symplectic transformations for clockwise and counterclockwise encirclings

Consider a general case of a multimode Hermitian bosonic system which corresponds (via the QMFS mapping) to a time-dependent non-Hermitian Hamiltonian. We take this latter Hamiltonian to be symmetric and periodic (period T_0), i.e.

$$\mathcal{H}_N(t) = \mathcal{H}_N^T(t) = \mathcal{H}_N(t + T_0). \tag{3.143}$$

As discussed in Appendix 3.7.7, the corresponding symplectic transformations in the QMFS setup are fully characterized by the non-unitary time-evolution matrices $\mathcal{U}_N(T_0)$ and $\tilde{\mathcal{U}}_N(T_0)$, which are $t = T_0$ solutions to the equations of motion

$$i\partial_t \mathcal{U}_N(t) = \mathcal{H}_N(t)\,\mathcal{U}_N(t), \tag{3.144a}$$

$$i\partial_t \tilde{\mathcal{U}}_N(t) = \mathcal{H}_N(-t)\,\tilde{\mathcal{U}}_N(t). \tag{3.144b}$$

As (by assumption) $\mathcal{H}_N(t)$ is a symmetric matrix, one finds:

$$\tilde{\mathcal{U}}_N(t) = \left[\mathcal{U}_N^T(-t)\right]^{-1}. \tag{3.145}$$

Furthermore, periodicity of $\mathcal{H}_N(t)$ leads to the relation that $\mathcal{U}_N(-T_0) = [\mathcal{U}_N(T_0)]^{-1}$, so

that we have

$$\tilde{\mathcal{U}}_N(T_0) = \left[\mathcal{U}_N^T(-T_0)\right]^{-1} = \mathcal{U}_N^T(T_0). \tag{3.146}$$

We see that the classical amplitude-evolution matrices associated with forward and backwards evolution are related by a simple transpose operation. We can use this and the results of Appendix 3.7.7 to then directly relate the unitary evolutions in the corresponding four-mode bosonic QMFS systems. It follows that the BM decompositions for forward and backwards evolution are related via:

$$\tilde{U}_{\mathrm{BM}}(T_0) = V_{\mathrm{BM}}^*(T_0), \tag{3.147a}$$

$$\tilde{V}_{\mathrm{BM}}(T_0) = U_{\mathrm{BM}}^*(T_0), \tag{3.147b}$$

$$\tilde{D}_A(T_0) = D_A(T_0) \;\Leftrightarrow\; \tilde{D}_B(T_0) = D_B(T_0). \tag{3.147c}$$

Here, tildes indicate backwards evolution. Note that the squeezing aspect of the evolution (as parameterized by the D matrices) is the same irrespective of the direction. Finally, note that these results apply directly to our two-mode problem of interest (i.e. $\mathcal{H}_N(t) \to \mathcal{H}_\omega(t)$, $\mathcal{U}_N(t) \to \mathcal{U}_\omega(t)$), as $\mathcal{H}_\omega(t)$ satisfies Eq. (3.143).

Evolution of quantum states via EP encircling

Having built up the necessary machinery, we can now study how the switching dynamics encoded in $\mathcal{U}_\omega(t)$ influences the evolution of quantum states in our four-mode bosonic system (lowering operators $\hat{a}_1, \hat{a}_2, \hat{b}_1, \hat{b}_2$). The unitary evolution operator $\hat{U}_\omega(t)$ of our system is defined by

$$i\partial_t \hat{U}_\omega(t) = \hat{H}_{\omega\mathrm{PA}}(t)\,\hat{U}_\omega(t), \quad \hat{U}_\omega(t=0) = \mathbb{I}, \tag{3.148}$$

where $\hat{H}_{\omega\mathrm{PA}}(t)$ is given by Eq. (3.22). $\hat{U}_\omega(t)$ generates a symplectic (i.e. commutation-relation preserving) linear transformation of the system's mode operators. As established in

Appendix 3.7.9, the form of this transformation is completely determined by the amplitude-evolution matrix $\mathcal{U}_\omega(t)$ of the original non-Hermitian problem.

As in the main text, we consider a cyclic evolution where $(g(t), \omega(t))$ evolve along a closed circle, starting and ending at the same point in parameter space. The non-Hermitian system's evolution is different for these two directions, corresponding to two distinct evolution matrices $\mathcal{U}_{\circlearrowleft}(t)$ and $\mathcal{U}_{\circlearrowright}(t)$. When transformed to the instantaneous eigenmode basis of $\mathcal{H}_\omega(t)$, one of these encodes the switching behaviour seen in Fig. 3.4, the other has no switching behaviour.

Using our mapping, we have two corresponding unitary transformations $\hat{U}_{\circlearrowleft}(t)$ and $\hat{U}_{\circlearrowright}(t)$ for our quantum four-mode system; we wish to understand their asymmetry. This is best accomplished by using the Bloch-Messiah decomposition (see Appendix 3.7.9), which represents each transformation as a product of two beam-splitter transformations, interspersed with a (diagonal) squeezing transformation. We find that the squeezing associated with both $\hat{U}_{\circlearrowleft}(T)$ and $\hat{U}_{\circlearrowright}(T)$ are identical, with the asymmetry manifesting itself only in the beamsplitter operations (c.f. Eqs.(3.147))

To see the the physical consequences of this asymmetry, consider first the case where all four modes start in vacuum, and parameters are cyclically evolved on the path shown in Fig. 3.4(a). CW or CCW traversal of this path results in two different final states for our four bosonic modes, $|\Psi_{\circlearrowleft}(t=T)\rangle$ versus $|\Psi_{\circlearrowright}(t=T)\rangle$. These final states are necessarily Gaussian and have zero means, and are thus fully characterized by their covariance matrix. First, consider beam-splitter type correlations between a and b modes. Due to the block structure of the symplectic transformation in Eqs. (3.127), these vanish for all times t, i.e.

$$\left\langle \hat{a}_j^\dagger(t)\,\hat{b}_{j'}(t)\right\rangle = \left\langle \hat{b}_j^\dagger(t)\,\hat{a}_{j'}(t)\right\rangle = 0. \tag{3.149}$$

Moreover, the photon numbers are identical for all four modes:

$$\left\langle \hat{a}_j^\dagger(t)\,\hat{a}_{j'}(t)\right\rangle = \left\langle \hat{b}_j^\dagger(t)\,\hat{b}_{j'}(t)\right\rangle = \delta_{jj'}\sinh^2\lambda_s$$
$$= \frac{\delta_{jj'}}{4}\left(\mathrm{tr}\left[\mathcal{U}_\omega^\dagger(t)\,\mathcal{U}_\omega(t)\right]-2\right). \tag{3.150}$$

As the squeezing parameter λ_s is the same at the final time T irrespective of encircling direction, the same is necessarily true for these average photon numbers.

Finally, the only non-zero anomalous (squeezing) correlators are given by

$$\left\langle \hat{a}_j(t)\,\hat{b}_{j'}(t)\right\rangle = \left\langle \hat{b}_{j'}(t)\,\hat{a}_j(t)\right\rangle = D_{jj'} \tag{3.151}$$
$$D = \frac{1}{4}\mathcal{U}_\omega(t)\,\mathcal{U}_\omega^\dagger(t) - \frac{1}{4}\left[\mathcal{U}_\omega(t)\,\mathcal{U}_\omega^\dagger(t)\right]^{-1}, \tag{3.152}$$

where D is a Hermitian matrix. These correlators (at the final time $t=T$) will depend on the direction of the encircling.

Finally, we could look at bipartite entanglement between different subsystems. Consider for example the entanglement between the a subsystem (formed by modes a_1, a_2) and the b subsystem (formed by modes b_1, b_2). Quantifying the entanglement via the logarithmic negativity E_N [78, 79], one finds:

$$E_N\left[\rho_{ab}(t)\right] = (\cosh\lambda_s+1)\log(\cosh\lambda_s)$$
$$-(\cosh\lambda_s-1)\log(\sinh\lambda_s). \tag{3.153}$$

The entanglement only depends on the squeezing paramter λ_s. As this is identical for both encircling directions, the generated $a-b$ entanglement is thus also insensitive to direction. The net result is that if we start with a vacuum state, the asymmetry between the states $|\Psi_{\circlearrowleft}(t=T)\rangle$ and $|\Psi_{\circlearrowright}(t=T)\rangle$ is subtle: both have the same average photon number and entanglement properties, and differ only in the phase of two-mode squeezing correlators

between a and b modes.

We now finally turn to the case presented in Section 3.5.2 of the main text, where we consider an initial, pure quantum state that corresponds to selectively populating one of the two eigenmodes of $\mathcal{H}_\omega(0)$. In the classical case, the chiral mode switching behaviour depends crucially on having such an asymmetric initial state. The same is true in the quantum case.

To construct a suitable initial state, we first consider the classical two-mode problem. Using our convention for the instantaneous eigenvectors $\vec{r}_+(t)$, $\vec{r}_-(t)$ of $\mathcal{H}_\omega(t)$, one finds that the vectors $\vec{r}_+(t)$ and $(\vec{r}_-(t))^*$ are orthogonal. They thus serve as a good basis, and we can write any initial set of amplitudes in the classical problem as:

$$\vec{z} = \xi \frac{\vec{r}_+}{|\vec{r}_+|} + \xi_\perp \frac{(\vec{r}_-)^*}{|\vec{r}_-|}, \tag{3.154}$$

where ξ and $\xi_\perp$ are complex numbers. $\xi_\perp$ is proportional to the amplitude c_- defined in Eq. (3.55), whereas ξ describes the amount of population in the mode $\vec{r}_+$ (when we make this vector part of an orthonormal basis).

We could now imagine a random classical state which selectively populates the + eigenmode with a random phase. In particular, take $\xi, \xi_\perp$ to be complex Gaussian random variables with zero mean, and where the only non-zero covariances are:

$$\overline{(\mathrm{Re}\ \xi)^2} = \overline{(\mathrm{Im}\ \xi)^2} = \frac{1}{2} e^{2\lambda_0}, \tag{3.155a}$$

$$\overline{(\mathrm{Re}\ \xi_\perp)^2} = \overline{(\mathrm{Im}\ \xi_\perp)^2} = \frac{1}{2} e^{-2\lambda_0}. \tag{3.155b}$$

The parameter $\lambda_0 > 0$ determines the asymmetry of the initial state.

Turning to our quantum system, the components of $\hat{z}$ become operators as per Eq. (3.16) and (3.21): they are linear combinations of the QMFS collective quadrature operators $(\hat{x}_{+,1}, \hat{x}_{+,2}, \hat{p}_{-,1}, \hat{p}_{-,2})$. It immediately follows that the amplitudes ξ, $\xi_\perp$ become commuting operators that are linear combinations of these QMFS collective quadrature operators; one

can easily find the relevant orthogonal transformation.

We can now construct a quantum Gaussian state where the operators $\hat{\xi}$, $\hat{\xi}_\perp$ have a covariance matrix that coincides with Eqs. (3.155). This in turn defines the covariance matrix of the QMFS collective quadrature operators. This of course does not specify the entire state: we also need to specify covariances involving collective quadratures conjugate to those in the QMFS, i.e. $\left(\hat{p}_{+,1}, \hat{p}_{+,2}, -\hat{x}_{-,1}, -\hat{x}_{-,2}\right)$. We do this by insisting on two additional requirements:

- The covariance matrix of the entire system describes a physical state compatible with the uncertainty principle [98].
- The covariance matrix of the entire system describes a pure state.
- There are no classical (i.e. symmetrized) correlations between a collective quadrature from the main QMFS, and the secondary QMFS

These conditions allow us to find a pure zero-mean Gaussian state parameterized by λ_0, where the amplitude-operators $\hat{\xi}, \hat{\xi}_\perp$ have covariances given by Eqs. (3.155). This is the kind of initial state used for the calculations of entanglement dynamics in Section 3.5.2.

Note that while our state clearly has a strong asymmetry favouring the + instantaneous eigenmode, there is still some population of the − eigenmode, as $\xi_\perp$ is not exactly zero. One cannot find a physical state where $\langle \hat{\xi}_\perp^\dagger \hat{\xi}_\perp \rangle$ is strictly zero as this would violate the uncertainty principle (i.e. as this quantity becomes smaller and smaller, the covariances of operators outside of the QMFS would diverge).

3.7.10 Relating non-Hermitian and bosonic topological invariants

In this subsection, we exploit the mappings established earlier to show that non-Hermitian Chern numbers [84] are equivalent to the Chern numbers for anomalous bosonic problems.

Relating Bogoliubov transformations to non-Hermitian eigenvectors

As a prerequisite, we will establish the connection between Bogoliubov transformations (in the bosonic problem) to the eigenvectors of the non-Hermitian problem.

Consider first a translationally-invariant Hermitian bosonic 2D lattice model having a primitive unit cell with N sites. The Hamiltonian can be written as $\hat{H} = \frac{1}{2}\sum_{\mathbf{k}} \hat{H}_{\mathbf{k}}$, where the Bloch Hamiltonian for quasimomentum $\mathbf{k}$ has the general form

$$\begin{aligned}\hat{H}_{\mathbf{k}} = &\sum_{i,j=1}^{N} \Big(\mu_{\mathbf{k},ij}\hat{a}^{\dagger}_{\mathbf{k},i}\hat{a}_{\mathbf{k},j} + \mu_{-\mathbf{k},ij}\hat{a}^{\dagger}_{-\mathbf{k},i}\hat{a}_{-\mathbf{k},j}\Big) \\ &+ \sum_{i,j=1}^{N} \Big(\nu_{\mathbf{k},ij}\hat{a}^{\dagger}_{\mathbf{k},i}\hat{a}^{\dagger}_{-\mathbf{k},j} + h.c.\Big),\end{aligned} \tag{3.156}$$

where $\hat{a}_{\mathbf{k},i}$ is the annihilation operator corresponding to quasi-momentum $\mathbf{k}$ and site i in the unit cell. Hermiticity requires $\mu_{\mathbf{k}} = \mu^{\dagger}_{\mathbf{k}}$; further, $\nu_{\mathbf{k}} = \nu^{T}_{-\mathbf{k}}$ as bosonic lowering operators commute.

The Heisenberg equations of motion now take the compact form

$$i\partial_t|\hat{a}_{\mathbf{k}}\rangle = \begin{pmatrix} \mu_{\mathbf{k}} & \nu_{\mathbf{k}} \\ -\nu^{\dagger}_{\mathbf{k}} & -\mu^{T}_{-\mathbf{k}} \end{pmatrix} |\hat{a}_{\mathbf{k}}\rangle, \tag{3.157}$$

where we define the column vector $|\hat{a}_{\mathbf{k}}\rangle$ formed by the $2N$ coupled operators as

$$|\hat{a}_{\mathbf{k}}\rangle = \Big(\hat{a}_{\mathbf{k},1}, \hat{a}_{\mathbf{k},2}, \cdots, \hat{a}_{\mathbf{k},N}, \hat{a}^{\dagger}_{-\mathbf{k},1}, \hat{a}^{\dagger}_{-\mathbf{k},2}, \cdots, \hat{a}^{\dagger}_{-\mathbf{k},N}\Big)^{T}. \tag{3.158}$$

We can now interpret the dynamical matrix of our driven bosonic system as an effective

non-Hermitian Bloch Hamiltonian $\mathcal{H}_{\text{eff}}(\mathbf{k})$ of a lattice with $2N$ sites in the unit cell,

$$\mathcal{H}_{\text{eff}}(\mathbf{k}) = \begin{pmatrix} \mu_{\mathbf{k}} & \nu_{\mathbf{k}} \\ -\nu_{\mathbf{k}}^{\dagger} & -\mu_{-\mathbf{k}}^{T} \end{pmatrix}. \tag{3.159}$$

This non-Hermitian Bloch Hamiltonian is related to the Hermitian Bogoliubov-de Gennes (BdG) Bloch Hamiltonian $H_{\text{BdG}}(\mathbf{k})$ by $\mathcal{H}_{\text{eff}}(\mathbf{k}) = \sigma_{N,z} H_{\text{BdG}}(\mathbf{k})$, where

$$H_{\text{BdG}}(\mathbf{k}) = \begin{pmatrix} \mu_{\mathbf{k}} & \nu_{\mathbf{k}} \\ \nu_{\mathbf{k}}^{\dagger} & \mu_{-\mathbf{k}}^{T} \end{pmatrix}. \tag{3.160}$$

and $\sigma_{N,z}$ is a z Pauli matrix in particle-hole space.

We next define the left and right eigenvectors of the matrix $\mathcal{H}_{\text{eff}}(\mathbf{k})$:

$$\mathcal{H}_{\text{eff}}(\mathbf{k}) |\mathbf{k}, j\rangle_{\text{R}} = E_j(\mathbf{k}) |\mathbf{k}, j\rangle_{\text{R}}, \tag{3.161}$$

$${}_{\text{L}}\langle \mathbf{k}, j| \mathcal{H}_{\text{eff}}(\mathbf{k}) = E_j(\mathbf{k}) {}_{\text{L}}\langle \mathbf{k}, j|. \tag{3.162}$$

Here $j = 1, 2, \cdots, 2N$, and we choose the eigenvectors to satisfy the biorthonormal condition

$${}_{\text{L}}\langle \mathbf{k}, j \mid \mathbf{k}, j' \rangle_{\text{R}} = \delta_{j,j'}. \tag{3.163}$$

We will focus exclusively on the regime where the parametric driving is sufficiently weak that our system is stable, and the spectrum $E_j(\mathbf{k})$ is purely real. $\hat{H}_{\mathbf{k}}$ can then be diagonalized via a Bogoliubov transformation. Not surprisingly, the quasiparticle operators that diagaonlize the Hamiltonian are directly related to the eigenvectors of $\mathcal{H}_{\text{eff}}(\mathbf{k})$. To see this explicitly, we use the fact that all left eigenvectors either have a real, non-zero "expectation" of $\sigma_{N,z}$ that is either positive or negative (see e.g. [99]). They can thus be chosen to obey

the symplectic normalization condition

$$ {}_{\mathrm{L}}\left\langle \mathbf{k}, n, \pm \right| \sigma_{N,z} \left| \mathbf{k}, n', \pm \right\rangle_{\mathrm{L}} = \pm \delta_{n,n'}, \tag{3.164} $$

All left eigenvectors are now labelled by a sign $\pm$, and the index n runs from 1 to N. We denote the corresponding eigenvalues $E_{n,\pm}(\mathbf{k})$. With this convention, it follows from Eq. (3.163) that the corresponding right eigenvectors are given by

$$ \left| \mathbf{k}, n, \pm \right\rangle_{\mathrm{R}} = \pm \sigma_{N,z} \left| \mathbf{k}, n, \pm \right\rangle_{\mathrm{L}}. \tag{3.165} $$

The eigenvectors now let us express the equations of motion in diagonal form; this can be accommplished by using the positive-norm eigenvectors only. We introduce new bosonic quasiparticles via

$$ \hat{\beta}_{\mathbf{k},n} = {}_{\mathrm{L}}\left\langle \mathbf{k}, n, + \right| \hat{a} \rangle . $$

They satisfy

$$ i\partial_t \hat{\beta}_{\mathbf{k},n} = E_{n,+}\left(\mathbf{k}\right) \hat{\beta}_{\mathbf{k},n}. $$

This represents a canonical Bogoliubov transformation, and the Hamiltonian is diagonal when expressed in terms of these operators. We thus see the (expected) relation between the Bogoliubov transformation and the eigenvectors of our non-Hermitian Hamiltonian.

Equivalence of bosonic and non-Hermitian Chern numbers

With the above relations in hand, we can now show that the non-Hermitian Chern number introduced in Ref. [84] coincides with the previously introduced Chern number for anomalous bosonic problems [85].

We start with the bosonic system. The Berry connection $A_{nn}\left(\mathbf{k}\right)$ for the n^{th} band was

introduced in Refs. [71, 85, 86] as

$$A_{nn}(\mathbf{k}) = i \cdot {}_{\mathrm{L}}\langle \mathbf{k}, n | \sigma_{N,z} \nabla_{\mathbf{k}} | \mathbf{k}, n \rangle_{\mathrm{L}}, \tag{3.166}$$

and the corresponding (quantized) Chern number is given by:

$$C_n = \frac{1}{2\pi} \int_{\mathrm{BZ}} (\nabla \times A_{nn}) \cdot \hat{z}\, d^2\mathbf{k} \tag{3.167}$$

This serves as a topological invariant to characterize bands in an anomalous, stable bosonic system.

Now, using Eq. (3.165), we can equivalently write this Chern number in terms of left and right eigenvectors of the non-Hermitian Hamiltonian $\mathcal{H}_{\mathrm{eff}}(\mathbf{k})$

$$\begin{aligned} C_n =& \frac{1}{2\pi} \int_{\mathrm{BZ}} (\nabla \times A_{nn}) \cdot \hat{z} d^2\mathbf{k} \\ =& \frac{i}{2\pi} \int_{\mathrm{BZ}} \epsilon_{3ij} \partial_i \left({}_{\mathrm{L}}\langle \mathbf{k}, n, + | \, \partial_j | \mathbf{k}, n, + \rangle_{\mathrm{R}} \right) d^2\mathbf{k} \\ =& \frac{i}{2\pi} \int_{\mathrm{BZ}} \epsilon_{3ij} \left(\partial_i \, \langle \mathbf{k}, n, + |_{\mathrm{L}} \right) \left(\partial_j | \mathbf{k}, n, + \rangle_{\mathrm{R}} \right) d^2\mathbf{k}. \end{aligned} \tag{3.168}$$

We can now compare this expression against the generalized Chern numbers $N_n^{\alpha\beta}$ introduced in Ref. [84] for 2D non-Hermitian Hamiltonians. These are defined as

$$B_{n,ij}^{\alpha\beta}(\mathbf{k}) = i \left\langle \partial_i \psi_n^{\alpha}(\mathbf{k}) \right| \partial_j \psi_n^{\beta}(\mathbf{k}) \Big\rangle, \tag{3.169}$$

$$N_n^{\alpha\beta} = \frac{1}{2\pi} \int_{BZ} \epsilon_{ij} B_{n,ij}^{\alpha\beta}(\mathbf{k})\, d^2\mathbf{k}. \tag{3.170}$$

Here, the indices $\alpha, \beta = \mathrm{L}, \mathrm{R}$, and $\left|\psi_n^{\mathrm{L}}(\mathbf{k})\right\rangle$ ($\left|\psi_n^{\mathrm{R}}(\mathbf{k})\right\rangle$) denotes the left (right) eigenvector of the given non-Hermitian Bloch Hamiltonian $\mathcal{H}(\mathbf{k})$. Ref. [84] shows that all four Chern

numbers $N_n^{\alpha\beta}$ for a given band n are identical.

We see now that the bosonic Chern number in Eq. (3.168) is identical to the generalized non-Hermitian Chern number N_n^{LR}. Thus, as long as the bosonic Hamiltonian $\hat{H}_{\mathbf{k}}$ has well-defined Chern numbers, we can always find the corresponding non-Hermitian lattice model $\mathcal{H}_{\mathrm{eff}}(\mathbf{k})$ whose topological invariants are exactly the same.

While the correspondence found here here may not seem that surprising, it provides an interesting recipe for constructing non-trivial non-Hermitian topological models: start with a topological bosonic model, and then construct its non-Hermitian analogue. We pursue this approach in the next section.

3.7.11 Correspondence between the dimer Kagome Hamiltonian and the topological bosonic parametric model

Due to the correspondence between the Chern number based on the bosonic symplectic normalization relation and the generalized Chern number for the non-Hermitian dynamical matrix, the analysis in Ref. [86] on the topological phases of the system also applies to the equivalent non-Hermitian problem. One interesting and probably exotic feature for the bosonic model is that the nontrivial topological phases are completely due to the parametric drive, without which we would only have a trivial Kagome lattice model with nearest neighbor tunnel couplings. Thus for the non-Hermitian model, nontrivial topological phases can only exist if the effective Hamiltonian has nonzero non-Hermitian components. This is in contrast to some previous work based on a topologically nontrivial coherent Hamiltonian on non-Hermitian topological systems, where the anti-Hermitian part of dynamics is usually introduced as a perturbation [70, 80]. Here we combine the correspondence of topological phases and the mapping between some parametric models and $\mathcal{PT}$-symmetric systems to construct a non-Hermitian $\mathcal{PT}$-symmetric lattice model, where nontrivial topological phase emerges from an otherwise topologically trivial Hermitian model when one adds balanced

onsite gain and loss terms to the model properly.

In Ref. [86], non-trivial topological states can be created by adding parametric coupling with proper arrangement of phases to a topologically trivial Kagome lattice model that only have identical coherent hopping. We consider a parametric Hamiltonian $\hat{H}_{\text{p.a.,Kagome}} = \hat{H}_0 + \hat{H}_{\text{L}}$ consisting of a topologically trivial tight-binding Kagome lattice model that conserves particle number

$$\hat{H}_0 = \omega_0 \sum_{\mathfrak{j}} \hat{a}_{\mathfrak{j}}^{\dagger} \hat{a}_{\mathfrak{j}} - J \sum_{\langle \mathfrak{j}, \mathfrak{j}' \rangle} \hat{a}_{\mathfrak{j}'}^{\dagger} \hat{a}_{\mathfrak{j}'}, \tag{3.171}$$

and a local parametric drive term H_{L}

$$\hat{H}_{\text{L}} = -\frac{1}{2} \nu \sum_{\mathfrak{j}} e^{i\phi_s} \hat{a}_{\mathfrak{j}}^{\dagger} \hat{a}_{\mathfrak{j}}^{\dagger} + h.c., \tag{3.172}$$

where the index $\mathfrak{j} = (\mathbf{j}, s) = (j_1, j_2, s)$ incorporates both periodicity in real space and sublattices $s = A, B, C$, and ν, ϕ_s denote the parametric drive strength and phase, respectively. Transforming the mode operators to the reciprocal $\mathbf{k}$ space, the system dynamics is closed with respect to the set of operators $|\hat{a}_{\mathbf{k}}\rangle = \left(\hat{a}_{\mathbf{k},A}, \hat{a}_{\mathbf{k},B}, \hat{a}_{\mathbf{k},C}, \hat{a}_{-\mathbf{k},A}^{\dagger}, \hat{a}_{-\mathbf{k},B}^{\dagger}, \hat{a}_{-\mathbf{k},C}^{\dagger}\right)^T$, so that as a special case of Eq. (3.157), the equations of motion can be written in the compact form

$$i\partial_t \left|\hat{a}_{\mathbf{k}}\right\rangle = \mathcal{H}_{\text{eff,K.}}\left(\mathbf{k}\right) \left|\hat{a}_{\mathbf{k}}\right\rangle, \tag{3.173}$$

where the dynamical matrix is given by

$$\mathcal{H}_{\text{eff,K.}}\left(\mathbf{k}\right) = \begin{pmatrix} \omega_0 \mathbb{I}_3 - J\tau\left(\mathbf{k}\right) & h \\ -h^{\dagger} & -\omega_0 \mathbb{I}_3 + J\tau\left(\mathbf{k}\right) \end{pmatrix}. \tag{3.174}$$

The matrix $\tau(\mathbf{k})$ is formed by geometrical factors of the tight-binding Kagome lattice

$$\tau(\mathbf{k}) = \begin{pmatrix} 0 & 1+e^{-i\mathbf{k}\cdot\mathbf{a_1}} & 1+e^{i\mathbf{k}\cdot\mathbf{a_3}} \\ 1+e^{i\mathbf{k}\cdot\mathbf{a_1}} & 0 & 1+e^{-i\mathbf{k}\cdot\mathbf{a_2}} \\ 1+e^{-i\mathbf{k}\cdot\mathbf{a_3}} & 1+e^{i\mathbf{k}\cdot\mathbf{a_2}} & 0 \end{pmatrix}, \tag{3.175}$$

where $\mathbf{a_1} = \left(-1, -\sqrt{3}\right), \mathbf{a_2} = (2, 0)$ are the lattice vectors, and $\mathbf{a_3} = \left(-1, \sqrt{3}\right)$; the coefficient matrix $h = -\nu \exp(i\Phi)$, $\mathbb{I}_3$ is the 3×3 identity matrix, and Φ is the diagonal matrix formed by the phases carried by local parametric drives

$$\Phi = \mathrm{diag}(\phi_A, \phi_B, \phi_C) = \mathrm{diag}(0, \phi, 2\phi), \quad \phi = \frac{2\pi}{3}. \tag{3.176}$$

The off-diagonal tunnelings in h can be rotated to onsite gain and loss via a unitary transformation

$$\mathcal{U}_{\mathrm{K.}} = \frac{1}{\sqrt{2}} \begin{pmatrix} e^{2i\Phi} & e^{2i\Phi} \\ ie^{-2i\Phi} & -ie^{-2i\Phi} \end{pmatrix}. \tag{3.177}$$

so that $\mathcal{H}_{\mathcal{PT},\mathrm{K.}}(\mathbf{k}) = \mathcal{U}_{\mathrm{K.}}^{\dagger} \mathcal{H}_{\mathrm{eff,K.}}(\mathbf{k}) \mathcal{U}_{\mathrm{K.}}$ is

$$\mathcal{H}_{\mathcal{PT},\mathrm{K.}}(\mathbf{k}) = \begin{pmatrix} \Sigma(\mathbf{k}) - i\nu\mathbb{I}_3 & \Delta(\mathbf{k}) \\ \Delta(\mathbf{k}) & \Sigma(\mathbf{k}) + i\nu\mathbb{I}_3 \end{pmatrix}, \tag{3.178}$$

where $\Sigma(\mathbf{k})$ and $\Delta(\mathbf{k})$ are Hermitian matrices with matrix elements given by

$$\Sigma_{ss'}(\mathbf{k}) = iJ\tau_{ss'}(\mathbf{k}) \sin(2\phi_s - 2\phi_{s'}), \tag{3.179a}$$

$$\Delta_{ss'}(\mathbf{k}) = \omega_0 \delta_{ss'} - J\tau_{ss'}(\mathbf{k}) \cos(2\phi_s - 2\phi_{s'}). \tag{3.179b}$$

The corresponding real space Hamiltonian $\hat{\mathcal{H}}_{\mathrm{Kagome}}$ for the lattice model $\mathcal{H}_{\mathcal{PT},\mathrm{K.}}(\mathbf{k})$ is presented in Section 3.5.3 in the main text.

Before ending this section, we note that the unitary mapping $\mathcal{U}_{\mathrm{K.}}$ in Eq. (3.177) is local in real space, so that any topological edge modes of the parametric Kagome lattice model $\hat{H}_{\mathrm{p.a.,Kagome}}$ will also be mapped to topological edge modes of the $\mathcal{PT}$-symmetric model.

CHAPTER 4

SPECTRAL CHARACTERIZATION OF NON-GAUSSIAN QUANTUM NOISE: KELDYSH APPROACH AND APPLICATION TO PHOTON SHOT NOISE

4.1 Overview of results

Having accurate tools to describe non-classical, non-Gaussian environmental fluctuations is crucial for designing effective quantum control protocols and understanding the physics of underlying quantum dissipative environments. In this chapter, we show how the Keldysh approach to quantum noise characterization can be usefully employed to characterize frequency-dependent noise, focusing on the quantum bispectrum (i.e. frequency-resolved third cumulant). Using the paradigmatic example of photon shot noise fluctuations in a driven bosonic mode, we show that the quantum bispectrum can be a powerful tool for revealing distinctive non-classical noise properties, including an effective breaking of detailed balance by quantum fluctuations. The Keldysh-ordered quantum bispectrum can be directly accessed using existing noise spectroscopy protocols.

4.2 Introduction

An accurate description of environmental fluctuations is crucial for quantum information processing and quantum control. While it is common to assume noise that is both classical and Gaussian, there are many physically-relevant situations where these assumptions fail [101–105]. Understanding how to usefully characterize non-Gaussian, non-classical noise

in a frequency-resolved manner could enable the design of more optimal dynamical decoupling protocols, enhancing qubit coherence. It could also provide fundamental insights into the nature of the underlying dissipative environment.

For classical noise, the frequency-resolved higher noise cumulants (so-called polyspectra [106]) provide a full characterization. These have been previously measured for classical non-Gaussian fluctuations in a single-electron transistor [107]. More recent work has proposed [103, 105] and demonstrated [104] protocols to reconstruct polyspectra using a qubit driven by classical non-Gaussian noise; Ref. [103] also studied the specific class of linearly coupled oscillator baths, where operator ordering does not play a role[1]. The full generalization of these ideas to quantum non-Gaussian noise as produced by a *generic* quantum environment (i.e. one where operator ordering matters) remains an interesting open question; for this general problem, the non-commutativity of noise operators at different times poses a challenge as to how one should appropriately define polyspectra.

In this paper, we show that the Keldysh approach [108–112], a method used extensively to characterize low-frequency noise, also provides an unambiguous and practically useful way to describe non-Gaussian quantum bath noise in the frequency domain. It provides a systematic way to construct a quasiprobability distribution to describe the noise, and to assess whether the noise can be faithfully mimicked by completely classical noise processes [109, 111]. It also has a direct operational meaning: the "quantum polyspectra" we introduce are *exactly* the quantities that contribute to the dephasing of a coupled qubit at each order in the coupling. Moreover, these quantities can be measured using *the same* non-Gaussian noise spectroscopy techniques designed for classical noise sources [103, 104, 113]; one does not have to decide in

1. Ref. [103] defines higher noise cumulants without specifying a particular time ordering of bath operators, i.e. our Eq. (4.3) but without any time or anti-time ordering symbols. They state that this is valid for a very specific class of problems: harmonic oscillator baths, where the noise operator $\hat{\xi}(t)$ is linear in bath creation and annihilation operators. In Appendix 4.8.1, we provide a rigorous justification for ignoring the operator ordering in these quantum noise models. Further, we discuss the conditions where ignoring the Keldysh ordering is (not) valid, and provide additional examples of quantum noise processes where the Keldysh ordering leads to nontrivial corrections.

advance whether the noise is classical or quantum to perform the characterization. Note that a recent work presented a method to measure arbitrary quantum bath correlation functions [113]; in contrast, our work focuses on characterizing the most physically-relevant correlation function at each order and identifying a corresponding quasiprobability.

To highlight the utility of our approach, we apply it to the concrete but non-trivial case of photon shot noise in a driven-damped bosonic mode (a relevant source of dephasing noise in circuit QED systems [114, 115] among others). Prior work used the Keldysh approach to study this noise at zero frequency [111, 116]; here we instead focus on the behaviour of the frequency-resolved third cumulant, the "quantum bispectrum" (QBS). We show that the QBS reveals important new physics and distinct quantum signatures: at low temperatures, qualitatively new features emerge that would never be present in a classical model with only thermal fluctuations. We also show that the QBS is a generic tool for revealing the breaking of detailed balance and violation of Onsager-like symmetry relations. We find that the photon shot noise QBS violates detailed balance at low temperatures.

4.3 Keldysh ordering and quantum polyspectra

Consider first a classical noise process $\xi(t)$. Its moment generating function (MGF) is defined as

$$\Lambda_{\text{class}}[F(t); t_f] = \overline{\exp\left[-i\int_0^{t_f} F(t)\xi(t)\right]}, \tag{4.1}$$

where the bar indicates a stochastic average. Functional derivatives of Λ_{class} with respect to $F(t)$ can be used to calculate arbitrary-order correlation functions of $\xi(t)$, while functional derivatives of $\ln \Lambda_{\text{class}}$ generate the cumulants of $\xi(t)$ (see e.g. [117]). Fourier transforming these cumulants yields the polyspectra, which completely characterize the noise in the frequency domain [106].

In the quantum case, our noise is a Heisenberg picture operator $\hat{\xi}(t)$ whose evolution is generated by the Hamiltonian of some bath; we take $\hat{\xi}(t)$ to be Hermitian for simplicity. Defining correlation functions now has some subtlety, as $\hat{\xi}(t)$ will not in general commute with itself at different times; hence, different time-ordering choices yield different results. Correlation functions at a given order describe both how the bath responds to external perturbations, as well as its intrinsic fluctuations [118]. We are interested here in characterizing the latter quantity, and asking whether these fluctuations are equivalent to an effective classical noise process.

The well-developed machinery of Keldysh quantum field theory provides a precise method for accomplishing our task [108–112]. While this approach is completely general, the simplest derivation is to imagine coupling an ancilla qubit to $\hat{\xi}$, such that the only qubit dynamics is from the interaction picture Hamiltonian $\hat{H}_{\rm int}(t) = \frac{1}{2}F(t)\hat{\xi}(t)\hat{\sigma}_z$. We then use the dephasing of the qubit to *define* the MGF of the noise in the quantum case, exactly like we would if the noise were classical:

$$\Lambda[F(t);t_f] \equiv \langle\hat{\sigma}_-(t_f)\rangle/\langle\hat{\sigma}_-(0)\rangle, \tag{4.2}$$

$$=\mathrm{Tr}\left[\mathcal{T}e^{-\frac{i}{2}\int_0^{t_f}dt'F(t')\hat{\xi}(t')}\hat{\rho}_{\rm B}\tilde{\mathcal{T}}e^{-\frac{i}{2}\int_0^{t_f}dt'F(t')\hat{\xi}(t')}\right]. \tag{4.3}$$

Here $\hat{\rho}_B$ is the initial bath density matrix, the trace is over bath degrees of freedom, and $\mathcal{T}$ ($\tilde{\mathcal{T}}$) is the time-ordering (anti-time ordering) symbol. Expanding Λ in powers of $F(t')$ defines correlation functions at a given order with a particular time-ordering prescription (the so-called Keldysh ordering). We stress that this approach amounts to trying to ascribe the qubit evolution to an effective classical stochastic process; this correspondence then defines cumulants (and implicitly a quasiprobability) for the quantum noise of interest.

For truly classical noise, the definition in Eq. (4.3) reduces to the classical MGF in Eq. (4.1). For quantum baths comprising of harmonic oscillators, and with a noise operator

$\hat{\xi}(t)$ that is linear in bath raising and lowering operators, operator ordering plays no role in the definition of cumulants. This is because commutators of $\hat{\xi}(t)$ with itself at different times are numbers, not operators (see Appendix 4.8.1 for an explicit proof). As a result, the Keldysh-ordered MGF in Eq. (4.3) is equivalent to the classical MGF in Eq. (4.1) with $\xi(t)$ directly replaced by the quantum noise operator $\hat{\xi}(t)$. This is the only kind of bath explicitly discussed in Ref. [103] (though the neglect of operator ordering issues is not discussed). We stress that ignoring operator ordering (i.e. not using the full definition in Eq. (4.3)) fails in almost any other situation. In particular, it is not valid for non-Gaussian quantum baths with nonlinear coupling or intrinsic nonlinearity, where the Keldysh ordering in Eq. (4.3) leads to nontrivial corrections in the quantum noise cumulants (see Appendix 4.8.1 for further discussion.)

The moments and corresponding quasiprobability defined via Eq. (4.3) are intrinsic to the noisy system; they predict the outcomes of a wide class of schemes designed to measure this noise[2]. They also have a direct role in Keldysh non-equilibrium field theory: they characterize the fluctuations of the "classical" field associated with the operator $\hat{\xi}(t)$. This provides an alternate, extremely physical way to understand the Keldysh-ordered cumulants, one that transcends simply viewing this prescription as a formal consequence of expanding interaction-picture operators. At each order, the Keldysh-ordered correlation function describes the intrinsic fluctuations of the system [118]. In contrast, the remaining independent correlation functions at the same order describe how the system responds to external fields which couple to $\hat{\xi}(t)$ (see Appendix 4.8.3 for a complete discussion). We stress again that at each order, the Keldysh-ordered correlation function is precisely the correlation function "seen" by the qubit.

2. The utility of Keldysh ordering to characterizing generic quantum noise, which is independent of the specific measurement scheme used to measure such noise, has been discussed in great detail in Refs. [109, 112]. As an illustration, Nazarov and Kindermann [109] has considered an alternate measurement setup that involves no qubit at all, where Keldysh-ordered quasiprobability provides a physical characterization. In Appendix 4.8.2, we briefly discuss their result for the reader's convenience.

It follows that the Keldysh-ordered cumulants $C^{(k)}(\vec{t}_k) \equiv \langle\langle \hat{\xi}\,(t_1)\cdots\hat{\xi}\,(t_k)\rangle\rangle_{\mathcal{K}}$ of the noise can be generated from $\chi[F(t);t_f] \equiv \ln\Lambda[F(t);t_f]$ via

$$\chi[F(t);t_f] = \sum_{\ell=1}^{\infty}\frac{(-i)^\ell}{\ell!}\prod_{j=1}^{\ell}\left[\int_0^{t_f} dt_j F(t_j)\right] C^{(\ell)}(\vec{t}_\ell), \tag{4.4}$$

where we define $\vec{t}_n \equiv (t_1,\ldots,t_n)$. Explicit expressions for the first few Keldysh-ordered cumulants are provided in Eqs. (4.27) and (4.28) of Appendix 4.8.4. The Keldysh-ordered second cumulant is simply a symmetrized correlation function, whereas the third cumulant corresponds to suppressing time-orderings where the earliest operator appears in the middle of an expectation value.

For stationary noise, the k-th order cumulant $C^{(k)}(\vec{t}_k)$ only depends on the $k-1$ time separations $\tau_j \equiv t_{j+1}-t_1$, $j=1,\ldots,k-1$. We define the quantum polyspectra as Fourier transforms of the Keldysh-ordered cumulants:

$$S_n[\vec{\omega}_n] \equiv \int_{\mathbb{R}^n} d\vec{\tau}_n\, e^{-i\vec{\omega}_n\cdot\vec{\tau}_n} C^{(n+1)}(\vec{\tau}_n), \quad n\geq 1. \tag{4.5}$$

For discussion of classical polyspectra, see Refs. [103, 105, 119]. The $\omega_j \to 0$ limit of $S_n[\vec{\omega}_n]$ characterize fluctuations in $\hat{m} = \int_0^t dt'\hat{\xi}(t')$ in the long-time limit (so-called full counting statistics (FCS)). This is the typical setting where the Keldysh approach has found great utility, largely for studying electronic current fluctuations. Here we extend the method to study non-classical, non-Gaussian noise *at non-zero frequencies* (see also Ref. [120] for an application to frequency-dependent current noise).

4.4 Quantum noise model

The utility of our approach can be illustrated by studying a concrete, nontrivial example of quantum non-Gaussian noise: the energy fluctuations of a driven-damped bosonic mode.

In what follows, we focus on the physics of the frequency-dependent third cumulant, the so-called quantum bispectrum (QBS) $S_2[\omega_1, \omega_2]$; we drop the subscript 2 hereafter. The QBS reveals a host of physics here that is not manifest in the low-frequency fluctuations (as studied in [111, 116, 121]).

Our "bath" here is a driven damped cavity mode c (frequency ω_c, Markovian energy decay rate γ). As discussed, the Keldysh-ordered cumulants of the photon-number shot noise can be derived by coupling the number operator $\hat{n} = \hat{c}^\dagger \hat{c}$ of the driven cavity to an ancilla qubit via $\hat{H}_{\rm int}(t) = F(t)\hat{n}\hat{\sigma}_z/2$; the desired quantities are then encoded in the qubit coherence via Eq. (4.2). Working in a rotating frame at the drive frequency, and letting $\hat{\rho}$ denote the qubit-cavity reduced density matrix, the system dynamics follows the master equation

$$\dot{\hat{\rho}} = -i[\hat{H}_0 + \hat{H}_{\rm int}(t), \hat{\rho}] + \gamma(\bar{n}_{\rm th} + 1)\mathcal{D}[\hat{c}]\hat{\rho} + \gamma\bar{n}_{\rm th}\mathcal{D}[\hat{c}^\dagger]\hat{\rho}. \tag{4.6}$$

Here $\mathcal{D}[\hat{A}]\hat{\rho} = \hat{A}\rho\hat{A}^\dagger - (\hat{A}^\dagger\hat{A}\hat{\rho} + \hat{\rho}\hat{A}^\dagger\hat{A})/2$ is the Lindblad dissipator and $\bar{n}_{\rm th}$ the thermal photon number associated with the cavity dissipation. The cavity Hamiltonian reads $\hat{H}_0 = -\delta\hat{c}^\dagger\hat{c} - (f\hat{c} + \text{H.c.})$, where f (δ) denotes the drive amplitude (detuning).

The Keldysh-ordered MGF Λ can now be computed by solving the master equation in Eq. (4.6); we stress that the qubit is introduced here as a theoretical tool for extracting the cumulants to appropriately characterize the quantum noise of interest. Even with an arbitrary time-dependent coupling $F(t)$, the qubit dephasing can be solved exactly using an extension of the phase space method in Ref. [122] (see also Appendix 4.8.5). An equivalent approach is to calculate correlation functions using standard techniques (e.g. quantum regression theorem, Heisenberg-Langevin equations) [76], and then apply the Keldysh ordering defined in Eqs. (4.3) and (4.4). In what follows, we will always take the long time limit $t_f \to \infty$, making the fluctuations stationary. One finds the QBS can be written as:

$$S[\omega_1, \omega_2] = S_{\rm th}[\omega_1, \omega_2] + S_{\rm dr}[\omega_1, \omega_2], \tag{4.7}$$

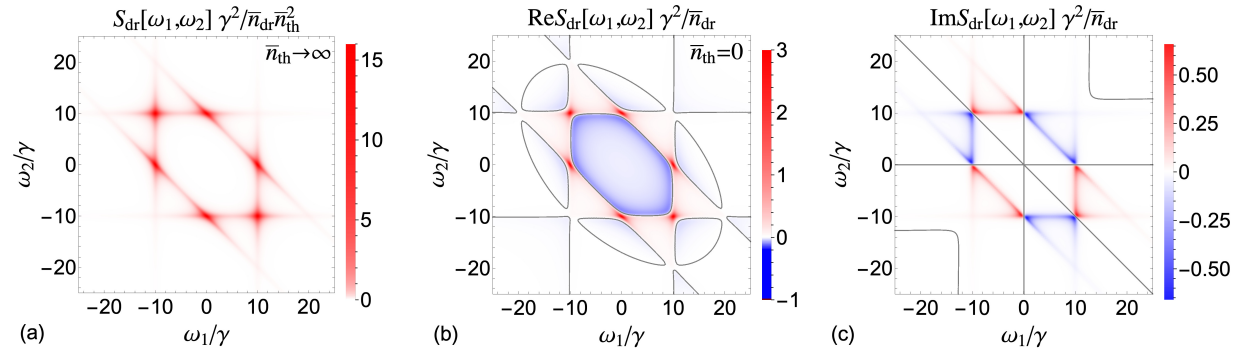

Fig. 4.1: Normalized quantum bispectra of drive-dependent photon fluctuations for large detuning $\delta = 10\gamma$ (a) in the classical limit $\bar{n}_{\rm th} \to \infty$, and (b) real part $\mathrm{Re}S_{\rm dr}[\omega_1, \omega_2]$, and (c) imaginary part $\mathrm{Im}S_{\rm dr}[\omega_1, \omega_2]$ in the extreme quantum limit $\bar{n}_{\rm th} = 0$. γ is the cavity damping rate, $\bar{n}_{\rm th}$ is the bath thermal number. The red (blue) regions correspond to positive (negative) values, while the gray contour lines indicate zeros. While the classical-limit bispectrum in (a) is real and positive (as expected from a classical calculation), the quantum-limit bispectrum exhibits negativity in (b) and an imaginary part in (c).

where the first term is completely independent of the drive f, and the second term is proportional to $|f|^2$.

4.5 Quantum bispectrum

4.5.1 Drive-independent fluctuations

The f-independent QBS $S_{\rm th}[\omega_1, \omega_2]$ can be calculated by solving Eq. (4.6) with $f = 0$. In this case, the cavity relaxes to a thermal steady state with no coherence between different Fock states. Its fluctuations can thus be mapped to a classical Markovian master equation. For such a classical and thermal Markov process, the bispectrum $S_{\rm th}[\omega_1, \omega_2]$ *must* always be real [123, 124]. In Appendix 4.8.7, we also show that in our case, $S_{\rm th}[\omega_1, \omega_2]$ must also be positive semidefinite. Letting $\omega_3 \equiv -\omega_1 - \omega_2$ in all equations that follow, our full calculation for the Keldysh-ordered QBS yields as expected a real, positive function:

$$S_{\rm th}[\omega_1, \omega_2] = \mathcal{C}_{\bar{n}_{\rm th}} \gamma^2 \left(6\gamma^2 + \sum_{j=1}^{3} \omega_j^2 \right) \Big/ \prod_{j=1}^{3} (\gamma^2 + \omega_j^2), \tag{4.8}$$

with $\mathcal{C}_{\bar{n}_{\rm th}} = \bar{n}_{\rm th}(\bar{n}_{\rm th}+1)(2\bar{n}_{\rm th}+1)$. The frequency dependence of this contribution to the bispectrum is the same both in the classical high-temperature limit $\bar{n}_{\rm th} \to \infty$, and in the extreme quantum limit $\bar{n}_{\rm th} \to 0$; the only temperature dependence is in the prefactor. $S_{\rm th}[\omega_1, \omega_2]$ vanishes in the absence of thermal fluctuations (i.e. $\bar{n}_{\rm th} \to 0$). In the limit $\bar{n}_{\rm th} \to 0$, this expression corresponds (as expected) to the bispectrum of asymmetric telegraph noise (see e.g., [125]), corresponding to fluctuations between the $n = 0$ and $n = 1$ Fock states. While our general result here suggests that the ω dependence of the QBS is not sensitive to quantum corrections, we will see that this is not true as soon as a coherent drive is added.

4.5.2 Driven fluctuations

We now consider the drive-dependent contribution to the bispectrum, $S_{\rm dr}[\omega_1, \omega_2]$ in Eq. (4.7). This quantity only depends on the drive amplitude f through the overall prefactor $\bar{n}_{\rm dr} = 4|f|^2/(\gamma^2 + 4\delta^2)$ (the intracavity photon number generated by f). Note that $S_{\rm dr}[\omega_1, \omega_2]$ remains non-zero at zero temperature, and is the only contribution to the QBS in this limit.

We find that the drive-dependent QBS shows striking quantum signatures. In the classical limit of high temperatures, it is always real and positive (similarly to the purely thermal contribution, see Appendix 4.8.7 for detail). However, as temperature is lowered and quantum fluctuations dominate, this quantity can have a negative real part, and even a non-zero imaginary part. These quantum features become more pronounced as the magnitude of the drive detuning δ is increased. The real and imaginary parts of $S_{\rm dr}[\omega_1, \omega_2]$ are plotted for zero temperature in Figs. 4.1(b) and 4.1(c) for a large drive detuning ($\delta/\gamma = 10$).

Consider first the surprising negativity of the real part of the zero-temperature QBS. Negativity in the zero-frequency limit was already discussed in [111, 116]. These works showed that this is a purely quantum effect, and that for large detunings it makes it impossible to describe the fluctuations by a positive-definite quasiprobability. Our results show how this striking non-classicality also manifests itself in the *non-zero* frequency fluctuations. We

find that the QBS $S_{\rm dr}[\omega_1, \omega_2]$ has a different frequency dependence in the quantum limit ($\bar{n}_{\rm th} = 0$) versus the classical limit $\tilde{S}_{\rm cl}[\omega_1, \omega_2]$. To see this, we write

$$\frac{S_{\rm dr}[\omega_1, \omega_2]}{\bar{n}_{\rm dr}} = (2\bar{n}_{\rm th} + 1)^2 \tilde{S}_{\rm cl}[\omega_1, \omega_2] + \tilde{S}_{\rm q}[\omega_1, \omega_2]. \tag{4.9}$$

The first term is the classical contribution which dominates in the high-temperature limit; $\tilde{S}_{\rm cl}[\omega_1, \omega_2]$ is independent of both $\bar{n}_{\rm dr}, \bar{n}_{\rm th}$, and is real and positive for all frequencies. Its form can be found directly from a classical Langevin equation calculation (see Eq. (4.42) of Appendix 4.8.7). In contrast, the second term is the temperature-independent quantum correction. It has a *completely different* frequency dependence from the classical limit, as described by $\tilde{S}_{\rm q}[\omega_1, \omega_2]$

$$\tilde{S}_{\rm q}[\omega_1, \omega_2] = -\frac{1}{2} \sum_{\substack{\alpha \neq \beta \\ \alpha, \beta = 1,2,3}} \frac{\frac{\gamma}{2} + i\omega_\beta}{(\gamma - i\omega_\alpha)[(\frac{\gamma}{2} + i\omega_\beta)^2 + \delta^2]}. \tag{4.10}$$

This function can have both a negative real part, and a non-zero imaginary part. In the quantum limit $\bar{n}_{\rm th} = 0$, one finds that real part of the QBS only becomes negative above a critical value of the detuning $|\delta|$. Moreover, the initial onset of negativity occurs at $\omega_1 = \omega_2 = 0$. In the large-detuning regime $|\delta| \gg \gamma$, the negative region of the QBS is peaked near a polygon whose shape is defined by the resonance conditions $\omega_j = \pm\delta$ $(j = 1, 2, 3)$.

4.6 Imaginary bispectrum and violations of detailed balance

We now turn to another striking feature of the photon shot noise QBS: while in the classical, high-temperature limit it is always real, the quantum correction $\tilde{S}_{\rm q}[\omega_1, \omega_2]$ has a non-zero imaginary part (see Fig. 4.2). This non-trivial imaginary bispectrum can *only* be probed at finite frequency: by its very definition in Eq. (4.5), the imaginary part of the QBS must vanish if either $\omega_1 = 0$ or $\omega_2 = 0$.

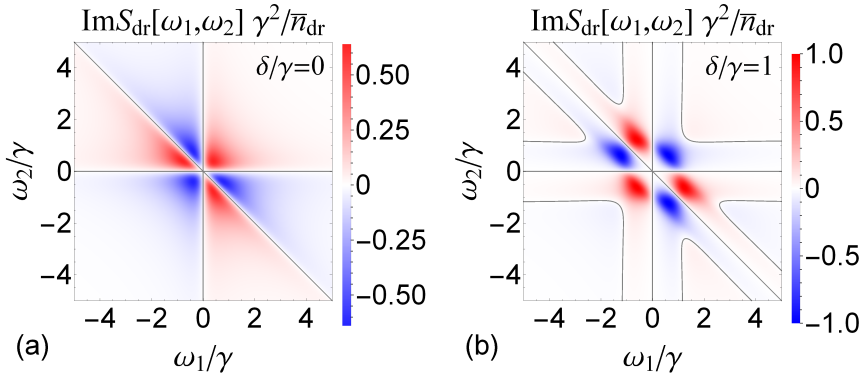

Fig. 4.2: Frequency dependence of the imaginary parts of the photon-shot noise bispectrum $\mathrm{Im}S[\omega_1,\omega_2]$ in the extreme quantum limit $\bar{n}_{\rm th}=0$ at different detunings. Parameters: (a) $\delta/\gamma=0$, (b) $\delta/\gamma=1$. Note that for $\bar{n}_{\rm th}=0$ the full quantum bispectrum coincides with the drive-dependent contribution $S_{\rm dr}[\omega_1,\omega_2]$.

The non-zero imaginary QBS is directly related to the basic symmetries of our quantum noise process, in particular the violation of Onsager-like time symmetry [123, 124, 126]. If a temporal cumulant $C^{(n+1)}(\vec{\tau}_n)$ is invariant under $\vec{\tau}_n \to -\vec{\tau}_n$ (i.e. the noise process satisfies microscopic reversibility), then the corresponding polyspectrum must be real [127]. Further, a classical Markov process obeying detailed balance always respects this symmetry. In our system quantum corrections (as described by $\tilde{S}_{\rm q}[\omega_1,\omega_2]$) cause a breaking of this symmetry and hence of detailed balance. There is a long history of studying detailed balance in driven-dissipative quantum systems (see e.g. [128–133]); the QBS provides yet another tool for exploring this physics. In Appendix 4.8.8, we discuss another related quantum system which exhibits an apparent breaking of detailed balance, namely a cavity driven by squeezed noise.

For a heuristic understanding of this symmetry breaking, we consider a simpler object, the temporal (Keldysh-ordered) third cumulant $C^{(3)}(\tau_1,\tau_2)$ at $\tau_1=\tau_2=t$. The non-zero imaginary QBS implies that this correlator differs for t and $-t$ (see Fig. 4.3). Using the definition of Keldysh ordering in Eqs. (4.3) and (4.4) we find:

$$\langle\delta\hat{n}(0)\delta\hat{n}(t)\delta\hat{n}(t)\rangle_{\mathcal{K}}=\frac{1}{2}\langle\{\delta\hat{n}(0),[\delta\hat{n}(t)]^2\}\rangle-\frac{\Theta(-t)}{4}\langle[\delta\hat{n}(t),[\delta\hat{n}(t),\delta\hat{n}(0)]]\rangle, \tag{4.11}$$

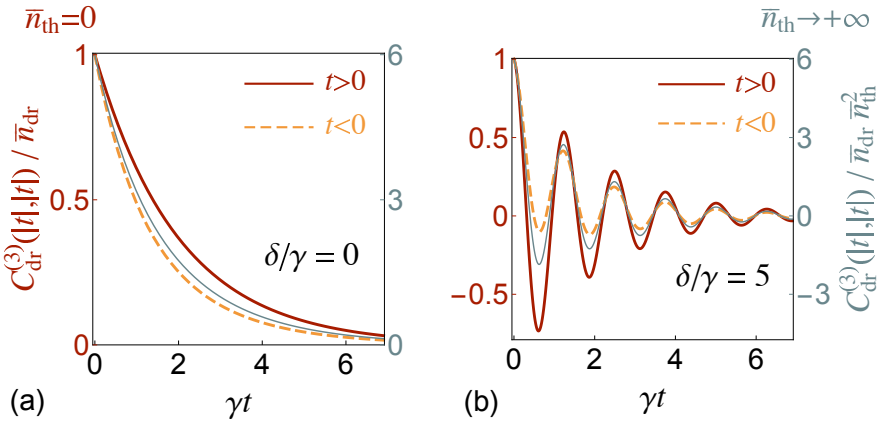

Fig. 4.3: Time-dependent Keldysh-ordered photon-shot noise third cumulant $C^{(3)}_{\rm dr}(|t|,|t|)$ in the quantum limit $\bar{n}_{\rm th} = 0$ for $t > 0$ (red solid lines) and $t < 0$ (orange dashed lines). Difference between curves highlights asymmetry under time reversal $t \to -t$. In contrast, the thin blue curves correspond to the same correlator $C^{(3)}_{\rm dr}(|t|,|t|)$ in the classical limit normalized by thermal photon number, which is symmetric. All correlation functions are normalized by in-cavity drive photon number $\bar{n}_{\rm dr}$. Detunings are: (a) $\delta = 0$, and (b) $\delta/\gamma = 5$.

where $\delta\hat{n}(t) = \hat{n}(t) - \langle\hat{n}(t)\rangle$, and $\Theta(t)$ is the Heaviside step-function. One finds that any imaginary quantum correction $\mathrm{Im}\tilde{S}_q[\omega_1,\omega_2]$ is entirely due to the second term on the RHS; it is thus completely responsible for the lack of time-symmetry.

What does this mean physically? As we have emphasized, the Keldysh ordering is relevant for any measurement protocol that directly probes $\hat{n}(t)$ [109, 112]. In contrast, the first term on the RHS of Eq. (4.11) would be relevant if we correlated a measurement of $\delta\hat{n}$ with a separate, direct measurement of $\delta\hat{n}^2$ (i.e. the Keldysh approach would give this answer for this sort of setup [112]). These protocols are not equivalent: measuring $\delta\hat{n}$ and then squaring the result has a different back-action than if one directly measured $\delta\hat{n}^2$. The latter measurement provides less information (and hence has less backaction), as it provides no information on the sign of $\delta\hat{n}$. This now provides a heuristic way of understanding the second term on the RHS of Eq. (4.11) (and the consequent lack of time symmetry). For $t < 0$, one is first measuring $\delta\hat{n}^2$. As a result, the two measurement protocols have different backaction effects, and the two correlation functions are distinct. In contrast, for $t > 0$, the earlier measurement is the same in both protocols, hence the backaction effect is identical,

and the two protocols agree.

While our heuristic explanation here invokes measurement backaction, we stress that the Keldysh-ordered correlation function is an *intrinsic* property of the driven cavity system [109, 118], with a relevance that goes beyond the analysis of just a single measurement setup. Further, this is the ordering that is "chosen" by our qubit: if one simply interprets the qubit dephasing as arising from classical noise, then the Keldysh ordered bispectrum (with its imaginary part) plays the role of the bispectrum of this effective classical noise.

4.7 Conclusions

We have shown how the Keldysh approach to quantum noise provides a meaningful way to define the polyspectra of non-classical, non-Gaussian noise. In the experimentally-relevant case of photon shot noise fluctuations in a driven-damped resonator, the quantum bispectrum reveals distinct quantum features and a surprising quantum-induced breaking of detailed balance. We stress that our approach amounts to interpreting the dephasing of a qubit by quantum noise as arising from an effective classical noise process. As such, the same noise spectroscopy techniques that have been used successfully to measure classical bispectra with qubits [103, 104] can be directly used (without modification) to measure our quantum bispectra.

4.8 Appendices

4.8.1 When is it necessary to consider Keldysh ordering, and when is it safe to ignore operator ordering in defining quantum noise cumulants?

In the main text, we have defined Keldysh-ordered cumulants in Eq. (4.3) to characterize a generic quantum noise process; the Keldysh ordering follows directly from standard rules of time evolution in the interaction picture. At first glance, this would seem to contradict

the definition in Ref. [103], which directly extends the definition of classical noise cumulants to the quantum case without specifying any particular time-ordering of bath operators (see unnumbered equation on page 2 of Ref. [103]). Their definition of the k-th cumulant can be written as

$$C^{(k)}(\vec{t}_k) \equiv \langle\langle \hat{\xi}\,(t_1) \cdots \hat{\xi}\,(t_k) \rangle\rangle, \tag{4.12}$$

where $\langle\langle \cdot \rangle\rangle$ relates the k-th cumulant to j-th moments $\langle \hat{\xi}\,(t_1) \cdots \hat{\xi}\,(t_j) \rangle$ for $j \leq k$, in exactly the same way as if $\hat{\xi}\,(t)$ were classical stochastic variables. Again, we stress that there is no time-ordering prescription specified here.

As we now show, there is in fact no contradiction between Eq. (4.12) and our definition in Eq. (4.3). This is because Ref. [103] at the outset restricts their discussion to the specific class of linearly coupled quantum oscillator baths (as is stated explicitly in the introduction of Ref. [103]). We discuss this more in what follows. Note that while Ref. [103] discussed some specific cases where their approach is valid, general conditions for its validity were not provided. As we show below, the basic requirement is that the commutator of the bath noise operator $\hat{\xi}(t)$ with itself at different times must simply be a number (or more generally, an operator that always commutes with $\hat{\xi}(t)$). This is only satisfied if the bath is a collection of harmonic oscillators, and the bath noise operator is linear in mode raising and lowering operators. We show this explicitly in what follows.

We start with the quantum bath models considered in Ref. [103], which consist of non-interacting bosonic modes a_k with Hamiltonian H_B and noise operator $B(t)$ of the form

$$H_B = \hbar \sum_k \Omega_k a_k^\dagger a_k, \tag{4.13}$$

$$B(t) = \sum_k (g_k e^{i\Omega_k t} a_k^\dagger + \text{h.c.}), \tag{4.14}$$

where noise operator is linear in raising and lowering operators, and the bath initial state $\rho_B(0)$ is chosen to be diagonal in the Fock basis to ensure stationarity. We now prove that the noise cumulants defined by Eq. (4.12), which ignores any operator ordering, agrees with the Keldysh-ordered quantum noise cumulants for these quantum baths. This is equivalent to showing that the Keldysh-ordered moment generating function (MGF) $\Lambda[F(t);t_f]$ in Eq. (4.3) now agrees with the MGF without any time ordering

$$\Lambda_{\rm cl}[F(t);t_f] \equiv {\rm Tr}\left[e^{-i\int_0^{t_f} dt' F(t')\hat{\xi}(t')}\hat{\rho}_{\rm B}\right], \tag{4.15}$$

where $\hat{\rho}_B$ is again the initial bath density matrix, and we use $\hat{\xi}(t)$ to denote general bath operators. It is straightforward to see that the cumulants in Eq. (4.12) (and in Ref. [103]) can be generated by $\ln\Lambda_{\rm cl}[F(t);t_f]$.

We thus seek to prove that $\Lambda_{\rm cl}[F(t);t_f] = \Lambda[F(t);t_f]$ for quantum bath described by Eqs. (4.13) and (4.14). Noting that for these baths, the commutators of bath noise operators $[\hat{\xi}(t'),\hat{\xi}(t'')]$ are just numbers. The following identity relations will then hold for generic $F(t)$

$$\mathcal{T}e^{-\frac{i}{2}\int_0^{t_f} dt' F(t')\hat{\xi}(t')} = \exp\left[-\hat{M}_1(t_f) - \hat{M}_2(t_f)\right], \tag{4.16}$$

$$\tilde{\mathcal{T}}e^{-\frac{i}{2}\int_0^{t_f} dt' F(t')\hat{\xi}(t')} = \exp\left[-\hat{M}_1(t_f) + \hat{M}_2(t_f)\right], \tag{4.17}$$

where

$$\hat{M}_1(t_f) = \frac{i}{2}\int_0^{t_f} dt' F(t')\hat{\xi}(t'), \tag{4.18}$$

$$\hat{M}_2(t_f) = \frac{1}{8}\int_0^{t_f} dt' \int_0^{t'} dt'' F(t')F(t')[\hat{\xi}(t'),\hat{\xi}(t'')], \tag{4.19}$$

and $[\hat{\xi}(t'),\hat{\xi}(t'')]$ is just a complex-valued function of t' and t''. Both equations can be rigorously proved by discretizing the time integral into N infinitesimal time intervals $\delta t = t_f/N$, so that the time- and anti-time-ordered operators can be rewritten as an ordered

product of propagators over these time increments, applying the Baker–Campbell–Hausdorff formula, and then taking the continuum limit $\delta t \to 0$ [76, 134]. Substituting Eqs. (4.16) and (4.17) into Eq. (4.3) for the Keldysh-ordered MGF $\Lambda[F(t); t_f]$, we obtain

$$\begin{aligned}
&\Lambda[F(t); t_f] \\
=&\mathrm{Tr}\left[\mathcal{T} e^{-\frac{i}{2}\int_0^{t_f} dt' F(t')\hat{\xi}(t')} \hat{\rho}_{\mathrm{B}} \tilde{\mathcal{T}} e^{-\frac{i}{2}\int_0^{t_f} dt' F(t')\hat{\xi}(t')}\right] \\
=&\mathrm{Tr}\left[e^{-2\hat{M}_1(t_f)}\hat{\rho}_{\mathrm{B}}\right] = \mathrm{Tr}\left[e^{-i\int_0^{t_f} dt' F(t')\hat{\xi}(t')}\hat{\rho}_{\mathrm{B}}\right] \\
=&\Lambda_{\mathrm{cl}}[F(t); t_f], \qquad (4.20)
\end{aligned}$$

which completes our proof. Incidentally, Eqs. (4.16) and (4.17) will also hold if the commutators $[\hat{\xi}(t'), \hat{\xi}(t'')]$ are still operators, but always commute with the bath operator $\hat{\xi}(t)$ at all times; for this scenario, the commutators $[\hat{\xi}(t'), \hat{\xi}(t'')]$ can be viewed equivalently as numbers as far as dynamics is concerned.

When the bath noise operator is given by Eq. (4.14), the bath dynamics will be completely linear, and any nontrivial non-Gaussianity can only be introduced via a non-Gaussian initial state. For example, Ref. [103] considered an initial bath state $\rho_B(0) = \rho_{T_1}/2 + \rho_{T_2}/2$ as a classical mixture of two thermal states at different temperatures T_1 and T_2. The non-Gaussian statistics here can be viewed as a result of the classical uncertainty in two different Gaussian distributions (i.e. uncertainty in temperature).

We also note that for any quantum bath where Eq. (4.20) is not true, Keldysh ordering cannot be ignored when defining noise cumulants. Further, there exist a variety of physical quantum baths where operator ordering plays an important role, and the Keldysh ordering leads to nontrivial corrections in non-Gaussian noise cumulants:

- Harmonic oscillator bath, where the bath operator is not linear in raising and lowering operators of the bosonic modes, e.g. the photon shot noise considered in the main text. Here the nonlinearity in the system-bath interaction induces nontrivial non-Gaussian

statistics with distinct quantum features.

- Interacting oscillator bath, i.e. bosonic bath with nonlinear dynamics, where the bath operator is linear in raising and lowering operators of the bosonic modes; this includes phonon bath with interactions. Keldysh ordering matters here due to the inherently nonlinear dynamics of the bath.

- Spin bath that exhibits non-Gaussian fluctuations. In this case, both the bath dynamics and the bath operator can induce non-Gaussian statistics, and it is in general nontrivial to apply the Keldysh ordering.

At the formal level, the Keldysh ordering is essential in these cases because the commutator $[\hat{\xi}(t'), \hat{\xi}(t'')]$ between bath operators at different times is a nontrivial operator (i.e. nonzero and does not commute with $\hat{\xi}(t)$). Due to the existence of these realistic examples of noise models where operator ordering is nontrivial, depending on the nature of quantum environments of interest, it may be important to be aware of the distinction between the most generic definition in Eq. (4.3), incorporating the Keldysh ordering, and the special case of linearly coupled oscillator baths, where Eq. (4.15) applies and the ambiguity in operator ordering can be ignored. In the main text, we also provide a concrete example where the Keldysh ordering results in unique quantum features in the quantum bispectrum, revealing a surprising breaking of detailed balance due to quantum fluctuations.

4.8.2 Keldysh-ordered quasiprobability distribution as a description of intrinsic noise

In the main text, we have focused on using the quantum bispectrum to understand the physics of the nontrivial energy fluctuations in a driven damped harmonic oscillator, and we state that a quasiprobability distribution can be defined for the Keldysh-ordered moment generating function (MGF) Λ. To elaborate on this and illustrate the generality of the

Keldysh approach, here we briefly summarize a pragmatic measurement setup, where the Keldysh-ordered quasiprobability distribution explicitly determines the measurement result. For more detailed discussions, the reader can refer to Refs. [109, 111, 112].

Nazarov and Kindermann [109] considered an idealized setup for measuring the statistics of a generic quantum observable $\hat{\phi}[F(t);t_f] = \int_0^{t_f} dt' F(t')\hat{\xi}(t')$ making use of an infinitely heavy mass. Without loss of generality, we assume that the detector mass is moving in 1-dimensional space with the Hamiltonian $\hat{H}_{\rm bath} = \hat{V}(\hat{x}) + \hat{p}^2/2m$. We also take the limit where the detector mass is infinitely heavy, i.e. $m \to \infty$, to avoid classical back action of the detector, so that it only measures *fluctuation* properties of the bath. The bath operator $\hat{\xi}(t)$ is coupled to the detector mass via the position operator $\hat{x}$, described by the Hamiltonian

$$\hat{H}_{\rm int}\,(t) = F(t)\hat{\xi}(t)\hat{x}, \tag{4.21}$$

and the detector-bath coupling $\hat{H}_{\rm int}(t)$ is on for time t_f.

If we were measuring a classical variable $\xi(t)$, the net effect of the coupling would be to simply shift the detector momentum by an amount $\phi = \int_0^{t_f} dt' F(t')\xi(t')$. For a classical stochastic process $\xi(t)$, the final momentum probability distribution function of the detector is just given by a convolution of the initial momentum distribution, and the probability distribution of momentum shifts $P(\phi)$. In the quantum regime, the detector state can no longer be represented by a classical probability distribution, but the aforementioned physical intuition still applies to a quasiprobability distribution, i.e. the Wigner function $W(x,p)$ of the detector state. However, for an operator $\hat{\xi}(t)$, the classical probability distribution $P(\phi)$ should be replaced by a Keldysh-ordered quasiprobability distribution $P(\phi;x)$, which is dependent on the detector position x. The Wigner function of the detector at final time t_f can thus be written as

$$W(x,p;t_f) = \int d\phi P(\phi;x) W(x,p-\phi;0), \tag{4.22}$$

which reproduces Eq. (15) in Ref. [109]. The Keldysh-ordered MGF discussed in Eq. (4.3) in the main text directly characterizes the quasiprobabilities $P(\phi; x)$. The idealized measurement here can be viewed as an illustration of the fact that Keldysh-ordered noise cumulants are intrinsic properties of the quantum bath, characterizing fluctuation properties. In the following section, we will also provide a rigorous justification, making use of the path-integral formulation of the Keldysh technique.

4.8.3 Distinguishing fluctuations from response properties

As discussed in the main text, a general n-point quantum correlation function describes both the intrinsic fluctuation properties of the system of interest (i.e. quantities that play the role of classical noise), as well as the response properties of the system to external applied fields. The situation is very clear at second order, where the product $\hat{\xi}(t)\hat{\xi}(t')$ can be decomposed as the sum of a commutator and an anti-commutator. The commutator determines the retarded Green function

$$G^R(t) \equiv -i\Theta(t) \left\langle [\hat{\xi}(t), \hat{\xi}(0)] \right\rangle . \tag{4.23}$$

This describes how the average value $\langle \hat{\xi}(t) \rangle$ changes to first order in response to an external perturbing field $V(t)$ entering the Hamiltonian as

$$\hat{H}_{\text{ext}}(t) = V(t)\hat{\xi}. \tag{4.24}$$

The relevant Kubo formula is:

$$\delta\langle \hat{\xi}(t) \rangle = \int_{-\infty}^{\infty} dt' G^R(t - t')V(t'). \tag{4.25}$$

In contrast, the anti-commutator describes the symmetrized noise spectral density:

$$S[\omega] \equiv \frac{1}{2}\int dt e^{i\omega t}\langle\{\hat{\xi}(t),\hat{\xi}(0)\}\rangle. \tag{4.26}$$

As has been discussed in many places (see e.g. Ref. [23]), this spectral density plays the role of a classical noise spectral density.

The Keldysh technique provides an unambiguous way of extending this separation between noise and response to higher orders. A full exposition of this method is beyond the scope of this paper; we refer the reader to Ref. [118]. We sketch the main ideas needed here. In the path-integral formulation of the Keldysh technique, each operator corresponds to two different fields, the classical field $\xi_{\rm cl}(t)$ and the quantum field $\xi_{\rm q}(t)$. Averages of these fields (weighted by the appropriate Keldysh action describing the system) then correspond to operator averages with a particular time ordering. One finds that:

- Averages only involving quantum fields are necessarily zero.
- Averages involving at least one classical field $\xi_{\rm cl}(t)$ and one or more quantum fields $\xi_{\rm q}(t)$ can always be interpreted as response coefficients to an external perturbation of the form $\hat{H}_{\rm ext}(t)$.
- Averages *only* involving classical fields $\xi_{\rm cl}(t)$ do not correspond to any kind of response function. Instead, they describe the intrinsic fluctuation properties of the system

Formally, this dichotomy arises because the perturbation $\hat{H}_{\rm ext}(t)$ enters the action of the system as a term that *only* involves the quantum field, i.e. $S_{\rm ext} = \int dt V(t)\xi_{\rm q}(t)$. Perturbation theory in $V(t)$ thus necessarily introduces powers of the quantum field. For example, at second order we have:

- The average $\overline{\xi_{\rm cl}(t)\xi_{\rm q}(0)}$ is directly proportional to the retarded Green function $G^R(t)$, and thus describes linear response to the external field.

- The average $\overline{\xi_{\rm cl}(t)\xi_{\rm cl}(0)}$ is proportional to $\langle\{\hat{\xi}(t),\hat{\xi}(0)\}\rangle$ and thus determines the usual symmetrized noise spectral density.

The same decomposition applies at higher orders. Consider third order correlators. The average of three classical fields $\overline{\xi_{\rm cl}(t_1)\xi_{\rm cl}(t_2)\xi_{\rm cl}(0)}$ is precisely the Keldysh ordered correlator discussed in the main text; it cannot be associated with a response coefficient. The remaining non-zero correlators describe different kinds of response:

- The average $\overline{\xi_{\rm cl}(t)\xi_{\rm q}(t')\xi_{\rm q}(t'')}$ represents a second-order Kubo response coefficient. It determines to second order how $\langle\hat{\xi}(t)\rangle$ is modified by $\hat{H}_{\rm ext}(t')$ at earlier times (i.e. how it depends on $V(t')$ and $V(t'')$).

- The average $\overline{\xi_{\rm cl}(t)\xi_{\rm cl}(t')\xi_{\rm q}(t'')}$ describes a first order noise-susceptibility [135]. It determines how the symmetrized correlator $\langle\{\hat{\xi}(t),\hat{\xi}(t')\}\rangle$ is modified to first order by $\hat{H}_{\rm ext}(t'')$

The arguments sketched here provided perhaps the deepest justification for considering Keldysh ordered correlation functions: they provide a clear and unambiguous way to distinguish fluctuation properties from response properties. We stress that an arbitrary correlation function could always be written as a linear combination of the Keldysh-ordered correlator (which describes pure noise) and additional terms describing response properties.

4.8.4 Explicit expressions for the second and third Keldysh-ordered cumulants

For concreteness, here we provide explicit expressions for the first few Keldysh-ordered cumulants $C^{(k)}(\vec{t}_k) \equiv \langle\langle\hat{\xi}\,(t_1)\cdots\hat{\xi}\,(t_k)\rangle\rangle_{\mathcal{K}}$ defined by Eqs. (4.3) and (4.4) in the main text. The second order cumulant function $C^{(2)}(\vec{t}_2)$ is just the auto-correlation function of $\hat{\xi}(t)$

$$C^{(2)}(\vec{t}_2) = \langle\langle\hat{\xi}\,(t_1)\,\hat{\xi}\,(t_1)\rangle\rangle_{\mathcal{K}} = \frac{1}{2}\langle\{\delta\hat{\xi}\,(t_1)\,,\delta\hat{\xi}\,(t_1)\}\rangle, \tag{4.27}$$

where $\delta\hat{\xi} = \hat{\xi} - \langle\hat{\xi}\rangle$. However, the third cumulant corresponds to a more complex ordering

$$C^{(3)}(\vec{t}_3) = \langle\langle\hat{\xi}\,(t_1)\,\hat{\xi}\,(t_2)\,\hat{\xi}\,(t_3)\rangle\rangle_{\mathcal{K}}$$
$$= \frac{1}{4}\sum_{\vec{\pi}_3\in\mathcal{P}_3} K(t_{\pi_1}, t_{\pi_2}, t_{\pi_3})\langle\delta\hat{\xi}(t_{\pi_1})\delta\hat{\xi}(t_{\pi_2})\delta\hat{\xi}(t_{\pi_3})\rangle, \tag{4.28}$$

$$K(\vec{t}_3) = 1 - \Theta(t_1 - t_2)\Theta(t_3 - t_2), \tag{4.29}$$

where $\mathcal{P}_3$ denotes the set of all possible permutations of (123) indices, and $\Theta(t)$ is the Heaviside step function. Such ordering is given by an average over all permutations of the three displaced operators $\delta\hat{\xi}(t_j)$, except for the terms where the earliest time appears in the middle position (as implied by the step functions), in agreement with expansion of the operator in Eq. (4.3) in powers of coupling $F(t')$. A similar expression of Keldysh-ordered third cumulant has also been derived for current operators in Ref. [120].

4.8.5 Phase space method for computing Keldysh-ordered cumulants of a driven damped cavity

In this subsection, we outline the phase space method to calculate Keldysh-ordered cumulants. However, we remark that once we have defined the unique Keldysh ordering for each higher cumulant using Eqs. (4.3) and (4.4), standard techniques for computing multi-point correlation functions (e.g. Langevin equations of motion, and quantum regression theorem) work equally well for the Keldysh-ordered cumulants.

In the phase space method, we need to solve the time evolution of qubit coherence operator $\hat{\rho}_{\uparrow\downarrow}(t) \equiv \langle\uparrow|\hat{\rho}(t)|\downarrow\rangle$, so that the qubit coherence can be computed as $\langle\hat{\sigma}_-(t)\rangle = \mathrm{Tr}[\hat{\rho}_{\uparrow\downarrow}(t)]$. We first restrict to the qubit off-diagonal block of the master equation in Eq. (4.6)

in the main text as

$$\dot{\hat{\rho}}_{\uparrow\downarrow} = -i[\hat{H}_0, \hat{\rho}_{\uparrow\downarrow}] - i\frac{\lambda}{2}\{F(t)\hat{n}, \hat{\rho}_{\uparrow\downarrow}\} + \gamma(\bar{n}_{\rm th}+1)\mathcal{D}[\hat{c}]\hat{\rho}_{\uparrow\downarrow} + \gamma\bar{n}_{\rm th}\mathcal{D}[\hat{c}^\dagger]\hat{\rho}_{\uparrow\downarrow}, \tag{4.30}$$

which is a direct extension, with a time-modulation $F(t)$ in interaction $\hat{H}_{\rm int}(t) = \lambda F(t)\hat{n}\hat{\sigma}_z/2$, of the technique used in Ref. [122]. Here we use a constant coefficient λ to keep track of orders in expansion on the coupling; by the end of the calculation, one can always set $\lambda = 1$. We stress that if we replace the time-independent coupling λ with a time-dependent one, the relevant derivations in Ref. [122] still hold rigorously, and we refer interested readers to this paper for more detail.

Without loss of generality, the system initial state can be chosen as a product state between the qubit and the cavity, with the cavity in thermal equilibrium. Thus, Wigner function $W(x,p;t)$ of the coherence operator $\hat{\rho}_{\uparrow\downarrow}(t)$ is Gaussian throughout time evolution. Moreover, for the Fourier transform of $W(x,p;t)$, we can assume the following ansatz [122]

$$W[k,q;t] = e^{-\nu(t)}\exp\left(-i[k\bar{x}(t)+q\bar{p}(t)] - \frac{1}{2}(k^2+q^2)\sigma_s(t)\right), \tag{4.31}$$

from which the moment generating function can be computed as $\Lambda[F(t);t_f] = e^{-\nu(t_f)}$. Substituting this ansatz into the master equation in Eq. (4.30), we then need to solve a set of ordinary differential equations for the coefficient functions

$$\dot{\nu}_{\rm th} = i\lambda F(t)\left(\sigma_s - \frac{1}{2}\right), \tag{4.32a}$$

$$\dot{\sigma}_s = \gamma\left(\bar{n}_{\rm th}+\frac{1}{2}\right) - \gamma\sigma_s - iF(t)\lambda\sigma_s^2 + \frac{i\lambda F(t)}{4}, \tag{4.32b}$$

$$\dot{\nu}_{\rm dr} = \frac{i\lambda}{2}F(t)(\bar{x}^2+\bar{p}^2), \tag{4.32c}$$

$$\dot{\bar{x}} = -\delta\bar{p} + \sqrt{2}\,{\rm Im}f - iF(t)\lambda\sigma_s\bar{x} - \frac{\gamma}{2}\bar{x}, \tag{4.32d}$$

$$\dot{\bar{p}} = \delta\bar{x} + \sqrt{2}\,{\rm Re}f - iF(t)\lambda\sigma_s\bar{p} - \frac{\gamma}{2}\bar{p}, \tag{4.32e}$$

where the exponent $\nu(t) = \nu_{\rm th}(t) + \nu_{\rm dr}(t)$ can be written as a sum of drive-independent and drive-dependent parts.

The Keldysh-ordered cumulants $C^{(\ell)}(\vec{t}_\ell)$ can now be extracted using the equation (see Eq. (4.4) in the main text)

$$\nu(t_f) = -\sum_{\ell=1}^{\infty} \lambda^\ell \frac{(-i)^\ell}{\ell!} \prod_{j=1}^{\ell} \left[\int_0^{t_f} dt_j F(t_j) \right] C^{(\ell)}(\vec{t}_\ell), \tag{4.33}$$

i.e. the cumulants can be obtained by solving Eqs. (4.32) perturbatively in orders of λ, and comparing the results to the integrals above. Since the cumulant functions $C^{(\ell)}(\vec{t}_\ell)$ must be symmetric over permutations of its variables $\{\vec{t}_\ell\}$, such procedure will lead to a unique result. For example, for the photon shot noise in a driven damped cavity discussed in the main text, first few drive-independent contributions to cumulants are given by

$$C^{(1)}_{\rm th}(t_1) = \bar{n}_{\rm th}, \tag{4.34a}$$

$$C^{(2)}_{\rm th}(\vec{t}_2) = \bar{n}_{\rm th}(\bar{n}_{\rm th}+1) e^{-\gamma|t_1 - t_2|}, \tag{4.34b}$$

$$C^{(3)}_{\rm th}(\vec{t}_3) = \bar{n}_{\rm th}(\bar{n}_{\rm th}+1)(2\bar{n}_{\rm th}+1) \exp\left(-\frac{\gamma}{2}|t_1 - t_2| - \frac{\gamma}{2}|t_2 - t_3| - \frac{\gamma}{2}|t_1 - t_3| \right). \tag{4.34c}$$

Taking Fourier transform of Eq. (4.34c) for the third cumulant, we obtain the drive-independent QBS, as given by Eq. (4.8) in the main text.

4.8.6 Quantum bispectrum (QBS) probed by qubit dephasing

In the main text and above, we introduced the ancilla qubit mostly as a theoretical tool to characterize the quantum bath fluctuations. However, as mentioned in the main text, the qubit-bath system is also a well-studied experimental probe to measure the QBS of a given quantum bath. The QBS of the bath can be extracted, by measuring the qubit coherence function $\langle \hat{\sigma}_-(t_f) \rangle$ evolving under given filter functions $F(t)$. Ref. [103] discusses a systematic

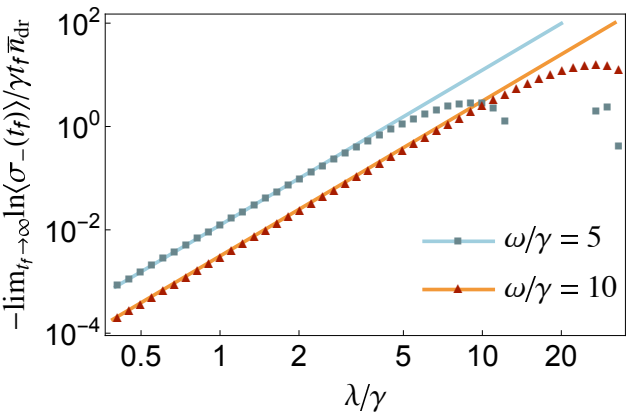

Fig. 4.4: Photon shot noise induced qubit frequency renormalization, as defined from the long time limit of the qubit coherence function, $-\lim_{t_f\to\infty}\mathrm{Im}\ln\langle\hat{\sigma}_-(t_f)\rangle/t_f$. We use here a filter function $F(t) = \lambda(\sin 2\omega t + \cos\omega t)$, and plot the frequency shift as function of coupling strength λ. The two curves correspond to two different choices of filter function center frequencies ω (as indicated in the legend). Solid lines depict contributions from QBS and have exact slopes of 3, as these terms are proportional to λ^3, whereas the data points are exact results by solving Eqs. (4.32) numerically (and thus include contributions from all higher-order odd noise cumulants). The QBS prediction describes the induced phase shift accurately over a range of weak to moderate couplings. Data points with an opposite frequency shift are not shown (the QBS approximation completely breaks down for these points). Parameters: $\delta = 10\gamma$, $\bar{n}_{\rm th} = 0$, $\bar{n}_{\rm dr} = 1$.

approach to reconstruct the bispectrum using this technique of qubit noise spectroscopy.

Here, we apply this idea to the specific noise model discussed in the main text. We consider qubit dephasing due to photon shot noise of a driven damped cavity mode, as described by the master equation in Eq. (4.6). As an illustration, we focus on the idealized filter function

$$F(t) = \lambda(\sin 2\omega t + \cos\omega t), \quad t \in [0, t_f], \tag{4.35}$$

where λ characterizes the coupling strength. This filter function is chosen such that for any coupling strength, the qubit coherence has no dependence on the real part of the QBS, i.e.

$$\mathrm{Im}\ln\langle\hat{\sigma}_-(t_f)\rangle = \mathrm{Im}\chi[F(t); t_f] = \frac{\lambda^3 t_f}{16}\mathrm{Im}S[\omega,\omega] + o(\lambda^5). \tag{4.36}$$

As discussed in the main text, the imaginary part of the QBS, which can be computed from Eq. (4.10), is a unique quantum feature and only depends on driven fluctuations. This phase shift is solely due to the non-Gaussian noise cumulants, and will be absent if we treat the noise operator as Gaussian. We compare above prediction based on the QBS to the induced frequency shift in the exact qubit coherence function in the long time limit

$$\lim_{t_f\to\infty} \frac{\mathrm{Im}\ln\langle\hat{\sigma}_-(t_f)\rangle}{t_f}, \tag{4.37}$$

which is calculated numerically by solving Eqs. (4.32). The results are plotted in Fig. 4.4 for the case of zero temperature $\bar{n}_{\rm th} = 0$, where the qubit dephasing is solely due to driven fluctuations. As shown in the plot, the QBS prediction agrees excellently with the exact result for small coupling λ as expected, but will deviate from the exact result as coupling λ increases. The QBS prediction works even at moderate couplings $\lambda/\gamma \sim 1$, because the higher cumulants here are suppressed by the large detuning $\delta/\gamma \gg 1$. The QBS thus has a concrete operational interpretation: it quantifies the leading order non-Gaussian correction in the qubit dephasing due to a given quantum noise process $\hat{\xi}(t)$.

4.8.7 Proof of non-negative energy shot noise bispectrum in a classical driven damped oscillator

In the classical limit $\bar{n}_{\rm th} \to \infty$, the cavity mode annihilation operator $\hat{c}$ in the main text can be described by a classical stochastic variable $c(t)$, describing the amplitude of a driven damped classical harmonic oscillator. The equation of motion is now given by

$$dc = -(\gamma/2 - i\delta)c dt + i f dt + \sqrt{\gamma\bar{n}_{\rm eff}}dW, \tag{4.38}$$

where $\bar{n}_{\rm eff} = \bar{n}_{\rm th} + 1/2 \simeq \bar{n}_{\rm th}$ (the 1/2 correction is added so that second-order correlators between $c(t)$, $c^*(t')$ match their symmetrized quantum counterparts), and dW is a complex-

valued Wiener increment. The solution to this stochastic differential equation can be written as $c(t) = c_0 + \zeta(t)$, where $c_0 = \langle c(t) \rangle$ is a complex constant number, and $\zeta(t)$ is a complex zero-mean stochastic variable. In the long time limit, $\zeta(t)$ is Gaussian and stationary, satisfying the equation

$$\langle \zeta^*(t)\zeta(t') \rangle = \bar{n}_{\text{eff}} \exp\Big[-i\delta(t-t') - \frac{\gamma}{2}|t-t'|\Big], \tag{4.39}$$

whereas all other second correlators vanish $\langle \zeta(t)\zeta(t') \rangle = \langle \zeta^*(t)\zeta^*(t') \rangle^* \equiv 0$. The photon number operator $\hat{n}$ then corresponds to the energy of the classical oscillator $n(t) = |c(t)|^2$, so that its Fourier transform can be expressed using Fourier components of $\zeta(t)$ as

$$\begin{aligned} n[\omega] =& \int dt e^{i\omega t} n(t) \\ =& |c_0|^2 + \int d\omega' \zeta^*[\omega - \omega']\zeta[\omega'] + c_0^* \zeta[\omega] + c_0 \zeta^*[\omega]. \end{aligned} \tag{4.40}$$

Since the Fourier transform $\zeta[\omega]$ of a Gaussian variable must also be Gaussian, polyspectra of $n(t)$ can be calculated using the expression above by applying Wick's theorem. Noting that all the anomalous correlators vanish, the only contractions that contribute would be given by terms of the following form

$$\langle \zeta^*[\omega]\zeta[\omega'] \rangle = \frac{\gamma \bar{n}_{\text{eff}}}{(\omega - \delta)^2 + \left(\frac{\gamma}{2}\right)^2} \delta(\omega + \omega'), \tag{4.41}$$

which is always non-negative. It is then straightforward to show that both drive-independent and drive-dependent contributions to polyspectra must also be non-negative for all frequencies. In particular, the frequency dependence $\tilde{S}_{\text{cl}}[\omega_1, \omega_2]$ of the drive-dependent bispectrum in the classical limit (see main text for definition) is real and positive semidefinite, which

can be explicitly written as

$$\tilde{S}_{\rm cl}[\omega_1,\omega_2]=\frac{1}{\gamma^2}\sum_{\substack{\alpha\neq\beta\\ \alpha,\beta=1,2,3}}\frac{1}{\left[1+4\left(\frac{\omega_\alpha+\delta}{\gamma}\right)^2\right]\left[1+4\left(\frac{\omega_\beta-\delta}{\gamma}\right)^2\right]}. \tag{4.42}$$

4.8.8 Temporal skewness for squeezed bath photon fluctuations

In the main text, we show a violation of higher-order Onsager reciprocity relations solely due to quantum corrections in the temporal third cumulant (skewness), which can be probed by an imaginary part in the QBS. Here we provide an example where the temporal skewness exhibits time asymmetry in both the classical and the quantum limits, and the skewness function also reveals insights into non-equilibrium dynamics in well-defined classical systems. We again consider photon shot noise in a dissipative bosonic mode, but now driven by squeezed noise. The master equation is

$$\dot{\hat{\rho}}=-i[\hat{H}_0+\hat{H}_{\rm int},\hat{\rho}]+\gamma(\bar{n}_{\rm cl}+1)\mathcal{D}[\hat{s}_r]\hat{\rho}+\gamma\bar{n}_{\rm cl}\mathcal{D}[\hat{s}_r^\dagger]\hat{\rho}, \tag{4.43}$$

where $\hat{s}_r=\hat{c}\cosh r+\hat{c}^\dagger\sinh r$ denotes the squeezed bath operator. In the rotating frame, the oscillator Hamiltonian is $\hat{H}_0=-\delta\hat{c}^\dagger\hat{c}$, and its interaction with the qubit is $\hat{H}_{\rm int}(t)=\frac{1}{2}F(t)\hat{n}(t)\hat{\sigma}_z$. Such noise model has a well-defined classical limit if we let $\bar{n}_{\rm cl}\to\infty$, where the bosonic mode can be equivalently described by a classical stochastic variable $c(t)$. We note that the steady state of the corresponding classical model is not thermal equilibrium, enabling a violation of Onsager-like relations even in the classical limit.

For concreteness, we again consider the temporal third cumulant $C^{(3)}(t,t)$, which can be written as a sum of classical and quantum contributions as

$$C^{(3)}(t,t)=(2\bar{n}_{\rm cl}+1)^3 f(t)\left[\tilde{C}^{(3)}_{\rm cl}(t)-\frac{1}{(2\bar{n}_{\rm cl}+1)^2}\right], \tag{4.44}$$

where $f(t) = e^{-\gamma|t|}\cosh(2r)/4$ is an even function of time t and independent of $\bar{n}_{\rm cl}$. The coefficient function $\tilde{C}^{(3)}_{\rm cl}(t)$ for the classical contribution is given by

$$\tilde{C}^{(3)}_{\rm cl}(t) = \cosh^2(2r) + \frac{\gamma^2 \sinh^2(2r)}{\gamma^2 + 4\delta^2}[1 + 2\cos(\delta t + \delta|t|)]. \tag{4.45}$$

The situation is now reversed: the quantum correction is symmetric under time reversal $t \to -t$, whereas the classical contribution is asymmetric for a generic nonzero detuning $\delta \neq 0$.

The time asymmetry in $C^{(3)}(t,t)$ has its roots in classical non-equilibrium dynamics: in the classical limit $\bar{n}_{\rm cl} \gg 1$, we can introduce two real quadratures x and p defined by $c = (x + ip)/\sqrt{2}$ to describe the corresponding classical oscillator. Their dynamics satisfies the stochastic differential equations

$$dx = (-\delta p - \frac{\gamma}{2}x)dt + e^r\sqrt{\gamma\bar{n}_{\rm eff}}dW_1, \tag{4.46a}$$

$$dp = (\delta x - \frac{\gamma}{2}p)dt + e^{-r}\sqrt{\gamma\bar{n}_{\rm eff}}dW_2, \tag{4.46b}$$

where $\bar{n}_{\rm eff} = \bar{n}_{\rm cl} + 1/2 \simeq \bar{n}_{\rm cl}$, and dW_1 and dW_2 are independent Wiener increments. These equations formally also describe time evolution of a resonantly coupled pair of real harmonic modes, where the interaction strength is given by $|\delta|$, and each oscillator is also coupled to a thermal reservoir with thermal excitations $e^{\pm 2r}\bar{n}_{\rm eff}$. This coupled two-mode system for $r \neq 0$ is a typical example of non-equilibrium system that violates detailed balance, manifested as time asymmetry in cross correlation functions $\langle A(0)B(t)\rangle$ [131–133]. Noting that $n(t)$ corresponds to the total energy in the classical limit, the skewness $C^{(3)}(t,t)$ can then be viewed as a correlation function between energy fluctuations $\delta n(0)$ and its higher order fluctuations $[\delta n(t)]^2$ at a different time. Thus, the time asymmetry in $C^{(3)}(t,t)$ is again a signature of detailed balance violation, which in turn is due to the imbalanced thermal baths set by the nonzero r.

CHAPTER 5

INTRINSIC AND INDUCED QUANTUM QUENCHES FOR ENHANCING QUBIT-BASED QUANTUM NOISE SPECTROSCOPY

5.1 Overview of results

Quantum sensing protocols that exploit the dephasing of a probe qubit are powerful and ubiquitous methods for interrogating an unknown environment. They have a variety of applications, ranging from noise mitigation in quantum processors, to the study of correlated electron states. In this chapter, we discuss a simple strategy for enhancing these methods, based on the fact that they often give rise to an inadvertent quench of the probed system: there is an effective sudden change in the environmental Hamiltonian at the start of the sensing protocol. These quenches are extremely sensitive to the initial environmental state, and lead to observable changes in the sensor qubit evolution. We show how these new features give access to environmental response properties. This enables methods for direct measurement of bath temperature, and for detecting non-thermal equilibrium states. We also discuss how to deliberately control and modulate this quench physics, which enables reconstruction of the bath spectral function. Extensions to non-Gaussian quantum baths are also discussed, as is the application of our ideas to a range of sensing platforms (e.g., nitrogen-vacancy (NV) centers in diamond, semiconductor quantum dots, and superconducting circuits).

5.2 Introduction

A key technique in quantum sensing is to use a suitably driven sensor qubit to characterize a noisy, dissipative environment. Commonly referred to as quantum noise spectroscopy (QNS) [137], this modality allows one to understand and possibly mitigate sources of decoherence that degrade a quantum processor [103, 104, 124, 138–152]. It also serves as a powerful means to probe a complicated many-body target system via its fluctuation properties (see, e.g., [153–157]). While many QNS protocols focus on the more specific problem of characterizing classical Gaussian noise [140–148], recent work has explored methods that go beyond these assumptions [100, 103, 104, 113, 124, 149–152, 158–161].

One crucial difference between a true quantum environment and a simple classical noise source is that the former is dynamical: its properties can change in response to an external perturbation. At a simple linear response level, this is encoded in the environment's susceptibility functions, or equivalently, asymmetric-in-frequency quantum noise spectral densities [23, 162–165]. The most direct (and perhaps extreme) way to probe these properties is to induce a quantum quench, where the environment experiences a sudden change in its Hamiltonian. Studying the consequences of deliberate quenches has been an extremely useful tool for probing a variety of phenomena in correlated systems [166].

In this chapter, we show that the basic physics of a quantum quench is relevant to a wide variety of commonly employed QNS schemes and systems; crucially, this is the case even if the protocol does not involve a deliberate quenching of the environment. We show how these quenches (whether intrinsic or deliberate) can be harnessed as a powerful new sensing modality: they reveal environmental response properties in previously unexplored ways. By analyzing standard T_2-type qubit-based QNS protocols, we identify generic conditions under which an inadvertent quench of the environment influences the sensor qubit's evolution. Surprisingly, the existence and properties of this quench effect are not simply a function of the initial environmental Hamiltonian, but instead depend on the initial environmental state.

The dominant effect of the quench is an unexpected phase shift of the sensor qubit coherence. For common cases where the environment is either a Gaussian quantum bath or the sensor-environment coupling is weak, we derive a simple, analytical expression connecting this quench phase shift (QPS) to a dissipative susceptibility of the environment (i.e. an effective density of states). We then use this to address a number of phenomena. In particular, using the extra information provided by the QPS, a standard T_2-based QNS protocol can be enhanced to independently characterize both fluctuation and response properties. As we discuss, such information lets us determine the temperature of a thermal equilibrium environment, making only mild assumptions encompassing a wide range of realistic scenarios (including sub-, super-, and Ohmic environments, environments generating $1/f$ noise, etc.). For the paradigmatic case of an environment with an Ohmic spectral density, we show that one can use the QPS (along with standard decoherence measurements) in a simple Hahn-echo protocol to directly extract the environmental temperature (something that cannot be done from decoherence measurements alone). We also show that the quench mechanism is relevant to generic initial bath states beyond equilibrium, and can be used to probe response properties in nonequilibrium systems. We further discuss extensions of this physics in regimes beyond the validity of linear response.

5.3 Intrinsic quantum quenches in standard T_2-type sensing protocols

While our ideas apply to a wide variety of settings, we focus throughout this chapter on a standard QNS experiment where the sensor qubit is coupled to an environment via a pure-dephasing interaction. Transforming to the standard toggling frame set by the choice of qubit control pulses (see e.g. [137]), as well as the rotating frame with respect to free qubit

Hamiltonian $\Omega\hat{\sigma}_z/2 = (\Omega/2)\left(|\uparrow\rangle\langle\uparrow| - |\downarrow\rangle\langle\downarrow|\right)$, the qubit-bath Hamiltonian is given by

$$\hat{H}_{\rm tot} = |\uparrow\rangle\langle\uparrow| \otimes \hat{H}_{{\rm b},\uparrow} + |\downarrow\rangle\langle\downarrow| \otimes \hat{H}_{{\rm b},\downarrow}, \tag{5.1}$$

where $\hat{H}_{{\rm b},\uparrow}$ ($\hat{H}_{{\rm b},\downarrow}$) describes the bath Hamiltonian conditioned on qubit being in the state $|\uparrow\rangle$ ($|\downarrow\rangle$). We set $\hbar = 1$ throughout. As in standard T_2-type measurements, the probe qubit is initialized in $|\downarrow\rangle$ and is initially unentangled with the bath. The quench physics we describe is crucially sensitive to the initial state of the bath. For illustrative purposes, we first focus on a simple but generic situation where the qubit $|\downarrow\rangle$ state lifetime can be viewed as infinite, and the bath has relaxed to a thermal equilibrium state with respect to $\hat{H}_{{\rm b},\downarrow}$. The initial density matrix of the qubit-bath system is thus

$$\hat{\rho}_{\rm tot}(t = 0^-) = |\downarrow\rangle\langle\downarrow| \otimes \hat{\rho}_{\rm b,i}, \tag{5.2a}$$

$$\hat{\rho}_{\rm b,i} = e^{-\hat{H}_{{\rm b},\downarrow}/k_B T}/Z_T, \tag{5.2b}$$

where Z_T is a normalization factor and T is the initial bath temperature. We stress that the initial bath state $\hat{\rho}_{\rm b,i}$ closely depends on the initial qubit state: again assuming the system has reached thermal equilibrium prior to start of the sensing protocol, and if instead the qubit is initialized in $|\uparrow\rangle$, then $\hat{\rho}_{\rm b,i}$ would be a thermal state with respect to $\hat{H}_{{\rm b},\uparrow}$.

We consider a standard T_2-based sensing protocol. At the start of the protocol ($t = 0$), an instantaneous $\pi/2$-pulse is applied to prepare the qubit in an equal superposition state $|+\rangle \equiv \left(|\uparrow\rangle + |\downarrow\rangle\right)/\sqrt{2}$; the system then evolves under $\hat{H}_{\rm tot}$ for time t_f, while the qubit is subject to a sequence of instantaneous control π-pulses. At the end of the protocol, one measures qubit Pauli operator $\hat{\sigma}_x$ or $\hat{\sigma}_y$. By repeating the measurements and varying t_f, one can obtain the qubit coherence $\langle\hat{\sigma}_-(t_f)\rangle$ as a function of t_f.

Surprisingly, in many cases an intrinsic effective bath quench occurs as part of this stan-

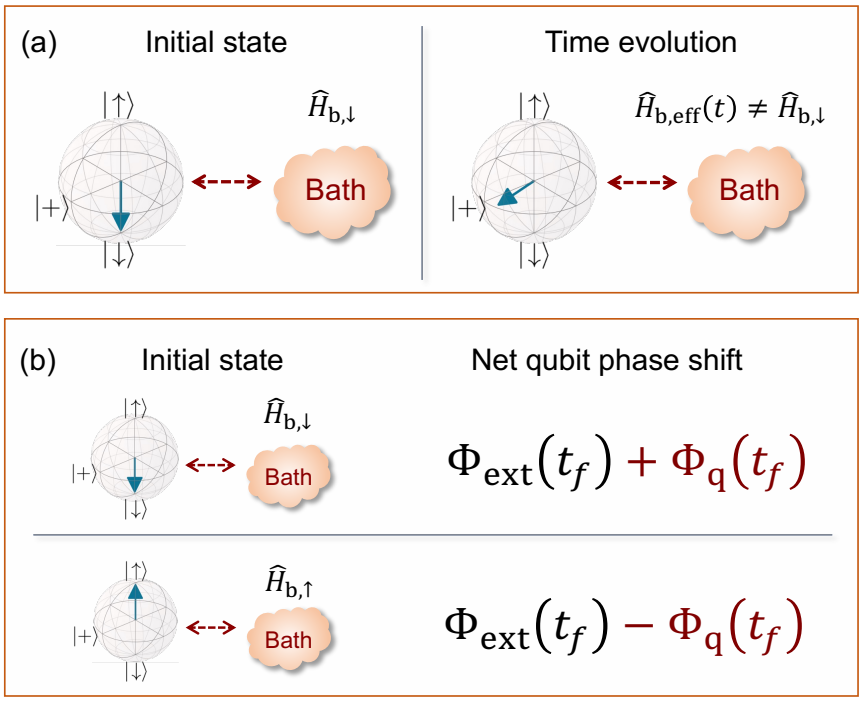

Fig. 5.1: Quantum quenches in standard dephasing-based quantum sensing (noise spectroscopy) protocols. (a) Schematic illustrating an "intrinsic" quantum quench arising in standard T_2-type experiments, where the effective bath Hamiltonian undergoes a sudden change at the start of the protocol, c.f. Eq. (5.4). (b) The quench manifests itself as an additional quench phase shift (QPS) $\Phi_q(t_f)$ of the sensor qubit. The QPS can be distinguished from a phase $\Phi_{\text{ext}}(t_f)$ resulting from an external field: in the simplest case, it is crucially sensitive to the initial qubit state before the start of the sensing protocol.

dard sensing protocol. To see this, we first rewrite $\hat{H}_{\text{tot}}$ as

$$\hat{H}_{\text{tot}} = \frac{1}{2}\hat{\sigma}_z \otimes \hat{\xi} + \hat{\sigma}_0 \otimes \frac{1}{2}(\hat{H}_{b,\uparrow} + \hat{H}_{b,\downarrow}), \tag{5.3}$$

with $\hat{\xi} \equiv \hat{H}_{b,\uparrow} - \hat{H}_{b,\downarrow}$, $\hat{\sigma}_0 \equiv |\uparrow\rangle\langle\uparrow| + |\downarrow\rangle\langle\downarrow|$. This suggests a simple picture for understanding the qubit evolution during the protocol: the qubit dephases due to coupling to the bath noise operator $\hat{\xi}$, while the bath evolves under an effective averaged bath Hamiltonian. Note that these two processes are not independent, as the effective bath Hamiltonian would affect $\hat{\xi}$ during time evolution and hence influence qubit dynamics.

Notably, the averaged bath Hamiltonian in Eq. (5.3) may or may not commute with the

initial bath state, which in our example is determined by $\hat{H}_{\mathrm{b},\downarrow}$. As shown in Fig. 5.1, this motivates defining a time-dependent effective bath Hamiltonian $\hat{H}_{\mathrm{b,eff}}(t)$ whose form reflects the change of the qubit state $\hat{\rho}_{\mathrm{qb}}$ at $t = 0$:

$$\hat{H}_{\mathrm{b,eff}}(t) \equiv \mathrm{Tr}_{\mathrm{qb}}[\hat{\rho}_{\mathrm{qb}}(t)\hat{H}_{\mathrm{tot}}(t)], \tag{5.4a}$$

$$= \begin{cases} \hat{H}_{\mathrm{b},\downarrow}, & t \leq 0, \\ (\hat{H}_{\mathrm{b},\uparrow} + \hat{H}_{\mathrm{b},\downarrow})/2, & 0 < t < t_f. \end{cases} \tag{5.4b}$$

We see that except for the trivial case $\hat{H}_{\mathrm{b},\uparrow} = \hat{H}_{\mathrm{b},\downarrow}$, the bath Hamiltonian $\hat{H}_{\mathrm{b,eff}}(t)$ exhibits a sudden change (i.e., a quench) that is solely due to the sudden change in qubit state at $t = 0$. As we show below in Eq. (5.8), this quench is physically meaningful: it directly determines the evolution of the qubit coherence $\langle\hat{\sigma}_-(t_f)\rangle$, the very quantity that is measured in the protocol.

For our subsequent discussion, it is useful to rewrite $\hat{H}_{\mathrm{b,eff}}(t)$ to make the quench more explicit:

$$\hat{H}_{\mathrm{b,eff}}(t) = \hat{H}_{\mathrm{b,i}} + \eta(t)\hat{V}. \tag{5.5}$$

Here $\eta(t)$ is an effective quench control function, which encodes the temporal profile of the quench. $\hat{V}$ represents the quench operator, which is defined as

$$\hat{V} \equiv \hat{H}_{\mathrm{b,eff}}(t = 0^+) - \hat{H}_{\mathrm{b,eff}}(t = 0^-). \tag{5.6}$$

For the specific example considered here, we have $\hat{H}_{\mathrm{b,i}} = \hat{H}_{\mathrm{b},\downarrow}$ and

$$\eta(t) = \Theta(t)\Theta(t_f - t), \tag{5.7a}$$

$$\hat{V} = \hat{\xi}/2, \tag{5.7b}$$

where $\Theta(t)$ is the Heaviside step function. If the total initial state is in thermal equilibrium with respect to $\hat{H}_{\rm tot}$ in Eq. (5.1), we can again define $\hat{H}_{\rm b,i}$ using Eq. (5.4a) as the bath Hamiltonian contingent on the initial qubit state. The quench operator $\hat{V}$ in this case is sensitive to the initial qubit state: if the qubit was initialized in $|\uparrow\rangle$, then we would have $\hat{H}_{\rm b,i} = \hat{H}_{\rm b,\uparrow}$ and $\hat{V} = -\hat{\xi}/2$. If the total system is initially out of equilibrium, the definitions in Eqs. (5.5) and (5.6) can describe quench physics corresponding to a much wider range of nonequilibrium initial bath states, even beyond the specific case in Eqs. (5.2b) and (5.7b). In the more general case, $\hat{H}_{\rm b,i}$ in Eq. (5.5) is directly controlled by the initial bath state (see Appendix 5.6.1).

We stress that in contrast to conventional quench experiments which require external temporal control of the bath, here the quench is intrinsic to the measurement protocol: it occurs unavoidably simply through the "back-action" of the qubit on the bath associated with the start of the QNS protocol. While we have discussed a simple example here, the same physics also applies to more general initial bath states and more general quench functions $\eta(t)$. We show explicitly in Appendix 5.6.1 how in general, one can find the form of the effective quench operator $\hat{V}$ from the initial bath state (even if it is a non-thermal state unrelated to $H_{\rm b,\uparrow/\downarrow}$). Further, one can also generate more complicated quench functions $\eta(t)$: as we will show, one approach to achieve this is to use a qubit embedded in a multilevel physical system, e.g. a nitrogen-vacancy center defect in diamond (see discussion on Eq. (5.27)).

As our approach is more general than the specific example of Eq. (5.2b), in what follows, we will allow $\eta(t)$ to have generic time dependence during the time evolution ($0 < t < t_f$), and we will assume a general $\hat{V}$ (unless specified otherwise).

5.3.1 General sensor qubit evolution including effective quench

We now rigorously show how the effective quench physics described in Eqs. (5.5) and (5.6) manifests itself in our standard T_2-based sensing protocol. We first transform to an appro-

priate interaction picture, determined by the initial (static) bath Hamiltonian $\hat{H}_{\mathrm{b,i}}$, and we again assume the standard toggling frame defined by qubit control pulses. We thus have time-dependent interaction-picture bath operators $\hat{V}(t)$ and $\hat{\xi}(t)$ whose time dependence is generated by $\hat{H}_{\mathrm{b,i}}$. Note that as the initial bath state is stationary in our interaction picture (i.e., $[\hat{\rho}_{\mathrm{b,i}}, \hat{H}_{\mathrm{b,i}}] = 0$), $\hat{\xi}(t)$ will describe stationary quantum noise: all its correlation functions will respect time-translational invariance.

Working in the above interaction picture, and letting $F(t)$ denote the usual filter function (also known as the switching function in time domain) that encodes the timing of qubit control π-pulses, the time-dependent qubit coherence is given by (see Appendix 5.6.2 for detail)

$$\langle \hat{\sigma}_-(t_f) \rangle = \frac{1}{2} \mathrm{Tr}(\hat{U}_\uparrow \hat{\rho}_{\mathrm{b,i}} \hat{U}_\downarrow^\dagger), \tag{5.8a}$$

$$\hat{U}_{\uparrow(\downarrow)} = \mathcal{T} \exp\left\{ -i \int_{-\infty}^{+\infty} \left[\eta(t') \hat{V}(t') \pm \frac{F(t')}{2} \hat{\xi}(t') \right] dt' \right\}. \tag{5.8b}$$

We stress that Eq. (5.8) is valid for a generic form of quench function $\eta(t)$ and operator $\hat{V}(t)$, and not limited to the specific case described by Eq. (5.4). Note crucially that we do not include the quench operator $\hat{V}$ in the definition of our interaction picture. While one could work in this alternate frame, it would obscure the fact that in general, $\hat{V}$ does not commute with the initial bath state. It would also lead to a time-dependent bath noise operator $\hat{\xi}'(t)$ that is nonstationary.

To discuss the sensor qubit evolution, it is convenient to separately parametrize the magnitude and phase of the qubit coherence function in Eq. (5.8):

$$\langle \hat{\sigma}_-(t_f) \rangle = \frac{1}{2} e^{-\zeta(t_f)} e^{-i\Phi(t_f)}. \tag{5.9}$$

The effects of the environment are now fully described by the (real, nonnegative) dephasing function $\zeta(t_f)$ (which controls the magnitude of the coherence) and the real bath-induced

phase shift function $\Phi(t_f)$. Standard QNS protocols use information in $\zeta(t_f)$ to probe properties of the environment [137]. As we will now see, due to our effective quench physics, key new features of the environment will also reveal themselves through the unexpected phase shift.

5.3.2 Quench-induced sensor-qubit phase shift

T_2-based QNS protocols typically have a sole focus on the fluctuation properties of the bath, specifically fluctuations of the bath noise operator $\hat{\xi}$. The simplest quantity characterizing these is the symmetrized noise spectral density $\bar{S}[\omega]$, given by:

$$\bar{S}[\omega] \equiv \frac{1}{2}\int_{-\infty}^{+\infty} dt e^{i\omega t}\langle\{\hat{\xi}(t),\hat{\xi}(0)\}\rangle \tag{5.10}$$

The average value here is with respect to the initial bath density matrix $\hat{\rho}_{\mathrm{b,i}}$. As discussed in many places (see e.g. [23]), this quantity is symmetric in frequency, and plays the role of a classical noise spectral density.

Another generic environmental property that is not typically probed in standard T_2-based QNS schemes is the dynamical response properties of the bath: how does it change in response to a time-dependent external perturbation? At the simplest linear-response level, this is described by conventional linear response susceptibilities (or equivalently, retarded Green's functions). We will be interested in a particular susceptibility, describing how the average value of the noise operator $\hat{\xi}$ changes in response to a perturbation coupling to the quench operator $\hat{V}$. This is described by the Green-Kubo linear response function (see, e.g., [24] for a pedagogical introduction)

$$G^R_{\xi V}[\omega] \equiv -i\int_{-\infty}^{+\infty} dt e^{i\omega t}\Theta(t)\langle[\hat{\xi}(t),\hat{V}(0)]\rangle. \tag{5.11}$$

We stress that in general, this susceptibility is distinct from the noise spectral density $\bar{S}[\omega]$.

Hence, being able to measure it would provide new information on the properties of our environment.

We return now to the evolution of our sensor qubit during the QNS protocol. For a generic environment, Eqs. (5.8) and (5.9) (which describe the sensor qubit coherence) can be analyzed perturbatively in both $\hat{\xi}$ and $\hat{V}$; for the simple example of Eq. (5.4), this amounts to perturbation theory in the qubit-bath coupling. The leading-order contributions to the dephasing and phase-shift functions in Eq. (5.9) can be succinctly written as (see Appendix 5.6.3)

$$\zeta(t_f) \simeq \int_{-\infty}^{+\infty} \frac{d\omega}{4\pi} |F[\omega]|^2 \bar{S}[\omega], \tag{5.12a}$$

$$\Phi(t_f) = \Phi_{\rm q}(t_f) \simeq \int_{-\infty}^{+\infty} \frac{d\omega}{2\pi} F^*[\omega] \eta[\omega] G^R_{\xi V}[\omega]. \tag{5.12b}$$

Here we use the notation $z[\omega] \equiv \int_{-\infty}^{+\infty} z(t) e^{i\omega t} dt$ to denote the Fourier transform of a temporal function. We stress that these expressions are valid for a general quench, and not just the specific example described by Eq. (5.4).

Eqs. (5.12) are generally valid for generic environments in the weak coupling limit; they also become exact for Gaussian quantum environments (i.e. linear coupling to a bath of independent bosonic modes). This covers many experimentally-relevant situations (e.g. environments comprised of phononic or photonic modes [167, 168], interacting disordered spin baths [157], $1/f$ charge and flux noise sources [169], etc.). Eq. (5.12a) is a standard textbook expression: at the Gaussian level, the qubit dephasing is controlled by the environmental noise spectral density, weighted by the filter function. In contrast, Eq. (5.12b) is less appreciated: because of the effective quench physics described above, and the dynamical nature of the bath, there is a bath-induced phase shift of the qubit sensor. This phase shift $\Phi_{\rm q}(t_f)$ depends both on the relevant bath susceptibility, the filter function $F[\omega]$ as well as the quench control function $\eta[\omega]$. As we will see, this phase provides a new route to learning about the environment. Note that the consequences of the quench can also be discussed beyond linear

response, as would apply to more general environments and sensor-environment couplings (see Appendix 5.6.4).

We stress that the quench-induced sensor phase shift $\Phi_{\rm q}(t_f)$ can be accessed in exactly the same type of experiments one would use to sense external DC or AC fields, making use of standard Ramsey, Hahn echo or more complex dynamical decoupling sequences [137].

A natural concern is whether this quench phase could be distinguished from more trivial phases resulting from external ambient magnetic fields. In the presence of such fields, the net qubit phase shift in Eq. (5.9) is now given by

$$\Phi(t_f) = \Phi_{\rm ext}(t_f) + \Phi_{\rm q}(t_f), \tag{5.13}$$

$$\Phi_{\rm ext}(t_f) = \int_{-\infty}^{+\infty} \frac{d\omega}{2\pi} F^*[\omega] B_{\rm ext}[\omega], \tag{5.14}$$

where $B_{\rm ext}(t)$ is the external ambient magnetic field, and the QPS $\Phi_{\rm q}(t_f)$ is again given by Eq. (5.12b). There is a critical difference between $\Phi_{\rm ext}$ and $\Phi_{\rm q}$: only the latter is sensitive to the initial state of the qubit (see discussion below Eq. (5.7b)). One can thus easily exploit this feature to distinguish the QPS from other more trivial phase-shift mechanisms (see Fig. 5.1(b) for an example). Further, we note that this feature lets one distinguish the QPS $\Phi_{\rm q}(t_f)$ from nontrivial qubit phase shifts due to non-Gaussianity of the noise source (the latter has been studied in e.g., Refs. [103, 104]).

We note that related phase shifts were discussed in previous works as an anomalous effect emerging in T_2-type QNS protocols in systems with an unusual "biased" qubit-environment coupling [164, 165]. In contrast, as we show the quench-induced phase shifts can in fact arise in a far wider set of systems, including ones with an "unbiased" coupling that according to previous works, would exhibit no extra phase shift. We again stress that it is the initial bath state (and not the qubit-bath coupling) that plays a key role in the quench physics. This realization will provide an important new control knob, as one can controllably change

the properties of the quench via seemingly subtle changes in the initial bath state. As we discuss, this provides a powerful tool for reconstructing environmental spectral functions.

5.4 Quench phase shift as a direct probe of environmental density of states

While the above discussion applies to the most general quench scenario, we will often be interested in cases where the quench Hamiltonian is static in the lab frame once the sensing protocol starts. This corresponds to a quench control function $\eta(t) = \Theta(t)\Theta(t_f - t)$. This is the case for the specific example situation in Eq. (5.4). As we will show in Eqs. (5.32) and (5.34b), this also encompasses the case of more general forms of quench operator $\hat{V}$ beyond Eq. (5.4), corresponding to a wide number of T_2-based sensing protocols with generic initial bath states.

For the above cases, the QPS can be further recast in a form that only involves the imaginary part of response function $\mathrm{Im}G^R_{\xi V}[\omega]$. For spin-echo control pulses satisfying $F[0] \equiv \int_0^{t_f} F(t)dt = 0$, the expression for the QPS further simplifies (see Appendix 5.6.5)

$$\Phi_{\mathrm{q}}(t_f) = -\int_{-\infty}^{+\infty} \frac{d\omega}{\pi\omega} \mathrm{Re}F[\omega]\, \mathrm{Im}G^R_{\xi V}[\omega]. \tag{5.15}$$

For a general pulse sequences, $F[\omega]$ above should be replaced by $F[\omega] - F[0]$.

Eq. (5.15) becomes even more revealing in cases like our example of Eq. (5.4), where the quench operator $\hat{V}$ is proportional to the noise operator $\hat{\xi}$, $\hat{V} = \beta\hat{\xi}$, where β is a real constant. We can thus write:

$$\Phi_{\mathrm{q}}(t_f) = \beta \int_{-\infty}^{+\infty} \frac{d\omega}{\omega} \mathrm{Re}F[\omega]\, \mathcal{J}[\omega], \tag{5.16}$$

where we have introduced the environmental spectral function

$$\mathcal{J}[\omega] = -\frac{1}{\pi}\mathrm{Im}G^R_{\xi\xi}[\omega], \tag{5.17}$$

which determines the dissipative response of the environment, and also plays the role of an effective density of states (DOS). $\mathcal{J}[\omega]$ also corresponds to the asymmetric part of the (unsymmetrized) quantum noise spectrum [23]. Eq. (5.16) shows that the quench phase shift provides a direct route to learning about properties of the environmental spectral function, a quantity that plays an important role both in quantum noise theory [167] and in various areas of many body physics. Note that a related expression was derived in Ref. [164] (though this work did not consider the more general situations analyzed here, see e.g. Eqs. (5.12b) and (5.15)).

While the importance and utility of $\mathcal{J}[\omega]$ is clear in many contexts, it is useful to provide a simple but ubiquitous example. Consider an environment comprised of independent bosonic modes b_k with $H_{\mathrm{b},\downarrow} = \sum_k \Omega_k \hat{b}^\dagger_k \hat{b}_k$ and a noise operator $\hat{\xi}(t) = \sum_k g_k e^{i\Omega_k t}\hat{b}^\dagger_k + \mathrm{H.c.}$. In this case, we have $\mathcal{J}[\omega] = \sum_k g_k^2 \delta(\omega - \Omega_k)$: it is indeed a weighted DOS, with each mode's contribution weighted by its coupling constant. This bosonic bath model can be used to describe a variety of phononic or electromagnetic dephasing environments [167, 168]. In this simple bosonic case, $\mathcal{J}[\omega]$ is completely independent of the environmental state. However, we stress that our results in subsequent sections remain valid for interacting baths, and/or baths that are not purely bosonic.

The above example highlights a general fact: to understand whether a large bath noise spectral density $\bar{S}[\omega]$ (as revealed by a standard QNS measurement) is due to a large bath DOS or a large mode-occupancy (i.e. temperature), one needs to also know the spectral function $\mathcal{J}[\omega]$. As such, the information provided by the QPS provides crucial additional information which complements information provided by the dephasing factor. To see this explicitly, consider the case where the initial bath state $\hat{\rho}_{b,i}$ is in thermal equilibrium at

temperature T. In this case, the quantum fluctuation-dissipation theorem (FDT) yields [128, 170]

$$\bar{S}[\omega] = \pi \mathcal{J}[\omega] \coth \frac{\omega}{2k_B T}. \tag{5.18}$$

This relation suggests something we will investigate in detail further: if one knows both the noise spectrum and spectral function at a given frequency, one can extract (in a parameter free manner) the environmental temperature. A standard dephasing-based QNS measurement does not provide sufficient information for such an extraction. Only the extra information provided by the QPS makes this possible. Note that our focus here is on dephasing-type couplings between a sensor qubit and the environment. If one instead had a transverse coupling, then an extended version of T_1 relaxometry could also be used in principle to extract $\mathcal{J}[\omega]$, see Appendix 5.6.6.

Finally, we point out that the above characterization is useful even in more general situations where the initial bath state is not in thermal equilibrium. In that case, the FDT relation in Eq. (5.18) can be used to define (at each frequency) an effective temperature $T_{\text{eff}}[\omega]$ (see, e.g., [23, 171, 172])

$$\coth \frac{\omega}{2k_B T_{\text{eff}}[\omega]} \equiv \frac{\bar{S}[\omega]}{\pi \mathcal{J}[\omega]}. \tag{5.19}$$

The fact that this quantity varies as a function of frequency would then be direct evidence of an initial nonequilibrium bath state. This is also the kind of nontrivial information that can be addressed in a standard T_2-style QNS protocol using the extra information provided by the QPS.

5.4.1 Probing low-frequency environmental properties and non-thermal states

As an example of its utility, we show here how the quench phase shift can be used to extract low-frequency spectral properties of a generic environment (encompassing sub-, super-, and Ohmic cases), going beyond what could be done by studying the dephasing factor alone. This information directly allows one to determine if the bath is in thermal equilibrium, i.e. whether the FDT relation of Eq. (5.18) is violated. In the case where the bath is in equilibrium, it provides a direct means to extract the environmental temperature. While the estimation protocol we discuss here applies to general quench operators, for concreteness we focus on the specific quench configuration in Eq. (5.4), where $\hat{V}(t) = \hat{\xi}(t)/2$. The protocol applies essentially the same way for more general situations as long as the lab-frame quench operator is static during the protocol (i.e. Eq. (5.15) must hold).

Our focus here is on a very generic scenario where both the environmental symmetrized noise spectrum and spectral function exhibit power-law behavior at low-frequency limit:

$$\bar{S}[\omega] \sim S_0 \omega^p \quad (\omega \to 0^+), \tag{5.20a}$$

$$\mathcal{J}[\omega] \sim \frac{A_0}{\pi} \omega^s \quad (\omega \to 0^+). \tag{5.20b}$$

Note this includes the case where these quantities tend to a constant asymptotically as $\omega \to 0^+$. Note also that even if one or both of the exponents p, s are negative, Eqs. (5.20) can still describe a physical bath, as long as one also introduces a low-frequency IR cutoff. We thus have four parameters characterizing the low-frequency features of the environment. As shown in Eq. (5.19), a general, non-thermal environment can always be characterized by a frequency-dependent effective temperature $T_{\text{eff}}[\omega]$. Using the asymptotic forms above, we have in the low-frequency limit:

$$T_{\text{eff}}[\omega] \sim \frac{S_0}{2k_B A_0} \omega^{p+1-s} \tag{5.21}$$

If the environment is in thermal equilibrium then $T_{\text{eff}}[\omega]$ will be frequency independent and equal to the bath temperature. We see this requires $p = s - 1$.

Our goal is thus to estimate the power-law exponents p, s, and overall coefficients S_0, A_0 from the sensor qubit dynamics. As we now show, this can be achieved by looking at both the phase and magnitude of the qubit coherence in the long-time limit. As long as the asymptotic power-law dependence of bath NSD (response function) does not exhibit too strong a low-frequency divergence, the asymptotic long-time behavior of the dephasing function $\zeta(t_f)$ (QPS $\Phi_{\text{q}}(t_f)$) under any specific spin-echo or dynamical-decoupling pulse becomes independent of details about the cutoff, and is solely determined by the low-frequency asymptotic behavior of NSD (spectral function) in Eq. (5.20). The needed conditions are satisfied by most physical environments (including, e.g., Ohmic baths and baths producing $1/f$ noise)

Using Eqs. (5.12a) and (5.15) we can rigorously show (see Appendix 5.6.7 for a detailed derivation)

$$\zeta(t_f) \sim \mathcal{C}_\zeta S_0 t_f^{1-p} \quad (t_f \to +\infty, -3 < p < 1), \tag{5.22a}$$

$$\Phi_{\text{q}}(t_f) \sim \mathcal{C}_\Phi A_0 t_f^{1-s} \quad (t_f \to +\infty, -2 < s < 2), \tag{5.22b}$$

where $\mathcal{C}_\zeta$ and $\mathcal{C}_\Phi$ are nonzero dimensionless coefficients determined by details of the qubit control pulse. Eqs. (5.22) are valid for some of the most common types of physical environments, including Ohmic baths ($p = 0$, $s = 1$) and baths generating $1/f$ noise ($p = -1$, $s = 0$). Comparing against Eq. (5.21), we see that the combined information in the dephasing function and quench phase shift is exactly what is needed to characterize the effective temperature $T_{\text{eff}}[\omega]$. If this quantity is frequency-dependent, the bath is not in a thermal state. Note that for exponents p and s falling out of the range of validity given in Eq. (5.22), the long-time regime of qubit dynamics would also be sensitive to details of the cutoff, but it would still be possible to extract information about the bath NSD (response function) from

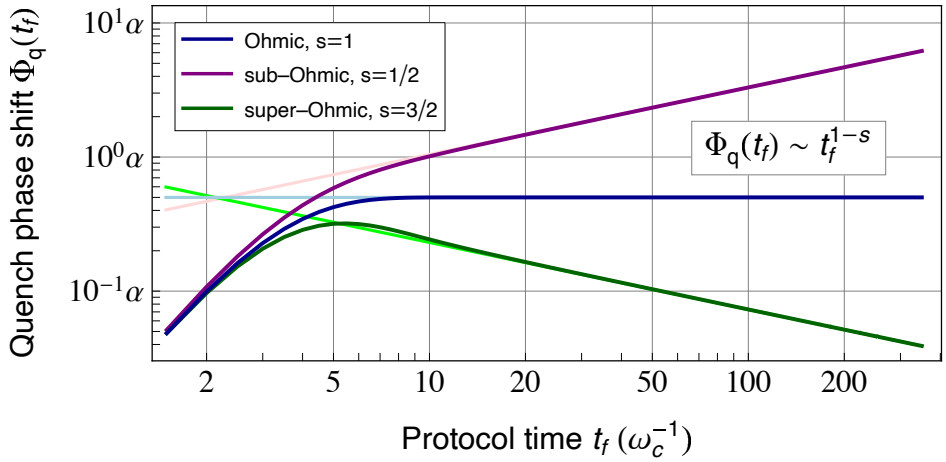

Fig. 5.2: Quench phase shift (QPS) $\Phi_{\rm q}(t_f)$ of a sensor qubit coupled to a Gaussian quantum environment, acquired during a Hahn echo sequence, as a function of protocol time t_f. We assume the environment has spectral function which behaves as a power law at low frequencies, i.e. $\mathcal{J}[\omega] = (\alpha/\pi)\omega_{\rm c}\,(\omega/\omega_{\rm c})^s\,e^{-(\omega/\omega_{\rm c})^2}$. Curves correspond to different power laws: Ohmic ($s=1$, dark blue curve), sub-Ohmic ($s=1/2$, purple curve), and super-Ohmic ($s=3/2$, dark green curve). We see that the QPS is extremely sensitive to the spectral function power law s. Light-colored lines depict the asymptotic long-time dependence of the QPS $\Phi_{\rm q}(t_f) \sim t_f^{1-s}$ (see also Eq. (5.22b)), which shows excellent agreement with the exact results in the long-time regime $t_f \gg \omega_{\rm c}^{-1}$, as expected. Note that for Gaussian, bosonic environments, the QPS is independent of temperature.

the dephasing function $\zeta(t_f)$ (QPS $\Phi_{\rm q}(t_f)$) using parametric spectral estimation techniques.

The asymptotic result in Eq. (5.22a) for dephasing is well established [173–175] and has been utilized for QNS in various experimental platforms [140, 143, 147]. The corresponding result for the quench phase shift in Eq. (5.22b) provides complementary information, on the properties of the spectral function. We stress that to assess whether the bath is in equilibrium, and if so what the temperature is, both these quantities are needed. In Fig. 5.2, we show the evolution of the quench phase shift for a simple Hahn echo pulse sequence; curves correspond to Gaussian Ohmic, sub- and super-Ohmic baths with Gaussian cutoffs, where $s = 1, \frac{1}{2}, \frac{3}{2}$ respectively. As expected, the exact QPS is accurately described by the asymptotic power-law function in the long-time regime. For Hahn echo, the constants appearing in Eqs. (5.22) are given by $\mathcal{C}_{\zeta,\rm H} = \frac{1-2^{p+1}}{\pi}\Gamma\,(p-1)\sin\frac{p\pi}{2}$ and $\mathcal{C}_{\Phi,\rm H} = \frac{1-2^{s}}{\pi}\Gamma\,(s-1)\cos\frac{s\pi}{2}$, where $\Gamma(\cdot)$ is the gamma function.

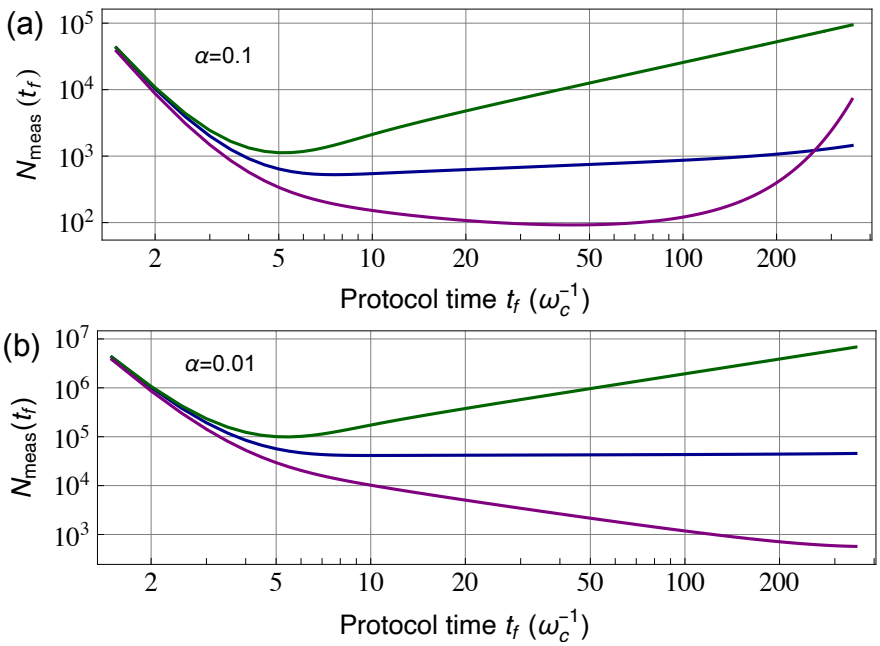

Fig. 5.3: Minimum number of measurements $N_{\rm meas}$ needed to resolve the quench phase shift with a unit signal-to-noise ratio in a Hahn echo protocol of time t_f: $N_{\rm meas}(t_f) \equiv \left|\langle\hat{\sigma}_y(t_f)\rangle\right|^{-2}$. Because of bath induced dephasing, it will in general take many repeated measurements to resolve the quench phase shift (QPS). We use the same Gaussian baths (and labelling) as in Fig 5.2. Panel (a) corresponds to a dimensionless coupling parameter $\alpha = 0.1$, while (b) corresponds to $\alpha = 0.01$. All plots correspond to a temperature $k_B T = 0.01\omega_{\rm c}$.

We have shown that the long-time properties of the sensor qubit coherence (both its magnitude and phase) reveal key features of our environment. This sensing modality of course has a natural tension: in the long-time limit, the loss of qubit coherence described by Eq. (5.12a) will make it difficult to resolve the quench phase shift (c.f. Eq. (5.12b)). This is not a fundamental problem, but necessitates sufficient averaging, i.e. repeated evolutions and measurements of the sensor qubit under the chosen pulse protocol. In what follows, we characterize the amount of averaging needed for given environmental parameters.

For convenience, in what follows we express the coefficient A_0 in Eq. (5.20b) as $A_0 = \alpha\omega_{\rm c}^{1-s}$, i.e. the product of a dimensionless parameter α quantifying the qubit-bath coupling strength, and powers of a UV-cutoff frequency scale $\omega_{\rm c}$ characterizing the regime where Eq. (5.20b) is valid. In the weak coupling limit $\alpha \ll 1$, we can calculate the number

of repeated measurements required to achieve a unit signal-to-noise ratio (SNR) for the measurement of the quench phase shift. Focusing only on fundamental projection noise, this is given (as is standard) by the squared inverse norm of the qubit coherence signal [137], $N_{\mathrm{meas}}(t_f) = \left|\langle\hat{\sigma}_y(t_f)\rangle\right|^{-2}$. This figure-of-merit is plotted in Fig. 5.3 for weakly-coupled baths with different spectral functions $\mathcal{J}[\omega]$. Note that in many experimentally-relevant situations, the effective environment temperature scale is much lower than the UV energy scale, i.e. $k_B T_{\mathrm{eff}} \ll \omega_{\mathrm{c}}$. As a result, measuring the long-time quench phase shift is within reach of state-of-the-art systems realizing QNS.

5.4.2 Case study: $1/f$ noise sources

In this subsection, we focus on low-frequency $1/f$ noise, where the NSD $\bar{S}[\omega] \propto 1/f^a$ ($f < k_B T$, $0 < a < 2$; often a is close to 1). The $1/f$ noise constitutes a dominating dephasing noise source in semiconductor and superconducting qubits [169]. We first show the asymptotic long-time behavior of the QPS $\Phi_{\mathrm{q}}(t_f)$ can now be recast into a simple form, in terms of a few experimentally relevant parameters. We also compute the Hahn-echo signal corresponding to two realistic charge noise models, which can be readily measured using superconducting qubits.

For low-frequency $1/f^a$ noise, the NSD $\bar{S}[\omega]$ satisfies Eq. (5.20a) with a power-law exponent $p = -a$. Assuming the corresponding quantum bath is in thermal equilibrium, we can reformulate the asymptotic results in Eqs. (5.22) in terms of three parameters: Hahn echo dephasing time $T_{2\mathrm{e}}$, the noise exponent a, and temperature T. More specifically, the asymptotic qubit dephasing function $\zeta(t_f)$ in Eq. (5.22a) now reads $\zeta(t_f) \sim (t_f/T_{2\mathrm{e}})^{1+a}$, so that we can rewrite the QPS in Eq. (5.22b) as

$$\Phi_{\mathrm{q}}(t_f) \sim \frac{a+1}{2k_B T T_{2\mathrm{e}}}\left(\frac{t_f}{T_{2\mathrm{e}}}\right)^a \quad (t_f \to +\infty, -1 < a < 3). \tag{5.23}$$

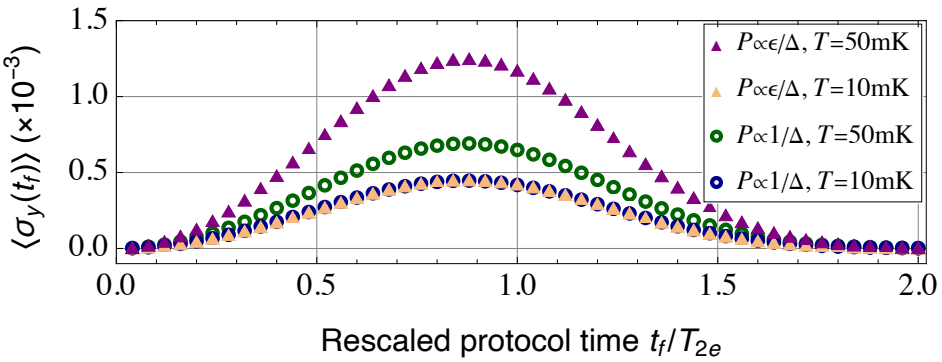

Fig. 5.4: Numerically simulated Hahn-echo qubit coherence function $\langle\hat{\sigma}_y(t_f)\rangle$ corresponding to two charge-noise baths. The bath spectral functions are generated by an ensemble of two-level fluctuators (TLFs) with $\hat{H}_{\rm TLF} = \epsilon\hat{\Sigma}_z + \Delta\hat{\Sigma}_x$, which are coupled to a phonon bath via $\hat{\Sigma}_x$. Two TLF distributions $P(\epsilon,\Delta)$ are used in the simulation: $P(\epsilon,\Delta) \propto \epsilon/\Delta$ (triangles), and $P(\epsilon,\Delta) \propto 1/\Delta$ (circles). The qubit-bath coupling strength is chosen such that the qubit coherence time is $T_{2\rm e} = 1$ μs at $T = 10$ mK (orange triangles and blue circles). As we increase bath temperature to $T = 50$ mK, the two models predict qualitative difference in the behavior of the Hahn echo signal $\langle\hat{\sigma}_y(t_f)\rangle$ (purple triangles and green circles), which in turn encodes dynamics of the quench phase shift (QPS).

Thus, to observe the QPS effect it is desirable to have qubits whose Hahn-echo coherence times are smaller than or comparable to the timescale set by temperature, i.e. $T_{2\rm e} \lesssim (k_B T)^{-1}$.

While the asymptotic result in Eq. (5.23) remains valid for low-frequency charge noise as well as $1/f$ flux noise, we now focus on the former case to estimate the QPS effects in realistic superconducting qubits. In this case we can approximate $T \sim 10^1$ mK, corresponding to a timescale of 1 ns. Experimentally, one can deliberately build superconducting qubits sensitive to charge noise [176] so that QPS effects become measurable.

To obtain a concrete estimate, we adopt two physically motivated microscopic model for charge noise, both consisting of two-level fluctuators (TLFs) coupled to a phonon bath (see [177] for detail). Making use of the bath spectral function generated by the models, we numerically compute qubit coherence signal $\langle\hat{\sigma}_y(t_f)\rangle$ under Hahn echo at two different temperatures ($T = 10$ mK and 50 mK). The results are plotted against rescaled protocol time $t_f/T_{2\rm e}$ in Fig. 5.4, where we set qubit-bath coupling such that the qubit coherence time

is $T_{2e} = 1\ \mu$s at $T = 10$ mK. We note that the two different models lead to marked difference in the QPS $\Phi_q(t_f)$, and hence the Hahn echo signal as one increases temperature.

While the $1/f^a$ noise spectrum has been observed in numerous experiments (see e.g. [178, 179]), we reiterate that the QPS $\Phi_q(t_f)$ offers a direct means to probe the low-frequency bath spectral function $\mathcal{J}[\omega]$, an independent spectral property from the standard NSD $\bar{S}[\omega]$. This is important for understanding decoherence mechanisms in recent designs of superconducting qubits with intrinsic noise protection [180]. On the other hand, despite existing theoretical models that could successfully capture multiple aspects of the $1/f^a$ noise spectra [169], a consensus on the microscopic origin of such noise remains elusive. Having access to the noise temperature (as opposed to the ambient temperature) can also help resolve the open question of origin of $1/f^a$ noise.

5.4.3 Case study: Ohmic baths

Baths with an Ohmic spectral density $\mathcal{J}[\omega]$ are both extremely well studied theoretically, and are good descriptions of various dissipative environments [181]. Perhaps the best known examples are the voltage and current fluctuations (i.e., Johnson-Nyquist noise [182, 183]) of an electromagnetic environment described by an impedance that is frequency-independent at low frequencies. Such electromagnetic environments are relevant to many systems, including superconducting qubits [184–187]. In this subsection, we specialize to the case of an environment that is approximately Ohmic at low frequencies, i.e. the low-frequency spectral function $\mathcal{J}[\omega]$ is proportional to frequency. As we now show, this sole assumption allows one to directly extract the environmental temperature via simple measurements that require no curve fitting.

When in thermal equilibrium, an Ohmic environment has a flat NSD at low frequencies, i.e. $\bar{S}[\omega] \sim 2A_0 k_B T$, c.f. Eq. (5.20). A measurement of the low-frequency NSD alone only yields the product of A_0 and T, and hence does not permit direct thermometry. Luckily,

the missing information (i.e. the value of the coupling constant A_0) is directly provided by the long-time limit quench phase shift. Defining $\Phi_{\rm q}(\infty) \equiv \lim_{t_f\to+\infty}\Phi_{\rm q}(t_f)$, we find from Eq. (5.22b):

$$\Phi_{\rm q}(\infty) = \frac{\pi}{2}\left.\frac{d\mathcal{J}[\omega]}{d\omega}\right|_{\omega=0} = \frac{1}{2}A_0. \tag{5.24}$$

See Appendix 5.6.8 for an alternative, intuitive derivation of this expression.

Given this simple result, one can now directly extract the environment temperature T from the quench phase shift $\Phi_{\rm q}(t_f)$ and low-frequency noise spectral density $\bar{S}[0]$, via the following relation

$$T = \frac{\bar{S}[0]}{4k_B}\left[\lim_{t_f\to+\infty}\Phi_{\rm q}(t_f)\right]^{-1}. \tag{5.25}$$

Note that this result assumes the NSD is flat in the low-frequency limit, in which case the qubit Ramsey and Hahn-echo coherence times are necessarily identical. However, realistic systems may also experience a large amount of quasistatic noise, leading to deviations from perfect Ohmic behavior at infinitesimal frequencies. Here we stress that even in these circumstances where the qubit Hahn-echo time T_2 differs from the Ramsey coherence time $T_{\rm FID}$, a modified version of Eq. (5.25) is still applicable, as long as the slow noise disrupting Ohmic NSD behavior emerges at a much lower frequency scale compared to the Ohmic regime. More specifically, this means the NSD $\bar{S}[\omega]$ and the spectral function $\mathcal{J}[\omega]$ has a low-frequency cutoff $\omega_{\rm ir}$, below which the Ohmic behavior $\bar{S}[\omega] \sim$ const. and $\mathcal{J}[\omega] \sim \omega$ breaks down. As mentioned, this includes the common physical situations, where the environment also has a large amount of quasistatic noise, which can be described as an additional delta function peak in the NSD. It then follows that, our thermometry protocol is applicable to baths with asymptotic low-frequency Ohmic behavior, which may exhibit a high- as well as a low-frequency cutoff. For this more general scenario, we should use asymptotic low-

frequency NSD $\lim_{\omega\to 0}\bar{S}[\omega] = 2/T_2$, instead of strictly zero-frequency noise $\bar{S}[0] = 2/T_{\rm FID}$ in Eq. (5.25). This justifies the use of Hahn-echo coherence time T_2 in the main text.

$$k_B T = \frac{1}{2T_2\,\Phi_{\rm q}(\infty)}. \tag{5.26}$$

The upshot is that for a thermal, Ohmic environment, simply measuring the Hahn-echo T_2 and the long-time quench phase shift directly yields the environmental temperature. We stress that this does not require any curve fitting, nor further assumptions. Furthermore, our protocol is also applicable if in addition to low-frequency Ohmic noise, we also have large quasistatic noise; this is a common scenario in many systems.

While Eq. (5.26) is exact, it is also useful to understand how long one must wait to achieve the asymptotic long-time limit of the QPS. The answer to this question depends on features in the spectral function away from $\omega = 0$. For convenience, in following discussion we rewrite the spectral function as $\mathcal{J}[\omega] = (\alpha/\pi)\omega\phi\,(\omega/\omega_{\rm c})$, where $\phi(\cdot)$ encodes high-frequency dependence of the spectral function. As illustrated in Fig. 5.5, there are two possible scenarios for the crossover dynamics of QPS. First, if the spectral function $\mathcal{J}[\omega]$ exhibits narrow peak(s) in the high-frequency regime, then the crossover timescale is given by $\Gamma_{\rm min}^{-1}$, where $\Gamma_{\rm min} < \omega_{\rm c}$ is the smallest linewidth of these peaked features. This is shown in Fig. 5.5(b), where the corresponding spectral function exhibits a high-frequency narrow Lorentzian peak with linewidth $2\Gamma_{\rm min} = 2\epsilon\omega_{\rm c} = 0.2\omega_{\rm c}$, as encoded by $\phi(x) = (1+\epsilon^2)^2/[(x-1)^2+\epsilon^2][(x+1)^2+\epsilon^2]$. Such spectral function can describe e.g., low-frequency photon shot noise generated by a driven damped cavity [100] (see also Appendix 5.6.9 for detail). The second generic case is where there are no such sharp features at high frequencies, and only a smooth cutoff in $\mathcal{J}[\omega]$ characterized by the UV cutoff frequency $\omega_{\rm c}$. In this case, the timescale for the QPS to saturate is $1/\omega_{\rm c}$ and independent of specific details of the form of the cutoff. This is confirmed in Fig. 5.5(c), where QPS crossover dynamics is plotted for step-function cutoff $\phi(x) = \Theta(1-x)$ (dashed blue), Lorentzian cutoff $\phi(x) = 1/(1+x^2)$ (dotted orange), exponential

cutoff $\phi(x) = e^{-x}$ (dot-dashed green), and Gaussian cutoff $\phi(x) = e^{-x^2}$ (dashed purple curve), respectively.

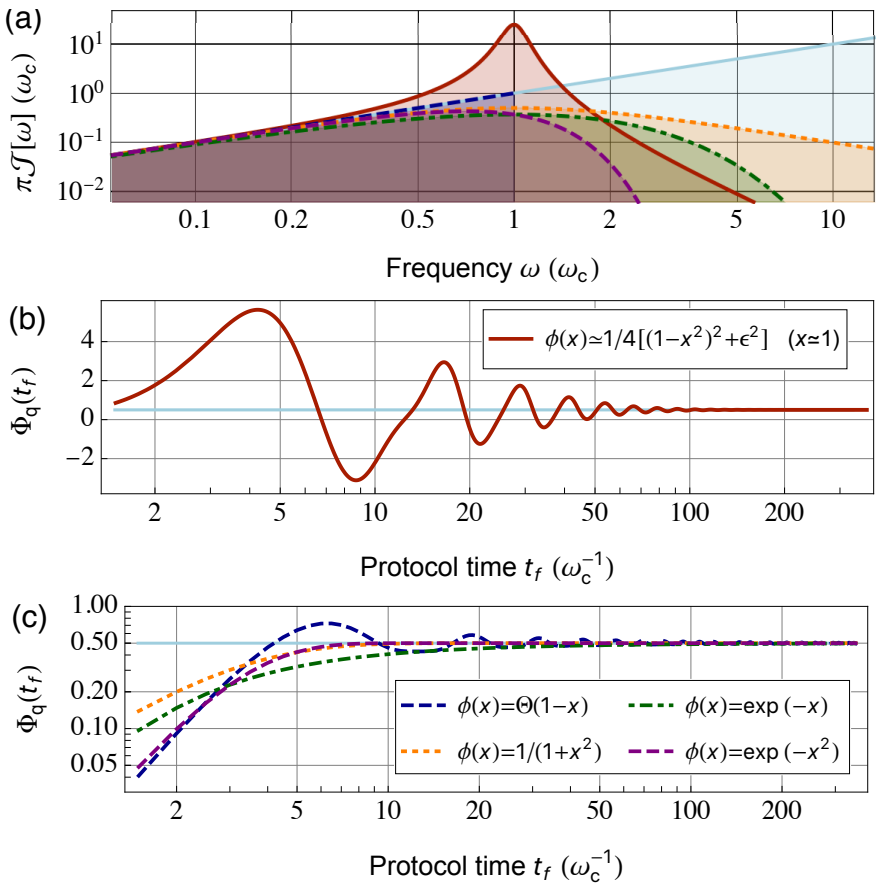

Fig. 5.5: Crossover dynamics of the Hahn-echo quench phase shift (QPS) $\Phi_q(t_f)$ for environments that are Ohmic at low frequencies. For practical applications, the crossover timescale at which the QPS approaches the asymptotic power law behavior (c.f. Eq. (5.22b)) becomes important. This timescale depends on high-frequency deviations in the bath spectral function $\mathcal{J}[\omega]$ from power law; plotted here are two generic scenarios for this crossover dynamics. As shown in (a), we consider bath spectral functions that are asymptotically Ohmic (i.e., proportional to frequency) at low frequencies. (b) Crossover dynamics for QPS with spectral function exhibiting a narrow Lorentzian peak in the range of high frequencies, i.e., $\mathcal{J}[\omega] \sim \alpha\omega_c^3/4\pi[(\omega-\omega_c)^2+\Gamma_{\rm min}^2]$ for $\omega \simeq \omega_c$ (red solid curve in (a)). For narrow peak with linewidth $2\Gamma_{\rm min}/\omega_c = 0.2 < 1$, the crossover timescale is given by $\Gamma_{\rm min}^{-1}$. (c) QPS for spectral functions that are Ohmic at low frequencies with a simple UV cutoff. In this case, the crossover time is given by inverse of the cutoff frequency ω_c^{-1}, and is independent of details about the cutoff. Cutoff functions $\phi(x)$ used: step-function (dashed blue), Lorentzian (dotted orange), exponential (dot-dashed green), and Gaussian cutoff (dashed purple curve). We assume $\alpha = 1$ in all panels. See the main text for specific forms of $\mathcal{J}[\omega]$ used in (b) and (c).

5.4.4 Spectral reconstruction of response functions

In this subsection, we restrict attention to situations where the quench (whether intentional or accidental) yields a quench operator $\hat{V}$ (c.f. Eq.(5.5)) which commutes with the noise operator ξ (Eq. (5.3)). In the simple and standard case where the quench temporal function $\eta(t)$ is a step function (c.f. Eq. (5.7a)), we showed in Eqs. (5.20-5.22) that the quench phase shift can be used to extract the low-frequency properties of the environment's spectral function $\mathcal{J}[\omega]$ (i.e. response function). A natural question is to ask whether it is possible to perform a complete reconstruction of $\mathcal{J}[\omega]$ in some finite bandwidth window. This would be then analogous to spectral reconstruction techniques used in conventional QNS measurements to reconstruct $\bar{S}[\omega]$.

It is worth noting that for the specific QPS given by Eq. (5.16), Ref. [164] has proven a no-go theorem, which prevents systematical reconstructions of spectral function $\mathcal{J}[\omega]$ using the restricted form of quenches in Eq. (5.4). Here we are interested in a more general question: can we utilize quenches with a more complex time-dependence, as encoded in quench function $\eta(t)$, to overcome the limitation set by aforementioned no-go theorem? Indeed, as we show in Appendix 5.6.10, the extra tunability in the quench function allows us to use the more general form of QPS in Eq. (5.12b) and reconstruct $\mathcal{J}[\omega]$ in a generic target frequency range.

The protocol we introduce below makes use of a generic structure, where the sensor qubit is controllably embedded in a multi-level system. While this can be realized in many different experimental platforms (e.g. a superconducting transmon qubit, as implemented in Ref. [152]), we focus here on sensor based on a $S = 1$ nitrogen-vacancy (NV) defect in diamond [155]. For this system, we discuss a specific protocol to reconstruct finite-frequency spectral function $\mathcal{J}[\omega]$ by engineering time-dependent quenches. We stress that our strategy can be used to implement generic forms of quench functions $\eta(t)$.

We start by showing how to engineer time-dependent quenches using NV centers in diamond. NV-based qubits are an ideal candidate to implement T_2-style QNS: the spin re-

Table 5.1: Quench operator dependence on subspaces of NV center used to form the sensor qubit, assuming fixed initial NV state $|m_z = 0\rangle$. The environment is coupled magnetically to the NV spin with $\hat{B} \equiv \hat{H}_{\mathrm{b},0} - \hat{H}_{\mathrm{b},-1} = \hat{H}_{\mathrm{b},+1} - \hat{H}_{\mathrm{b},0}$ (see Eq. (5.27)).

$\|\uparrow\rangle$	$\|\downarrow\rangle$	Quench operator $\hat{V}$	Noise operator $\hat{\xi}$
$\|m_z = 0\rangle$	$\|m_z = -1\rangle$	$-\hat{B}/2$	$\hat{B}$
$\|m_z = +1\rangle$	$\|m_z = 0\rangle$	$+\hat{B}/2$	$\hat{B}$
$\|m_z = +1\rangle$	$\|m_z = -1\rangle$	0	$2\hat{B}$

laxation timescale T_1 of NV centers is typically much longer than the dephasing timescale, so that $\hat{S}_z$ is conserved to a great approximation during T_2-type protocols. The dominating dephasing typically comes from coupling to environmental magnetic noise (due to surrounding nuclear spins, etc.); alternatively, this makes them a powerful magnetic sensor. We can thus write NV-bath Hamiltonian as

$$\hat{H}_{\mathrm{NV-bath}} = \sum_{m_z=0,\pm1} |m_z\rangle\langle m_z| \otimes \hat{H}_{\mathrm{b},m_z}. \tag{5.27}$$

We will consider the NV-bath coupling to correspond to an effective bath-induced magnetic field $\hat{B}$, which then satisfies $\hat{B} = \hat{H}_{\mathrm{b},0} - \hat{H}_{\mathrm{b},-1} = \hat{H}_{\mathrm{b},+1} - \hat{H}_{\mathrm{b},0}$.

The most common and straightforward way to experimentally initialize the NV center is via optical illumination, which prepares it in the $|m_z = 0\rangle$ state [188]. Given this specific initial NV center state, the initial bath Hamiltonian $\hat{H}_{\mathrm{b,i}}$ in Eq. (5.5) should be replaced by $\hat{H}_{\mathrm{b},0}$ (i.e., the bath Hamiltonian conditioned on qubit in $|m_z = 0\rangle$ state). Turning to the sensing protocol, it is relatively easy and straightforward to rapidly produce a superposition state using any two of the three $|m_z\rangle$ states. This provides us then with three different choices for the specific form of the sensor qubit, each corresponding to different effective quench physics. This is summarized in Table 5.1: the form of the quench physics given by Eqs. (5.5) and (5.6) can be controlled or even turned off by choosing the sensor qubit subspace: $\{m_z = 0, m_z = 1\}$, $\{m_z = 0, m_z = -1\}$ or $\{m_z = +1, m_z = -1\}$. This extra knob in NV-based qubits can be used to distinguish the quench phase shift effect from other

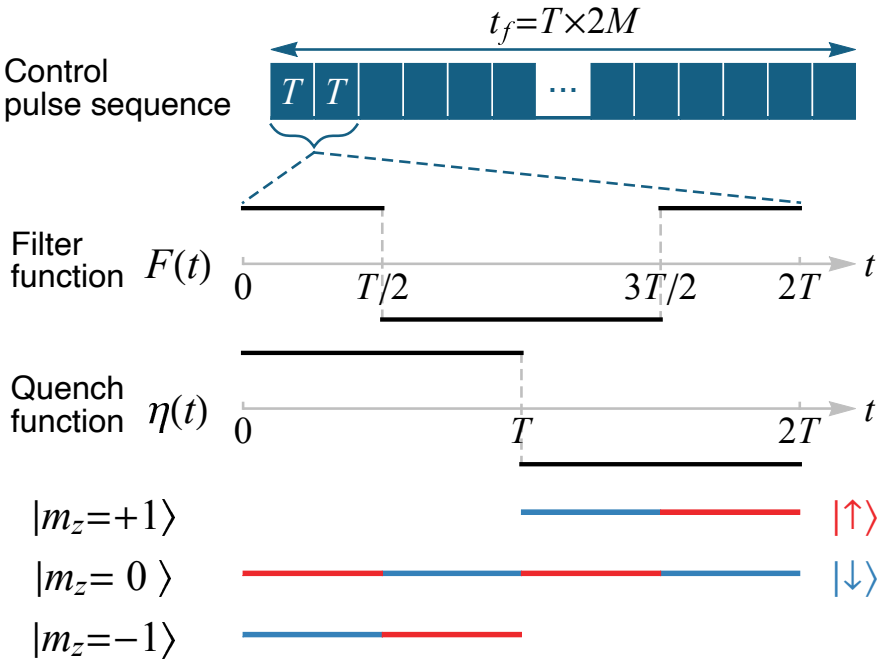

Fig. 5.6: Schematic for example NV center control pulse sequence realizing time modulations in both the noise filter function $F(t)$ and quench function $\eta(t)$. As shown in Eq. (5.31), this control sequence in turn enables reconstruction of spectral function $\mathcal{J}[\omega]$. The control pulses are periodically structured as $2M$ repetitions of a base sequence (period $T = t_f/2M$), so that $F(t)$ and $\eta(t)$ have period $2T = t_f/M$. The noise filter function $F(t)$ encodes timings of the standard dynamical decoupling π-pulses within the qubit subspace. In addition, we can further engineer a modulating quench function $\eta(t)$ by periodically switching between qubit subspaces of $\{m_z = 0, m_z = -1\}$ and $\{m_z = 0, m_z = +1\}$ (see also Table 5.1). The corresponding time-dependent NV levels used as sensor qubit states during the protocol are illustrated in the bottom part of the schematic.

spurious phases due to the environment [165].

We can now harness this freedom to generate a powerful new kind of quench protocol. The basic idea is to engineer a nontrivial time-dependence of the quench function $\eta(t)$ (c.f. Eq. (5.5)) by deliberately switching the sensor spin between the different possible qubit subspaces at prescribed times during the protocol. As we show below, the time dependent $\eta(t)$ generated by this approach can be utilized to generate comb-based filter functions that enable spectral reconstruction of the response function. Figure 5.6 illustrates a concrete example of control pulses that realize such time-dependent quenches: by periodically switching between the $\{m_z = 0, m_z = -1\}$ and $\{m_z = 0, m_z = +1\}$ qubit

subspaces (pulse period $T = t_f/2M$) in addition to applying standard qubit-control π-pulses at $\ell T/2$ ($\ell = 1, 3, \ldots, 4M-1$), we effectively realize the more general quench in Eq. (5.5) with $\hat{H}_{\rm b,i} = \hat{H}_{\rm b,0}$ and $\hat{V} = -\hat{B}/2$, whereas the corresponding quench function $\eta(t) = \sum_{n=0}^{2M-1}(-)^n\Theta(t-nT)\Theta(nT+T-t)$ is shown in Fig. 5.6.

For the more general control sequence discussed above, the qubit dynamics is again given by Eq. (5.8). The lab-frame noise operator is given by $\hat{\xi} = \hat{B}$; as before, we transform to the toggling frame defined by the standard qubit-control π-pulses (the control pulses switching between qubit subspaces do not contribute here), with the resulting filter function shown in Fig. 5.6.

We thus obtain the filter function $F[\omega]$ and quench function $\eta[\omega]$ in frequency space as

$$F[\omega] = -\frac{4}{\omega}e^{i\frac{\omega t_f}{2}}\sin\frac{\omega t_f}{2}\frac{\sin^2\frac{\omega t_f}{8M}}{\cos\frac{\omega t_f}{4M}}, \tag{5.28a}$$

$$\eta[\omega] = -\frac{2i}{\omega}e^{i\frac{\omega t_f}{2}}\sin\frac{\omega t_f}{2}\tan\frac{\omega t_f}{4M}. \tag{5.28b}$$

Substituting above equations into Eq. (5.12b), together they generate a frequency-comb filter function in the large pulse number $M \gg 1$ limit, which can be directly used to probe the spectral function $\mathcal{J}[\omega]$ (i.e. response function). More specifically, noting that $\hat{V} = -\hat{B}/2 = -\hat{\xi}/2$ we have

$$\Phi_{\rm q}(t_f) \simeq \int_{-\infty}^{+\infty} d\omega \mathcal{F}_{\mathcal{J}}[\omega; t_f]\mathcal{J}[\omega], \tag{5.29}$$

$$\mathcal{F}_{\mathcal{J}}[\omega; t_f] = -{\rm Im}(F^*[\omega]\eta[\omega])/4, \tag{5.30}$$

and $\mathcal{F}_{\mathcal{J}}[\omega; t_f]$ forms a comb-like structure in frequency space if we fix pulse periodicity

$T = t_f/2M$ and take the asymptotic large pulse number limit, i.e.

$$\mathcal{F}_{\mathcal{J}}[\omega; t_f] \sim -\frac{M}{\omega_0} \sum_{\ell=-\infty}^{+\infty} \mathcal{A}_\ell \delta(\omega - \ell\omega_0) \quad (M \gg 1), \tag{5.31a}$$

$$\omega_0 = \pi/T = 2M\pi/t_f, \tag{5.31b}$$

where $\mathcal{A}_\ell = (4/\ell^2)\sin(\ell\pi/2)$ are constant coefficients that depend on the control sequence and can be derived using Eq. (5.28).

Thus, by making use of all three levels of our spin-1 sensor, we can engineer a time-dependent quench function $\eta(t)$ that enables the construction of a standard comb-based filter function. This in turn allows spectral reconstruction of the imaginary bath response function (i.e. the spectral function $\mathcal{J}[\omega]$) over a large frequency range.

Note that Ref. [164] developed related techniques for reconstructing spatially correlated noise and response functions using multiple qubits; we stress that these are distinct from our multilevel protocols. More specifically, the multiqubit protocols crucially require 2-qubit SWAP gates in addition to standard dynamical-decoupling-type controls; further, the spectral function $\mathcal{J}[\omega]$ is not directly accessible via those existing protocols. In contrast, the quench physics in Eq. (5.5) provides a tool for directly probing bath response properties (i.e. its density of states), and our quench-based protocols can be straightforwardly implemented using only local spin-echo-type, or dynamical-decoupling control sequences.

5.5 Summary and outlook

In this work, we have shown how intrinsic quenches arise in standard T_2-style noise spectroscopy experiments, and how quench-induced phase shift effects to the sensor qubit can be utilized to estimate or reconstruct the spectral function, or more general response functions of the environment. These response properties provide an independent and complementary

environmental characterization from the standard noise spectral density, and encode useful information: in combination with standard NSD, we can use the estimated spectral function to extract effective temperature of a generic nonequilibrium bath. For environments in thermal equilibrium, the quench-enhanced QNS based on a single probe qubit also allows one to extract environmental temperature.

Our work highlights the critical role played by the initial state in controlling the effective quench physics associated with a generic T_2-style QNS experiment. As such, our quench formalism greatly expands previous works that considered related examples of environment-induced phase shift effects: by analyzing quenches that arise in the most general settings of T_2-based QNS protocols, we show that one can engineer a generic quench operator, or a quench with complex time dependence. These generalizations allow us to further use the quench phase shift to probe general response functions, or reconstruct the spectral function in a generic frequency range, respectively. Qubit magnetic noise spectroscopy has been used to probe electronic correlation functions in 2-dimensional systems [155, 189, 190]; it would be interesting to apply our technique to those system to also probe low-frequency electronic spectral function.

Our discussion so far on effective quench physics in standard T_2-type QNS has focused on the common case where the environment is either a quantum Gaussian bath, or where the sensor is weakly coupled to a quantum environment. While these cases make it convenient to describe the result emergence of a quench-induced sensor qubit phase shift, the physics we have discussed is far more general. In particular, the quench has nontrivial consequences on the sensor qubit even beyond the weak-coupling or Gaussian regime. In Appendix 5.6.4, we briefly discuss how these effect can be directly related to nonlinear response functions and noise susceptibilities of the environment. An interesting open question is how to design sensing protocols to extract those higher order response functions. Alternatively, quantum quenches have conventionally been used to explore correlated phenomena in many-body

systems [166]; our quench approach to QNS also opens up possibilities to explore new physics in these systems. We leave these to future works.

5.6 Appendices

5.6.1 Generalized quenches based on arbitrary initial bath states

Our discussion so far has focused on "incidental" environment quenches occurring during a generic QNS sensing protocol; for the most part, we considered a specific scenario where before the protocol starts, the environment is in the initial state described by Eq. (5.2b). We now show that the basic quench physics we have described (and its impact on the sensor qubit) applied to a far wider set of circumstances, where the bath starts in an arbitrary initial state $\hat{\rho}_{\mathrm{b,i}}$. This provides an entire new modality for sensing: one could deliberately prepare the environment in an interesting target state before the start of the sensing sequence, and then use the resulting quench physics (namely the influence on the sensor qubit's phase) to probe the environment.

The simplest generalization is when the environment is initially in a thermal state corresponding to some arbitrary (bath-only) Hamiltonian $\hat{H}_{\mathrm{b,i}}$:

$$\hat{\rho}_{\mathrm{b,i}} = e^{-\hat{H}_{\mathrm{b,i}}/k_B T}/Z_T, \tag{5.32}$$

In this case, we can directly use Eq. (5.5) to define our quench, and identify the quench operator $\hat{V}$ via Eq. (5.6). We stress that in this more general case, the initial bath Hamiltonian $\hat{H}_{\mathrm{b,i}}$ need not have any simple relation to the qubit-conditioned bath Hamiltonians $\hat{H}_{\mathrm{b},\uparrow(\downarrow)}$ appearing in Eq. (5.1). As a result, the quench operator $\hat{V}$ will now be independent of the noise operator $\hat{\xi} \equiv \hat{H}_{\mathrm{b},\uparrow} - \hat{H}_{\mathrm{b},\downarrow}$. For systems where it is possible to initialize the environment in different initial equilibrium states, this provides a powerful new way to probe the environment: different initial states yield different quenches, and hence different quench

phase shifts via Eq. (5.15).

An even more general scenario is when the bath starts in an arbitrary non-thermal equilibrium initial state $\hat{\rho}_{\mathrm{b,i}}$ that has no simple relation to a static Hamiltonian. This could be achieved in numerous ways, e.g. by explicitly driving the bath [191, 192]. As we have stressed repeatedly, our general quench mechanism is ultimately controlled by the initial state $\hat{\rho}_{\mathrm{b,i}}$ of the environment. A quench will occur as part of our T_2-style QNS protocol any time

$$[\hat{\rho}_{\mathrm{b,i}}, \hat{H}_{\mathrm{b,eff}}(t)] \neq 0, \quad 0 < t < t_f. \tag{5.33}$$

In cases where this state was thermal, this $\hat{\rho}_{\mathrm{b,i}}$ could easily be related to an initial bath Hamiltonian $\hat{H}_{\mathrm{b,i}}$, which we then used to identify the quench operator $\hat{V}$ in Eq. (5.6). In contrast, for our more general case, there is no unique way to identify $\hat{H}_{\mathrm{b,i}}$. In general, we may choose any bath Hamiltonian compatible with the initial bath state, i.e. satisfying $[\hat{H}_{\mathrm{b,i}}, \hat{\rho}_{\mathrm{b,i}}] = 0$. The choice of $\hat{H}_{\mathrm{b,i}}$ would then determine $\hat{V}$. We stress that this seeming ambiguity is only a choice of bookkeeping: the actual evolution of the sensor qubit (and the quench phase shift) is of course only determined by $\hat{\rho}_{\mathrm{b,i}}$ (see Appendix 5.6.2).

Given these caveats, we now present a simple (though non-unique) method to usefully parametrize the quench in the most general case. We define the initial bath Hamiltonian $\hat{H}'_{\mathrm{b,i}}$ and quench operator $\hat{V}'$ as the "longitudinal" (maximally commuting) and "transverse" (minimally non-commuting) components of the effective bath Hamiltonian with respect to $\hat{\rho}_{\mathrm{b,i}}$. We can make this prescription explicit by first diagonalizing the initial bath state as $\hat{\rho}_{\mathrm{b,i}} = \sum_{n=0}^{N} p_n \hat{P}_n$. Here the eigenvalues p_n are distinct with $p_0 = 0$, and $\hat{P}_n$ is the projector onto the eigenspace corresponding to p_n [193]. The initial bath Hamiltonian $\hat{H}'_{\mathrm{b,i}}$ and the

quench $\hat{V}'$ can now be defined as

$$\hat{H}'_{\mathrm{b,i}} \equiv \sum_{n=0}^{N} \hat{P}_n(\hat{H}_{\mathrm{b},\uparrow} + \hat{H}_{\mathrm{b},\downarrow})\hat{P}_n/2, \tag{5.34a}$$

$$\hat{V}' \equiv \sum_{m,n=0;\, m\neq n}^{N} \hat{P}_m(\hat{H}_{\mathrm{b},\uparrow} + \hat{H}_{\mathrm{b},\downarrow})\hat{P}_n/2. \tag{5.34b}$$

For concreteness, we provide an example of this procedure for a bosonic bath that couples linearly to the sensor qubit:

$$\hat{H}_{\mathrm{b},\downarrow} = \sum_k \Omega_k \hat{b}_k^\dagger \hat{b}_k, \tag{5.35a}$$

$$\hat{H}_{\mathrm{b},\uparrow} = \hat{H}_{\mathrm{b},\downarrow} + \sum_k \left(g_k \hat{b}_k^\dagger + \mathrm{H.c.}\right). \tag{5.35b}$$

We also assume that the initial bath state is not a thermal state, but a squeezed thermal state. As a result, the initial state of the sensor and bath is given by

$$\hat{\rho}_{\mathrm{tot}}(t = 0^-) = |{\downarrow}\rangle\langle{\downarrow}| \otimes \hat{\rho}_{\mathrm{b,i}}, \tag{5.36a}$$

$$\hat{\rho}_{\mathrm{b,i}} = \hat{S}(\vec{r})\, e^{-\hat{H}_{\mathrm{b},\downarrow}/k_B T} \hat{S}^\dagger(\vec{r})/Z_T, \tag{5.36b}$$

where $\hat{S}(\vec{r}) \equiv \exp\left(\sum_k r_k \hat{b}_k^2/2 - \mathrm{H.c.}\right)$ denotes the squeezing operator, with real constants r_k the corresponding mode squeezing parameters [76].

Using our above prescription, we find that initial bath Hamiltonian $\hat{H}'_{\mathrm{b,i}}$ and the quench

operator $\hat{V}'$ in Eq. (5.34) are given by

$$\hat{H}'_{\mathrm{b,i}} = \sum_k \Omega_k \left[\hat{b}_k^\dagger \hat{b}_k \cosh^2 2r_k + \frac{\sinh 4r_k}{4} \left(\hat{b}_k^{\dagger 2} + \mathrm{H.c.} \right) \right], \tag{5.37a}$$

$$\begin{aligned} \hat{V}' = &- \sum_k \Omega_k \hat{b}_k^\dagger \hat{b}_k \sinh^2 2r_k \\ &+ \frac{1}{4} \sum_k \left(-\Omega_k \hat{b}_k^{\dagger 2} \sinh 4r_k + 2g_k \hat{b}_k^\dagger + \mathrm{H.c.} \right). \end{aligned} \tag{5.37b}$$

While the quench operator $\hat{V}'$ in Eq. (5.37b) still contains an incidental contribution which depends on qubit-bath couplings g_k, it also includes deliberate quenches that can be tuned via the initial squeezing parameters r_k. We again note that it is not the only way to introduce a quench operator $\hat{V}$ satisfying Eq. (5.8). However, this convention is useful for understanding effects on qubit dynamics due to the quench.

5.6.2 Qubit dynamics during a standard T_2-type experiment

In this subsection, we provide a detailed derivation of Eq. (5.8) in the main text, which describes qubit dynamics due to pure-dephasing baths in a general T_2-type (e.g., spin echo, or general dynamical decoupling) experiment. For concreteness, we first reiterate the general setup of the T_2-type experiment; more detail can be found in the main text. As standard, we assume that the qubit is initialized into a pure state with no qubit-bath entanglement, so that an instantaneous $\pi/2$-pulse at the beginning of the protocol ($t = 0$) prepares the system in a product state given by

$$\hat{\rho}_{\mathrm{tot}}(t = 0^+) = |+\rangle\langle+| \otimes \hat{\rho}_{\mathrm{b,i}}, \tag{5.38a}$$

$$|+\rangle \equiv \left(|\uparrow\rangle + |\downarrow\rangle \right) / \sqrt{2}. \tag{5.38b}$$

The system then evolves under a pure-dephasing-type total Hamiltonian $\hat{H}_{\rm tot}$ for time t_f, while the qubit is subject to a sequence of instantaneous control π-pulses. At each instant t during the time evolution, the total qubit-bath system Hamiltonian can be rewritten as

$$\hat{H}_{\rm tot} = |\uparrow\rangle\langle\uparrow| \otimes \hat{H}_{\rm b,\uparrow} + |\downarrow\rangle\langle\downarrow| \otimes \hat{H}_{\rm b,\downarrow} \tag{5.39a}$$

$$= \hat{\sigma}_0 \otimes H_{\rm b,avg} + \frac{\hat{\sigma}_z}{2} \otimes \hat{\xi}, \qquad 0 < t < t_f, \tag{5.39b}$$

where we introduce

$$\hat{\sigma}_0 \equiv |\uparrow\rangle\langle\uparrow| + |\downarrow\rangle\langle\downarrow|\,, \quad \hat{\sigma}_z \equiv |\uparrow\rangle\langle\uparrow| - |\downarrow\rangle\langle\downarrow|\,, \tag{5.40a}$$

$$H_{\rm b,avg} \equiv \frac{1}{2}(\hat{H}_{\rm b,\uparrow} + \hat{H}_{\rm b,\downarrow}), \quad \hat{\xi} \equiv \hat{H}_{\rm b,\uparrow} - \hat{H}_{\rm b,\downarrow}. \tag{5.40b}$$

To keep our discussion general, we will assume a generic initial bath state $\hat{\rho}_{\rm b,i}$, and a corresponding initial bath Hamiltonian $\hat{H}_{\rm b,i}$ satisfying $[\hat{H}_{\rm b,i}, \hat{\rho}_{\rm b,i}] = 0$ (see also the preceding section). It is thus convenient to introduce a time-dependent effective bath Hamiltonian $\hat{H}_{\rm b,eff}(t)$ as

$$\hat{H}_{\rm b,eff}(t) \equiv \begin{cases} \hat{H}_{\rm b,i}, & t \leq 0, \\ H_{\rm b,avg}, & 0 < t < t_f. \end{cases} \tag{5.41}$$

As shown in Eq. (5.33), a nontrivial quench $\hat{V}$ generally arises in this standard T_2-type protocol, if the initial bath state $\hat{\rho}_{\rm b,i}$ does not commute with the effective bath Hamiltonian governing subsequent bath dynamics, i.e., $[\hat{\rho}_{\rm b,i}, \hat{H}_{\rm b,avg}] \neq 0$. We can rewrite $\hat{H}_{\rm b,eff}(t)$ in terms of the initial $\hat{H}_{\rm b,i}$ and this quench operator $\hat{V}$ as (see the preceding section and Eq. (5.5) in the main text)

$$\hat{H}_{\rm b,eff}(t) = \hat{H}_{\rm b,i} + \eta(t)\hat{V}, \tag{5.42}$$

where the quench function $\eta(t)$ vanishes, i.e. $\eta(t)=0$, unless $0<t<t_f$.

Transforming to the standard toggling frame with respect to qubit control pulses, as well as the rotating frame defined by initial bath Hamiltonian $\hat{H}_{\rm b,i}$, we obtain the rotating-frame Hamiltonian

$$\hat{H}_{\rm I}(t)=\eta(t)\hat{\sigma}_0\otimes\hat{V}(t)+F(t)\frac{\hat{\sigma}_z}{2}\otimes\hat{\xi}(t),\quad 0<t<t_f, \tag{5.43}$$

where $F(t)$ denotes the usual noise filter function that encodes the timing of qubit control π-pulses, and $\hat{V}(t)$ and $\hat{\xi}(t)$ refer to the rotating-frame bath-only operators. Thus, we can compute the qubit coherence function $\langle\hat{\sigma}_-(t_f)\rangle=\langle\uparrow|{\rm Tr}_{\rm bath}\left[\hat{\rho}_{\rm tot}(t_f)\right]|\downarrow\rangle$ in this toggle-rotating frame as

$$\hat{\rho}_{\rm tot}(t_f)=\mathcal{T}e^{-i\int_0^{t_f}dt'\hat{H}_{\rm I}(t')}\hat{\rho}_{\rm tot}(t=0^+)\tilde{\mathcal{T}}e^{i\int_0^{t_f}dt'\hat{H}_{\rm I}(t')}, \tag{5.44}$$

$$\Rightarrow\frac{\langle\hat{\sigma}_-(t_f)\rangle}{\langle\hat{\sigma}_-(0^+)\rangle}={\rm Tr}\left\{\mathcal{T}e^{-i\int_0^{t_f}dt'\hat{H}_\uparrow(t')}\hat{\rho}_{\rm b,i}\tilde{\mathcal{T}}e^{i\int_0^{t_f}dt'\hat{H}_\downarrow(t')}\right\}, \tag{5.45}$$

$$\hat{H}_{\uparrow(\downarrow)}(t)\equiv\eta(t)\hat{V}(t)\pm\frac{1}{2}F(t)\hat{\xi}(t), \tag{5.46}$$

where $\mathcal{T}$ and $\tilde{\mathcal{T}}$ denote time- and anti-time orderings, respectively. From Eq. (5.38) we have $\langle\hat{\sigma}_-(0^+)\rangle=1/2$, so that the qubit coherence function $\langle\hat{\sigma}_-(t_f)\rangle$ can be rewritten as

$$\langle\hat{\sigma}_-(t_f)\rangle=\frac{1}{2}{\rm Tr}(\hat{U}_\uparrow\hat{\rho}_{\rm b,i}\hat{U}_\downarrow^\dagger), \tag{5.47a}$$

$$\hat{U}_{\uparrow(\downarrow)}=\mathcal{T}\exp\left\{-i\int_{-\infty}^{+\infty}\left[\eta(t')\hat{V}(t')\pm\frac{F(t')}{2}\hat{\xi}(t')\right]dt'\right\}, \tag{5.47b}$$

i.e., we obtain Eq. (5.8) in the main text. Note that we adopt the convention where the filter and quench functions vanish (i.e., $F(t)=\eta(t)=0$) unless $0\le t\le t_f$.

From above derivation, it is straightforward to see that the exact qubit dynamics only depends on initial bath state $\hat{\rho}_{\rm b,i}$, and Eq. (5.47) (i.e., Eq. (5.8) in the main text) holds for a generic quench operator $\hat{V}$ associated with any $\hat{H}_{\rm b,i}$ satisfying $[\hat{H}_{\rm b,i},\hat{\rho}_{\rm b,i}]=0$. For

a generic bath initial state $\hat{\rho}_{\mathrm{b,i}}$, as discussed in the preceding section), a useful way to resolve such ambiguity in $\hat{V}$ is to choose the particular $\hat{V}' \equiv H_{\mathrm{b,avg}}(t = 0^+) - \hat{H}'_{\mathrm{b,i}}$ as the minimally non-commuting component of $H_{\mathrm{b,avg}}$ with respect to $\hat{\rho}_{\mathrm{b,i}}$. While this is not the only workable choice, it highlights the fact that the quench is more directly controlled by the initial bath state rather than the physical bath Hamiltonian at the beginning of the protocol. Identifying the quench in this way also allows us to compute qubit dynamics using a systematic perturbative expansion of Eq. (5.47) in terms of the quench operator $\hat{V}$.

5.6.3 Leading order qubit time evolution due to a quenched environment

In Eqs. (5.12) in the main text, we present general formulae relating leading order bath-induced dephasing (quench-induced phase shift) effects to the bath noise spectral density (linear response susceptibility function). While there are multiple ways to derive this result, in this subsection we provide a detailed derivation based on the Keldysh field theory technique and cumulant expansion [100]. Our approach is directly applicable to non-Gaussian baths, and elucidates the regime where Eqs. (5.12) becomes exact.

We start with Eq. (5.45) (of which Eq. (5.8) constitutes a special case), where the sensor-qubit coherence function by the end of a T_2-type experiment is given by

$$\frac{\langle \hat{\sigma}_-(t_f)\rangle}{\langle \hat{\sigma}_-(0^+)\rangle} = \mathrm{Tr}\left\{ \mathcal{T} e^{-i\int_0^{t_f} dt' \hat{H}_\uparrow(t')} \hat{\rho}_{\mathrm{b,i}} \tilde{\mathcal{T}} e^{i\int_0^{t_f} dt' \hat{H}_\downarrow(t')} \right\}, \tag{5.48a}$$

$$\hat{H}_{\uparrow(\downarrow)}(t) = \eta(t)\hat{V}(t) \pm \frac{1}{2} F(t)\hat{\xi}(t). \tag{5.48b}$$

For convenience, we introduce the Keldysh-ordered cumulant generating function (CGF) $\chi[F(t), \eta(t); t_f]$ of the bath noise and quench operators as

$$\chi[F(t), \eta(t); t_f] \equiv \ln\left[\frac{\langle \hat{\sigma}_-(t_f)\rangle}{\langle \hat{\sigma}_-(0^+)\rangle} \right]. \tag{5.49}$$

See Ref. [100] for discussions on the physical implications of this function. In terms of qubit dynamics, the real and imaginary parts of $\chi[F(t),\eta(t);t_f]$ correspond to qubit dephasing and bath-induced phase shift effects, respectively.

We can now compute qubit coherence $\langle\hat{\sigma}_-(t_f)\rangle$ by perturbatively expanding the CGF $\chi[F(t),\eta(t);t_f]$ in terms of $\hat{\xi}(t)$ and $\hat{V}(t)$. The Keldysh technique offers a systematic way to perform this expansion [100, 194, 195]. In the Keldysh approach, for each bath operator $\hat{A}$ there are a corresponding classical field $A_{\rm cl}(t)$ and a quantum field $A_{\rm q}(t)$. Stochastic averages between these fields can be computed in a well-defined way, with respect to the so-called Keldysh action. The very construction of the Keldysh action (see, e.g., Ref. [100]) ensures that the quantum operator expectation value in Eq. (5.48a) can be directly related to averages that only involve $\xi_{\rm cl}$ and $V_{\rm q}$. Taking the logarithm of Eq. (5.48a), the CGF $\chi[F(t),\eta(t);t_f]$ is in turn given by

$$\chi[F(t),\eta(t);t_f] = \sum_{\ell=1}^{\infty}\sum_{m=0}^{\infty}\frac{(-i)^{\ell+m}}{\ell!m!}\chi^{(\ell,m)}[F(t),\eta(t);t_f], \tag{5.50}$$

$$\chi^{(\ell,m)}[F(t),\eta(t);t_f] = \prod_{j=1}^{\ell}\left[\int_0^{t_f}dt_j F(t_j)\right]\prod_{k=\ell+1}^{\ell+m}\left[\int_0^{t_f}dt_k\eta(t_k)\right]C^{(\ell,m)}(\vec{t}_{\ell+m}), \tag{5.51}$$

where we define $\vec{t}_n \equiv (t_1,\ldots,t_n)$. Here $C^{(\ell,m)}(\vec{t}_{\ell+m})$ denote Keldysh-ordered cumulants, which can be directly generated from Keldysh-ordered moments of the form

$$\overline{\xi_{\rm cl}(t_1)\ldots\xi_{\rm cl}(t_\ell)V_{\rm q}(t_{\ell+1})\ldots V_{\rm q}(t_{\ell+m})}, \tag{5.52}$$

and lower-order averages. Note that the terms in Eq. (5.50) involving cumulants of the form $C^{(\ell,0)}(\vec{t}_\ell)$ correspond to contributions solely from noise fluctuations, which would determine qubit dynamics in the absence of quenches. In contrast, the cumulants $C^{(\ell,m)}(\vec{t}_{\ell+m})$ for $m>0$ encode bath (linear and nonlinear) response properties ($\ell=1$), as well as noise susceptibilities ($\ell>1$).

Without loss of generality, we assume zero-average noise operator, i.e. $\langle\hat{\xi}\rangle = 0$. The first order contribution to the cumulant expansion in Eq. (5.50) thus vanishes, and the leading-order nontrivial Keldysh-ordered cumulants can be written explicitly as

$$C^{(2,0)}(\vec{t}_2) = \overline{\xi_{\rm cl}(t_1)\xi_{\rm cl}(t_2)} = \frac{1}{2}\langle\{\hat{\xi}(t_1), \hat{\xi}(t_2)\}\rangle, \tag{5.53a}$$

$$C^{(1,1)}(\vec{t}_2) = \overline{\xi_{\rm cl}(t_1)V_{\rm q}(t_2)} = \Theta(t_1 - t_2)\langle[\hat{\xi}(t_1), \hat{V}(t_2)]\rangle, \tag{5.53b}$$

where the bath operator average is defined with respect to $\hat{\rho}_{\rm b,i}$ as $\langle\hat{A}\rangle \equiv {\rm Tr}(\hat{A}\hat{\rho}_{\rm b,i})$. These leading order cumulants can be directly related to the bath noise spectral density (NSD) $\bar{S}[\omega]$ and response susceptibility function $G^R_{\xi V}[\omega]$, as

$$\bar{S}[\omega] \equiv \frac{1}{2}\int_{-\infty}^{+\infty} dt e^{i\omega t}\langle\{\hat{\xi}(t), \hat{\xi}(0)\}\rangle = \int_{-\infty}^{+\infty} dt e^{i\omega t} C^{(2,0)}(t, 0), \tag{5.54a}$$

$$G^R_{\xi V}[\omega] \equiv -i\int_{-\infty}^{+\infty} dt e^{i\omega t}\Theta(t)\langle[\hat{\xi}(t), \hat{V}(0)]\rangle = -i\int_{-\infty}^{+\infty} dt e^{i\omega t} C^{(1,1)}(t, 0). \tag{5.54b}$$

Substituting above relations into Eqs. (5.49) and (5.50), we can rewrite the leading order contributions in terms of bath NSD and linear response susceptibility, so that we obtain

$$\frac{\langle\hat{\sigma}_-(t_f)\rangle}{\langle\hat{\sigma}_-(0^+)\rangle} = e^{-\zeta(t_f) - i\Phi(t_f)}, \tag{5.55a}$$

$$\zeta(t_f) \simeq \frac{1}{2}\int_{-\infty}^{+\infty} dt_1 F(t_1)\int_{-\infty}^{+\infty} dt_2 F(t_2) C^{(2,0)}(\vec{t}_2) = \int_{-\infty}^{+\infty}\frac{d\omega}{4\pi}|F[\omega]|^2\bar{S}[\omega], \tag{5.55b}$$

$$\Phi(t_f) \simeq -i\int_{-\infty}^{+\infty} dt_1 F(t_1)\int_{-\infty}^{+\infty} dt_2 \eta(t_2) C^{(1,1)}(\vec{t}_2) = \int_{-\infty}^{+\infty}\frac{d\omega}{2\pi}F^*[\omega]\eta[\omega]G^R_{\xi V}[\omega]. \tag{5.55c}$$

Above equations reproduce Eqs. (5.12).

The cumulant expansion in Eq. (5.50) terminates at the second order if $\xi_{\rm cl}(t)$ and $V_{\rm q}(t)$ are Gaussian random variables, which is satisfied by linearly coupled harmonic oscillator bath models discussed in the main text. For this case, the dephasing and phase shift expressions in Eqs. (5.55b) and (5.55c) become exact. Thus, we conclude that Eqs. (5.12), or equivalently

Eqs. (5.55b) and (5.55c), hold exactly for Gaussian baths, where noise and quench operators can take arbitrarily strong coupling strengths. Alternatively for more general non-Gaussian baths, Eqs. (5.55) describe leading-order approximations for qubit dynamics in terms of bath noise and quench operators.

It is worth unpacking Eq. (5.12b), or equivalently Eq. (5.55c), to provide a physical understanding of the quench-induced phase. As shown in Eq. (5.5), the effective quench at the start of our protocol at $t = 0$ suddenly turns on a term $\eta(t)\hat{V}$ in the effective bath Hamiltonian (c.f. Eq. (5.5)). At the linear response level, this perturbation causes a time-dependent shift in the average of the bath operator $\hat{\xi}$ that couples to the qubit. This shift is given from linear response by $\langle\delta\hat{\xi}(t)\rangle_V = \int_{-\infty}^{+\infty} dt_2 \eta(t_2) G^R_{\xi V}(t - t_2)$. Next, this induced average value of $\hat{\xi}$ has a direct consequence on the qubit: it is equivalent to a time-dependent z magnetic field on the sensor qubit. This then leads to a net phase shift given by the integral of this effective field weighted by the filter function $F(t)$: $\Phi_{\rm q}(t_f) = \int_{-\infty}^{+\infty} dt_1 F(t_1)\langle\delta\hat{\xi}(t_1)\rangle_V$. Connections between sensor phase shifts and linear response were also discussed in Ref. [165]. Note that our expression for the quench phase shift can be written as $\Phi_{\rm q}(t_f) = \int_{-\infty}^{+\infty} dt_1 F(t_1) \int_{-\infty}^{+\infty} dt_2 \eta(t_2) G^R_{\xi V}(t_1 - t_2)$. This is similar but not identical to Eq. (15) in Ref. [165], where the filter function $F(t_1)$ erroneously occurs at a later time than the quench function $\eta(t_2)$.

5.6.4 Generalizations beyond Gaussian bath approximation

For the case of a general environment, the qubit dynamics is still generally described by Eq. (5.8). For the general case, a powerful means of attack is provided by Keldysh field theory techniques [100, 194, 195]. One finds that the quench does more that just induce a phase shift $\Phi_{\rm q}(t_f)$ (c.f. Eq. (5.12b)). The quench physics can also modify the noise properties of the bath, changing the dephasing function in Eq. (5.9).

A general way to describe these effects is to use non-linear response theory, something that

can be effectively calculated using the Keldysh approach. For weakly coupled (or Gaussian) environments, the quench only induces a nonzero average of the noise operator $\xi(t)$ that is linear in the quench operator $\hat{V}$. In the more general cases, this shift in mean will have higher-order terms in $\hat{V}$; in addition, the symmetrized noise correlator of $\xi(t)$ will also be modified. Keeping terms to leading orders in $\hat{V}$, these effects can formally be written in terms of nonlinear response functions as

$$\begin{aligned}\langle\delta\hat{\xi}(t)\rangle_V &= \int_{-\infty}^{+\infty} dt_1 \eta(t_1) G^R_{\xi V}(t-t_1) \\ &\quad + \iint_{-\infty}^{+\infty} dt_1 dt_2 \eta(t_1)\eta(t_2) G^R_{\xi,VV}(t-t_2, t_1-t_2) + \ldots, \qquad (5.56)\\ \langle\delta\hat{\xi}(t)\delta\hat{\xi}(t')\rangle_V &= \int_{-\infty}^{+\infty} dt_1 \eta(t_1) G^R_{\xi\xi,V}(t-t_1, t'-t_1) + \ldots, \qquad (5.57)\end{aligned}$$

where the susceptibility functions $G^R_{\xi V}(t)$, $G^R_{\xi,VV}(t_1,t_2)$, and $G^R_{\xi\xi,V}(t_1,t_2)$ can be systematically computed using Keldysh field theory techniques [100, 195]. Note the appearance of a new function here, $G^R_{\xi\xi,V}(t_1,t_2)$. This is often referred to as a noise susceptibility, and describes how the environmental symmetrized noise spectral density is modified by the quench. Noise susceptibilities often reveal subtle features of a physical system, and have been studied in a variety of contexts (e.g. to uncover subtle features of coherent quantum electronic transport [196]).

The upshot is that the quench physics described here is not limited to weakly-coupled or Gaussian environments. For the general case, it can be described using both linear and nonlinear response functions [100, 196, 197]. This also highlights another utility of our quench approach to QNS: it provides in principle access to higher-order nonlinear response properties of an unknown environment using T_2-type measurements. More specifically, one can design general quench control protocol (e.g., making use of the multilevel probe qubit shown in Fig. 5.6) to generate comb-based filter functions and reconstruct these higher-order response spectral functions of a non-Gaussian quantum environment. We leave details to

future work.

5.6.5 *Derivation of the relation between the quench phase shift and the bath density of states*

In Eq. (5.12b) of the main text, we provide a general formula to compute the quench-induced phase shift using the Green-Kubo linear response theory, which relates the phase shift to the bath susceptibility function $G^R_{\xi V}[\omega]$. We then claim that for the specific quench function $\eta(t) = \Theta(t)\Theta(t_f - t)$ emerging in a typical T_2-type experiment, this phase shift can be rewritten as Eq. (5.15), which only involves the imaginary part of response function. In this subsection, we explicitly derive the latter equation using the general formula. Recall that for a generic Gaussian bath, the quench phase shift (QPS) is given by Eq. (5.12b) as

$$\Phi_{\rm q}(t_f) = \int_{-\infty}^{+\infty} \frac{d\omega}{2\pi} F^*[\omega]\eta[\omega]G^R_{\xi V}[\omega] \tag{5.58}$$

$$= \int_{-\infty}^{+\infty} dt_1 F(t_1) \int_{-\infty}^{+\infty} dt_2 \eta(t_2) G^R_{\xi V}(t_1 - t_2), \tag{5.59}$$

where $G^R_{\xi V}(t) \equiv -i\Theta(t)\langle[\hat{\xi}(t), \hat{V}(0)]\rangle$ is the standard Green-Kubo linear response susceptibility function. Noting that the real and imaginary parts of the spectral response function $G^R_{\xi V}[\omega]$ are related to each other via the Kramers-Kronig relation, we can rewrite the QPS in terms of only ${\rm Im}G^R_{\xi V}[\omega]$. More specifically, given that the retarded Green's function $G^R_{\xi V}(t)$ is real by definition, the imaginary part of the response function ${\rm Im}G^R_{\xi V}[\omega]$ can be written as

$${\rm Im}G^R_{\xi V}[\omega] = \frac{1}{2i}\int_{-\infty}^{+\infty} dt e^{i\omega t}\left[G^R_{\xi V}(t) - G^R_{\xi V}(-t)\right]. \tag{5.60}$$

Thus, we can rewrite the QPS as

$$\begin{aligned}\Phi_{\rm q}(t_f) =& \int_{-\infty}^{+\infty} dt_1 F(t_1) \int_{-\infty}^{+\infty} dt_2 \eta(t_2) G^R_{\xi V}(t_1 - t_2) \\ =& \int_0^{t_f} dt_1 F(t_1) \int_0^{t_1} dt_2 \eta(t_2) [G^R_{\xi V}(t_1 - t_2) - G^R_{\xi V}(t_2 - t_1)] \\ =& 2 \int_{-\infty}^{+\infty} \frac{d\omega}{2\pi} {\rm Im} G^R_{\xi V}[\omega] \mathcal{F}_\Phi[F(t), \eta(t); t_f], \end{aligned} \tag{5.61}$$

where we have made use of the fact that the susceptibility $G^R_{\xi V}(t) = 0$ for $t < 0$. The general weighting function $\mathcal{F}_\Phi[F(t), \eta(t); t_f]$ is now given by

$$\mathcal{F}_\Phi[F(t), \eta(t); t_f] \equiv \int_0^{t_f} dt_1 F(t_1) \int_0^{t_1} dt_2 \eta(t_2) \sin\omega(t_1 - t_2). \tag{5.62}$$

Substituting into above equation the specific quench function $\eta(t) = \Theta(t)\Theta(t_f - t)$, we can explicitly compute the integral involving $\eta(t_2)$ in Eq. (5.62) to obtain

$$\Phi_{\rm q}(t_f) = \int_{-\infty}^{+\infty} \frac{d\omega}{\pi} \frac{{\rm Re}F[0] - {\rm Re}F[\omega]}{\omega} {\rm Im} G^R_{\xi V}[\omega], \tag{5.63}$$

so that for spin-echo or dynamical-decoupling control pulses with $F[0] \equiv \int_0^{t_f} F(t) dt = 0$, we recover Eq. (5.15). For the specific form of the quench operator $\hat{V}(t) = \hat{\xi}(t)/2$ as given by Eq. (5.7b), we can rewrite above expression for the QPS $\Phi_{\rm q}(t_f)$ in terms of imaginary part of the response function ${\rm Im} G^R_{\xi\xi}[\omega]$ as

$$\Phi_{\rm q}(t_f) = \int_{-\infty}^{+\infty} \frac{d\omega}{2\pi} \frac{{\rm Re}F[0] - {\rm Re}F[\omega]}{\omega} {\rm Im} G^R_{\xi\xi}[\omega]. \tag{5.64}$$

Alternatively, for general forms of quench function $\eta(t)$, it is still possible to represent the QPS using a frequency-space integral of imaginary part of the response function, as weighted by the control functions $F[\omega]$ and $\eta[\omega]$. However, in general the integral would be nonlocal in frequency space. From the general expression in Eq. (5.62), we can rewrite the general

transfer function for the quench phase shift $\mathcal{F}_\Phi[F(t), \eta(t); t_f]$ as

$$\mathcal{F}_\Phi[F(t), \eta(t); t_f] = -\,\mathrm{Re}F[\omega]\mathrm{Im}\eta[\omega] + \mathcal{P}\int_{-\infty}^{+\infty} \frac{d\omega_1}{\pi} \frac{\mathrm{Re}F[\omega_1]\mathrm{Re}\eta[\omega_1]}{\omega - \omega_1}. \tag{5.65}$$

As shown in Eq. (5.63), the above function $\mathcal{F}_\Phi[F(t), \eta(t); t_f]$ greatly simplifies when using the specific quench function $\eta(t) = \Theta(t)\Theta(t_f - t)$.

5.6.6 QPS in comparison to relaxometry-based techniques to measure response

In the main text, we have focused on the specific type of quantum noise spectroscopy measurements where a sensor qubit is coupled to its environment via pure-dephasing-type interactions. Within this setting, we have shown the quench phase shift (QPS) lets one probe the response properties, or spectral function of the environment, which would be otherwise inaccessible using standard dephasing-based noise spectroscopy.

Interestingly, in principle one can extract similar information about the imaginary part of response function $\mathrm{Im}G^R_{\xi\xi}[\omega]$, or equivalently the spectral function, using an extended version of standard T_1 relaxometry experiments. Conventional T_1-type experiments specifically probes transversely coupled bath fields (e.g., via $\hat{H}_{\mathrm{int}} = \hat{\sigma}_x \otimes \hat{\xi}$), which induces transitions between the qubit levels. In this setting, typically one would measure the qubit population decay rate $\Gamma_{\mathrm{tot}} \equiv 1/T_1$ [198], which corresponds to the sum of qubit relaxation and excitation rates. A straightforward calculation based on Fermi's Golden rule can then relate Γ_{tot} to the symmetrized noise spectral density (NSD) via $\Gamma_{\mathrm{tot}} = 2\bar{S}[\Omega]$, whereas the difference between relaxation and excitation rates corresponds to the response function $\mathrm{Im}G^R_{\xi\xi}[\Omega]$ (see the following paragraph for more detail). While the bath NSD can be directly inferred from T_1-decay rate Γ_{tot}, to further probe response function $\mathrm{Im}G^R_{\xi\xi}[\omega]$ one would also need to measure the qubit steady state population $\langle\hat{\sigma}_z\rangle_{\mathrm{ss}}$: the latter measurement is not a part of standard

T_1 relaxometry [137, 199]. In comparison, the QPS in Eq. (5.12b) is readily accessible in standard T_2-type measurements, and as we show in the main text, arguably offers a more direct knob to probe the response properties of longitudinal bath fields. We also note that standard T_1-type experiments are not sensitive to dephasing baths. Although in principle one can use the spin-locking technique (also known as $T_{1\rho}$ measurements) [137], i.e. continuously drive the qubit to measure longitudinal bath fields via relaxometry-based experiments, in practice the drive strength needs to be higher than the inhomogeneous linewidth of the qubit. Thus, the range of frequencies that can be probed using the spin-locking technique often does not correspond to the dominating dephasing source for the undriven qubit (see e.g. [142, 200, 201]). In contrast, T_2-type experiments with QPS measurements are more suitable for probing low-frequency dephasing noise source.

We now concretely show the relation between qubit decay rate Γ_{tot} and the steady state population $\langle\hat{\sigma}_z\rangle_{\text{ss}}$ to environmental properties. For the case of transverse coupling to the bath, it is more illuminating to represent bath properties in terms of the quantum noise spectra $S[\omega] \equiv \int_{-\infty}^{+\infty} dt e^{i\omega t}\langle\hat{\xi}(t)\hat{\xi}(0)\rangle$, so that the Fermi's Golden rule transition rates for qubit excitation and relaxation $\Gamma_{\pm}$ are given by $\Gamma_{\pm} = S[\mp\Omega]$ (Ω denotes qubit transition frequency; see Ref. [23] for a pedagogical introduction). One can use a few lines of algebra to show that the symmetrized and anti-symmetrized components of $S[\omega]$ are related to the bath NSD $\bar{S}[\omega] = (S[+\omega] + S[-\omega])/2$, and the imaginary part of response function $\text{Im}G^R_{\xi\xi}[\omega] = (S[-\omega] - S[+\omega])/2$, respectively. The qubit population decay rate Γ_{tot} and the steady state population $\langle\hat{\sigma}_z\rangle_{\text{ss}}$ can then be computed explicitly as $\Gamma_{\text{tot}} = \Gamma_+ + \Gamma_- = 2\bar{S}[\Omega]$, and $\langle\hat{\sigma}_z\rangle_{\text{ss}} = \text{Im}G^R_{\xi\xi}[\Omega]/\bar{S}[\Omega]$. Thus, given both the qubit decay rate and steady state population simultaneously, we can use them to infer the response function [23, 150, 162, 202].

5.6.7 Asymptotic analysis on qubit evolution due to environments with power-law noise spectra and response functions

In the main text, we present the asymptotic long-time behavior of qubit dephasing function and quench phase shift (QPS) in Eqs. (5.22), assuming that the bath noise spectral density (NSD) and density of states functions exhibit power-law dependence in the asymptotic low-frequency limit. For clarity, here we provide a detailed derivation of the asymptotic results. We start with the general expressions for the dephasing function $\zeta(t_f)$ and QPS $\Phi_{\rm q}(t_f)$ under any spin-echo qubit control pulse, given by Eqs. (5.12a) and (5.15) in the main text as

$$\zeta(t_f) = \int_{-\infty}^{+\infty} \frac{d\omega}{4\pi} |F[\omega]|^2 \bar{S}[\omega], \tag{5.66a}$$

$$\Phi_{\rm q}(t_f) = -\int_{-\infty}^{+\infty} \frac{d\omega}{\pi\omega} {\rm Re}F[\omega]\, {\rm Im}G^R_{\xi V}[\omega]. \tag{5.66b}$$

We also assume that the bath NSD $\bar{S}[\omega]$ and response functions ${\rm Im}G^R_{\xi V}[\omega]$ exhibit power-law dependence in the asymptotic low-frequency regime (see Eqs. (5.20) in the main text)

$$\bar{S}[\omega] \sim S_0 \omega^p \quad (\omega \to 0^+), \tag{5.67a}$$

$${\rm Im}G^R_{\xi V}[\omega] \sim -\frac{A_0}{2}\omega^s \quad (\omega \to 0^+). \tag{5.67b}$$

For convenience, we rewrite the bath NSD $\bar{S}[\omega]$ and response functions ${\rm Im}G^R_{\xi V}[\omega]$ in the full frequency range in terms of cutoff functions $\mu_A(x)$ $(A = S, G)$ as

$$\bar{S}[\omega] = S_0 \omega^p \mu_S(\omega/\omega_{\rm c}), \tag{5.68a}$$

$${\rm Im}G^R_{\xi V}[\omega] = -\frac{A_0}{2}\omega^s \mu_G(\omega/\omega_{\rm c}), \tag{5.68b}$$

where we introduce a UV cutoff frequency $\omega_{\rm c}$ below which the asymptotic power-law function provides a good approximation for the exact function. By definition, the cutoff functions

$\mu_A(x)$ satisfy following conditions

$$\mu_A(0)=1, \quad \lim_{x\to\infty}\mu_A(x)=0, \quad (A=S,G), \tag{5.69}$$

and we further assume both cutoff functions $\mu_A(x)$ $(A=S,G)$ corresponding to any physical bath are smooth near $x=0$.

We now consider a generic qubit control pulse satisfying $F[0]=0$, which consists of L instantaneous π-pulses at times $t=\alpha_\ell t_f$. Without loss of generality, we assume the coefficients α_ℓ $(\ell=1,2,\ldots,L)$ satisfy following conditions

$$\alpha_1<\alpha_2<\ldots<\alpha_L, \quad F[0]=0 \Leftrightarrow 2\sum_{\ell=1}^{L}(-)^\ell\alpha_\ell+(-)^{L+1}=0, \tag{5.70}$$

so that we can explicitly compute the filter function $F[\omega]$ as

$$F[\omega]=\int_0^{t_f}dt_1F(t_1)e^{i\omega t_1}=\frac{2\sum_{\ell=1}^{L}(-)^{\ell-1}e^{i\alpha_\ell\omega t_f}-1+(-)^Le^{i\omega t_f}}{i\omega}. \tag{5.71}$$

Substituting above equation into Eqs. (5.66) and noting that the integrands are even functions of frequency, we obtain

$$\begin{aligned}\zeta(t_f)&=\frac{S_0}{2\pi}\int_0^{+\infty}\omega^{p-2}\left|2\sum_{\ell=1}^{L}(-)^\ell e^{i\alpha_\ell\omega t_f}+1+(-)^{L+1}e^{i\omega t_f}\right|^2\mu_S(\omega/\omega_c)\,d\omega\\&=\frac{S_0}{2\pi}t_f^{1-p}\int_0^{+\infty}x^{p-2}\left|2\sum_{\ell=1}^{L}(-)^\ell e^{i\alpha_\ell x}+1+(-)^{L+1}e^{ix}\right|^2\mu_S\left(x/\omega_ct_f\right)dx, \qquad (5.72a)\\ \Phi_q(t_f)&=\frac{A_0}{\pi}\int_0^{+\infty}\omega^{s-2}\left[2\sum_{\ell=1}^{L}(-)^{\ell-1}\sin\alpha_\ell\omega t_f+(-)^L\sin\omega t_f\right]\mu_G(\omega/\omega_c)\,d\omega\\&=\frac{A_0}{\pi}t_f^{1-s}\int_0^{+\infty}x^{s-2}\left[2\sum_{\ell=1}^{L}(-)^{\ell-1}\sin\alpha_\ell x+(-)^L\sin x\right]\mu_G\left(x/\omega_ct_f\right)dx. \qquad (5.72b)\end{aligned}$$

In the long-time limit $t_f \to +\infty$, the integrals above would tend asymptotically to universal limits that are independent of details about the physical cutoffs, if and only if the integrals when setting $\mu_A(x) \equiv 1$ $(A = S, G)$ are well defined. For this scenario, the asymptotic limits of dephasing function and phase shift functions can be derived as

$$-3 < p < 1 : \zeta(t_f) \sim \mathcal{C}_\zeta(p) S_0 t_f^{1-p} \quad (t_f \to +\infty), \tag{5.73a}$$

$$-2 < s < 2 : \Phi_{\mathrm{q}}(t_f) \sim \mathcal{C}_\Phi(s) \frac{A_0}{2} t_f^{1-s} \quad (t_f \to +\infty), \tag{5.73b}$$

where the dimensionless coefficients $\mathcal{C}_\zeta(p)$ and $\mathcal{C}_\Phi(s)$ are determined by the spin-echo pulse parameters as

$$\begin{aligned}\mathcal{C}_\zeta(p) =& \frac{\Gamma(p-1)}{\pi} \left\{ 4 \sum_{\ell > \ell'}^{L} (-)^{\ell+\ell'} (\alpha_\ell - \alpha_{\ell'})^{1-p} \right. \\ & \left. + 2 \sum_{\ell=1}^{L} (-)^{\ell} \left[(-)^{L+1} (1-\alpha_\ell)^{1-p} + \alpha_\ell^{1-p} \right] + (-)^{L+1} \right\} \sin \frac{p\pi}{2}, \end{aligned} \tag{5.74a}$$

$$\mathcal{C}_\Phi(s) = \frac{\Gamma(s-1)}{\pi} \left[2 \sum_{\ell=1}^{L} (-)^{\ell} \alpha_\ell^{1-s} + (-)^{L+1} \right] \cos \frac{s\pi}{2}, \tag{5.74b}$$

and $\Gamma(\cdot)$ is the gamma function. For Hahn echo, the control pulse parameters are $L = 1$, $\alpha_1 = \frac{1}{2}$, and substituting the parameters into equation above lets us obtain the coefficients $\mathcal{C}_{\zeta,\mathrm{H}} = \frac{1-2^{p+1}}{\pi} \Gamma(p-1) \sin \frac{p\pi}{2}$ and $\mathcal{C}_{\Phi,\mathrm{H}} = \frac{1-2^{s}}{\pi} \Gamma(s-1) \cos \frac{s\pi}{2}$ in the main text. Note that above equations are still well-defined if p, s are exact integers, where the gamma function in Eqs. (5.74) alone might diverge: in this case, we could obtain the asymptotic coefficients by taking the continuous limit of Eqs. (5.74) as the exponent approaches the corresponding integer value. The asymptotic limit of quench phase shift can be further simplified if the

response function exponent take the value of 1, as

$$s = 1 : \lim_{t_f \to +\infty} \Phi_{\rm q}(t_f) = A_0/2. \tag{5.75}$$

For exponents beyond the range of validity specified in Eqs. (5.73), the long-time behavior of the dephasing function (phase shift) may not have a well-defined asymptotic limit, or the asymptotic behavior would depend on details of the low- or high-frequency cutoff of the bath NSD (response function). To illustrate this, we discuss a concrete example where the long-time phase shift dynamics explicitly depends on details of the cutoff. We compare the Hahn echo phase shift dynamics for response function $\mathrm{Im}G^R_{\xi V}[\omega] = -(A_0/2)\omega^s \mu_G\left(\omega/\omega_{\rm c}\right)$ with exponent $s = 5/2$, and two different UV cutoff functions: exponential cutoff with $\mu_{G,\rm exp}\left(x\right) = e^{-x}$, and step-function cutoff with $\mu_{G,\rm sp}\left(x\right) = \Theta(1-x)$, where $\Theta(\cdot)$ is the Heaviside step function. The quench phase shift is generally given by Eq. (5.72b), which for Hahn echo can be computed analytically to yield

$$\Phi_{\rm q,exp}(t_f) = \frac{4A_0}{\pi}\int_0^{+\infty} \omega^{\frac{1}{2}} e^{-\frac{\omega}{\omega_{\rm c}}} \sin\frac{\omega t_f}{2}\sin^2\frac{\omega t_f}{4} d\omega \tag{5.76}$$

$$= \frac{A_0}{2\sqrt{\pi}} t_f^{-\frac{3}{2}} \left[2^{\frac{3}{2}} e^{i\frac{\pi}{4}} \left(1 + \frac{2i}{\omega_{\rm c} t_f}\right)^{-\frac{3}{2}} - 2^{-1} e^{i\frac{\pi}{4}} \left(1 + \frac{i}{\omega_{\rm c} t_f}\right)^{-\frac{3}{2}} + \text{c.c.} \right], \tag{5.77}$$

$$\Phi_{\rm q,sp}(t_f) = \frac{4A_0}{\pi}\int_0^{\omega_{\rm c}} \omega^{\frac{1}{2}} \sin\frac{\omega t_f}{2}\sin^2\frac{\omega t_f}{4} d\omega \tag{5.78}$$

$$= \frac{8A_0}{\pi}\left[\frac{\sqrt{\omega_{\rm c}}}{t_f}\sin^4\frac{\omega_{\rm c} t_f}{4} - \frac{\sqrt{\omega_{\rm c}}}{2t_f}\int_0^1 x^{-\frac{1}{2}} \sin^4\frac{x\omega_{\rm c} t_f}{4} dx \right]. \tag{5.79}$$

While the asymptotic $t_f \gg \omega_{\rm c}^{-1}$ limit of Hahn echo phase shift $\Phi_{\rm q,exp}(t_f)$ assuming exponential cutoff agrees with the universal result in Eq. (5.73b), it is straightforward to see that the phase shift dynamics with step-function cutoff does not have a well-defined asymptotic long-time limit, and does not agree with Eq. (5.73b). Although the oscillatory behavior of the first term in the square bracket in Eq. (5.79) is typical when we have response functions

with a step-function cutoff (e.g. see the dashed blue curve in Fig. 5.5(c) in the main text, depicting the QPS for Ohmic bath spectral function with a step-function UV cutoff), for exponents within the range of validity of Eq. (5.79) such oscillations are negligible in the asymptotic long-time limit. However, as shown in Eq. (5.79), for exponents outside this range the oscillatory contribution is important even in the long-time limit. Generally, for bath NSD (response function) of the form given by Eqs. (5.67) with exponent $p \geq 1$ ($s \geq 2$), the long-time behavior of the dephasing function $\zeta(t_f)$ (quench phase shift $\Phi_{\rm q}(t_f)$) depend on the detail of the UV cutoff of the spectrum. Similarly, for exponents $p \leq -3$ ($s \leq -2$) below the regime of validity in Eq. (5.73), the corresponding long-time behavior would depend on the low-frequency cutoff.

5.6.8 Alternative derivation of quench phase shift in Ohmic environments

As discussed in Sec. 5.4.3, specifically for baths that exhibit Ohmic behavior (a flat NSD and a linear bath spectral function) in the asymptotic low-frequency limit, i.e., satisfying Eq. (5.67) with $p = 0$, $s = 1$, the quench phase shift (QPS) under spin-echo or dynamical-decoupling control sequences tends to a constant in the long-time regime, as shown in Eq. (5.24) (see also Eq. (5.75) in Appendix 5.6.7). In this section, we provide an intuitive derivation of this result, which for a generic control sequence can be written as

$$\lim_{t_f\to+\infty} \Phi_{\rm q}(t_f) = \frac{F[0]}{2}{\rm Re}G^R_{\xi\xi}[\omega = 0^+] - \frac{1}{2}\left.\frac{d{\rm Im}G^R_{\xi\xi}[\omega]}{d\omega}\right|_{\omega=0^+}, \tag{5.80}$$

where $F[0] \equiv \int_0^{t_f} F(t)dt$. We start with the general linear response formula for QPS, assuming quench operator $\hat{V} = \hat{\xi}/2$, quench function $\eta(t) = \Theta(t)\Theta(t_f - t)$, and a generic filter function, which in the time domain is given by (see Eq. (5.59))

$$\Phi_{\rm q}(t_f) = \frac{1}{2}\int_0^{t_f} dt_1 F(t_1) \int_0^{t_1} dt_2 G^R_{\xi\xi}(t_1 - t_2). \tag{5.81}$$

We can rewrite the expression on the right hand side using integration by parts as

$$\Phi_{\rm q}(t_f) = \frac{F[0]}{2}\int_0^{t_f} dt_1 G^R_{\xi\xi}(t_1) - \frac{1}{2}\int_0^{t_f} dt_1 G^R_{\xi\xi}(t_1)\int_0^{t_1} dt_2 F(t_2). \tag{5.82}$$

The first term on the RHS can be viewed as the net phase shift due to a constant qubit frequency shift $\int_0^{t_f} dt G^R_{\xi\xi}(t)$ accumulated during the time evolution, whereas the second term accounts for a residual phase correction due to the fact that the quench-induced frequency shift to the qubit is time dependent. For Ohmic baths whose response functions exhibit linear dependence in the asymptotic low-frequency regime, it is straightforward to show that the asymptotic long-time behaviors of these two terms are given by

$$\lim_{t_f\to+\infty}\frac{F[0]}{2}\int_0^{t_f} dt G^R_{\xi\xi}(t) = \frac{F[0]}{2}\int_0^{+\infty} G^R_{\xi\xi}(t)dt = \frac{F[0]}{2}{\rm Re}G^R_{\xi\xi}[\omega=0^+], \tag{5.83}$$

$$-\frac{1}{2}\lim_{t_f\to+\infty}\int_0^{t_f} dt_1 G^R_{\xi\xi}(t_1)\int_0^{t_1} dt_2 F(t_2) = -\frac{1}{2}\int_0^{+\infty} tG^R_{\xi\xi}(t)dt = -\frac{1}{2}\left.\frac{d{\rm Im}G^R_{\xi\xi}[\omega]}{d\omega}\right|_{\omega=0^+}. \tag{5.84}$$

Thus, the asymptotic long-time behavior of QPS with Ohmic baths can be viewed as the sum of phase shift due to a static frequency shift in the long-time limit, which is proportional to $F[0]$, and a residual phase correction. Noting that the bath spectral function $\mathcal{J}[\omega]$ is related to the response function via $\mathcal{J}[\omega] = -\frac{1}{\pi}{\rm Im}\ G^R_{\xi\xi}[\omega]$ (see also Eq. (5.17) in the main text), we have

$$\begin{aligned}\lim_{t_f\to+\infty}\Phi_{\rm q}(t_f) &= \frac{F[0]}{2}{\rm Re}G^R_{\xi\xi}[\omega=0^+] - \frac{1}{2}\left.\frac{d{\rm Im}G^R_{\xi\xi}[\omega]}{d\omega}\right|_{\omega=0^+}\\ &= \frac{F[0]}{2}{\rm Re}G^R_{\xi\xi}[\omega=0^+] + \frac{\pi}{2}\left.\frac{d\mathcal{J}[\omega]}{d\omega}\right|_{\omega=0^+}.\end{aligned} \tag{5.85}$$

Specifically for dynamical-decoupling-type control pulses with $F[0] = 0$, the first term would vanish, and we recover Eq. (5.24) in the main text. As a result, for approximately Ohmic baths with spectral function satisfying $\mathcal{J}[\omega] \sim \omega$ at low frequencies, the asymptotic behavior of QPS under spin-echo control pulses in the long time $t_f \to \infty$ regime is universal (i.e., it only depends on the asymptotic linear dependence of the spectral function), and is independent of the specific UV cutoff of the response function and details of the qubit control sequence.

5.6.9 QPS generated by a driven damped environmental cavity mode

In the main text, we have considered a quantum bath whose spectral function is asymptotically Ohmic in the low-frequency limit (i.e. $\bar{S}[\omega] \sim$ const. and $\mathcal{J}[\omega] \sim \omega$ as $\omega \to 0^+$) and also exhibits a Lorentzian peak at a finite frequency; the Hahn-echo quench phase shift (QPS) dynamics due to this bath is illustrated in Fig. 5.5b. As mentioned in the main text, such spectral function can describe dephasing environments generated by a driven damped electromagnetic (EM) cavity. In this subsection, we provide a detailed discussion on the corresponding physical system.

Consider a qubit dispersively coupled to a driven damped bosonic mode b (resonance frequency $\omega_{\rm c}$, decay rate κ) via the Hamiltonian

$$\hat{H}_{\rm int} = \frac{1}{2}\hat{\sigma}_z \otimes \hat{\xi}, \quad \hat{\xi} = \lambda \hat{b}^\dagger \hat{b}. \tag{5.86}$$

For instance, we may have a superconducting transmon qubit coupled to a microwave cavity mode; the photon shot noise fluctuations due to the cavity mode then induce qubit frequency shift and dephasing during time evolution. Transforming to the interaction picture defined by the free qubit Hamiltonian $\Omega\hat{\sigma}_z/2$, as well as frame rotating at the drive frequency $\omega_{\rm dr}$ of the cavity mode, the dynamics of the total system can be described by the quantum master

equation as follows

$$\dot{\hat{\rho}} = -i[\hat{H}_0 + \hat{H}_{\rm int} + \hat{H}_{\rm dr}, \hat{\rho}] + \kappa(\bar{n}_{\rm th} + 1)\mathcal{D}[\hat{b}]\hat{\rho} + \kappa\bar{n}_{\rm th}\mathcal{D}[\hat{b}^\dagger]\hat{\rho}, \tag{5.87}$$

where $\bar{n}_{\rm th}$ is the thermal photon number. For simplicity, we assume zero temperature ($\bar{n}_{\rm th} = 0$) hereafter, but we stress that our approach also applies to the case with finite $\bar{n}_{\rm th}$. In the above equation, $\hat{H}_0$ and $\hat{H}_{\rm dr}$ are rotating-frame Hamiltonians accounting for free cavity dynamics and the linear cavity drive, respectively, as

$$\hat{H}_0 = -\Delta\hat{b}^\dagger\hat{b}, \quad \hat{H}_{\rm dr}(t) = y(t)f_{\rm dr}\hat{b}^\dagger + \text{H.c.}, \tag{5.88}$$

where $\Delta \equiv \omega_{\rm dr} - \omega_{\rm c}$ denotes the cavity detuning, and $f_{\rm dr}$ is the drive strength. We introduce a dimensionless envelope function $y(t)$ to encode possible time dependence of the drive. For the purpose of our discussion, we can assume the cavity drive is switched on at some earlier time before the start of the Hahn-echo protocol, so that we have $y(t) = 1$ during the protocol ($0 < t < t_f$). For convenience, we define the stationary intracavity driven photon number in the absence of the qubit (i.e., setting $\lambda = 0$ in Eq. (5.87)) as $\bar{n}_{\rm dr}$, so that we have (here $\langle\cdot\rangle$ denotes stationary state expectation values of bath operator)

$$\bar{n}_{\rm dr} = |\beta_{\rm dr}|^2, \quad \beta_{\rm dr} = \langle\hat{b}\rangle = \frac{f_{\rm dr}}{\Delta + i\frac{\kappa}{2}}. \tag{5.89}$$

In this specific setup, the photon shot noise coupled to the qubit is generally non-Gaussian [100]. Thus, in order to apply our results in the main text (based on Eqs. (5.66)) to describe the photonic environment, we first need to ensure non-Gaussian effects are small. Without loss of generality, we focus on the mean-field regime where the Gaussian approxi-

mation is well justified, i.e. we have approximately

$$\delta\hat{\xi} \equiv \lambda\hat{b}^\dagger\hat{b} - \lambda\langle\hat{b}^\dagger\hat{b}\rangle \simeq \lambda\beta_{\rm dr}\delta\hat{b}^\dagger + \text{H.c.}, \tag{5.90}$$

which holds if we require parameters to satisfy following conditions

$$\bar{n}_{\rm dr} > 1, \quad \sqrt{\bar{n}_{\rm dr}}\frac{\lambda}{\kappa} \lesssim 1. \tag{5.91}$$

Substituting the mean field approximation (Eq. (5.90)) into definition of symmetrized noise spectral density $\bar{S}[\omega]$ (see Eq. (5.10) in the main text)

$$\bar{S}[\omega] \equiv \frac{1}{2}\int_{-\infty}^{+\infty} dt e^{i\omega t}\langle\{\delta\hat{\xi}(t), \delta\hat{\xi}(0)\}\rangle, \tag{5.92}$$

and making use of solution to the master equation in Eq. (5.87), we can straightforwardly obtain the NSD as

$$\bar{S}[\omega] = \bar{n}_{\rm dr}\lambda^2\left[\frac{\frac{\kappa}{2}}{\left(\frac{\kappa}{2}\right)^2 + (\Delta+\omega)^2} + \frac{\frac{\kappa}{2}}{\left(\frac{\kappa}{2}\right)^2 + (\Delta-\omega)^2}\right]. \tag{5.93}$$

Similarly we can derive the bath spectral function $\mathcal{J}[\omega]$ as

$$\mathcal{J}[\omega] = -\frac{1}{\pi}\text{Im}G^R_{\xi\xi}[\omega] = \frac{\bar{n}_{\rm dr}\lambda^2}{\pi}\left[\frac{\frac{\kappa}{2}}{\left(\frac{\kappa}{2}\right)^2 + (\Delta-\omega)^2} - \frac{\frac{\kappa}{2}}{\left(\frac{\kappa}{2}\right)^2 + (\Delta+\omega)^2}\right]. \tag{5.94}$$

Note that we can rewrite the spectral function in Eq. (5.94) as

$$\mathcal{J}[\omega] = \omega\frac{\bar{n}_{\rm dr}\lambda^2}{\pi\Delta^2}\frac{\frac{2\kappa}{\Delta}}{\left[\left(\frac{\omega}{\Delta}+1\right)^2 + \left(\frac{\kappa}{2\Delta}\right)^2\right]\left[\left(\frac{\omega}{\Delta}-1\right)^2 + \left(\frac{\kappa}{2\Delta}\right)^2\right]}, \tag{5.95}$$

which recovers the form of spectral function used to compute data shown in Fig. 5.5b, if we redefine centers of Lorentzian peaks as $\pm\Delta$. It is straigtforward to check that the photon

shot noise exhibits Ohmic behavior in the asymptotic low-frequency limit, i.e. we have

$$\bar{S}[\omega] \sim \bar{n}_{\rm dr}\lambda^2 \frac{\kappa}{\left(\frac{\kappa}{2}\right)^2+\Delta^2} \quad (\omega \to 0^+), \tag{5.96a}$$

$$\mathcal{J}[\omega] \sim \frac{\bar{n}_{\rm dr}}{\pi} \frac{2\kappa\Delta\lambda^2}{\left[\left(\frac{\kappa}{2}\right)^2+\Delta^2\right]^2}\omega \quad (\omega \to 0^+). \tag{5.96b}$$

Making use of results in Eqs. (5.73), we thus obtain the asymptotic behavior of dephasing function $\zeta(t_f)$ and the quench phase shift $\Phi_{\rm q}(t_f)$

$$\zeta(t_f) \sim \bar{n}_{\rm dr} \frac{\lambda^2}{\left(\frac{\kappa}{2}\right)^2+\Delta^2} \frac{\kappa t_f}{2} \quad (t_f \to +\infty), \tag{5.97a}$$

$$\Phi_{\rm q}(t_f) \sim \bar{n}_{\rm dr} \frac{\kappa\Delta\lambda^2}{\left[\left(\frac{\kappa}{2}\right)^2+\Delta^2\right]^2} \quad (t_f \to +\infty). \tag{5.97b}$$

We now compare the predicted asymptotic results to exact dynamics from directly solving the master equation Eq. (5.87). We consider qubit dynamics corresponding to standard Hahn-echo protocol, where the qubit-bath system is initialized as follows: i) we first prepare the qubit in one of eigenstates, $|\uparrow\rangle$ or $|\downarrow\rangle$; ii) we then switch on cavity drive, and wait for long enough so that the cavity reaches a stationary state at the start ($t = 0$) of the Hahn echo protocol. Denoting the qubit phase shift corresponding to initial state $|\uparrow\rangle$ ($|\downarrow\rangle$) as $\Phi_\uparrow(t_f)$ ($\Phi_\downarrow(t_f)$), we thus have

$$\lim_{t_f\to+\infty}\left[\Phi_\downarrow(t_f)-\Phi_\uparrow(t_f)\right] = 2\lim_{t_f\to+\infty}\Phi_{\rm q}(t_f) = \pi \left.\frac{d\mathcal{J}[\omega]}{d\omega}\right|_{\omega=0^+} \tag{5.98}$$

$$= \bar{n}_{\rm dr}\frac{2\kappa\Delta\lambda^2}{\left[\left(\frac{\kappa}{2}\right)^2+\Delta^2\right]^2}. \tag{5.99}$$

Because the master equation conserves qubit polarization (i.e., $\hat{\sigma}_z$), and is quadratic in terms of bosonic mode operators, we can numerically simulate the exact qubit-cavity system dynamics efficiently (see [100] for details). Figure 5.7 illustrates the exact qubit phase shift

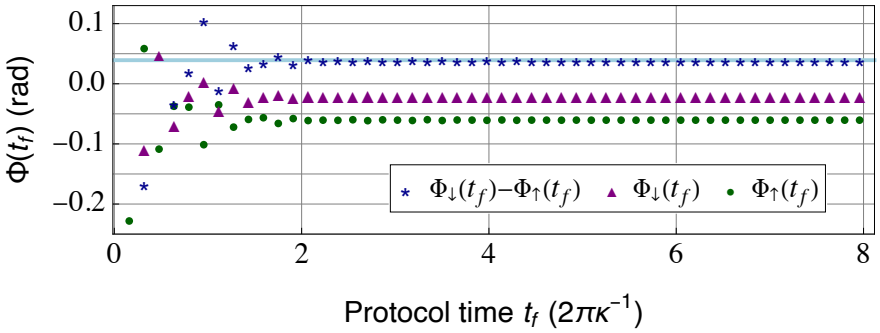

Fig. 5.7: Numerically simulated Hahn-echo qubit phase shift and the quench phase shift dynamics, corresponding to the photonic environment generated by a driven, damped cavity mode. The purple triangles (green circles) depict qubit phase shifts $\Phi_{\downarrow}(t_f)$ ($\Phi_{\uparrow}(t_f)$) using initial qubit state $|\downarrow\rangle$ ($|\uparrow\rangle$), which are computed numerically from solving the qubit-cavity master equation in Eq. (5.87). The difference between the two qubit phase shifts $\left[\Phi_{\downarrow}(t_f) - \Phi_{\uparrow}(t_f)\right]$ (dark blue asterisks) in the long-time limit can be well described by the asymptotic expression based on quench phase shift in Eq. (5.99), as expected. Parameters: $\Delta/\kappa = 5$, $\lambda/\kappa = 0.5$, $\bar{n}_{\rm dr} = 10$, and $\bar{n}_{\rm th} = 0$.

dynamics corresponding to initial qubit state $|\downarrow\rangle$ and $|\uparrow\rangle$ (purple triangles and green circles, respectively) for the choice of parameters $\Delta/\kappa = 5$, $\lambda/\kappa = 0.5$, and $\bar{n}_{\rm dr} = 10$. As shown in Fig. 5.7, the difference in qubit phase shifts $\left[\Phi_{\downarrow}(t_f) - \Phi_{\uparrow}(t_f)\right]$ (dark blue asterisks) in the long-time limit is in good agreement with the asymptotic result in Eq. (5.99) (light blue line), verifying our approach. The corresponding Hahn-echo coherence functions are plotted in Fig. 5.8, and can be readily measured using, e.g., state-of-the-art implementations of superconducting qubits.

The results above on quench phase shift encode intriguing information about nature of the corresponding environment. Comparing the asymptotic results in Eqs. (5.97) to the temperature estimation formula in Eq. (5.25), the qubit quench phase shift dynamics, which can be detected by measuring $\left[\Phi_{\downarrow}(t_f) - \Phi_{\uparrow}(t_f)\right]$, indicates that low-frequency photon shot noise has a finite temperature. At first glance, this might seem surprising, as the system master equation in Eq. (5.87) only includes a purely cooling dissipator when we assume zero thermal photon number ($\bar{n}_{\rm th} = 0$), and does not involve any explicit heating. We note that there is in fact no contradiction: the finite temperature of low-frequency fluctuations reflects

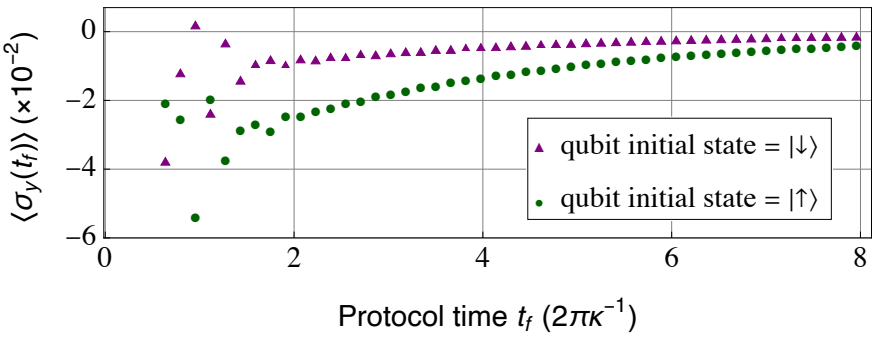

Fig. 5.8: Numerically simulated Hahn-echo qubit coherence function $\langle\hat{\sigma}_y(t_f)\rangle$ corresponding to the photonic environment generated by a driven damped cavity mode. The purple triangles (green circles) depict qubit Hahn-echo coherence function $\langle\hat{\sigma}_y(t_f)\rangle$ using initial qubit state $|\downarrow\rangle$ ($|\uparrow\rangle$), which are computed numerically from solving the qubit-cavity master equation in Eq. (5.87). Note that data points with small protocol times ($t_f < \pi/\kappa$) fall out of range of the figure and are not shown here; however, the short-protocol-time behavior is determined by the high-frequency components of the spectral function, and does not affect our conclusion. The parameters are the same as in Fig. 5.7.

the fact that Markovian dissipation actually corresponds to a non-equilibrium environment, and the quench approach provides a direct knob to probe this physics.

5.6.10 General strategy for reconstructing the environmental spectral function using time-dependent quenches

In the main text, we discussed using sensor qubits based on a single nitrogen vacancy center in diamond to engineer a time-dependent quench (c.f. Fig. 5.6), and we discussed its application in reconstructing the bath spectral function for a specific type of control pulses. In this subsection, we discuss a general recipe to construct more general periodic control pulses, which lead to a powerful set of varying spectral filters that can be utilized to reconstruct the spectral function $\mathcal{J}[\omega]$ in a broad range of frequencies.

As discussed in the main text (see discussions following Eq. (5.27)), to illustrate the idea we focus on case where the quench operator is directly related to noise, with $\hat{V} = \hat{\xi}/2$. Without loss of generality, we also focus on periodic NV control pulses, which are suitable for reconstructing the spectral function at finite target frequencies. Recall that the spin-1

structure of the NV lets us effectively realize a nontrivial quench function $\eta(t)$, in addition to the standard noise filter function. More specifically, we can apply a periodic sequence of NV control pulses (period T with $2M$ repetitions, $M \in \mathbb{Z}$), switching between the qubit subspaces $\{m_z = 0, m_z = +1\}$ and $\{m_z = 0, m_z = -1\}$ (see also Fig. 5.6 in the main text), to realize a periodic quench function as

$$\eta(t) = \sum_{m=0}^{M-1} \eta_0(t - 2mT; 2T), \tag{5.100}$$

where $\eta_0(t; 2T)$ denotes the base quench function, and satisfies the following relation

$$\eta_0(t; 2T) = \begin{cases} +1 \text{ or } -1, & 0 \leq t \leq 2T, \\ 0, & t < 0 \text{ or } t > 2T. \end{cases} \tag{5.101}$$

The structure of switching pulses also ensure that $\eta_0(t; 2T) = (-)^N \eta_0(t + T; 2T)$ for $0 < t < T$, where N is the total number of switching pulses per period T. For the example control pulse sequence depicted in Fig. 5.6, we have $N = 1$ and $\eta_0(t; 2T) = -\Theta(t)\Theta(T - t) + \Theta(t - T)\Theta(2T - t)$, where $\Theta(\cdot)$ denotes the Heaviside step function. Again introducing the total protocol time satisfying $t_f = 2MT$, we can straightforwardly rewrite Fourier transform of the quench function as

$$\eta[\omega] = e^{i(M-1)\frac{\omega t_f}{2M}} \frac{\sin \frac{\omega t_f}{2}}{\sin \frac{\omega t_f}{2M}} \eta_0[\omega; 2T], \tag{5.102}$$

$$\eta_0[\omega; 2T] \equiv \int_0^{2T} \eta_0(t; 2T) e^{i\omega t} dt. \tag{5.103}$$

For reasons that will become clear, we also assume a periodic sequence of standard qubit control π-pulses, with a same period T and total evolution time $t_f = 2MT$, so that we

similarly have

$$F(t) = \sum_{m=0}^{M-1} F_0(t - 2mT; 2T), \tag{5.104}$$

$$F[\omega] = e^{i(M-1)\frac{\omega t_f}{2M}} \frac{\sin\frac{\omega t_f}{2}}{\sin\frac{\omega t_f}{2M}} F_0[\omega; 2T]. \tag{5.105}$$

Substituting Eqs. (5.105) and (5.102) above into Eq. (5.12b) in the main text, which described the general quench phase shift, and noting that $\hat{V} = \hat{\xi}/2$, we obtain

$$\begin{aligned}
\Phi_{\rm q}(t_f) &= \int_{-\infty}^{+\infty} \frac{d\omega}{2\pi} F^*[\omega]\eta[\omega] G^R_{\xi V}[\omega] \\
&= \int_{-\infty}^{+\infty} \frac{d\omega}{4\pi} F^*[\omega]\eta[\omega] G^R_{\xi\xi}[\omega] \\
&= \int_{-\infty}^{+\infty} \frac{d\omega}{4\pi} \frac{\sin^2\frac{\omega t_f}{2}}{\sin^2\frac{\omega t_f}{2M}} F_0^*[\omega; 2T]\eta_0[\omega; 2T] G^R_{\xi\xi}[\omega].
\end{aligned} \tag{5.106}$$

We are now ready to present the recipe, or the necessary and sufficient conditions, to construct spectral filters that specifically probe the bath spectral function $\mathcal{J}[\omega]$ (see also Eq. (5.17) in the main text)

$$\mathcal{J}[\omega] = -\frac{1}{\pi} {\rm Im} G^R_{\xi\xi}[\omega]. \tag{5.107}$$

We essentially require that the base filter and quench functions exhibit the same periodicity, and satisfy the following conditions

- The base filter and quench functions must be mirror symmetric or anti-symmetric with respect to $t = T$, i.e., $F_0(t; 2T) = s_F F_0(2T - t; 2T)$, and $\eta_0(t; 2T) = s_\eta \eta_0(2T - t; 2T)$, where s_F, $s_\eta = \pm 1$.

- The base filter and quench functions exhibit opposite mirror symmetries with respect to $t = T$, i.e., $s_F = -s_\eta = +1$ or -1.

Above constraints ensure that the quench phase shift in Eq. (5.106) is only sensitive to the

imaginary part of the response function $\mathrm{Im}G^R_{\xi\xi}[\omega]$, or equivalently the spectral function $\mathcal{J}[\omega]$, so that we have

$$\Phi_{\mathrm{q}}(t_f) = \int_{-\infty}^{+\infty} \mathcal{F}_{\mathcal{J}}[\omega; t_f]\mathcal{J}[\omega]d\omega = 2\int_{0}^{+\infty} \mathcal{F}_{\mathcal{J}}[\omega; t_f]\mathcal{J}[\omega]d\omega, \tag{5.108}$$

$$\mathcal{F}_{\mathcal{J}}[\omega; t_f] = \frac{\sin^2\frac{\omega t_f}{2}}{4\sin^2\frac{\omega t_f}{2M}}\mathrm{Im}(F_0^*[\omega; 2T]\eta_0[\omega; 2T]). \tag{5.109}$$

The spectral filter $\mathcal{F}_{\mathcal{J}}[\omega; t_f]$ for $\mathcal{J}[\omega]$ forms a comb-like structure in frequency space, if we fix pulse periodicity $T = t_f/2M$ and take the asymptotic large pulse number limit, i.e.

$$\mathcal{F}_{\mathcal{J}}[\omega; t_f] \sim \frac{M\omega_0}{4}\sum_{\ell=-\infty}^{+\infty} \mathrm{Im}(F_0^*[\ell\omega_0; 2T]\eta_0[\ell\omega_0; 2T])\,\delta(\omega - \ell\omega_0) \quad (M \gg 1), \tag{5.110a}$$

$$\omega_0 = \pi/T = 2M\pi/t_f. \tag{5.110b}$$

Thus, given a finite target frequency range, we can construct a corresponding set of NV control pulses that specifically realize frequency comb filters for the spectral function at target frequencies. We can then measure the quench phase shifts under these control pulses in the comb limit (fix $T = t_f/2M$ and choose $M \gg 1$), which in turn enable reconstruction of the spectral function $\mathcal{J}[\omega]$ via Eq. (5.108).

CHAPTER 6

QUANTUM NONRECIPROCAL INTERACTIONS VIA DISSIPATIVE GAUGE SYMMETRY

6.1 Overview of results

One-way nonreciprocal interactions between two quantum systems are typically described by a cascaded quantum master equation, and rely on an effective breaking of time-reversal symmetry (TRS) as well as the balancing of coherent and dissipative interactions. In this chapter, we present a new approach for obtaining nonreciprocal quantum interactions that is *completely distinct* from cascaded quantum systems, and that does not in general require broken TRS. Our method relies on a local gauge symmetry present in any Markovian Lindblad master equation. This new kind of quantum nonreciprocity has many implications, including a new mechanism for performing dissipative steady-state unitary gate operations on a target quantum system. We also introduce a new, extremely general quantum-information based metric for quantifying quantum nonreciprocity.

6.2 Introduction

The study of interactions and scattering that are intrinsically directional (i.e. nonreciprocal) is at the forefront of many areas of physics. Such interactions are of fundamental interest: for example, they can lead to exotic phase transitions in classical active matter systems [204–206], and can also be used to generate dimerized many-body entangled states [207–209]. They also have a myriad of practical applications in both classical and quantum information

processing tasks, in settings that range from classical photonic and acoustic systems [210–212], to quantum circuits and networks [213–222].

While classically, one can describe directional interactions using effective non-Hermitian Hamiltonians, in quantum settings one needs a description that conserves probability and accounts for quantum fluctuations. The standard quantum description of nonreciprocity is provided by the theory of cascaded quantum systems [223, 224]. It describes an extremely general class of fully directional interactions between two subsystems A and B that involve a pair of arbitrary "local" operators $\hat{A}$ and $\hat{B}$ (i.e. $\hat{A}$ only acts on subsystem A, $\hat{B}$ only acts on subsystem B). The directional dynamics is described by a Lindblad quantum master equation (QME) of the form [223–225]:

$$\frac{d\hat{\rho}}{dt} = -i[\hat{H}_{AB}, \hat{\rho}] + \mathcal{D}[\hat{A} - i\hat{B}]\hat{\rho} \equiv \mathcal{L}_{\mathrm{CS}}\hat{\rho}, \tag{6.1}$$

where $\hat{\rho}$ is the system density matrix, $\hat{H}_{AB} = (\hat{A}^\dagger\hat{B} + \hat{B}^\dagger\hat{A})/2$, and $\mathcal{D}[\hat{O}]\hat{\rho} = (\hat{O}\hat{\rho}\hat{O}^\dagger - \{\hat{O}^\dagger\hat{O}, \hat{\rho}\}/2)$ denotes the standard Lindblad dissipator. One can show that the dynamics encodes a fully one-way interaction where subsystem A affects the dynamics and evolution of subsystem B, but not vice versa.

Cascaded QMEs were first derived for setups involving an explicitly nonreciprocal element (e.g. a directional waveguide or circulator). More recently, it was realized that Eq. (6.1) provides a more general blueprint for engineering nonreciprocal interactions, based on balancing a coherent Hamiltonian interaction (described by $\hat{H}_{AB}$) and a dissipative interaction (described by the dissipator $\mathcal{D}[\hat{A} - i\hat{B}]\hat{\rho}$) [31, 225]. This can be realized by engineering suitable drives and couplings to dissipative environments, without using a conventional nonreciprocal element. This approach has been employed in a variety of experiments including quantum optomechanics (e.g. [216, 218–221]) and superconducting quantum circuits (e.g. [215, 217]). Note that the coefficient $-i$ in the dissipator of Eq. (6.1) ultimately implies that any physical means for realizing this dynamics requires an effective broken time-reversal symmetry

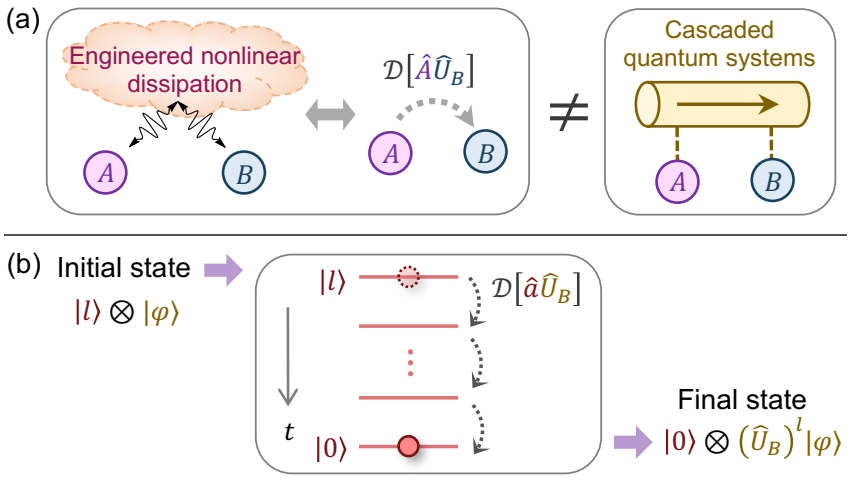

Fig. 6.1: (a) Schematic for quantum nonreciprocal interactions via gauge symmetry. This approach uses correlated dissipation, but is completely distinct from a cascaded quantum system. (b) Dissipative steady-state realization of a tunable unitary gate making use of the nonreciprocal interaction in (a), in a system where subsystem A is a cavity mode a that controls the gate, and subsystem B is the target qubit. One can selectively apply a unitary gate $(\hat{U}_B)^\ell$ on B by initializing A in the corresponding Fock state $|\ell\rangle$, and letting the system relax to the steady state (see Eq. (6.3) and Section 6.4.3).

(TRS). This can be achieved by using phases encoded in the drive tones applied to the system, in a manner that generates a synthetic gauge flux. This time-modulation approach to nonreciprocity is also well studied in completely classical contexts [210–212].

One might guess that the general structure of Eq. (6.1) is the only way to obtain fully-directional, Markovian quantum interactions between two systems. In this work we show that this is not the case. We introduce a new kind of quantum open system dynamics where correlated dissipation generates nonreciprocal interactions in a manner distinct from the cascaded QME. As we discuss in detail, we ultimately exploit a basic gauge symmetry present in any Lindblad master equation. This gives us a mechanism for nonreciprocity that, surprisingly, does not require any notion of broken TRS or a non-trivial synthetic gauge field. In its simplest form, the new nonreciprocal QME can be written in terms of a generic local

operator $\hat{A}$ on A and a unitary $\hat{U}_B$ on B, as (see Fig. 6.1(a))

$$\frac{d\hat{\rho}}{dt} = \Gamma\mathcal{D}[\hat{A}\hat{U}_B]\hat{\rho} \equiv \mathcal{L}_{\rm dir}\hat{\rho}. \tag{6.2}$$

As we show, this purely dissipative dynamics is strictly unidirectional (A influences B but not vice-versa), and moreover, cannot be written in the cascaded QME form of Eq. (6.1). We also show that this structure has a non-trivial generalization to more complex master equations with multiple dissipators.

Our work provides a thorough investigation of this new route to quantum nonreciprocity, including implementation methods. We also introduce a new, very general metric for quantum nonreciprocity that uses quantum-information theoretic tools, and use this to characterize the nonreciprocity of our mechanism in the presence of imperfections. Our study also goes beyond just fundamental considerations. We discuss a potentially powerful application of our new directional dynamics: a method for realizing dissipative steady-state unitary quantum gate operations. By this, we mean here that the gate operation is realized in the dissipative steady state of the dynamics. The basic idea is sketched in Fig. 6.1(b). Starting from a bipartite system having control (A) and target (B) subsystems, the goal is for the dissipative relaxation of the system (under a dynamics of the form of Eq. (6.2)) to implement a unitary operation on B whose form is dictated by the initial state of A. Specifically, for a set of initial states for A indexed by λ, we can achieve:

$$\begin{aligned}\hat{\rho}_B(\infty) &= \lim_{t\to\infty} \mathrm{Tr}_A\left[e^{t\mathcal{L}_{\rm dir}}(\hat{\rho}_A(\lambda)\otimes\hat{\rho}_B)\right] \\ &= \hat{U}_B(\lambda)\hat{\rho}_B\hat{U}_B(\lambda)^\dagger.\end{aligned} \tag{6.3}$$

The steady state of B is related to its initial state by a unitary, whose form is dictated by the initial A state. As we discuss in detail, this mechanism for performing gates has several attractive features: it does not require any timing control, and its dissipative nature makes

it robust against certain kinds of errors in initial A state preparation (as long as all such A states lead to the same B unitary). We stress that the mechanism of Eq. (6.3) is completely distinct from previous works exploring alternative dissipative approaches to quantum control [226–233]. While the dissipative implementation of quantum gates in Eq. (6.3) is not robust against loss in A, intriguingly, recent work [234] shows that it leads to a promising route to realizing autonomous quantum error correction schemes.

The remainder of the chapter is organized as follows. In Section 6.3, we set the stage for our discussions of quantum nonreciprocity by introducing a very general quantum information metric that quantifies quantum nonreciprocal (QNR) interactions in an arbitrary system, in a state-independent manner. Section 6.4 introduces our new mechanism for QNR in the simplest setting, and discusses its application to dissipative steady-state gate operations. Section 6.5 discusses physical implementation strategies that are compatible with state-of-the-art superconducting circuit and quantum optical platforms. Section 6.6 generalizes our new mechanism to more complex cases with multiple dissipators, and demonstrates that these QNR interactions can generate entanglement. We conclude in Section 6.7.

6.3 Quantifying nonreciprocity of general quantum dynamics

6.3.1 Basic notions

Before introducing our new mechanism, we start with a more basic question: what is a fundamental, system-agnostic way of identifying and quantifying nonreciprocal dynamics? While in simple linear settings one can just look at the asymmetry of scattering-matrix coefficients at a particular input frequency, we would like a more general metric that can apply even when there is no obvious connection to scattering, and which is not contingent on a particular choice of initial state. As we now discuss, we can formulate such a metric using well-known quantum information-theoretic quantities.

We start with a generic bipartite system with subsystems A and B, whose dynamics are described by the evolution superoperator $\mathcal{E}_t^{(AB)}$. This superoperator tells us how the system density matrix evolves, i.e.

$$\hat{\rho}_{AB}(t) = \mathcal{E}_t^{(AB)} \hat{\rho}_{AB}(0). \tag{6.4}$$

$\mathcal{E}_t^{(AB)}$ is also known as a quantum map or channel; any physical evolution corresponds to such a map, with the requirement that $\mathcal{E}_t^{(AB)}$ be completely positive and trace-preserving (CPTP) [22]. We stress that this description encompasses a full range of dynamics from non-dissipative unitary evolution, to highly complex non-Markovian dissipative evolution.

We now want a metric that tells us whether the dynamics describes by $\mathcal{E}_t^{(AB)}$ is nonreciprocal. We first introduce the *isolation function* of subsystem A, $I^{(A)}(t)$, which quantifies how sensitive the evolution of A is over this time interval to the initial state of subsystem B. The isolation function of subsystem B, $I^{(B)}(t)$, will be defined in an analogous manner. $I^{(A)}(t)$ can be directly connected to a standard task in quantum information theory. Suppose we first prepare subsystem B in one of two given states, $|\phi_1\rangle$ or $|\phi_2\rangle$ with equal probability. We also prepare A in some state $\hat{\rho}_A$. We then let the total system evolve for time t. We thus have two possible time-evolution maps for system A, contingent on the two subsytem B initial states:

$$\mathcal{E}_{|\phi_{\mathrm{i}}\rangle}^{(A)}(t)\hat{\rho}_A \equiv \mathrm{Tr}_B \left[\mathcal{E}_t^{(AB)} (\hat{\rho}_A \otimes |\phi_{\mathrm{i}}\rangle_B \langle \phi_{\mathrm{i}}|) \right]. \tag{6.5}$$

The goal is now to optimally guess which initial state B we started with, using only a *single* measurement on the A system at time t. We are interested in the maximum success probability where we optimize over all A initial states as well as the final A-subsystem measurement. This probability $p_{\max}(\{|\phi_1\rangle, |\phi_2\rangle\})$ gives us a measure of how different the A

system dynamics is depending on the choice of initial B state. One finds [235]:

$$p_{\max}(\{|\phi_1\rangle, |\phi_2\rangle\}) = \frac{1}{2} + \frac{1}{4}||\mathcal{E}^{(A)}_{|\phi_1\rangle}(t) - \mathcal{E}^{(A)}_{|\phi_2\rangle}(t)||_\diamond. \tag{6.6}$$

Here, $||\cdot||_\diamond$ denotes the so-called diamond norm and provides a distance measure between two quantum channels [236], which is stable with respect to tensor product operations (i.e. attaching ancillary quantum systems to A). Note that $p_{\max}$ must lie in the interval $[0.5, 1]$.

Eq. (6.6) thus provides a fundamental metric for the sensitivity of the A system dynamics to a change in the initial state of B. This then directly leads to a fundamental notion of how isolated the A system dynamics is from B: further optimize Eq. (6.6) over the choice of the B system initial states. This leads us to define the subsystem A isolation as:

$$I^{(A)}(t) \equiv 1 - \frac{1}{2} \max_{|\phi_1\rangle, |\phi_2\rangle \in \mathcal{H}_B} ||\mathcal{E}^{(A)}_{|\phi_1\rangle}(t) - \mathcal{E}^{(A)}_{|\phi_2\rangle}(t)||_\diamond, \tag{6.7}$$

where $\mathcal{H}_B$ denotes Hilbert space of B. The isolation function $I^{(A)}(t)$ lies in the interval $[0, 1]$, and measures the maximal influence a change of initial subsystem B state could have on the A subsystem dynamics. The case of complete isolation, $I^{(A)}(t) = 1$, implies that the dynamics of A is completely independent of the initial state of subsystem B. The isolation function for subsystem B is defined in a completely analogous manner. Note that if A and B are not coupled at all in the dynamics (i.e. the total channel is a tensor product of independent channels for each subsystem), then both subsystems are fully isolated at all times: $I^{(A)}(t) = I^{(B)}(t) = 1$. For $t = 0$, both systems are also of course always trivially isolated as the total channel is the identity.

6.3.2 Instantaneous nonreciprocity

These isolation functions now give us a simple way of identifying nonreciprocal dynamics as an evolution map that yields $I^{(A)}(t) \neq I^{(B)}(t)$, i.e. a situation where there is an asymme-

try in how strongly A influences B versus how strongly B influences A. One can discuss nonreciprocity for the instantaneous quantum map at a specific time, as well as for the entire evolution. If we focus on a specific time, we can define $\mathcal{E}_t^{(AB)}$ as being reciprocal or nonreciprocal at time t using the isolation functions, i.e.

$$\begin{aligned} &I^{(A)}(t) = I^{(B)}(t) \\ \Rightarrow &\mathcal{E}_t^{(AB)} \text{ is instantaneously reciprocal at } t; \end{aligned} \tag{6.8}$$

$$\begin{aligned} &I^{(A)}(t) \neq I^{(B)}(t) \\ \Rightarrow &\mathcal{E}_t^{(AB)} \text{ is instantaneously nonreciprocal at } t. \end{aligned} \tag{6.9}$$

6.3.3 Global nonreciprocity

One could also ask about whether the dynamics is nonreciprocal over an entire time interval $[0, t]$. In this case, we can define reciprocity by insisting the isolations are identical over the entire time interval:

$$\forall t \in (0, +\infty),\, I^{(A)}(t) = I^{(B)}(t) \;\Rightarrow\; \text{dynamics is reciprocal;} \tag{6.10}$$

$$\exists t \in (0, +\infty) \text{ s.t. } I^{(A)}(t) \neq I^{(B)}(t) \;\Rightarrow\; \text{dynamics is nonreciprocal.} \tag{6.11}$$

6.3.4 Fully nonreciprocal dynamics

Finally, one is also often interested in identifying situations with full nonreciprocity, where one system is unaffected by the other, but is nonetheless still able to influence it. We first consider quantum map at a specific time, and define instantaneous full nonreciprocity (i.e. unidirectionality) from A to B for $\mathcal{E}_t^{(AB)}$ at time t as

$$I^{(A)}(t) = 1,\, I^{(B)}(t) < 1 \Rightarrow \mathcal{E}_t^{(AB)} \text{ is instantaneously unidirectional } (A \to B). \tag{6.12}$$

Physically, the conditions on LHS can be understood as ensuring that states of A can affect evolution of B, but not vice versa. One can also define maximal unidirectionality from A to B (at time t) as any evolution that yields $I^{(A)}(t) = 1$ and $I^{(B)}(t) = 0$. More generally, one can also define fully nonreciprocal dynamics via the condition that dynamics of A is fully isolated at all times, but B is not fully isolated at some time, as

$$\forall t,\ I^{(A)}(t) = 1,\ \text{and}\ \exists t \text{ s.t. } I^{(B)}(t) < 1. \tag{6.13}$$

The case of B-to-A full nonreciprocity can be similarly defined by interchanging A and B in Eq. (6.13). We stress that having fully isolated A dynamics is a necessary but not sufficient condition for full nonreciprocity from A to B. In fact, it is possible to have dynamics generated by nontrivial interactions that is isolated in both directions, i.e. $I^{(A)}(t) = I^{(B)}(t) = 1$ (for an example, see Section 6.4.4).

6.3.5 Physical intuition and example cases

For a variety of simple test cases, our formal definitions of reciprocity and nonreciprocity agree with simple intuition. For example, it is easy to show that if the starting bipartite system is uncoupled, or is symmetric under permutation of A and B labels, then its dynamics is automatically reciprocal as per the definition in Eq. (6.10). Our definition also does more than simply quantify asymmetry of the bipartite system. As an example, in Appendix 6.8.1 we consider a class of highly asymmetric bipartite, non-dissipative systems that are always reciprocal as per our definition in Eq. (6.10). These systems take the B subsystem to be a qubit, the A system to be *arbitrary*, and take the two subsystems to interact via coupling Hamiltonian that commutes with the B-only Hamiltonian. Another interesting test case is where A and B are both single qubits. In this case, if the evolution is an arbitrary unitary, then it must be fully reciprocal (see Appendix 6.8.1).

To gain intuition about the opposite limit of full nonreciprocity, it is useful to examine cases where dynamics of A is fully isolated. This is of course a necessary condition for fully unidirectional dynamics (see Eq. (6.13)), but is of course not sufficient. One can show if B can be exactly traced out from the total system dynamics, then the A isolation by our definition stays unity throughout the time evolution, i.e.

$$\forall t,\ \mathrm{Tr}_B\left[\mathcal{E}_t^{(AB)}(\hat{\rho}_A\otimes\hat{\rho}_B)\right]=\mathcal{E}_t^{(A)}\hat{\rho}_A\Rightarrow\forall t,\ I^{(A)}(t)\equiv 1. \tag{6.14}$$

Here $\mathcal{E}_t^{(A)}$ is a local superoperator acting on A and is independent of $\hat{\rho}_B$. As a result, dynamics of a generic cascaded quantum systems from A to B (see Eq. (6.1)) must be fully isolated in terms of subsystem A. Furthermore, because A cannot be exactly traced out from the system dynamics, the dynamics of B can be affected by A, so that dynamics generated by Eq. (6.1) is fully nonreciprocal by Eq. (6.13).

6.4 Quantum nonreciprocity via generalized gauge symmetry

6.4.1 Gauge-invariance nonreciprocity with a single dissipator

We now introduce our new method for realizing nonreciprocal quantum dynamics via an open system Markovian dynamics that is *distinct* from cascaded quantum systems. We begin with the simplest case of a Lindblad master equation with a single dissipator, leaving generalizations to Section 6.6. We start with a seemingly trivial observation for a single, generic Lindblad dissipator on system A. Such a dynamics is described by

$$\mathcal{L}_{A,1}\hat{\rho}_A=\Gamma\mathcal{D}[\hat{A}]\hat{\rho}_A. \tag{6.15}$$

It is straightforward to see that this Lindbladian is invariant under an arbitrary gauge transformation of the jump operator $\hat{A}\rightarrow\hat{A}e^{i\theta(t)}$, where $\theta(t)$ can be an arbitrary time-

dependent real function. This invariance formally corresponds to a local (in time) gauge symmetry of a generic Lindblad dissipator.

We can use this trivial insensitivity of the dynamics to $\theta(t)$ to now obtain a nonreciprocal interaction between two systems: simply replace the classical time-dependent phase with a quantum operator acting on a different quantum system B: $\theta(t) \to \hat{\theta}_B$. As shown in Fig. 6.1(a), we now rewrite the phase factor in the jump operator as unitary operator $\hat{U}_B$ acting on subsystem B. We thus obtain a new QME (see also Eq. (6.2)):

$$\mathcal{L}_{\mathrm{dir}}\hat{\rho} = \Gamma\mathcal{D}[\hat{A}\hat{U}_B]\hat{\rho}. \tag{6.16}$$

One can easily show that gauge invariance property discussed above ensures that the dynamics of A is insensitive to B. More explicitly, consider a general master equation where the interaction between A and B is given by Eq. (6.16): $(d\hat{\rho}/dt) = (\mathcal{L}_{A,\mathrm{i}} + \mathcal{L}_{B,\mathrm{i}})\hat{\rho} + \Gamma\mathcal{D}[\hat{A}\hat{U}_B]\hat{\rho}$, with $\mathcal{L}_{A(B),\mathrm{i}}$ describing internal dynamics of A (B). One can exactly trace out B to obtain a QME for the A reduced density matrix $\hat{\rho}_A = \mathrm{Tr}_B\hat{\rho}$ alone, as

$$\frac{d\hat{\rho}_A}{dt} = \mathcal{L}_{A,\mathrm{i}}\hat{\rho}_A + \Gamma\mathcal{D}[\hat{A}]\hat{\rho}_A. \tag{6.17}$$

However, the converse is in general not true: B will be in general influenced by A, i.e. its evolution is sensitive to the initial state of A as well as $\mathcal{L}_{A,\mathrm{i}}$. The only exception is the case where $\hat{A}$ is proportional to a unitary, see also Section 6.4.4.

The more formal definitions of nonreciprocity introduced in Section 6.3 also yield an identical picture. Because the equation of motion of the A subsystem is independent of the B state (see Eq. (6.17)), it follows that the A isolation must be unity throughout time evolution, i.e. $I^{(A)}(t) \equiv 1$ for all t. For the B isolation, assuming $\hat{A}$ is not proportional to a unitary operator, one can generally show that $I^{(B)}(t) < 1$ for some time t; see also Section 6.4.2 for a concrete example with a bosonic lowering operator as $\hat{A}$. Thus, according to the new metric

based on isolation functions, the QME in Eq. (6.16) describes fully nonreciprocal dynamics from A to B as long as we have $\hat{A}^\dagger \hat{A} \not\propto \hat{\mathbb{I}}$.

We stress that Eq. (6.16) describes a generic nonreciprocal open-systems dynamics that is distinct from a cascaded quantum system: it *cannot* be written in the form of a cascaded QME, Eq. (6.1). Our new approach in Eq. (6.16) can be written as a Liouvillian that has no Hamiltonian part, and that has a single dissipator with a jump operator that is a *product* of an A operator and a B operator. In marked contrast, the cascaded quantum systems QME in Eq. (6.1) has a Hamiltonian in its Liouvillian, and a jump operator that is the *sum* of a subsystem-A operator and a subsystem-B operator. These cannot be made equivalent. At a more physical level, the differences in jump operators correspond to different forms of system-bath coupling. The inequivalence also implies that the nonreciprocal interaction described by Eq. (6.16) *cannot* be realized by coupling A and B to a directional waveguide (see Fig. 6.1(a)).

6.4.2 Example: photon-loss dissipator

To make our ideas more concrete, consider a simple case where the A subsystem in Eq. (6.16) is a bosonic mode, and $\hat{A}$ is taken to be the photon lowering operator $\hat{a}$ for this mode. Further, take an initial state where A is unentangled with B, and is prepared either in the vacuum state $|0\rangle$, or in the Fock state $|\ell\rangle$ ($\ell > 0$). From Eq. (6.7), we can thus obtain an upper limit of the corresponding B isolation in the long-time $t \to \infty$ limit as

$$I^{(B)}(\infty) \leq 1 - \frac{1}{2} \lim_{t\to\infty} ||\mathcal{E}^{(B)}_{|0\rangle}(t) - \mathcal{E}^{(B)}_{|\ell\rangle}(t)||_\diamond. \tag{6.18}$$

One can also show (see Section 6.4.3) that the subsystem-B evolution maps appearing in this equation have an extremely simple form:

$$\lim_{t\to\infty} \mathcal{E}^{(B)}_{|n\rangle}(t)\hat{\rho}_B = \hat{U}_B^n \hat{\rho}_B \hat{U}_B^{\dagger n}. \tag{6.19}$$

Intuitively, this describes a dissipative process where each time a photon is lost from the A cavity, subsystem B undergoes a unitary evolution $\hat{U}_B$. We can thus derive an upper bound for the corresponding B isolation in the long-time $t \to \infty$ limit as [237]

$$I^{(B)}(\infty) \leq 1 - \sqrt{1 - \min_{|\phi\rangle\in\mathcal{H}_B} |\langle\phi|\hat{U}_B^\ell\,|\phi\rangle\,|^2}. \tag{6.20}$$

Letting $e^{i\beta_m}$ denote the eigenvalues $\hat{U}_B$, the RHS of Eq. (6.20) can be further rewritten explicitly as

$$I^{(B)}(\infty) \leq 1 - \max_{m,n} \left|\sin\frac{\ell(\beta_m - \beta_n)}{2}\right|. \tag{6.21}$$

Thus, the B isolation in the long-time limit is less than 1 for any nontrivial unitary $\hat{U}_B^\ell$ (i.e. not proportional to identity map), signalling nontrivial influence from A to B. The isolation reaches minimal value of zero if $\hat{U}_B^\ell$ has two eigenvalues with relative π phase difference, in which case the long-time evolution becomes maximally nonreciprocal.

6.4.3 Dissipative quantum gates mediated by new form of nonreciprocal interaction

Our new nonreciprocal QME has many interesting features. Here, we focus on a potentially powerful application: the implementation of unitary gate operations on subsystem B that are realized in a dissipative steady state, and whose form is controlled by the initial state of subsystem A. The most generic way to realize this is to construct a dynamics of the form

of Eq. (6.16), where $\hat{A}$ has a subspace of dark states $\mathcal{D}$: if $|d\rangle \in \mathcal{D}$, then $\hat{A}|d\rangle = 0$. Further, let $\mathcal{S}$ denote the set of states in the intersection between the orthogonal complement of $\mathcal{D}$ and the inverse image of $\mathcal{D}$ under $\hat{A}$. A given state $|\psi\rangle \in \mathcal{S}$ is both orthogonal to the dark state subspace, and has the property $\hat{A}|\psi\rangle$ is in $\mathcal{D}$ (i.e. a single action of $\hat{A}$ results in a dark state). We now have a simple way to obtain our dissipative gate:

- At $t = 0$ the full system is taken to be in a product state $\hat{\rho}_{AB}(0) = \hat{\rho}_A(0) \otimes \hat{\rho}_B(0)$.
- If we don't want a gate operation to be performed on B, we start subsystem A in an arbitrary dark state in $\mathcal{D}$. In this case, there is no evolution under Eq. (6.16), and the subsystem B state is unchanged.
- To turn the gate on, we instead prepare subsystem A in an arbitrary state in $\mathcal{S}$. In this case, there is non-trivial evolution under Eq. (6.16). To achieve the gate operation, one just waits until the system reaches its steady state. The dissipative steady state will be

$$\hat{\rho}_{AB}(\infty) = \hat{\rho}'_A \otimes \left(\hat{U}_B \hat{\rho}_B(0) \hat{U}_B^\dagger\right), \tag{6.22}$$

  where $\hat{\rho}'_A$ is in $\mathcal{D}$, i.e. it is a dark state. The final state of B is related to the initial state by the unitary $\hat{U}_B$.

We stress that this approach realizes a gate operation on system B in the dissipative steady state; no precise timing control is needed. The only control that is needed is to prepare subsystem-A at $t = 0$ in a state in the subspace $\mathcal{S}$. Crucially, this control need not be perfect, as any state in this manifold (pure or impure) will lead to the desired gate operation. This resilience is similar in spirit to recent theoretical ideas for mixed-state encodings of quantum information (see e.g. [238]).

An even more versatile kind of controllable dissipative gate is possible if $\hat{A}$ has the general structure of a lowering operator. By this, we mean that within a given subspace,

$\hat{A}$ is a matrix that only has non-zero entries along the super-diagonal. This is exactly the situation we have if $\hat{A}$ is a bosonic lowering operator $\hat{a}$, hence we consider this case in what follows. As illustrated in Fig. 6.1(b), if the control subsystem A is initialized in a Fock state $|\ell\rangle$, the long-time dynamics of the target system effectively applies $\hat{U}_B$ ℓ times on the initial target state, so that we have

$$\lim_{t\to\infty} \mathrm{Tr}_A \left\{ e^{\mathcal{L}_{\mathrm{dir}} t} \left[|\ell\rangle\langle\ell| \otimes \hat{\rho}_B(0) \right] \right\} = (\hat{U}_B)^\ell \hat{\rho}_B(0) (\hat{U}_B^\dagger)^\ell. \tag{6.23}$$

This recipe allows one to apply e.g. tunable phase gates on a target qubit. We stress that this gate mechanism works for generic systems (see Appendix 6.8.7 for an example where it can be used to apply displacement gates on a harmonic oscillator).

We note that this approach to dissipative unitary gate operations is distinct from previous works exploring dissipative quantum control. For example, Ref. [226] focused on dissipatively realizing a *unique* steady state that effectively realizes a quantum computational task. In contrast, we are dissipatively implementing a steady-state unitary operation on subsystem B, not a unique state. Our dissipator in Eq. (6.16) has of course multiple steady states, something that is exploited by our protocol. Approaches for mimicking Hamiltonian evolution on a subsystem have also been formulated, using either strong dissipation [227–229], measurements [230–232], or fast repetitive resets [233]. In stark contrast to our work, these approaches do not yield a time-independent steady state. Instead, one needs to explicitly shut off the dynamics at a particular time in order to achieve a particular unitary (whereas we achieve the unitary in the long-time steady state). We stress that our dissipative unitary gate does not give rise to long time oscillations; as such it is completely distinct from recent mechanisms studied in the context of quantum synchronization [239, 240].

The dissipative steady-state gate mechanism described here suggests a fundamentally different physical architecture for constructing a quantum processor. In the standard architectures, the analog information parameterizing a target gate operation $\hat{U}_B$ (e.g. the angles

and axes of a single-qubit rotation) is contained in external control pulses, whose precision is subject to fluctuations of external control electronics. Here, the analog parameters of $\hat{U}_B$ are "hard-wired" within the engineered quantum system, whose precision is an inherent property of the quantum device itself. The subsystem A acts as a classical switch for the gate, and the only information flow needed to execute the quantum gate is a binary command. While it may be non-trivial to prepare subsystem A in the starting states in the basic examples presented in this work (Fock states), in principle the starting manifold $\mathcal{S}$ can be made large and macroscopically distinguishable from $\mathcal{D}$, so the control need not be perfect as any state in this $\mathcal{S}$ (pure or impure) will lead to the desired gate operation. Finally, to be clear, the non-reciprocal dissipator in the current scheme does not counter decoherence in $\hat{\rho}_B$. Interestingly, the mechanism of steady-state unitary gates here provides a powerful knob for implementing autonomous quantum error correction [241–245] using reservoir engineering, see [234].

6.4.4 Gauge-invariance nonreciprocity: other generic cases

We now discuss the physics of our nonreciprocal dynamics in Eq. (6.16) for different generic choices of the subsystem-A operator (beyond the lowering operator case discussed above). Consider first the case where $\hat{A}$ is itself unitary. In this case, there is no asymmetry in our dissipator (i.e. both subsystem operators are unitary), and correspondingly we would expect that there cannot be any directional interaction. This is indeed what occurs: in this case, it is easy to confirm that both systems are isolated from one another. The only way to see signatures of the interaction would be to consider the evolution of correlations between them. As discussed in [246, 247], this type of dissipative dynamics can be understood as coupling both A and B to the same classical Poisson point process. It is then straightforward to show that time evolution of both of subsystems is independent of the other, and the correlation between classical stochastic processes coupled to A versus B is only discernible if one looks

at AB correlators.

Another general case is where the $\hat{A}$ operator in Eq. (6.16) is Hermitian. While the dynamics in this case is directional from A to B, we can exactly solve for the time evolution in terms of eigenbasis of the jump operator. The system dynamics now allows a simple interpretation, i.e. B dephases at rates depending on A state, but not vice versa.

6.4.5 Connection to measurement-and-feedforward processes

Given that a large class of standard quantum cascaded systems can be intuitively understood as being equivalent to a measurement-and-feedforward (MF) process [31, 248], it is worth discussing the relation between our nonlinear dissipator in Eq. (6.16) and MF protocols. As shown in [248], dissipators given by Eq. (6.16) can be realized via a generalized MF process as $e^{\mathcal{L}_{\text{dir}}\delta t}\hat{\rho} = \sum_{\ell=1,2} \hat{M}_\ell \hat{\rho} \hat{M}_\ell^\dagger$. Here, the Kraus operators $\hat{M}_\ell$ are given by (to order δt)

$$\hat{M}_1 = \sqrt{\Gamma \delta t}\hat{A}\hat{U}_B, \quad \hat{M}_2 = 1 - \Gamma \hat{A}^\dagger \hat{A} \delta t, \tag{6.24}$$

which satisfy the normalization condition $\sum_{\ell=1,2} \hat{M}_\ell^\dagger \hat{M}_\ell = \hat{\mathbb{I}}$. Intuitively, this stochastic process corresponds to weakly measuring A, and subsequently applying unitary transformations on B conditioned on the measurement results. This interpretation provides a simple, complementary way to understand the directionality of our dynamics in the single dissipator case. It also tells us that this dynamics can never generate entanglement between A and B.

While for a single dissipator, both the gauge-invariance picture and MF picture let us understand the directionality, the same is not true for the multiple dissipator case analyzed in Section 6.6. In this case, the gauge invariance pictures ensures nonreciprocity, but there is no mapping onto a MF process (and in fact, the dynamics can create entanglement).

6.4.6 Non-Markovian effects

As we have stressed, the nonreciprocity of the dissipative dynamics in our basic dissipator of Eq. (6.16) is directly related to the local gauge invariance of a standard Lindblad dissipator. This effective gauge symmetry however only emerges in the limit of a Markovian bath, something we discuss in detail in Appendix 6.8.2. Physically, it requires the bath correlation time τ_{E} to be much smaller than the timescale associated with variation of the gauge phase $\theta(t)$: $\tau_{\mathrm{E}} \ll [\dot{\theta}(t)]^{-1}$. If this condition is met, then the bath is effectively only sensitive to the instantaneous value of $\theta(t)$, and there is no difference between a constant in time $\theta(t)$ versus a time varying phase. Conversely, if changes in the gauge phase $\theta(t)$ are not negligible during the bath correlation time, the dynamics of $\theta(t)$ will induce non-Markovian effects in the bath, and the system dynamics will no longer be gauge invariant.

The above picture can be made rigorous, and one can calculate leading non-Markovian corrections. In Appendix 6.8.3, we consider microscopic bath model with a system-environment (SE) interaction Hamiltonian of the form $\hat{H}_{\mathrm{SE}} = e^{i\theta(t)}\hat{\xi}^{\dagger}\hat{A} + \mathrm{H.c.}$. Here, $\hat{\xi}$ is the bath operator that couples to the system. We derive the leading-order correction to Eq. (6.15) due to a finite bath correlation time τ_{E}, a correction which scales as $\tau_{\mathrm{E}}\dot{\theta}(t)$. Further, in Section 6.5.2, we work with an explicit quantum realization of our dissipative scheme, and use the isolation functions defined in Section 6.3 to quantify how a finite bath correlation time causes deviations from full nonreciprocity.

6.5 Physical implementation in cavity QED systems

6.5.1 Basic setup

We now discuss methods for implementing the general nonreciprocal dynamics of Eq. (6.16) in a quantum optical setup. Note that incidentally, dissipators of the form in Eq. (6.16) have been used to describe e.g. decay of two-level atoms with recoil [249, 250]. However,

to the best of our knowledge, such processes have not been discussed in the context of engineering useful nonreciprocal interactions. The standard treatment of such processes also immediately expands out the unitary in Eq. (6.16) (see e.g. [251]), obscuring the fully nonreciprocal structure. In this section, in contrast, we focus on experimentally compatible methods for realizing a generic target dissipator. One direct approach would be to explicitly break TRS, and use standard nonreciprocal elements like a circulator or a chiral waveguide. Formally, such implementations involve starting with a larger system described by a cascaded master equation, eliminating degrees of freedom, and then obtaining the effective dynamics of Eq. (6.16). We discuss a generic method for doing this (starting with a chiral waveguide) in Appendix 6.8.4. Note that several recent circuit QED experiments using nonreciprocal elements could be usefully interpreted in this way [252–254] (see Appendix 6.8.4 for more details). We also stress that this recipe for realizing Eq. (6.16) using a larger cascaded quantum system does not imply that the two types of dynamics are equivalent. To see this, one may consider an analogical example involving open versus closed quantum systems: there, it is straightforward to understand that the two still correspond to very distinct forms of dynamics, even though any open quantum system can be realized by starting from a larger closed quantum system with auxiliary reservoir modes, and then eliminating the reservoir degrees of freedom.

We focus here on a more intriguing implementation strategy that uses reservoir engineering techniques but *does not require any elements that explicitly break time-reversal symmetry, i.e. the dynamics does not involve any nontrivial gauge-invariant phases*. We take subsystem A to be a resonator mode with bosonic annihilation operator $\hat{a}$, and subsystem B to be a qubit with Pauli z operator $\hat{\sigma}_z$. We wish to realize our nonreciprocal master equation Eq. (6.16) with the choices $\hat{A} = \hat{a}$, and $\hat{U}_B = \exp(-i\theta\hat{\sigma}_z/2)$, i.e.

$$\frac{d\hat{\rho}}{dt} = \mathcal{L}_{\text{gate}}\hat{\rho} = \Gamma\mathcal{D}[e^{-i\frac{\theta}{2}\hat{\sigma}_z}\hat{a}]\hat{\rho}. \tag{6.25}$$

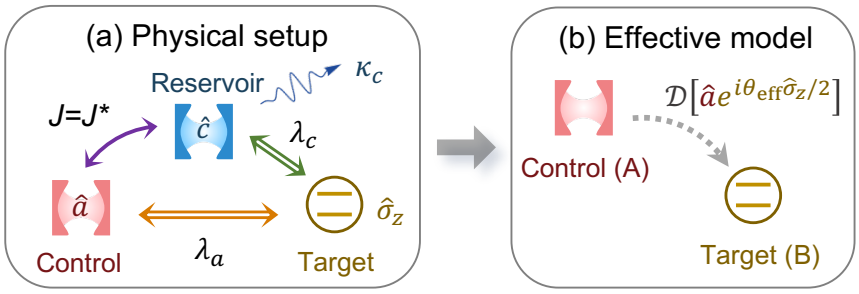

Fig. 6.2: (a) Schematic of a setup that realizes a nonreciprocal interaction from a cavity mode a (A) to a qubit (B). Both subsystems are coupled to an auxiliary damped bosonic mode c that plays the role of a reservoir, see Eq. (6.27). (b) The effective dissipator describing the nonreciprocal interaction in the Markovian reservoir limit $\kappa_c \gg J$.

To engineer the effective dynamics in Eq. (6.25), we couple both the cavity mode a and the qubit to an auxiliary, highly damped bosonic mode $\hat{c}$ (decay rate κ_c), via tunneling and dispersive interactions respectively (see Fig. 6.2(a)). The interaction Hamiltonian between the system and the c mode (i.e. the reservoir) is:

$$\hat{H}_{\rm int} = (J\hat{a}^\dagger\hat{c} + \text{H.c.}) + (\lambda_c/2)\hat{\sigma}_z\hat{c}^\dagger\hat{c}, \tag{6.26}$$

where J denotes the complex tunnel coupling rate. We will also include a direct Hamiltonian dispersive coupling between the cavity mode $\hat{a}$ and the qubit, $\hat{H}_{\rm S} = (\lambda_a/2)\hat{\sigma}_z\hat{a}^\dagger\hat{a}$. We take a and c modes to be resonant, and work in a rotating frame where the a, c and qubit frequencies are shifted to zero. The total dynamics (including the reservoir c mode) is then described by the QME:

$$\frac{d\hat{\rho}_{\rm tot}}{dt} = \mathcal{L}_{\rm SR}\hat{\rho}_{\rm tot} = -i[\hat{H}_{\rm S} + \hat{H}_{\rm int}, \hat{\rho}_{\rm tot}] + \kappa_c\mathcal{D}[\hat{c}]\hat{\rho}_{\rm tot}. \tag{6.27}$$

Note that Eq. (6.27) does not involve any explicit breaking of TRS, in that there is no nontrivial gauge phase. Even if J is complex, the corresponding hopping phase can always be eliminated by a gauge transformation on $\hat{a}$; hence, the phase of J plays no role. This can be understood physically from the fact that the setup in Eq. (6.27) does not host any closed

loops enclosing a nontrivial flux. We thus assume henceforth, without loss of generality, that the cavity-reservoir coupling amplitude in Eq. (6.27) is real and positive, i.e. $J = |J|$.

We next consider the limit where reservoir-mode photons decay much faster than their tunneling rate to the cavity, i.e. $\kappa_c \gg J$. We can then adiabatically eliminate the reservoir (see Appendix 6.8.5), yielding an effective QME for the cavity-qubit density matrix $\hat{\rho}$

$$\frac{d\hat{\rho}}{dt} = -i\left[\frac{\lambda_a + \lambda_{\text{eff}}}{2}\hat{\sigma}_z\hat{a}^\dagger\hat{a}, \hat{\rho}\right] + \Gamma_{\text{eff}}\mathcal{D}\left[e^{-i\frac{\theta_{\text{eff}}}{2}\hat{\sigma}_z}\hat{a}\right]\hat{\rho}. \tag{6.28}$$

For $\kappa_c \gg J$, the parameters in this QME are

$$\Gamma_{\text{eff}} = 4J^2\kappa_c/(\kappa_c^2 + \lambda_c^2), \tag{6.29}$$

$$\lambda_{\text{eff}} = -4J^2\lambda_c/(\kappa_c^2 + \lambda_c^2), \tag{6.30}$$

$$\theta_{\text{eff}} = 2\arctan(\lambda_c/\kappa_c). \tag{6.31}$$

The various coupling in Eq. (6.28) can be easily given a physical interpretation. In the regime $\kappa_c \gg J$, the reservoir and the qubit together forms a new effective, Markovian environment for the cavity mode. The corresponding effective cavity decay rate Γ_{eff} matches the Fermi's Golden rule expectation, and is independent of the qubit state. λ_{eff} is an induced dispersive coupling arising from weak hybridization of a and c modes. The most interesting parameter is the phase θ_{eff}. At a heuristic level, whenever a photon hops from the cavity mode to the reservoir mode and subsequently decays, the qubit is rotated by an angle θ_{eff} about the z axis. In the limit $\lambda_c \ll \kappa_c$, this phase shift can be understood as a product between photon dwell time in the reservoir c mode, $\tau_c \sim \kappa_c^{-1}$, and the bare qubit-reservoir dispersive coupling strength λ_c.

Finally, we imagine tuning the direct dispersive interaction so that it cancels the induced dispersive interaction, i.e. tune $\lambda_a = -\lambda_{\text{eff}}$. In this case, we are left only with the dissipator in Eq. (6.28), which corresponds exactly to the form in our general directional QME

Eq. (6.25). We thus obtain a completely directional dynamics from the cavity to the qubit. We stress that this physical implementation uses standard forms of qubit-cavity coupling, and does not use any explicitly nonreciprocal elements.

It is worth stepping back to ask what the essential ingredients were here to obtain quantum nonreciprocity without any explicit breaking of TRS. Like in our general QME in Eq. (6.2), it was crucial to have a final dissipator that was a product of A and B operators, corresponding to a nonlinear system-bath interaction (i.e. the environment couples to the composite operator $\hat{A}\hat{U}_B$). Further, we needed asymmetry: the B operator was unitary, the A operator was not. It is interesting to note that nonlinearity and broken inversion symmetry have been used in a very different manner to engineer nonreciprocal scattering without breaking TRS, both in classical [255, 256] and quantum [257–259] settings. However, the scattering in those works are only approximately nonreciprocal, and even then only for a limited range of incident field powers and frequencies. This is very different from our mechanism, which is unidirectional independent of initial state, and which is not equivalent to a simple scattering problem.

6.5.2 Non-Markovian effects in the qubit-cavity setup

The physical implementation given by Eq. (6.27) provides a concrete setup where we can quantitatively analyze the effects of non-Markovianity. In this case, the reservoir (i.e. the highly damped c mode) has a finite correlation time $\tau_c \sim \kappa_c^{-1}$, and the Markovian limit is only reached for large decay rate κ_c. As discussed in Section 6.4.6, the gauge symmetry that leads to isolation and nonreciprocity in our system only exists in the Markovian limit. We thus expect to see deviations from ideal behaviour away from this limit.

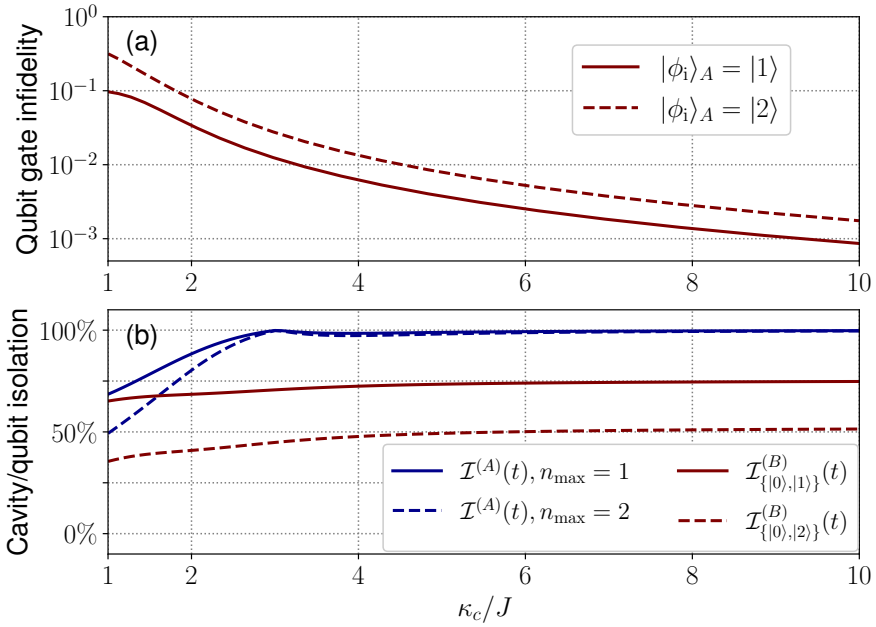

Fig. 6.3: (a) State-averaged infidelity of the cavity-controlled steady-state qubit gate, as a function of the non-Markovianity parameter κ_c/J. We consider different choices of initial cavity state: either the Fock state $|\phi_{\rm i}\rangle_A = |1\rangle$ (solid) or $|2\rangle$ (dashed), and take $\theta_{\rm eff} = \pi/6$. These different initial cavity states result in different gate operations. Infidelity tends to zero in the Markovian limit. (b) Isolation functions for both qubit and cavity as a function of the non-Markovianity parameter κ_c/J. We take a fixed evolution time $t = \pi/\Gamma_{\rm eff}$ and $\theta_{\rm eff} = \pi/6$. Blue curves: cavity isolation $I^{(A)}(t)$, c.f. Eqs. (6.7) and (6.32). Red curves: conditional qubit isolation function $I^{(B)}_{\{|0\rangle,|\ell\rangle\}}(t)$ ($\ell = 1, 2$) which is an upper bound for the qubit isolation $I^{(B)}(t)$, see Eq. (6.33). We see strongly nonreciprocal behaviour (i.e. $I^{(A)}(t) \simeq 1$, $I^{(B)}(t) < 1$) even away from the Markovian limit. As discussed in the main text, when calculating $I^{(A)}(t)$, we truncate the cavity Fock space to $n_{\rm max}$ photons for simplicity; the solid (dashed) curve is for $n_{\rm max} = 1$ ($n_{\rm max} = 2$).

In Fig. 6.3(a), we numerically investigate the infidelity [260] of the steady-state gate operation performed on B, as a function of the non-Markovianity parameter κ_c/J. Remaining parameters are also varied to keep the qubit gate angle θ in Eq. (6.31) fixed (here at a value $\theta_{\rm eff} = \pi/6$). As expected, the infidelity rapidly drops to zero in the Markovian large κ_c limit. This general trend remains true no matter what the chosen value of $\theta_{\rm eff}$.

We can also ask how non-Markovian effects impact nonreciprocity in this system. The isolation functions introduced in Section 6.3 let us quantitatively compare the nonreciprocity

of Eq. (6.27) for different values of κ_c. For cavity dynamics due to Eq. (6.27), one can show that the cavity isolation function can be expressed as

$$I^{(A)}(t) = 1 - \frac{1}{2}||\mathcal{E}^{(A)}_{|\uparrow\rangle}(t) - \mathcal{E}^{(A)}_{|\downarrow\rangle}(t)||_\diamond. \tag{6.32}$$

where $|\uparrow\rangle, |\downarrow\rangle$ are $\hat{\sigma}_z$ eigenstates. While the diamond norm can be calculated for quantum maps acting on an infinite-dimensional Hilbert space, to make the problem numerically tractable, we truncate the cavity Hilbert space to have at most one or two photons (as this is already sufficient to illustrate the effect of non-Markovianity). The numerically calculated cavity isolation for increasing cavity decay rates κ_c is plotted by the blue curves in Fig. 6.3(b). We see that even for modest values of κ_c (i.e. not strongly in the Markovian regime), the cavity is well isolated.

To characterize nonreciprocity, we also need to consider the qubit isolation $I^{(B)}(t)$. We can find a simple upper bound for this quantity using the conditional qubit isolation $I^{(B)}_{\{|0\rangle,|\ell\rangle\}}(t)$, corresponding to initial control cavity Fock states $\{|0\rangle, |\ell\rangle\}$ ($\ell = 1, 2$), as

$$I^{(B)}(t) \leq \left(I^{(B)}_{\{|0\rangle,|\ell\rangle\}}(t) \equiv 1 - \frac{1}{2}||\mathcal{E}^{(B)}_{|0\rangle}(t) - \mathcal{E}^{(B)}_{|\ell\rangle}(t)||_\diamond \right). \tag{6.33}$$

From definition of qubit isolation (c.f. Eq. (6.7)), one sees that $I^{(B)}_{\{|0\rangle,|\ell\rangle\}}(t)$ must be no less than the actual qubit isolation function $I^{(B)}(t)$. As shown in Fig. 6.3(b), in the fast reservoir limit $\kappa_c/J \gg 1$, $I^{(B)}_{\{|0\rangle,|\ell\rangle\}}(t)$ ($\ell = 1, 2$) (red curves) is considerably smaller than cavity isolation $I^{(A)}(t)$ (blue curves), demonstrating that the reservoir mode mediates an effective unidirectional interaction from control cavity to the qubit.

6.6 Generalized gauge-invariance nonreciprocity: the non-abelian case

6.6.1 Gauge symmetry of a multi-dissipator Lindblad master equation

We now discuss how our recipe for quantum nonreciprocity based on gauge invariance can be extended from Eq. (6.16) to a much broader class of dynamics. This generalized version involves dissipative dynamics with multiple dissipators, and the relevant local gauge symmetry can become non-abelian. As we show, this generalized version is in general *not* equivalent to unconditional evolution under measurement and feedforward, and is capable of generating entanglement. It is also (like the single dissipator case) distinct from the cascaded quantum systems master equation.

Similar to Section 6.4.1, we start by considering a single system A undergoing dissipative Lindblad dynamics, but now involving multiple dissipators:

$$\frac{d}{dt}\hat{\rho}_A = \Gamma \sum_{\ell=1}^{N} \mathcal{D}[\hat{A}_\ell]\hat{\rho}_A \equiv \mathcal{L}_A \hat{\rho}_A. \tag{6.34}$$

As is well known, multi-dissipator Liouvillians like $\mathcal{L}_A$ are invariant under a wide class of transformations that mix the jump operators $\hat{A}_l$. Let u_{lm} be the matrix elements of an arbitrary $N \times N$ complex unitary matrix $\check{\mathcal{U}}$ [261]. Then we necessarily have (see e.g. [20]):

$$\sum_{\ell=1}^{N} \mathcal{D}[\hat{A}_\ell] = \sum_{\ell=1}^{N} \mathcal{D}\left[\sum_{m=1}^{N} u_{\ell m}\hat{A}_m\right]. \tag{6.35}$$

The above invariance of $\mathcal{L}_A$ also trivially continues to hold if we make the unitary mixing matrix $\check{\mathcal{U}}(t)$ time dependent. Formally, this represents a local-in-time, non-abelian gauge symmetry, as for $N \geq 1$ different allowed $\check{\mathcal{U}}$ do not commute with one another.

For what follows, it will be helpful to give an intuitive picture of this multi-dissipator

gauge symmetry. Each of the N dissipators in our master equation (indexed by ℓ) can be interpreted as describing the influence of an independent dissipative bath. The operator $\sum_m u_{\ell m}\hat{A}_m$ is then interpreted as the particular system-A operator that couples to bath ℓ. $u_{\ell m}$ are thus system-bath coupling constants. Eq. (6.35) hence tells us that there are several distinct ways to couple our system to the N baths that results in identical dynamics; all that is required is that the $u_{\ell m}$ form a unitary matrix. At a physical level, this means that each independent bath should couple to an "orthogonal" set of system operators (i.e. the rows of $\check{\mathcal{U}}$ are orthogonal), and that the "total coupling strength" to bath l is always the same, i.e. $\sum_m |u_{lm}|^2 = 1$.

6.6.2 From gauge symmetry to a multi-dissipator non-reciprocal interaction

Similar to Section 6.4.1, Eq. (6.35) now provides a route to construct a nonreciprocal interaction with a second subsystem B: we make each matrix element $u_{\ell m}(t)$ of $\check{\mathcal{U}}(t)$ an operator $\hat{u}_{\ell m}$ acting on B. This results in a new master equation acting on the state of the bipartite A plus B system:

$$\frac{d}{dt}\hat{\rho}_{AB} = \Gamma \sum_{\ell=1}^{N} \mathcal{D}\left[\hat{z}_\ell\right]\hat{\rho} \equiv \mathcal{L}_{\text{multi}}\hat{\rho}, \tag{6.36}$$

with

$$\hat{z}_\ell = \sum_{m=1}^{N} \hat{A}_m \hat{u}_{\ell m}. \tag{6.37}$$

At a physical level, we can interpret this as a kind of generalized dissipative parametric coupling: system B controls the strength and form of the coupling between system A and the N dissipative baths in the problem. If the different $\hat{u}_{\ell m}$ operators fail to commute, then there will be unavoidable quantum noise in the magnitude and form of these couplings. Note that simpler parametric dissipative couplings have been studied in quantum optomechanics

(see e.g. [262, 263]), where a mechanical resonator controls the loss rate of a photonic cavity mode.

The dissipative parametric coupling between A and B in Eqs. (6.36) and (6.37) will not in general be directional; this requires a further constraint. We now come to the central result of this section: the master equation Eq. (6.36) mediates a fully nonreciprocal interaction from A to B if the B operators satisfy the generalized unitarity constraint

$$\sum_{\ell=1}^{N} (\hat{u}_{\ell m})^\dagger \hat{u}_{\ell m'} = E_B \delta_{mm'} \hat{\mathbb{I}}_B, \tag{6.38}$$

where $\hat{\mathbb{I}}_B$ is the identity operator on subsystem B, and E_B is a positive real constant. Noting that E_B can be absorbed into the definition of $\hat{u}_{\ell m}$, we set $E_B = 1$ going forward. If Eq. (6.38) is satisfied, it is easy to show that A is completely isolated from B: one can trace out B and derive a closed QME for the dynamics of A that is independent of any additional local dynamics acting on B. This isolation reflects the underlying gauge symmetry discussed above (see Appendix 6.8.6 for details). The converse is not true: B will in general be influenced by A. Note that if Eq. (6.38) is satisfied, the operators $\hat{u}_{\ell m}$ can be viewed as matrix elements of a generalized unitary transformation acting on a larger space (see Appendix 6.8.6).

We stress that Eq. (6.36) is not a trivial generalization of the single-dissipator case in Eq. (6.16), since each individual dissipator $\mathcal{D}[\hat{z}_\ell]$ need not generate fully nonreciprocal dynamics on its own. Unidirectionality is thus in general a collective property of the full Liouvillian, and not of each dissipator on its own. Further, there is no clever transformation that allows one in general to express the Liouvillian in such a form, i.e. $\mathcal{L}_{\text{multi}}\hat{\rho} \neq \sum_\ell \Gamma_\ell \mathcal{D}[\hat{A}'_\ell \hat{U}_{B,\ell}]\hat{\rho}$. At a physical level, Eq. (6.38) represents a constraint on our dissipative parametric interaction. While system B still parametrically controls the coupling of system A to the N dissipative baths in our problem, the coupling to each of these baths is fixed in magnitude

irrespective of the state of B. Further, each bath always sees an orthogonal combination of the system-A operators $\hat{A}_\ell$. This constraint ensures system A is independent of system B (by virtue of the symmetry in Eq. (6.35)), but still allows A to influence B.

6.6.3 Example: qubit-controlled photonic loss

As a concrete example, we consider a bipartite system where the A subsystem is comprised of two photonic cavity modes a_1, a_2, and the B subsystem is a single qubit (see Fig. 6.4(a)). We take the basic dissipative process to be single photon loss on each cavity mode, i.e. $\hat{A}_\ell = \hat{a}_\ell$ ($\ell = 1, 2$). Consider first the setup without the qubit. In this case, the RHS of the master equation in Eq. (6.35) describes a setup where each cavity couples to its own output waveguide, with the two waveguides then being routed through a beam splitter with scattering matrix $\check{\mathcal{U}}$. The two outputs of the beam splitter are then routed to zero-temperature reservoirs. One clearly sees that the particular form of the beam splitter unitary is immaterial to the two cavity modes: regardless of its form, each cavity mode experiences identical, independent single photon loss.

We now use our general recipe to make this into a nonreciprocal interaction between the two cavity modes and a qubit, by making the beam splitter a "quantum" beam splitter whose scattering properties depend on qubit operators. Such a qubit-controlled beam splitter can be characterized by a unitary operator $\hat{U}_{\text{qbs}}$ on the total cavity-qubit system. We take this operator to depend on both $\hat{\sigma}_z$ and $\hat{\sigma}_x$, with a total system dynamics that is described by:

$$\mathcal{L}_2\hat{\rho} = \Gamma \sum_{\ell=1}^{2} \mathcal{D}\left[\hat{z}_\ell\right]\hat{\rho}, \quad \hat{z}_\ell = \hat{U}_{\text{qbs}}\hat{a}_\ell(\hat{U}_{\text{qbs}})^\dagger, \tag{6.39}$$

with

$$\hat{U}_{\text{qbs}} = e^{i\varphi\hat{\sigma}_z\left(\hat{a}_1^\dagger\hat{a}_1 - \hat{a}_2^\dagger\hat{a}_2\right) + i\theta\hat{\sigma}_x\left(\hat{a}_1^\dagger\hat{a}_2 + \hat{a}_2^\dagger\hat{a}_1\right)}. \tag{6.40}$$

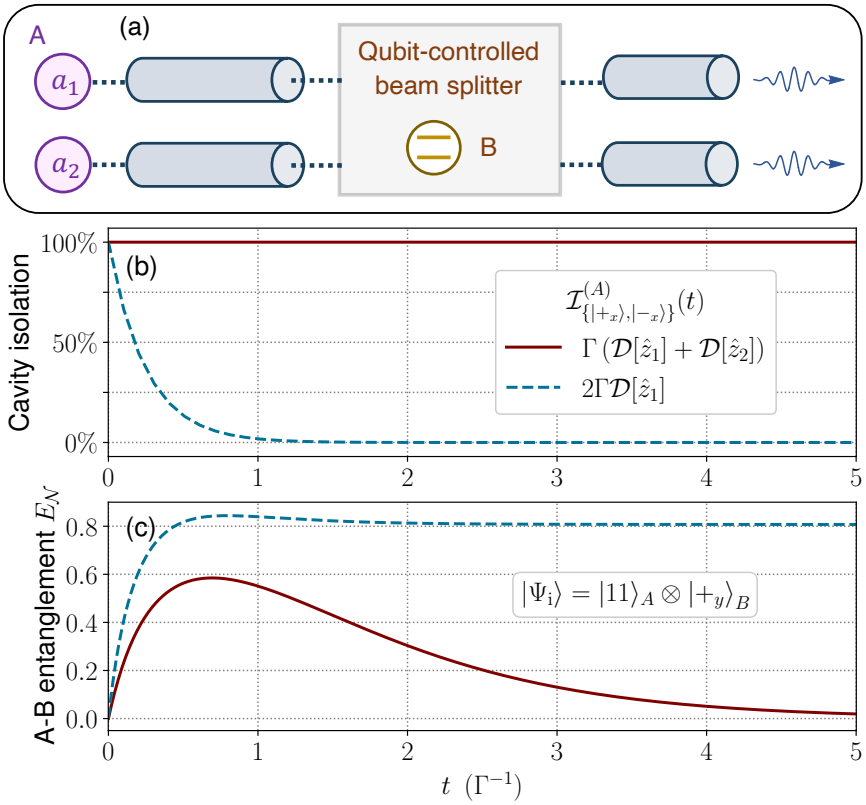

Fig. 6.4: (a) Schematic illustrating a 2-dissipator gauge symmetry nonreciprocal interaction. Two cavity modes a_1,a_2 are coupled each to waveguides, which are then sent to a beam splitter that depends on the state of a qubit. The dissipation is described by the Liouvillian $\Gamma(\mathcal{D}[\hat{z}_1]+\mathcal{D}[\hat{z}_2])$ (see Eqs. (6.39) and (6.41)). (b) Numerically computed cavity isolation $I^{(A)}_{\{|+_x\rangle,|-_x\rangle\}}(t)$ for dynamics generated by the 2-dissipator sum (solid red line), versus a single dissipator $2\Gamma\mathcal{D}[\hat{z}_1]$ (dashed blue curve). The A isolation stays unity in the former case, as expected for any dynamics that is fully nonreciprocal by design (see discussion on Eq. (6.39)). In contrast, individual dissipators from the setup in (a), e.g. $\mathcal{D}[\hat{z}_1]$, is not unidirectional. For illustrative purposes, the numerics plotted here is restricted to the subspace with at most two photons in A, but our result remains valid for a_1, a_2 modes with infinite levels. (c) Entanglement (logarithmic negativity $E_{\mathcal{N}}$) generation by the dissipations, assuming a product initial state $|11\rangle_A \otimes |+_y\rangle_B$. The fully nonreciprocal interactions generated by $\Gamma(\mathcal{D}[\hat{z}_1]+\mathcal{D}[\hat{z}_2])$ creates entanglement (solid red curve), signaling nontrivial influence from the cavity modes to the qubit.

The qubit-controlled beam splitter in Eq. (6.40) generalizes simpler constructions only involving a single qubit operator. The latter setups have been discussed theoretically (see e.g. [238, 264]) and even realized recently in experiment [265]. As we will see, using two non-commuting operators in our example will give us a new dynamical structure that is

distinct from the single-dissipator setup in Section 6.4.1.

The jump operators in Eq. (6.39) can be explicitly computed to be

$$\hat{z}_1 = e^{-i\varphi\hat{\sigma}_z}\left(\cos\theta\,\hat{a}_1 - i\sin\theta\,\hat{\sigma}_x\hat{a}_2\right), \tag{6.41a}$$

$$\hat{z}_2 = e^{i\varphi\hat{\sigma}_z}\left(-i\sin\theta\,\hat{\sigma}_x\hat{a}_1 + \cos\theta\,\hat{a}_2\right). \tag{6.41b}$$

Each of these dissipators has a non-trivial action on the composite system that in general will correlate the state of the qubit and cavities (see Fig. 6.4(a)). For example, the jump operator $\hat{z}_1$ has an amplitude for flipping the state of the qubit (correlated with loss from a_2) and for not flipping the qubit state (correlated with loss from a_1). The situation is reversed for $\hat{z}_2$. In general, neither of these jump operators can be written as a product of a qubit operator times a cavity operator. For simplicity, we assume $\theta = \varphi = \pi/4$ in what follows, but our results are valid as long as $\sin 2\theta \sin 2\varphi \neq 0$. Note that the latter constraint ensures that Eq. (6.39) cannot be decomposed into a trivial sum of single nonreciprocal dissipators.

The dissipators in the master equation Eq. (6.39) have the same form as those in the general nonreciprocal master equation Eq. (6.37). A direct computation also shows that the unitarity condition of Eq. (6.38) is satisfied. As a result, Eq. (6.39) *necessarily* describes a unidirectional interaction from the subsystem A cavity modes to subsystem B, the qubit. The cavity modes are unaffected by the qubit, and each experience simple loss at rate Γ. In contrast, the qubit remains non-trivially influenced by the cavity modes. It is interesting to ask what this nonreciprocal interaction means physically. To obtain intuition, one can consider the simple case where $\hat{a}_1$, $\hat{a}_2$ are replaced by c-numbers α_1, α_2. The form of qubit dissipation then crucially depends on the relative phase between the two amplitudes, i.e. the phase of α_1/α_2: if the ratio is real, the two qubit jump operators will be proportional to two unaligned unitaries, and the resulting qubit dynamics simply corresponds to coupling to classically stochastic Hamiltonians [247]. In contrast, if α_1/α_2 is complex, i.e. α_1, α_2 have different phases, then the jump operators will not be proprotional to unitaries, generating

richer dissipative dynamics for the qubit.

An alternative picture for Eq. (6.39) is provided by viewing the dynamics as due to an average over stochastic quantum jumps [266]. As we show, this is particularly useful for understanding entanglement generation by the nonreciprocal dynamics. Consider a product initial state, $|\Psi_{AB}\rangle = |11\rangle_A \otimes \left|\psi_{\rm qb}\right\rangle_B$ with a generic qubit state $\left|\psi_{\rm qb}\right\rangle_B$. With a single quantum jump, the initial state is acted once by $\hat{z}_1$ or $\hat{z}_2$ (see Eq. (6.41)). Because the action on qubit state by these jump operators is correlated with the action on the 2-photon state, the total qubit-cavity state will in general become entangled after the jump, indicating possible entanglement generation in the averaged dynamics. Later in this section, we further provide a concrete example for entanglement generation by Eq. (6.39).

To help see these properties more explicitly, and to see that the directionality is *not* a property of each dissipator on its own, we can calculate the isolation function of subsystem A (defined via Eqs. (6.5) and (6.7)). We compare the nonreciprocal dynamics as generated by Eq. (6.39), against the case with just a single dissipator, i.e.

$$\mathcal{L}_2'\hat{\rho} = 2\Gamma\mathcal{D}\left[\hat{z}_1\right]\hat{\rho}, \tag{6.42}$$

where the jump operator is again given by Eq. (6.41a). In Fig. 6.4(b), we plot the conditional subsystem A isolation $I^{(A)}_{\{|+_x\rangle,|-_x\rangle\}}(t)$, defined as:

$$I^{(A)}_{\{|+_x\rangle,|-_x\rangle\}}(t) \equiv 1 - (1/2)||\mathcal{E}^{(A)}_{|+_x\rangle}(t) - \mathcal{E}^{(A)}_{|-_x\rangle}(t)||_\diamond. \tag{6.43}$$

This quantity measures how sensitive the subsystem A dynamics is to the initial state of B, when B starts in a σ_x eigenstate $|\pm_x\rangle$. It sets an upper bound on the full A subsystem isolation $I^{(A)}(t)$. As shown in Fig. 6.4(b), the conditional cavity isolation stays unity at all times for the master equation Eq. (6.39). This is as expected, as the generalized unitarity constraint is satisfied. As a result, $I^{(A)}(t)$ should be unity according to Eq. (6.14). In

contrast, the A isolation is significantly smaller than 1 for the case where we only have one of the two required dissipators, see Eq. (6.42). In this case, A is not isolated from B. This shows concretely that the combined action of both dissipators in Eq. (6.39) leads to a fully directional dynamics, even though each on its own *does not* mediate a one-way interaction. Note that in this plot, we have calculated the isolation functions in a restricted cavity Hilbert subspace with at most 2 total photons. However, this does not affect the validity of our conclusion, since numerically computed isolation will set an upper bound for the isolation of the bosonic A subsystem with infinite levels. As such, our calculation clearly shows that we cannot get fully nonreciprocal interaction with only one of the dissipators in Eq. (6.41).

Of course, simply showing that subsystem A is isolated does not indicate a nonreciprocal interaction: we also need to verify that B is influenced by A, and that we have not simply cancelled any interaction between the two subsystems. To show that there is indeed a nonreciprocal interaction, in Fig. 6.4(c) we show that our master equation (Eq. (6.39)) can generate entanglement between the two subsystems. We show in that figure the time-dependent entanglement, as quantified by the logarithmic negativity, between A and B starting with an initial product state $|11\rangle_A \otimes |+_y\rangle_B$, with $|+_y\rangle_B$ denoting the qubit $\hat{\sigma}_y$ eigenstate. We see that entanglement is generated at intermediate times (red solid curve), even though system A is fully isolated at all times. This indicates that A must be influencing B, and that we have a nontrivial nonreciprocal interaction.

The fact that our dynamics can generate entanglement also leads to other important conclusions. It immediately implies that Eq. (6.39) cannot be realized via local measurement and feedforward processes, and as such, cannot be rewritten as a sum of single nonreciprocal dissipators, each having the form of Eq. (6.16). If such a decomposition were possible (see e.g. Appendix 6.8.6), then our dynamics would be equivalent to a local measurement-plus-feedforward protocol, something that cannot generate entanglement (c.f. discussion below

Eq. (6.24)). We note that this nonreciprocal entanglement generation is unique to the multi-dissipator version of our master equation.

Finally, as in the simpler single dissipator version of our mechanism, deviations from the Markovian limit will also impact the directionality of our interaction; this is discussed in more detail in Appendix 6.8.3.

6.7 Summary and outlook

In this work, we have introduced and analyzed a new kind of dissipative dynamics that leads to fully nonreciprocal interactions between two quantum systems. The crucial ingredient was a time-local gauge symmetry inherent in any Markovian, Lindblad master equation. Surprisingly, the explicit breaking of time-reversal or the use of synthetic gauge fields were not necessary. As such, our new class of directional quantum master equations do not have the form of a standard cascaded quantum master equation.

Nonreciprocal quantum interactions are being actively studied for both their fundamental and practical implications. Our results thus greatly expand the toolbox and class of interactions available for such studies. In terms of application, we have shown how our interactions can be used for a new kind of dissipative quantum gate; the application to more complex kinds of quantum control (using e.g. the multi-dissipator version of our dynamics) could be extremely fruitful. We note that in a very different context, engineered dissipation has been studied theoretically [241, 245] and demonstrated experimentally [242–244] as means to realize autonomous quantum error correction (AQEC). Here, dissipative processes are designed to mitigate errors by bringing the system back to a desired code space. While our dissipative nonreciprocity and dissipative gates are very different in nature, it is worth asking whether these ideas could be combined with autonomous error correction for even more robust forms of quantum information processing. In [234], the general nonreciprocal structure in Eq. (6.16) is shown to enable a novel AQEC scheme against excitation loss, a dominant er-

ror source in bosonic systems. In concatenation with discrete variable QEC codes, it further offers a promising route towards practical fault-tolerant quantum computation (see [234] for detail). In another example, cases of nonreciprocal dissipators Eq. (6.16) are also considered for achieving passively-protected quantum memory [267]. Unlike our work, Ref. [267] did not note the general underlying nonreciprocal structure in Eq. (6.16), nor provide any route to physically realizing the required dissipators. An important open question is under what circumstances such nonreciprocal dissipators would provide a practical advantage in applications; we leave a systematic study to future works.

Our work also has great potential for fundamental studies. For example, it provides a direct way of designing quantum analogues of classical kinetically constrained models that feature directionality (see e.g. [268]). Such models could provide a new setting to study glassy dynamics in the quantum regime. It would also be interesting to study our new kind of dissipative interactions in many-body lattice models. Here, our mechanism could be used to construct a class of directional models that are dissipative analogues of closed systems with dynamical gauge fields. The latter is a topic of intense interest in a variety of engineered quantum systems (see e.g. Refs. [269–272]).

6.8 Appendices

6.8.1 Examples of Hamiltonians dynamics that are fully reciprocal according to Eq. (6.10)

In Section 6.3 in the main text, we introduce a new metric of isolation to quantify the influence of one subsystem on the dynamics of another subsystem, which leads to a general definition of reciprocity and nonreciprocity in the quantum regime. It is interesting to ask what the isolation looks like, and how nonreciprocal it is, if one considers fully coherent (i.e. Hamiltonian) dynamics. In this Appendix, we provide two general classes of Hamiltonian

dynamics, which can be proven to be reciprocal as per Eq. (6.10). It is also intriguing to ask if fully Hamiltonian dynamics of generic systems should always be reciprocal by the definition in Eq. (6.10). While we conjecture that it should be case, in order for the definition of (non)reciprocity in Section 6.3 to align with the (breaking of) Onsager reciprocity relations, we leave a thorough study to future works.

Isolation function of reciprocal dynamics generated by Hamiltonians with local qubit (B) $\mathbb{Z}_2$ symmetry

While our proof can be straightforwardly generalized to Hamiltonian dynamics of generic bipartite systems with N_A (N_B)-dimensional subsystem A (B), as long as the total AB Hamiltonian has a local symmetry that is N_B-dimensional and nondegenerate within B subspace, for the sake of clarity, here we focus on bipartite systems AB where B is a single qubit. In this subsection, we explicitly derive the isolation functions for dynamics generated purely by Hamiltonians with a local qubit $\mathbb{Z}_2$ symmetry, and show that any such dynamics must be fully reciprocal by the definition in Eq. (6.10). We stress that such Hamiltonians, albeit having a constrained form, can be generally nonlinear and interacting.

Consider a generic bipartite system consisting of an N_A-dimensional system as A and a qubit as B. We assume the system evolves under a Hamiltonian $\hat{H}_{AB}$, where interaction between A and B commutes with the qubit-only Hamiltonian $\hat{H}_{B,0} \equiv \mathrm{Tr}_A \hat{H}_{AB}$. We can thus define, without loss of generality, the eigenstates of $\hat{H}_{B,0}$ as qubit $\hat{\sigma}_z$ eigenbasis, and rewrite the system Hamiltonian as follows

$$\hat{H}_{AB} = \hat{H}_A \otimes \hat{\mathbb{I}}_B + \hat{\xi}_A \otimes \hat{\sigma}_z. \tag{6.44}$$

For notation simplicity, it is convenient to rewrite the total Hamiltonian in terms of projectors

onto qubit $\hat{\sigma}_z$ eigenstates, as

$$\hat{H}_{AB} = \hat{H}^{(A)}_{\uparrow} \otimes |\uparrow\rangle\langle\uparrow| + \hat{H}^{(A)}_{\downarrow} \otimes |\downarrow\rangle\langle\downarrow|\,, \tag{6.45}$$

where the conditional A Hamiltonians contingent on qubit states $|\sigma\rangle$ ($\sigma = \uparrow, \downarrow$) are given by $\hat{H}^{(A)}_{\uparrow/\downarrow} = \hat{H}_A \pm \hat{\xi}_A$.

Following Eq. (6.5) in the main text, we can again define evolution superoperator of A, depending on initial qubit (B) state $|\phi_{\rm i}\rangle$, as

$$\mathcal{E}^{(A)}_{|\phi_{\rm i}\rangle}(t)\hat{\rho}_A \equiv \mathrm{Tr}_B \left[e^{-i\hat{H}_{AB}t} (\hat{\rho}_A \otimes |\phi_{\rm i}\rangle_B\langle\phi_{\rm i}|) e^{i\hat{H}_{AB}t} \right]. \tag{6.46}$$

Substituting Eq. (6.45) into above equation, the conditional A quantum map can be straightforwardly calculated as

$$\mathcal{E}^{(A)}_{|\phi_{\rm i}\rangle}(t)\hat{\rho}_A = \sum_{\sigma=\uparrow,\downarrow} |\langle\sigma|\phi_{\rm i}\rangle|^2 \, e^{-i\hat{H}^{(A)}_{\sigma}t} \hat{\rho}_A e^{i\hat{H}^{(A)}_{\sigma}t}. \tag{6.47}$$

Since the A evolution in this case can be rewritten as a probabilistic mixture of unitary gates, the A isolation can be shown to have a closed analytical form. For convenience, we first introduce the unitary operator $\hat{U}^{(A)}_{\downarrow\uparrow}(t)$ acting on A that describes the "overlap" between the two conditional unitary maps as

$$\hat{U}^{(A)}_{\downarrow\uparrow}(t) = e^{i\hat{H}^{(A)}_{\downarrow}t} e^{-i\hat{H}^{(A)}_{\uparrow}t}, \tag{6.48}$$

and define its eigenvalues as $e^{i\phi_\ell}$ ($\ell = 1, 2, \ldots, N_A$). One can thus show that

$$I^{(A)}(t) = 1 - \max_{1\le\ell<m\le N_A} \left| \sin\frac{(\phi_\ell - \phi_m)}{2} \right|. \tag{6.49}$$

Conversely, we can also compute the qubit (B) isolation exactly, since the qubit undergoes

a constrained form of dynamics that conserves the $\hat{\sigma}_z$ operator (c.f. the system Hamiltonian in Eq. (6.44)). In this case, the qubit experiences simple phase shift and/or dephasing during the time evolution. More specifically, given initial qubit state $\hat{\rho}_B$ and expanding it using $\hat{\sigma}_z$ basis, the qubit populations stay constant throughout the evolution. The qubit coherence due to Eq. (6.45) can be computed as

$$\frac{\langle\uparrow|\,\mathcal{E}^{(B)}_{|\phi_{\rm i}\rangle}(t)\hat{\rho}_B|\downarrow\rangle}{\langle\uparrow|\,\hat{\rho}_B|\downarrow\rangle} = \mathrm{Tr}\left(e^{-i\hat{H}^{(A)}_{\uparrow}t}\,|\phi_{\rm i}\rangle_A\langle\phi_{\rm i}|\,e^{i\hat{H}^{(A)}_{\downarrow}t}\right) \tag{6.50}$$

$$= \mathrm{Tr}\left(\hat{U}^{(A)}_{\downarrow\uparrow}(t)\,|\phi_{\rm i}\rangle_A\langle\phi_{\rm i}|\right), \tag{6.51}$$

where $\hat{U}^{(A)}_{\downarrow\uparrow}$ is again the overlap unitary in Eq. (6.48). Because the qubit map now takes a pure-dephasing form, the diamond norm between two such qubit maps can be explicitly derived as

$$\begin{aligned}||\mathcal{E}^{(B)}_{|\phi_1\rangle}(t) - \mathcal{E}^{(B)}_{|\phi_2\rangle}(t)||_\diamond &= \left|\mathrm{Tr}\left[\hat{U}^{(A)}_{\downarrow\uparrow}(t)(|\phi_1\rangle\langle\phi_1| - |\phi_2\rangle\langle\phi_2|)\right]\right| \\ &= \left|\langle\phi_1|\,\hat{U}^{(A)}_{\downarrow\uparrow}(t)\,|\phi_1\rangle - \langle\phi_2|\,\hat{U}^{(A)}_{\downarrow\uparrow}(t)\,|\phi_2\rangle\right|. \end{aligned} \tag{6.52}$$

Expanding the states $|\phi_1\rangle, |\phi_2\rangle$ in Eq. (6.52) using eigenbasis of $\hat{U}^{(A)}_{\downarrow\uparrow}$, and optimizing over all A initial states, one can compute the B isolation function $I^{(B)}(t)$ as follows

$$\begin{aligned} I^{(B)}(t) \equiv& 1 - \frac{1}{2}\max_{|\phi_1\rangle,|\phi_2\rangle\in\mathcal{H}_A}||\mathcal{E}^{(B)}_{|\phi_1\rangle}(t) - \mathcal{E}^{(B)}_{|\phi_2\rangle}(t)||_\diamond \\ =& 1 - \frac{1}{2}\max_{|\phi_1\rangle,|\phi_2\rangle\in\mathcal{H}_A}\left|\langle\phi_1|\,\hat{U}^{(A)}_{\downarrow\uparrow}(t)\,|\phi_1\rangle - \langle\phi_2|\,\hat{U}^{(A)}_{\downarrow\uparrow}(t)\,|\phi_2\rangle\right| \\ =& 1 - \max_{1\le\ell<m\le N_A}\left|\sin\frac{(\phi_\ell - \phi_m)}{2}\right|. \end{aligned} \tag{6.53}$$

Comparing above expression to Eq. (6.49), we thus have

$$I^{(A)}(t) = I^{(B)}(t). \tag{6.54}$$

Proof of reciprocity for arbitrary Hamiltonian dynamics of two-qubit systems

In this subsection, we restrict to bipartite systems where both A and B are single qubits, and we seek to prove that arbitrary Hamiltonian dynamics of this two-qubit system is reciprocal as per Eq. (6.10). To start, we note that the isolation function of A (B) is invariant under applications of local unitaries at the input and/or output ports of the quantum channel. More specifically, we consider two generic quantum maps $\mathcal{E}^{(AB)}$ and $\mathcal{F}^{(AB)}$ that are related by the following equation

$$\mathcal{E}^{(AB)}\hat{\rho}_{AB} = (\hat{W}_A \otimes \hat{W}_B)\left(\mathcal{F}^{(AB)}\hat{\rho}'_{AB}\right)(\hat{W}_A^\dagger \otimes \hat{W}_B^\dagger), \tag{6.55}$$

$$\hat{\rho}'_{AB} = \hat{V}_A \otimes \hat{V}_B \hat{\rho}_{AB} \hat{V}_A^\dagger \otimes \hat{V}_B^\dagger. \tag{6.56}$$

Making use of the fact that the diamond norm (c.f. Eq. (6.6)) is invariant under unitary transformations applied before or after the quantum channels [235], one can straightforwardly show that the corresponding isolation functions $I^{(A/B)}(\mathcal{E}^{(AB)})$ and $I^{(A/B)}(\mathcal{F}^{(AB)})$ are also equal for two maps, i.e.

$$I^{(A/B)}(\mathcal{E}^{(AB)}) = I^{(A/B)}(\mathcal{F}^{(AB)}). \tag{6.57}$$

The isolation functions in above equation are defined similarly to Eq. (6.7) for the two channels, and we omit any time variables (if applicable) for notation simplicity.

We next observe that, as pointed out in the main text, dynamics generated by any Hamiltonian symmetric under permutation of A and B is automatically reciprocal by our definition. For 2-qubit systems, and assuming no local Hamiltonians, we conclude that dynamics generated by so-called Heisenberg XYZ interactions should be reciprocal. Rewriting

the corresponding unitary evolution superoperator as

$$\mathcal{U}_{XYZ}^{(AB)}\hat{\rho}_{AB} = \hat{U}_{XYZ}\hat{\rho}_{AB}\hat{U}_{XYZ}^{\dagger}, \tag{6.58}$$

$$\hat{U}_{XYZ} = \exp\left[-i\left(\sum_{\alpha=x,y,z} J_{\alpha}\hat{\sigma}_{A,\alpha}\hat{\sigma}_{B,\alpha}\right)\right], \tag{6.59}$$

we thus have

$$I^{(A)}(\mathcal{U}_{XYZ}^{(AB)}) = I^{(B)}(\mathcal{U}_{XYZ}^{(AB)}). \tag{6.60}$$

Finally, we make use of the standard decomposition of any 2-qubit rotations into local unitaries and a Heisenberg unitary [273], which can be viewed as a special case of the KAK decomposition of Lie groups. For a generic 2-qubit unitary operator $\hat{U}_{AB}$, the decomposition states that there exist two local unitary unitaries $\hat{U}_{A,\ell} \otimes \hat{U}_{B,\ell}$ ($\ell = 1, 2$), such that the following equality holds

$$\hat{U}_{AB} = (\hat{U}_{A,1} \otimes \hat{U}_{B,1})\hat{U}_{\mathrm{H}}(\hat{U}_{A,2} \otimes \hat{U}_{B,2}), \tag{6.61}$$

$$\hat{U}_{\mathrm{H}} = \exp\left[-i\left(\sum_{\alpha=x,y,z} h_{\alpha}\hat{\sigma}_{A,\alpha}\hat{\sigma}_{B,\alpha}\right)\right]. \tag{6.62}$$

Comparing above equation with Eq. (6.55), we see that the unitary map generated by $\hat{U}_{AB}$ has the same isolation functions as that generated by $\hat{U}_{\mathrm{H}}$. From Eq. (6.60), we can further prove that for any 2-qubit unitary evolution $\mathcal{U}_2^{(AB)}\hat{\rho}_{AB} = \hat{U}_{AB}\hat{\rho}_{AB}\hat{U}_{AB}^{\dagger}$, we have

$$I^{(A)}(\mathcal{U}_2^{(AB)}) = I^{(B)}(\mathcal{U}_2^{(AB)}), \tag{6.63}$$

so that any 2-qubit Hamiltonian dynamics must be reciprocal.

6.8.2 The emergence of gauge symmetry in a single-dissipator Markovian Lindblad master equation

As discussed in the main text, the unidirectional nature of dynamics generated by the nonlinear dissipator $\mathcal{D}[\hat{A}\hat{U}_B]\hat{\rho}$ (see Eq. (6.16) in the main text) crucially depends on a fundamental gauge symmetry, which is inherent to Lindblad-form QMEs that describe Markovian environments. In this section, we illustrate this connection using a microscopic model for the quantum dissipation.

Let us consider a generic, single Lindblad dissipator of system A, given by

$$\mathcal{L}_{A,1}\hat{\rho} = \Gamma\mathcal{D}[\hat{A}]\hat{\rho}. \tag{6.64}$$

Without loss of generality, we could model the dissipation as due to a bosonic microscopic environment consisting of harmonic oscillator modes b_ℓ, so that the system-bath Hamiltonian can be written as

$$\hat{H}_{\rm tot} = \hat{H}_{\rm E} + \hat{H}_{\rm SE}, \quad \hat{H}_{\rm E} = \sum_\ell \omega_\ell \hat{b}_\ell^\dagger \hat{b}_\ell, \tag{6.65}$$

$$\hat{H}_{\rm SE} = \hat{A}\hat{\xi}^\dagger + {\rm H.c.}, \quad \hat{\xi} = \sum_\ell g_\ell^* \hat{b}_\ell. \tag{6.66}$$

The density of states (DOS) function $\mathcal{J}_0[\omega]$ of this bosonic environment can be explicitly computed in terms of the interaction picture bath operator $\hat{\xi}(t) = e^{i\hat{H}_{\rm E}t}\hat{\xi}e^{-i\hat{H}_{\rm E}t}$, as

$$\mathcal{J}_0[\omega] \equiv \frac{1}{2\pi}\int_{-\infty}^{\infty} \langle[\hat{\xi}(t), \hat{\xi}^\dagger(0)]\rangle e^{i\omega t}dt \tag{6.67}$$

$$= \sum_\ell |g_\ell|^2 \delta(\omega - \omega_\ell). \tag{6.68}$$

In the Markovian limit, the environmental DOS $\mathcal{J}_0[\omega]$ reduces to a constant, i.e. we have

$$\mathcal{J}_0[\omega] \equiv \Gamma \Leftrightarrow \langle[\hat{\xi}(t_1), \hat{\xi}^\dagger(t_2)]\rangle = \Gamma\delta(t_1 - t_2). \tag{6.69}$$

In this limit, we can integrate out the bath dynamics to obtain a standard Lindblad equation, as given by Eq. (6.64).

We now perform a standard gauge transformation that shifts the jump operator phase by a time-dependent real value $\theta(t)$, i.e. $\hat{A} \to \hat{A}' = \hat{A}e^{i\theta(t)}$, so that the new interaction picture system-bath interaction becomes

$$\hat{H}'_{\text{SE}}(t) = \sum_\ell \left(g_\ell \hat{A}\hat{b}_\ell^\dagger e^{i\omega_\ell t + i\theta(t)} + \text{H.c.}\right). \tag{6.70}$$

Mathematically, the gauge symmetry of the Lindblad dissipator can be understood from the fact that the microscopic bath DOS $\mathcal{J}'[\omega]$ stays invariant under the gauge transformation. More specifically, we can show rigorously

$$\mathcal{J}'[\omega] = \frac{1}{2\pi}\int_{-\infty}^{\infty}\sum_\ell |g_\ell|^2 e^{i\omega t - i\omega_\ell t}e^{-i\theta(t)+i\theta(0)}dt \tag{6.71}$$

$$= \Gamma\int_{-\infty}^{\infty}\delta(t)e^{-i\theta(t)+i\theta(0)}dt = \Gamma. \tag{6.72}$$

This derivation formally shows that the microscopic origin of the time-local gauge symmetry of the Lindbladian in Eq. (6.64) is due to a completely flat bath DOS function, i.e. due to a Markovian environment.

As mentioned, above derivation requires the bath is perfectly Markovian, so that the bath correlation function $\langle[\hat{\xi}(t), \hat{\xi}^\dagger(0)]\rangle$ is proportional to a delta function. We now discuss an intuitive way to understand the role of Markovianity in the emergence of the time-local gauge symmetry. Noting the gauge phase $e^{i\theta(t)}$ enters the interaction picture Hamiltonian in exactly the same manner as dynamical phases of the environmental modes $e^{i\omega_\ell t}$, we could

formally absorb time dependence of the gauge phase into the definition of environmental chemical potential, by going to the following rotating frame defined with respect to $\hat{H}_{\rm rot}$, as

$$\hat{H}'_{\rm E} \to \hat{H}''_{\rm E} = \hat{H}_{\rm E} - \hat{H}_{\rm rot}, \tag{6.73}$$

$$\hat{b}'_\ell \to \hat{b}''_\ell = e^{i\hat{H}_{\rm rot}t}\hat{b}_\ell e^{-i\hat{H}_{\rm rot}t} = \hat{b}_\ell e^{i\theta(t)}, \tag{6.74}$$

where we have

$$\hat{H}_{\rm rot} = -\dot{\theta}\,(t)\sum_\ell \hat{b}^\dagger_\ell \hat{b}_\ell. \tag{6.75}$$

We remark that the system-bath interaction in the rotating frame takes the same form as the original interaction Hamiltonian in Eq. (6.66), i.e. we have

$$\hat{H}''_{\rm E} = \sum_\ell \Big[\omega_\ell + \dot{\theta}\,(t)\Big]\,\hat{b}^\dagger_\ell \hat{b}_\ell, \tag{6.76}$$

$$\hat{H}''_{\rm SE} = \sum_\ell \Big(g_\ell \hat{A}\hat{b}^\dagger_\ell + {\rm H.c.}\Big)\,. \tag{6.77}$$

Noting that the bath Hamiltonian now varies in time, we can formally *define* a time-dependent bath DOS function $\mathcal{J}\,[\omega;t]$, as

$$\mathcal{J}\,[\omega;t] \equiv \sum_\ell |g_\ell|^2\,\delta\left(\omega - \omega_\ell - \dot{\theta}\,(t)\right), \tag{6.78}$$

which can be related to the original bath DOS function $\mathcal{J}_0[\omega]$ in Eq. (6.68) as

$$\mathcal{J}\,[\omega;t] = \mathcal{J}_0[\omega - \dot{\theta}\,(t)]. \tag{6.79}$$

In the Markovian limit we thus have $\mathcal{J}\,[\omega;t] \equiv \mathcal{J}_0[\omega] = \Gamma$, so that the bath DOS is invariant under generic gauge transformations. For a realistic environment, the bath bandwidth should

be finite and hence cannot be perfectly Markovian. In this case, above analysis would be valid as long as the bath correlation time τ_{E} is much smaller than timescale associated with dynamics of the gauge phase, i.e. $\tau_{\mathrm{E}}\dot{\theta}\left(t\right) \ll 1$.

6.8.3 Leading-order non-Markovian corrections to fully nonreciprocal master equations due to broken gauge symmetry

Single-dissipator case

The discussion in the preceding section relates an intrinsic gauge symmetry of any Lindbladian dissipative dynamics to the Markovian nature of the corresponding bath. In this subsection, we focus on Lindbladians with a single dissipator, and examine how the gauge symmetry can be broken if the bath deviates from the Markovian limit. We again start with the interaction picture system-bath Hamiltonian, where the system-bath coupling is modulated in time by a phase factor (which formally acts as a gauge transformation on the jump operator). The Hamiltonian is given by Eq. (6.70), as

$$\hat{H}'_{\mathrm{SE}}\left(t\right) = \hat{A}\hat{\xi}^{\dagger}e^{i\theta(t)} + \mathrm{H.c.} \tag{6.80}$$

$$= \sum_{\ell}\left(g_{\ell}\hat{A}\hat{b}_{\ell}^{\dagger}e^{i\omega_{\ell}t+i\theta(t)} + \mathrm{H.c.}\right). \tag{6.81}$$

Assuming the bosonic bath is in the vacuum state, we can derive a Markovian evolution equation for the system density matrix as

$$\frac{d}{dt}\hat{\rho}\left(t\right) = -i[\Sigma\left(t\right)\hat{A}^{\dagger}\hat{A}, \hat{\rho}\left(t\right)] + \Gamma_{\mathrm{BR}}\left(t\right)\mathcal{D}[\hat{A}]\hat{\rho}\left(t\right). \tag{6.82}$$

Note that above equation is an example of the so-called Bloch-Redfield equation, which generalizes standard Lindblad master equation by incorporating effects due to a finite bath correlation time. The Bloch-Redfield equation still assumes the bath is Gaussian, but allows

the bath to be non-Markovian. The first term on the RHS of Eq. (6.82) is analogous to the Lamb shift, and describes a correction to the coherent system Hamiltonian due to coupling to the environment. The second term takes the same form as the standard Lindblad dissipator, but the dissipator strength can now be negative because we have included effects from a non-Markovian bath.

To compute the coefficients $\Sigma(t)$ and $\Gamma_{\mathrm{BR}}(t)$ in Eq. (6.82), it is useful to view Eq. (6.81) as coupling the system to a new, effective bath operator, whose phase is modified by the gauge phase $e^{i\theta(t)}$. We refer to this new bath as the "gauge transformed bath" in the following discussions. We can thus introduce the 2-point correlation function $\mathcal{E}_\theta(t_1, t_2)$ of the new bath operator, which is given by

$$\mathcal{E}_\theta(t_1, t_2) \equiv \langle \hat{\xi}(t_1)\, \hat{\xi}^\dagger(t_2) \rangle e^{-i\theta(t_1)+i\theta(t_2)} \tag{6.83}$$

$$= \sum_\ell |g_\ell|^2 e^{-i\omega_\ell(t_1-t_2)-i\theta(t_1)+i\theta(t_2)}. \tag{6.84}$$

It is important to note that while the original bath is stationary, the new bath set by the gauge phase is generally nonstationary, except for the trivial case where the gauge phase $\theta(t)$ is only a linear function of time. This means that the correlation function $\mathcal{E}_\theta(t_1, t_2)$ in Eq. (6.84) would depend on both the time difference $t_1 - t_2$ and the "center of times" $(t_1 + t_2)/2$, unless we have $\theta(t) = \theta(0) + t\dot{\theta}(0)$. The Lamb shift coefficient $\Sigma(t)$ can now be related to the bath correlation function as

$$\Sigma(t) = \mathrm{Im} \int_0^t dt_1 \langle \hat{\xi}(t)\, \hat{\xi}^\dagger(t_1) \rangle e^{-i\theta(t)+i\theta(t_1)} \tag{6.85}$$

$$= \mathrm{Im} \int_0^t dt_1 \mathcal{E}_\theta(t, t_1), \tag{6.86}$$

and the dissipator strength $\Gamma_{\mathrm{BR}}(t)$ is in turn given by

$$\Gamma_{\mathrm{BR}}(t) = 2\mathrm{Re}\int_0^t dt_1 \mathcal{E}_\theta(t,t_1)\,. \tag{6.87}$$

If the original bath has a finite but short correlation time τ_{E} (the definition of short will become clear in discussion that follows), we can compute the leading order non-Markovian correction in the master equation, which depends on $\dot{\theta}(t)$. We first rewrite the correlation function of the gauge transformed bath in terms of the autocorrelation function of the old bath $\mathcal{E}(t_1,t_2)$ (setting $\theta(t)\equiv 0$ in Eq. (6.84)) as

$$\mathcal{E}_\theta(t_1,t_2) = \mathcal{E}(t_1,t_2)\, e^{-i\theta(t_1)+i\theta(t_2)}. \tag{6.88}$$

Without loss of generality, we assume the bath has a finite correlation time τ_{E}, so that the stationary bath autocorrelation function can be written as

$$\mathcal{E}(t_1,t_2) = \mathcal{E}_\theta(t_1,t_2)|_{\theta(t)\equiv 0} = g_{\mathrm{eff}}^2 e^{-|t_1-t_2|/\tau_{\mathrm{E}}}, \tag{6.89}$$

where $g_{\mathrm{eff}} = \sqrt{\mathcal{E}(0,0)}$ is a real coupling coefficient that characterizes the system-bath coupling strength. If the gauge phase changes much slower than the bath correlation time, i.e. we have

$$\tau_{\mathrm{E}}^2\ddot{\theta}(t) \ll \tau_{\mathrm{E}}\dot{\theta}(t) \ll 1, \quad \forall t, \tag{6.90}$$

and if we are interested in system dynamics over timescales that are much longer than the bath correlation time ($t \gg \tau_{\mathrm{E}}$), then we can approximate the integral entering Eqs. (6.86)

and (6.87) as

$$\begin{aligned}
&\int_0^t dt_1 \mathcal{E}_\theta\left(t,t_1\right)\\
=&g_{\text{eff}}^2\int_0^t e^{-(t-t_1)/\tau_{\text{E}}}e^{-i\theta(t)+i\theta(t_1)}dt_1 &(6.91)\\
\simeq&g_{\text{eff}}^2\int_{-\infty}^t e^{-(t-t_1)/\tau_{\text{E}}}e^{-i\dot{\theta}(t)(t-t_1)+\frac{i}{2}\ddot{\theta}(t)(t-t_1)^2}dt_1 &(6.92)\\
\simeq&g_{\text{eff}}^2\tau_{\text{E}}[1-i\tau_{\text{E}}\dot{\theta}\left(t\right)+i\tau_{\text{E}}^2\ddot{\theta}\left(t\right)-\tau_{\text{E}}^2\dot{\theta}\left(t\right)^2]. &(6.93)
\end{aligned}$$

Thus, we obtain first two leading-order contributions to the Lamb shift, and to the time-dependent decay rate, in terms of the small parameter $\tau_{\text{E}}\dot{\theta}\left(t\right)$ as

$$\begin{aligned}
\Sigma\left(t\right)&\simeq-g_{\text{eff}}^2\tau_{\text{E}}^2[\dot{\theta}\left(t\right)-\tau_{\text{E}}\ddot{\theta}\left(t\right)], &(6.94)\\
\Gamma_{\text{BR}}\left(t\right)&\simeq 2g_{\text{eff}}^2\tau_{\text{E}}\left(1-[\tau_{\text{E}}\dot{\theta}\left(t\right)]^2\right). &(6.95)
\end{aligned}$$

We can thus rewrite Eq. (6.82) as

$$\begin{aligned}
\frac{d}{dt}\hat{\rho}\left(t\right)\simeq&ig_{\text{eff}}^2\tau_{\text{E}}^2[\dot{\theta}\left(t\right)-\tau_{\text{E}}\ddot{\theta}\left(t\right)][\hat{A}^\dagger\hat{A},\hat{\rho}\left(t\right)]\\
&+2g_{\text{eff}}^2\tau_{\text{E}}\left(1-[\tau_{\text{E}}\dot{\theta}\left(t\right)]^2\right)\mathcal{D}[\hat{A}]\hat{\rho}\left(t\right). &(6.96)
\end{aligned}$$

It is also convenient to rewrite above equation in terms of original bath DOS $\mathcal{J}_0$ given in Eq. (6.68). The latter can now be calculated as

$$\begin{aligned}
\mathcal{J}_0\left[\omega\right]&\equiv\frac{1}{2\pi}\int_{-\infty}^{\infty}\langle[\hat{B}\left(t\right),\hat{B}^\dagger\left(0\right)]\rangle e^{i\omega t}dt &(6.97)\\
&=\frac{1}{2\pi}\int_{-\infty}^{\infty}\mathcal{E}\left(t,0\right)e^{i\omega t}=\frac{1}{\pi}g_{\text{eff}}^2\tau_{\text{E}}, &(6.98)
\end{aligned}$$

so that we have

$$\partial_t \hat{\rho}\,(t) \simeq i\pi \mathcal{J}_0\,[0]\,\tau_{\rm E}[\dot{\theta}\,(t) - \tau_{\rm E}\ddot{\theta}\,(t)][\hat{A}^\dagger \hat{A}, \hat{\rho}\,(t)] + 2\pi \mathcal{J}_0\,[0]\left(1 - [\tau_{\rm E}\dot{\theta}\,(t)]^2\right)\mathcal{D}[\hat{A}]\hat{\rho}\,(t)\,. \tag{6.99}$$

Generalization to the multi-dissipator case

The discussion in the previous subsection can be straightforwardly generalized to Lindbladian with multiple dissipators. In the main text, we stated that the invariance of a generic Lindbladian under time-dependent unitary transformations $\check{\mathcal{U}}\,(t)$ [261] on the jump operators is closely related to the Markovian nature of the bath. Here, we illustrate this connection by similarly deriving leading-order non-Markovian corrections to general Lindbladians with multiple dissipators. For concreteness, here we consider a general class of microscopic environments that can realize such dissipators in the Markovian limit, but our approach straightforwardly applies to generic environments.

We start by rewriting a general Lindbladian as (see Eq. (6.35))

$$\mathcal{L}_A \hat{\rho}_A = \Gamma \sum_{\ell=1}^{N} \mathcal{D}\left[\sum_{m=1}^{N} u_{\ell m}(t)\hat{A}_m\right]\hat{\rho}_A, \tag{6.100}$$

where $u_{\ell m}(t)$ are again matrix elements of the N-dimensional complex unitary matrix $\check{\mathcal{U}}(t)$. For the purpose of discussion, we consider a microscopic environment realizing such dissipative dynamics, by coupling the system to a harmonic oscillator bath with independent bath operators $\hat{\xi}_\ell$. In the interaction picture with respect to bath-only Hamiltonian $\hat{H}_{\rm E}$, the system-bath Hamiltonian is given by

$$\hat{H}_{\rm SE}\,(t) = \sum_{\ell,m=1}^{N} u_{\ell m}\,(t)\,\hat{A}_m \hat{\xi}_\ell^\dagger\,(t) + \text{H.c.}, \tag{6.101}$$

where the bath operators satisfy white-noise statistics

$$\langle \hat{\xi}_{\ell}^{(0)\dagger}(t_1)\,\hat{\xi}_{\ell'}^{(0)}(t_2)\rangle = 0, \tag{6.102}$$

$$\langle \hat{\xi}_{\ell}^{(0)}(t_1)\,\hat{\xi}_{\ell'}^{(0)\dagger}(t_2)\rangle = \Gamma\delta_{\ell\ell'}\delta(t_1 - t_2)\,. \tag{6.103}$$

In the Markovian limit, the resulting system (A modes) dynamics will be invariant under any unitary matrix $\check{\mathcal{U}}(t)$. To understand the role of Markovianity in the emergence of this time-local generalized gauge symmetry, we again assume that the bath modes have finite but very small correlation times, and we now derive the correction to A system dynamics due to non-Markovian effects. Towards this goal, it is useful to rewrite the system-bath coupling using a new set of bath operators $\hat{C}_{\ell}$, as

$$\hat{H}_{\rm SE}(t) = \sum_{\ell=1}^{N} \hat{A}_{\ell}\hat{C}_{\ell}^{\dagger}(t) + \text{H.c.}, \quad \hat{C}_{\ell}(t) = \sum_{m=1}^{N} u_{m\ell}^{*}(t)\,\hat{\xi}_{m}(t)\,. \tag{6.104}$$

In contrast to the original stationary bath operators $\hat{\xi}_{m}(t)$, similar to the single-dissipator case, the new bath operators $\hat{C}_{m}(t)$ is in general nonstationary due to the presence of the time-dependent coefficients $u_{m\ell}(t)$. As we show, such nonstationarity will in general give rise to nontrivial non-Markovian effects in A dynamics.

Making use of the standard Born-Markov approximation, we can integrate out the bath modes to obtain an effective master equation for system A

$$\begin{aligned}\frac{d\hat{\rho}(t)}{dt} =& -i\sum_{\ell,m=1}^{N}\Sigma_{\ell m}(t)\left[\hat{A}_{\ell}^{\dagger}\hat{A}_{m},\hat{\rho}(t)\right] \\ &+\sum_{\ell,m=1}^{N}\Gamma_{\ell m}(t)\left(\hat{A}_{m}\hat{\rho}(t)\,\hat{A}_{\ell}^{\dagger} - \frac{1}{2}\{\hat{A}_{\ell}^{\dagger}\hat{A}_{m},\hat{\rho}(t)\}\right).\end{aligned} \tag{6.105}$$

The effective Hamiltonian, also known as the Lamb shift term, and the dissipator coefficient

matrices are given by

$$\Sigma(t) = -\frac{i}{2}\left[\mathcal{S}(t) - \mathcal{S}^{\dagger}(t)\right], \tag{6.106}$$

$$\Gamma(t) = \mathcal{S}(t) + \mathcal{S}^{\dagger}(t), \tag{6.107}$$

$$\mathcal{S}_{\ell m}(t) = \int_0^t dt_1 \langle \hat{C}_{\ell}(t)\, \hat{C}_m^{\dagger}(t_1)\rangle. \tag{6.108}$$

While our discussion is applicable to generic forms of bath correlators in the small correlation time limit, for concreteness we assume that they take the diagonal form as follows

$$\langle \hat{\xi}_{\ell}^{(0)\dagger}(t_1)\, \hat{\xi}_{\ell'}^{(0)}(t_2)\rangle = 0, \tag{6.109}$$

$$\langle \hat{\xi}_{\ell}^{(0)}(t_1)\, \hat{\xi}_{\ell'}^{(0)\dagger}(t_2)\rangle = \Gamma\delta_{\ell\ell'}\frac{1}{2\tau_{\mathrm{E},\ell}} e^{-|t_1-t_2|/\tau_{\mathrm{E},\ell}}. \tag{6.110}$$

We can thus compute the master equation coefficients via the bath kernel function $\mathcal{S}_{\ell m}(t)$. For convenience, we introduce the time-dependent generator of $\check{\mathcal{U}}(t)$ as

$$\check{\mathcal{G}}(t) = -i\frac{d\check{\mathcal{U}}(t)}{dt}\check{\mathcal{U}}^{\dagger}(t). \tag{6.111}$$

Assuming small bath correlation time $\Gamma\tau_{\mathrm{E},\ell} \ll 1$, we can perturbatively compute the leading order corrections to $\mathcal{S}_{\ell m}(t)$, as

$$\mathcal{S}_{\ell m}(t) = \sum_{j,j'=1}^{N} u_{j\ell}^{*}(t) \int_0^t dt_1 \langle \hat{\xi}_j(t)\, \hat{\xi}_{j'}^{\dagger}(t_1)\rangle u_{j'm}(t_1) \tag{6.112}$$

$$\simeq \frac{1}{2}\sum_{j,j'=1}^{N} u_{j\ell}^{*}(t)\, u_{j'm}(t)\left[1 + i\tau_{\mathrm{E},j} g_{jj'}(t) - i\tau_{\mathrm{E},j}^2 \dot{g}_{jj'}(t) - \tau_{\mathrm{E},j}^2 g_{ja}(t)\, g_{aj'}(t)\right]. \tag{6.113}$$

The corresponding master equation Eq. (6.105) can now be conveniently rewritten in

terms of a new jump operator basis

$$\hat{z}_{\ell}\left(t\right)=\sum_{m=1}^{N}u_{\ell m}\left(t\right)\hat{A}_{m}, \tag{6.114}$$

so that we can write the effective master equation as

$$\begin{aligned}\mathcal{L}\hat{\rho}\left(t\right)\simeq&-i\sum_{\ell,m=1}^{N}\tilde{\Sigma}_{\ell m}\left(t\right)\left[\hat{z}_{\ell}^{\dagger}\left(t\right)\hat{z}_{m}\left(t\right),\hat{\rho}\left(t\right)\right]\\&+\sum_{\ell,m=1}^{N}\tilde{\Gamma}_{\ell m}\left(t\right)\left(\hat{z}_{m}\left(t\right)\hat{\rho}\left(t\right)\hat{z}_{\ell}^{\dagger}\left(t\right)-\frac{1}{2}\{\hat{z}_{\ell}^{\dagger}\left(t\right)\hat{z}_{m}\left(t\right),\hat{\rho}\left(t\right)\}\right).\end{aligned} \tag{6.115}$$

The Lamb shift term and dissipator coefficients in the new basis can thus be derived as follows

$$\begin{aligned}\tilde{\Sigma}_{\ell m}\left(t\right)=&\frac{1}{4}\left[\left(\tau_{\mathrm{E},\ell}+\tau_{\mathrm{E},m}\right)g_{\ell m}\left(t\right)-\left(\tau_{\mathrm{E},\ell}^{2}+\tau_{\mathrm{E},m}^{2}\right)\dot{g}_{\ell m}\left(t\right)\right.\\&\left.+i\left(\tau_{\mathrm{E},\ell}^{2}-\tau_{\mathrm{E},m}^{2}\right)g_{\ell a}\left(t\right)g_{am}\left(t\right)\right],\end{aligned} \tag{6.116}$$

$$\begin{aligned}\tilde{\Gamma}_{\ell m}\left(t\right)=&1+\frac{1}{2}\left[i\left(\tau_{\mathrm{E},\ell}-\tau_{\mathrm{E},m}\right)g_{\ell m}\left(t\right)\right.\\&-i\left(\tau_{\mathrm{E},\ell}^{2}-\tau_{\mathrm{E},m}^{2}\right)\dot{g}_{\ell m}\left(t\right)\\&\left.-\left(\tau_{\mathrm{E},\ell}^{2}+\tau_{\mathrm{E},m}^{2}\right)g_{\ell a}\left(t\right)g_{am}\left(t\right)\right].\end{aligned} \tag{6.117}$$

Before ending this subsection, we also discuss an intuitive way to understand the local-in-time gauge symmetry $\check{\mathcal{U}}(t)$ in the multi-dissipator case. Similar to the single-dissipator scenario, the addition of the unitary matrix elements $u_{\ell m}\left(t\right)$ in the Lindbladian $\mathcal{L}_{A}\hat{\rho}=\sum_{\ell=1}^{N}\mathcal{D}[\sum_{m=1}^{N}u_{\ell m}\left(t\right)\hat{A}_{m}]\hat{\rho}$ (see Eq. (6.100)) can be equivalently viewed as the result of shifting the Hamiltonian frequencies of a microscopic harmonic oscillator bath. Let us again consider a microscopic bath realizing the dissipators, with the system-bath Hamiltonian

given by

$$\hat{H}_{\text{tot}} = \hat{H}_{\text{E}} + \hat{H}_{\text{SE}}, \quad \hat{H}_{\text{E}} = \sum_{\alpha} \omega_{\alpha} \sum_{\ell=1}^{N} \hat{b}_{\ell,\alpha}^{\dagger} \hat{b}_{\ell,\alpha}, \tag{6.118}$$

$$\hat{H}_{\text{SE}}(t) = \sum_{\ell,m=1}^{N} u_{\ell m}(t) \hat{A}_m \hat{\xi}_{\ell}^{\dagger} + \text{H.c.}, \quad \hat{\xi}_{\ell} = \sum_{\alpha} g_{\alpha}^{*} \hat{b}_{\ell,\alpha}. \tag{6.119}$$

Note that we choose the bath mode frequencies ω_{α} and coupling strengths g_{α}^{*} to be identical for corresponding modes $\hat{b}_{\ell,\alpha}$ coupled to different system operators $\hat{A}_{\ell}$. This bath model is not necessarily physically motivated, but it allows a simple interpretation of the time-dependent coupling coefficients $u_{\ell m}(t)$. In fact, we can now transform to a new rotating frame

$$\hat{\rho}_{\text{SE}} \to \hat{\rho}'_{\text{SE}} = \hat{U}^{\dagger}(t) \hat{\rho}_{\text{SE}} \hat{U}(t), \quad \hat{U}(t) = \mathcal{T} e^{-i \int_0^t \delta \hat{H}_{\text{E}}(t_1) dt_1}, \tag{6.120}$$

so that the time dependence in system-bath couplings is converted into an additional term in the bath-only Hamiltonian, as

$$\hat{H}_{\text{SE}} \to \hat{H}'_{\text{SE}} = \hat{U}^{\dagger}(t) \hat{H}_{\text{SE}} \hat{U}(t) = \sum_{\ell=1}^{N} \hat{A}_{\ell} \hat{\xi}_{\ell}^{\dagger} + \text{H.c.} \tag{6.121}$$

$$\hat{H}_{\text{E}} \to \hat{H}'_{\text{E}}(t) = \hat{H}_{\text{E}} + \delta \hat{H}_{\text{E}}(t). \tag{6.122}$$

The correction term $\delta \hat{H}_{\text{E}}(t)$ takes the form of a beam splitter Hamiltonian, and can be written as

$$\delta \hat{H}_{\text{E}}(t) = \sum_{\alpha} \sum_{\ell,m=1}^{N} h_{\ell m}(t) \hat{b}_{\ell,\alpha}^{\dagger} \hat{b}_{m,\alpha}, \tag{6.123}$$

where the beam splitter matrix $h_{\ell m}(t) = \left[\check{\mathcal{H}}(t)\right]_{\ell m}$ is related to the unitary matrix $\check{\mathcal{U}}(t)$

via the following equation

$$\check{\mathcal{H}}(t) = i\frac{d\check{\mathcal{U}}^{\dagger}(t)}{dt}\check{\mathcal{U}}(t). \tag{6.124}$$

6.8.4 *Reservoir engineering implementation of nonreciprocal interactions in Eq.* (6.16) *via a unidirectional waveguide*

In Section 6.5.1 in the main text, we state that the nonreciprocal single-dissipator master equation in Eq. (6.16) can be straightforwardly realized via reservoir engineering, if one also has access to elements explicitly breaking TRS, e.g. an unidirectional waveguide. In this Appendix, we provide a detailed discussion about the physical setup in this case and its connection to related experiments [252, 253].

Recall the desired dissipator in Eq. (6.16), as given by $\mathcal{L}_{\text{dir}}\hat{\rho} = \Gamma\mathcal{D}[\hat{A}\hat{U}_B]\hat{\rho}$. For concreteness, in this Appendix we assume the A subsystem is a cavity mode with operator $\hat{A} = \hat{a}$ being a bosonic lowering operator, but we note that the scheme discussed below can be generalized to other systems as well. The corresponding Lindbladian is thus

$$\mathcal{L}_{\text{dir}}\hat{\rho} = \Gamma\mathcal{D}[\hat{a}\hat{U}_B]\hat{\rho}. \tag{6.125}$$

For purpose that will become clear later, it is convenient to rewrite the unitary in terms of a Hermitian generating operator $\hat{E}_B$, i.e.

$$\hat{U}_B = \exp\Big(-i\hat{E}_B\Big), \tag{6.126}$$

where eigenvalues of $\hat{E}_B$ are real and lie in the range $(-\pi, \pi]$. Noting that definition of unitary $\hat{U}_B$ has a global gauge phase degree of freedom, we can redefine it as $e^{-i\theta_0}\hat{U}_B$ with arbitrary phase θ_0 without affecting system dynamics; we will choose this phase such that -1 is not in the spectrum of $\hat{U}_B$, or equivalently, $\hat{E}_B$ does not contain the eigenvalue π.

We now introduce a fully directional coupling (e.g., mediated by a one-way waveguide) from A to an reservoir mode c, as well as a Hamiltonian interaction $\hat{H}_{BC}$ between B and the reservoir that shifts the c frequency. The total system-reservoir (SR) dynamics can thus be described by the following master equation

$$\begin{aligned}\frac{d\hat{\rho}_{\mathrm{SR}}}{dt} =& -i\left[\hat{H}_{AC}+\hat{H}_{BC},\hat{\rho}_{\mathrm{SR}}\right]\\ &+\mathcal{D}\left[\sqrt{\Gamma_a}\hat{a}-i\sqrt{\Gamma_c}\hat{c}\right]\hat{\rho}_{\mathrm{SR}}.\end{aligned} \tag{6.127}$$

Here, Γ_a, Γ_c denote the effective coupling rates between modes a, c and the directional waveguide, respectively. The coupling Hamiltonians $\hat{H}_{AC}$ and $\hat{H}_{BC}$ are now given by

$$\hat{H}_{AC} = \frac{1}{2}\sqrt{\Gamma_a\Gamma_c}\left(\hat{a}^\dagger\hat{c}+\hat{c}^\dagger\hat{a}\right), \tag{6.128}$$

$$\hat{H}_{BC} = \frac{1}{2}\lambda\hat{M}_B\hat{c}^\dagger\hat{c}, \tag{6.129}$$

where $\hat{M}_B$ is a dimensionless Hermitian operator on B that we will determine later. Note that if we ignore B and its coupling to the reservoir mode c, the remaining setup reduces to the standard cascaded quantum systems (see Eq. (6.1)). To realize the dissipator in Eq. (6.125), we take the limit where c serves as a Markovian reservoir for the AB system. More specifically, this requires $\Gamma_c \gg \Gamma_a$, in which case we can use standard adiabatic elimination techniques [76] to integrate out mode c. We thus obtain an effective master equation of the system AB, as

$$\frac{d\hat{\rho}}{dt} = \Gamma_a\mathcal{D}\left[\hat{a}\hat{U}_{B,\mathrm{eff}}\right]\hat{\rho}, \tag{6.130}$$

$$\hat{U}_{B,\mathrm{eff}} = \frac{\Gamma_c\hat{\mathbb{I}}_B - i\lambda\hat{M}_B}{\Gamma_c\hat{\mathbb{I}}_B + i\lambda\hat{M}_B}. \tag{6.131}$$

It is worth stressing that the validity of Eq. (6.130) does not depend on having a small coupling between reservoir and B subsystem, i.e. λ can be comparable or even greater than

Γ_c. Hence, we can use this recipe to realize general unitary operators $\hat{U}_B$.

Comparing Eq. (6.130) with Eq. (6.125), we can choose the a mode coupling rate Γ_a and subsystem B coupling operator $\hat{M}_B$ in the initial setup Eq. (6.127), such that the effective master equation Eq. (6.130) realizes the desired dynamics, i.e. we require

$$\Gamma_a = \Gamma, \tag{6.132}$$

$$\hat{M}_B = \frac{\Gamma_c}{\lambda} \tan \frac{\hat{E}_B}{2}. \tag{6.133}$$

We thus obtain a general recipe, as given by Eq. (6.127), that makes use of directional coupling and reservoir engineering techniques to implement a nonreciprocal quantum master equation of the form in Eq. (6.125). For the specific case where B is a single qubit, and assuming the target unitary is a Z-rotation $e^{-i\frac{\theta}{2}\hat{\sigma}_z}$, we further have

$$\hat{M}_B = \frac{\Gamma_c}{\lambda} \left(\tan \frac{\theta}{4} \right) \hat{\sigma}_z. \tag{6.134}$$

We note that the physical setup discussed in this Appendix is experimentally accessible using e.g. state-of-the-art superconducting qubit platforms. In fact, in a different context, specific cases of dynamics in Eq. (6.127) have been implemented for quantum-non-demolition (QND) measurement of itinerant microwave photons [252, 253]. In those works, the QND detector structure consists of a cavity dispersively coupled to a qubit. To perform the QND detection, an itinerant microwave field is sent through a circulator and then reflected off the cavity mode. By measuring the qubit phase shift, one can in turn extract average photon number of the input pulse. Comparing the QND setup to our master equation in Eq. (6.127), the cavity and the qubit would be mapped to the reservoir mode c and subsystem B, respectively. As a result, external coupling rate of the cavity would correspond to Γ_c, and the cavity-qubit dispersive interaction to Eq. (6.129). For Ref. [253], we can use a qubit in the place of mode a to describe the single-photon source in that work, so that the recipe

in Eq. (6.127) can be straightforwardly modified to describe the corresponding experimental system. In Ref. [252], the itinerant microwave has a Gaussian pulse shape, which can be formally mimicked via output of a cavity mode (A) with a time-dependent coupling rate $\Gamma_a(t)$. In both experiments, the unidirectional coupling is achieved by explicit use of a circulator.

Despite aforementioned similarities between the physical setups used in [252, 253] and our model, we note that those previous works did not really utilize the master equations in Eq. (6.127) or (6.130) to analyze dynamics of their systems. Our derivation thus reveals a striking new feature of dynamics in those types of setups: in the Markovian limit ($\Gamma_c \gg \Gamma_a$), if one starts from a product state of A cavity Fock state and a generic qubit (B) state, the qubit steady state in the long-time limit would undergo a *coherent* Z rotation from its initial state, with the phase shift controlled by the photon number of the initial A state. The experimental setup in [253] thus can be directly used to dissipatively realize steady-state unitary gates (see also Section 6.4.3 in the main text).

Finally, we note that the effective master equation in Eq. (6.130) describes an idealized case; in realistic settings, the fidelity of the unitary gate emerging from such dissipative steady-sate relaxation process will suffer from a range of imperfections, including non-Markovian effects due to a finite reservoir linewidth, nonzero thermal photon population in the reservoir and cavity modes, imperfect preparation of the initial A cavity state, etc. Still, in principle it is possible to carefully engineer the practical systems to suppress those factors and achieve gate fidelity comparable to typical pulse-based gates. Further, given an experimental system, one can incorporate those imperfections into the theory model in Eq. (6.127) and quantitatively examine how they affect the dissipative steady-state gate fidelity (e.g. see Section 6.5.2 for discussion on non-Markovian effects), which can be useful for designing new setups to improve the gate fidelity.

6.8.5 *The role of Markovianity in achieving unidirectional interaction for the physical implementation in Eq.* (6.27)

In Section 6.5.1 in the main text, we discuss physical implementation of the nonreciprocal dissipator $\mathcal{L}_{\text{gate}}\hat{\rho} = \Gamma\mathcal{D}[e^{-i\frac{\theta}{2}\hat{\sigma}_z}\hat{a}]\hat{\rho}$ via an intermediate reservoir mode (see Eq. (6.27)). We also state that this setup crucially requires that the reservoir mode is Markovian. In this Appendix, we provide a detailed discussion on the role of Markovianity in such physical realizations.

We start with a general setup consisting of a driven-cavity-qubit system coupled to a reservoir mode. In the rotating frame with respect to the drive frequency, the total system dynamics can be described by the master equation $(d\hat{\rho}/dt) = \mathcal{L}_0\hat{\rho}$, with the Lindbladian given by

$$\mathcal{L}_0\hat{\rho} = -i\left[\hat{H}_{\text{S}} + \hat{H}_{\text{E}} + \hat{H}_{\text{int}}, \hat{\rho}\right] + \kappa_a\mathcal{D}\left[\hat{a}\right]\hat{\rho} + \kappa_c\mathcal{D}\left[\hat{c}\right]\hat{\rho}, \tag{6.135}$$

$$\hat{H}_{\text{S}} = -\Delta_a\hat{a}^\dagger\hat{a} + \frac{\lambda_a}{2}\hat{\sigma}_z\hat{a}^\dagger\hat{a} + f^*_{\text{dr}}\left(t\right)\hat{a} + f_{\text{dr}}\left(t\right)\hat{a}^\dagger, \tag{6.136}$$

$$\hat{H}_{\text{E}} = -\Delta_c\hat{c}^\dagger\hat{c}, \quad \hat{H}_{\text{int}} = \left(J\hat{a}^\dagger\hat{c} + J^*\hat{c}^\dagger\hat{a}\right) + \frac{\lambda_c}{2}\hat{\sigma}_z\hat{c}^\dagger\hat{c}. \tag{6.137}$$

As discussed in Section 6.5.1, in the large reservoir linewidth limit, i.e. $\kappa_c \gg |J|$, one can treat the reservoir mode effectively as a Markovian environment for the cavity-qubit system. In this regime, one can follow standard adiabatic elimination procedures to integrate out reservoir mode and obtain the desired dynamics. To elucidate the role of Markovianity, here we consider instead the regime with small reservoir linewidth $\kappa_c \lesssim |J|$. As we show, the effects due to non-Markovianity now manifest as extra frequency-dependent corrections to the system Langevin equations of motion.

For concreteness, let us first write out the quantum Langevin equations of the system, as

$$i\partial_t \hat{a} = \left(-\Delta_a + \frac{\lambda_a}{2}\hat{\sigma}_z - i\frac{\kappa_a}{2}\right)\hat{a} + J\hat{c} - i\sqrt{\kappa_a}\hat{a}_{\text{in}} + f_{\text{dr}}(t), \tag{6.138}$$

$$i\partial_t \hat{c} = \left(-\Delta_c + \frac{\lambda_c}{2}\hat{\sigma}_z - i\frac{\kappa_2}{2}\right)\hat{c} + J^*\hat{a} - i\sqrt{\kappa_c}\hat{c}_{\text{in}}, \tag{6.139}$$

$$i\partial_t \hat{\sigma}_- = \left(\lambda_a \hat{a}^\dagger \hat{a} + \lambda_c \hat{c}^\dagger \hat{c}\right)\hat{\sigma}_-. \tag{6.140}$$

However, we note that similar analysis can be carried out at the level of e.g. system master equation as well. While our discussion can be straightforwardly generalized to a generic initial state, for convenience we assume that the cavity mode starts in a coherent state $|\alpha_0\rangle$, i.e. with amplitude α_0, and the reservoir is in vacuum state at initial time $t = t_0$. Thus, the system dynamics can be fully determined by solving the following set of linear equations for the cavity and reservoir mode amplitudes $\bar{a}_\sigma$ and $\bar{c}_\sigma$ ($\sigma = \uparrow, \downarrow$)

$$i\partial_t \bar{a}_\sigma = \left(-\Delta_a + \frac{\lambda_a}{2}\sigma_z - i\frac{\kappa_a}{2}\right)\bar{a}_\sigma + J\bar{c}_\sigma + f_{\text{dr}}(t), \tag{6.141a}$$

$$i\partial_t \bar{c}_\sigma = \left(-\Delta_c + \frac{\lambda_c}{2}\sigma_z - i\frac{\kappa_c}{2}\right)\bar{c}_\sigma + J^*\bar{a}_\sigma, \tag{6.141b}$$

where $\sigma_z = \pm 1$ correspond to $\sigma = \uparrow, \downarrow$. The qubit coherence function can thus be computed by solving the differential equation

$$\frac{1}{\langle\hat{\sigma}_-(t)\rangle}\frac{d\langle\sigma_-(t)\rangle}{dt} = -i\lambda_a \bar{a}_\uparrow \bar{a}_\downarrow^* - i\lambda_c \bar{c}_\uparrow \bar{c}_\downarrow^*. \tag{6.142}$$

We can formally integrate out the reservoir mode by transforming to the Fourier space and eliminating $\bar{c}_\sigma[\omega]$ from the equations, using the following relation

$$\bar{c}_\sigma[\omega] = \frac{J^*}{\omega + \Delta_c - \frac{\lambda_c}{2}\sigma_z + i\frac{\kappa_c}{2}}\bar{a}_\sigma[\omega]. \tag{6.143}$$

For notation convenience, we can rewrite the reservoir amplitude in terms of the reservoir

mode susceptibility function $\chi^{(0)}_{c,\sigma}[\omega]$, as

$$\bar{c}_\sigma[\omega] = J^* \chi^{(0)}_{c,\sigma}[\omega]\, \bar{a}_\sigma[\omega], \tag{6.144}$$

$$\chi^{(0)}_{c,\sigma}[\omega] \equiv \frac{1}{\omega + \Delta_c - \frac{\lambda_c}{2}\sigma_z + i\frac{\kappa_c}{2}}. \tag{6.145}$$

As a result, we obtain

$$\begin{aligned}\bar{a}_\sigma[\omega] &= \frac{1}{\omega + \Delta_a - \frac{\lambda_a}{2}\sigma_z + i\frac{\kappa_a}{2} - \frac{|J|^2}{\omega+\Delta_c-\frac{\lambda_c}{2}\sigma_z+i\frac{\kappa_c}{2}}} f_{\mathrm{dr}}[\omega] \\ &= \frac{1}{\omega + \Delta_a - \frac{\lambda_a}{2}\sigma_z + i\frac{\kappa_a}{2} - |J|^2 \chi^{(0)}_{c,\sigma}[\omega]} f_{\mathrm{dr}}[\omega]. \end{aligned} \tag{6.146}$$

Without loss of generality, and for illustrative purpose, we assume the drive is resonant with cavity mode a, and the local cavity loss is negligible, so that we have $\Delta_a = \kappa_a = 0$. In this case, we can further simplify the Fourier-space cavity amplitudes as

$$\bar{a}_\sigma[\omega] = \frac{1}{\omega - \frac{\lambda_a}{2}\sigma_z - |J|^2 \chi^{(0)}_{c,\sigma}[\omega]} f_{\mathrm{dr}}[\omega]. \tag{6.147}$$

Above equation allows one to express the cavity mode linear response susceptibilities $\chi_{a,\sigma}[\omega]$, as dressed by the coupling to reservoir mode, as

$$\bar{a}_\sigma[\omega] = \chi_{a,\sigma}[\omega]\, f_{\mathrm{dr}}[\omega], \tag{6.148}$$

$$\chi_{a,\sigma}[\omega] = \left(\omega - \frac{\lambda_a}{2}\sigma_z - |J|^2 \chi^{(0)}_{c,\sigma}[\omega]\right)^{-1}. \tag{6.149}$$

Noting that the phase of tunnel coupling rate J does not affect linear response susceptibilities of the cavity, we can use a local gauge transformation on the cavity mode to make J completely real. Therefore, without loss of generality we assume a real coupling constant J between reservoir and cavity modes hereafter.

Making use of the cavity susceptibilities in Eq. (6.149), we can define the self-energy of cavity mode as $\mathcal{E}_{a,\sigma_z}[\omega] \equiv \omega - \left(\chi_{a,\sigma}[\omega]\right)^{-1}$, so that we have

$$\bar{a}_\sigma[\omega] = \frac{1}{\omega - \mathcal{E}_{a,\sigma_z}[\omega]} f_{\mathrm{dr}}[\omega]. \tag{6.150}$$

The cavity mode self-energy can now be conveniently written in terms of qubit-independent and -dependent contributions, i.e.

$$\begin{aligned}\mathcal{E}_{a,\sigma_z}[\omega] =& \frac{\omega + \Delta_c + i\frac{\kappa_c}{2}}{\left(\omega + \Delta_c + i\frac{\kappa_c}{2}\right)^2 - \left(\frac{\lambda_c}{2}\right)^2} |J|^2 \\ &+ \left(\frac{\lambda_a}{2} + \frac{|J|^2}{\left(\omega + \Delta_c + i\frac{\kappa_c}{2}\right)^2 - \left(\frac{\lambda_c}{2}\right)^2} \frac{\lambda_c}{2} \right) \sigma_z.\end{aligned} \tag{6.151}$$

Since we are interested in dynamics at timescales much slower than reservoir correlation time $\tau_c \sim \kappa_c^{-1}$, we can choose a specific λ_a to minimize the qubit-state dependent term in Eq. (6.151) at low frequencies, as

$$\lambda_a = -\mathrm{Re}\left[\frac{|J|^2}{\left(\Delta_c + i\frac{\kappa_c}{2}\right)^2 - \left(\frac{\lambda_c}{2}\right)^2} \right] \lambda_c. \tag{6.152}$$

If the cavity mode is resonant with the reservoir mode, i.e. if $\Delta_c = \Delta_a = 0$, the qubit-dependent term in the self-energy (Eq. (6.151)) allows perfect cancellation in the stationary limit ($\omega = 0$). In contrast, for transient dynamics at fast frequencies ω, the cavity self-energy can have nontrivial dependence on qubit states, even in the resonant limit.

Let us examine such frequency-dependent corrections in more detail. For convenience, we can rewrite the self energy in terms of reservoir linewidth κ_c and effective parameters θ_{eff}

and Γ_{eff} that describe the stationary limit dissipation, i.e. letting

$$\lambda_c = \kappa_c \tan\frac{\theta_{\text{eff}}}{2}, \quad \Delta_c = 0, \tag{6.153}$$

$$\Gamma_{\text{eff}} = J^2 \frac{4\kappa_c}{\kappa_c^2 + \lambda_c^2} \Rightarrow J^2 = \frac{1}{4}\Gamma_{\text{eff}}\kappa_c \sec^2\frac{\theta_{\text{eff}}}{2}, \tag{6.154}$$

$$\lambda_a = J^2 \frac{4\lambda_c}{\kappa_c^2 + \lambda_c^2} = \Gamma_{\text{eff}} \tan\frac{\theta_{\text{eff}}}{2}, \tag{6.155}$$

so that the self-energy function can be reformulated as

$$\begin{aligned}&\mathcal{E}_{a,\sigma_z}[\omega] \\ =&\frac{\Gamma_{\text{eff}}}{2}\frac{\left(\omega + i\frac{\kappa_c}{2}\right)\frac{\kappa_c}{2}\sec^2\frac{\theta_{\text{eff}}}{2} + \omega\left(\omega + i\kappa_c\right)\tan\frac{\theta_{\text{eff}}}{2}\sigma_z}{\left(\omega + i\frac{\kappa_c}{2}\right)^2 - \left(\frac{\kappa_c}{2}\tan\frac{\theta_{\text{eff}}}{2}\right)^2}.\end{aligned} \tag{6.156}$$

For the sake of discussion, we can use a representative value for the effective phase shift $\theta_{\text{eff}} = \pi/2$, so that above expression further simplifies as

$$\mathcal{E}_{a,\sigma_z}[\omega] = \frac{\Gamma_{\text{eff}}}{2}\frac{\left(\omega + i\frac{\kappa_c}{2}\right)\kappa_c + \omega\left(\omega + i\kappa_c\right)\sigma_z}{\omega\left(\omega + i\kappa_c\right) - \frac{\kappa_c^2}{2}}. \tag{6.157}$$

The Markovian limit amounts to requiring that the self-energy scale near resonance, i.e. Γ_{eff}, is much smaller than the frequency range over which $\mathcal{E}_{a,\sigma_z}[\omega]$ significantly changes. The latter frequency scale is in turn set by reservoir mode linewidth κ_c. In the limit where $\Gamma_{\text{eff}} \ll \kappa_c$, we can expand the self energy function in the vicinity of $\omega = 0$, so that we obtain

$$\mathcal{E}_{a,\sigma_z}[\omega] \simeq -i\frac{\Gamma_{\text{eff}}}{2}\left(1 + 2\frac{\omega}{\kappa_c}\sigma_z\right). \tag{6.158}$$

The second term in the parenthesis in Eq. (6.158) represents leading-order non-Markovian corrections, which describes qubit backaction to the cavity and causes deviation from the full-nonreciprocity limit.

It is also interesting to consider qubit dynamics in this setup. Because of the nonlinear dispersive coupling, the qubit dynamics can be more complicated in the frequency space: taking Fourier transform of Eq. (6.142), we have

$$\begin{aligned}&\omega \ln\langle\sigma_{-}[\omega]\rangle\\&=\int_{-\infty}^{+\infty} d\omega_1 \left(\lambda_a \bar{a}_{\uparrow}[\omega_1]\,\bar{a}_{\downarrow}^{*}[\omega-\omega_1]+\lambda_c \bar{c}_{\uparrow}[\omega_1]\,\bar{c}_{\downarrow}^{*}[\omega-\omega_1]\right).\end{aligned} \tag{6.159}$$

We can again substitute Eq. (6.143) into this equation to obtain

$$\omega \ln\langle\sigma_{-}[\omega]\rangle=\int_{-\infty}^{+\infty} d\omega_1 \Lambda_a[\omega_1;\omega]\,\bar{a}_{\uparrow}[\omega_1]\,\bar{a}_{\downarrow}^{*}[\omega-\omega_1] \tag{6.160}$$

$$\Lambda_a[\omega_1;\omega]=\lambda_a+\lambda_c|J|^2\,\chi_{c,\uparrow}^{(0)}[\omega]\,\chi_{c,\downarrow}^{(0)}[\omega-\omega_1]. \tag{6.161}$$

In the Markovian limit, the cavity amplitude is approximately independent of the qubit state, so that we have $\bar{a}_{\uparrow}(t)\simeq\bar{a}_{\downarrow}(t)$. In this limit, the first term on the RHS of Eq. (6.161), which is given by λ_a, leads to a pure phase shift on the qubit, while the second term can induce both phase shift and dephasing in qubit dynamics.

6.8.6 Properties of multiple-dissipator generalization of gauge-symmetry nonreciprocal Lindbladians in Eq. (6.36)

In Section 6.6, we introduce the multi-dissipator generalization of gauge-symmetry nonreciprocal Lindbladians, which take the following form (c.f. Eq. (6.36))

$$\mathcal{L}_{\text{multi}}\hat{\rho}=\Gamma\sum_{\ell=1}^{N}\mathcal{D}\left[\sum_{m=1}^{N}\hat{u}_{\ell m}\hat{A}_m\right]\hat{\rho}. \tag{6.162}$$

In analogy to the classical gauge symmetry Eq. (6.35), the B operators $\hat{u}_{\ell m}$ can be thought of as operator-valued matrix elements of a generalized unitary, which acts on the composite

linear space $\mathbb{C}^N \otimes \mathcal{H}_B$ between the *dissipator* space $\mathbb{C}^N$ of the $\hat{A}_\ell$ operators, and the B system Hilbert space. In this Appendix, we provide more details about the general structure of this generalized unitary. Based on this construction, we also discuss a couple of typical examples illustrating the connections and differences between the multi- and single-dissipator nonreciprocal Lindbladians.

Connection to a generalized unitary operator

To motivate the generalized unitary, we again start with a multi-dissipator Lindbladian acting only on system A, as given by $\mathcal{L}_A\hat{\rho}_A = \Gamma \sum_{\ell=1}^{N} \mathcal{D}[\hat{A}_\ell]\hat{\rho}_A$. As noted in the main text, this Lindbladian is invariant under a generic unitary transformation on the jump operators $\hat{A}_\ell$

$$\mathcal{L}_A\hat{\rho}_A = \Gamma \sum_{\ell=1}^{N} \mathcal{D}\left[\sum_{m=1}^{N} u_{\ell m}\hat{A}_m\right]\hat{\rho}_A, \tag{6.163}$$

where $u_{\ell m}$ are matrix elements of a N-dimensional complex unitary matrix $u_{\ell m} = \left(\check{\mathcal{U}}\right)_{\ell m}$. We can also write the unitary matrix explicitly in terms of its Hermitian generator $\check{\mathcal{H}}$, i.e. $\check{\mathcal{U}} = \exp\left(-i\check{\mathcal{H}}\right)$. For discussion that follows, it is convenient to rewrite the Hermitian matrix $\check{\mathcal{H}}$ as a sum of N^2 basis matrices $\check{\mathcal{E}}_{\ell m}$ as

$$\check{\mathcal{H}} = \sum_{\ell,m=1}^{N} h_{\ell m}\check{\mathcal{E}}_{\ell m}. \tag{6.164}$$

Here, $\check{\mathcal{E}}_{\ell m} \equiv \mathbf{e}_\ell \left(\mathbf{e}_m\right)^\dagger$ are formed by outer products between N basis vectors $\mathbf{e}_\ell$ of the linear space $\mathbb{C}^N$, so that we have $\check{\mathcal{E}}^\dagger_{\ell'\ell}\check{\mathcal{E}}_{m'm} = \delta_{\ell' m'}\check{\mathcal{E}}_{\ell m}$.

We now turn to the nonreciprocal Lindbladian given by Eq. (6.162). In analogy to the gauge symmetry described in Eq. (6.163), we can generate B operators $\hat{u}_{\ell m}$ via a generalized

unitary operator acting on the composite linear space $\mathbb{C}^N \otimes \mathcal{H}_B$, as

$$\hat{u}_{\ell m} = \left(e^{-i\hat{H}_{\rm gen}}\right)_{\ell m}, \tag{6.165}$$

$$\hat{H}_{\rm gen} = \sum_{j,j'=1}^{N} \check{\mathcal{E}}_{jj'} \hat{h}_{jj'}, \tag{6.166}$$

where $\hat{h}_{jj'}$ are operators acting on B satisfying $\hat{h}_{jj'} = \hat{h}^{\dagger}_{j'j}$. One can further show that the unitarity conditions $\sum_{\ell} \hat{u}^{\dagger}_{\ell m} \hat{u}_{\ell m'} = \delta_{mm'} \hat{\mathbb{I}}_B$ (see Eq. (6.38)) hold if and only if the $\hat{u}_{\ell m}$ operators can be rewritten as Eq. (6.165). If Eq. (6.165) holds, as mentioned in the main text, one can exactly trace out system B to obtain a closed master equation acting on system A as $(d\hat{\rho}_A/dt) = \Gamma \sum_{\ell} \mathcal{D}[\hat{A}_{\ell}]\hat{\rho}_A$, so that the multimode master equation in Eq. (6.162) is again unidirectional.

Example cases of multi-dissipator nonreciprocity equivalent or inequivalent to incoherent sum of single fully directional dissipators

As discussed in the main text, Eq. (6.162) describes a much more general class of fully nonreciprocal dynamics as compared to the single-dissipator case (see Eq. (6.16)). Here we discuss in detail conditions for when the former multi-dissipator dynamics can or cannot be rewritten as an incoherent sum of unidirectional dissipators, i.e. if it is possible to write equality relation of the following form

$$\mathcal{L}_{\rm multi}\hat{\rho} \stackrel{?}{=} \Gamma \sum_{\ell} \mathcal{D}\left[\hat{U}_{B,\ell}\hat{A}'_{\ell}\right]\hat{\rho}. \tag{6.167}$$

While it is difficult to comprehensively characterize all the possible scenarios where such equivalence relation exists, here we discuss two independently sufficient conditions for Eq. (6.167) to hold. The first case can be easily understood in terms of the generalized Hermitian generator in Eq. (6.166). More specifically, if we can diagonalize it using a new local A basis as

defined by $\check{\mathcal{F}}_{\ell\ell'} = \sum_{j,j'=1}^{N} v_{\ell j'} \check{\mathcal{E}}_{j'j} v^*_{\ell' j}$, so that we have

$$\hat{H}_{\text{gen}} = \sum_{j,j'=1}^{N} \check{\mathcal{E}}_{jj'} \hat{h}_{jj'} = \sum_{\ell=1}^{N} \check{\mathcal{F}}_{\ell\ell} \hat{\Phi}_{B,\ell}, \tag{6.168}$$

where $v_{\ell m} = \left(\check{\mathcal{V}}\right)_{\ell m}$ are elements of a unitary matrix, then one can use a few lines of algebra to show that Eq. (6.162) in this case is equivalent to a sum of single fully nonreciprocal dissipators. More specifically, we obtain

$$\mathcal{L}_{\text{multi}} \hat{\rho} = \Gamma \sum_{\ell=1}^{N} \mathcal{D} \left[e^{-i\hat{\Phi}_{B,\ell}} \sum_{m=1}^{N} v^*_{\ell m} \hat{A}_m \right] \hat{\rho}. \tag{6.169}$$

Note that RHS of Eq. (6.169) is fully equivalent to the starting Lindbladian, but now each dissipator by itself implements a unidirectional interaction from A to B.

The second case is if we cannot diagonalize the generator in Eq. (6.166) (and hence the generalized unitary, see Eq. (6.165)) via a local basis change on A operators, but the B system only has a single qubit, and all qubit operators $\hat{u}_{\ell m}$ commute with each other. For such Lindbladians, we can again reformulate it as a sum of single nonreciprocal dissipators via a local linear transformation on $\hat{A}_\ell$ jump operators, so that Eq. (6.167) holds. To see this, we first note that the total system dynamics is easily solvable by jointly diagonalizing $\hat{u}_{\ell m}$ via a local B basis, which we assume to be $\hat{\sigma}_z$ basis for simplicity, so that time evolution under $\mathcal{L}_{\text{multi}}$ will conserve excitations in that basis. More concretely, the generalized unitary can now be decomposed using projectors $\hat{P}_{\uparrow(\downarrow)}$ onto $\hat{\sigma}_z$ eigenstates of B subsystem as

$$e^{-i\sum_{j,j'=1}^{N} \check{\mathcal{E}}_{jj'} \hat{h}_{jj'}} = \check{\mathcal{U}}_{\uparrow} \hat{P}_{\uparrow} + \check{\mathcal{U}}_{\uparrow} \hat{P}_{\downarrow}. \tag{6.170}$$

Again, we can transform the local A basis to $\check{\mathcal{U}}'_{\uparrow(\downarrow)} = \check{\mathcal{W}} \check{\mathcal{U}}_{\uparrow(\downarrow)} \check{\mathcal{W}}^\dagger$ via a unitary matrix $\check{\mathcal{W}}$; for the jump operators in this new dissipator frame to be unidirectional, we require that

$\check{\mathcal{U}}'_{\uparrow} = \exp\big(-i\check{\mathcal{D}}\big)\check{\mathcal{U}}'_{\downarrow}$, where $\big(\check{\mathcal{D}}\big)_{\ell m} = \delta_{\ell m} d_\ell$ denotes a real diagonal matrix. This relation can be realized by transforming to the eigenbasis of $\check{\mathcal{U}}_{\uparrow}\check{\mathcal{U}}_{\downarrow}^{\dagger}$, so that we have

$$\mathcal{L}_{\text{multi}}\hat{\rho} = \Gamma \sum_{\ell=1}^{N} \mathcal{D}\left[e^{-id_\ell \frac{\hat{\sigma}_z}{2}} \hat{A}'_\ell\right] \hat{\rho}. \tag{6.171}$$

As a concrete example, we consider A consisting of two bosonic modes. Using $\check{\mathcal{Z}}$ and $\check{\mathcal{X}}$ to denote Pauli matrices acting on $\mathbb{C}^2$, we focus on the dissipator generated by the following generalized unitary operator

$$\hat{u}_{\ell m} = \left[e^{-i\theta\left(\check{\mathcal{Z}}\hat{\sigma}_z \cos\varphi + \check{\mathcal{X}}\hat{\mathbb{I}}_B \sin\varphi\right)}\right]_{\ell m}. \tag{6.172}$$

The corresponding system Lindbladian is given by

$$\begin{aligned}\mathcal{L}\hat{\rho} =& \Gamma\mathcal{D}[\hat{a}_1 (\cos\theta - i\hat{\sigma}_z \cos\varphi \sin\theta) - i\hat{a}_2 \sin\theta \sin\varphi]\hat{\rho} \\ &+ \Gamma\mathcal{D}[\hat{a}_2 (\cos\theta + i\hat{\sigma}_z \cos\varphi \sin\theta) - i\hat{a}_1 \sin\theta \sin\varphi]\hat{\rho}.\end{aligned} \tag{6.173}$$

In this case $\check{\mathcal{U}}_{\uparrow(\downarrow)} = e^{-i\theta(\pm\check{\mathcal{Z}}\cos\varphi + \check{\mathcal{X}}\sin\varphi)}$, and we can generally rewrite the Lindbladian into the form in Eq. (6.171). For the specific case with $\theta = \pi/2$, the relevant nonlocal basis simplifies into $\hat{a}_{y,\pm} = (\hat{a}_1 \pm i\hat{a}_2)/\sqrt{2}$, so that we have

$$\mathcal{L}\hat{\rho} = \frac{\Gamma}{2}\mathcal{D}\left[e^{i(\pi/2-\varphi)\hat{\sigma}_z}\hat{a}_{y,+}\right]\hat{\rho} + \frac{\Gamma}{2}\mathcal{D}\left[e^{i(-\pi/2+\varphi)\hat{\sigma}_z}\hat{a}_{y,-}\right]\hat{\rho}. \tag{6.174}$$

More generally, if we cannot diagonalize the generator in Eq. (6.166) (and hence the generalized unitary) via a local basis change on A operators, and if $\hat{u}_{\ell m}$ operators do not commute or B has more complicated level structure than a qubit, then there are cases where it is impossible to write the Lindbladian $\mathcal{L}_{\text{multi}}$ as Eq. (6.167), i.e. incoherent sum of fully nonreciprocal dissipators. For example, We can again consider 2 bosonic modes as subsystem

A, where the generalized unitary is given by

$$\hat{u}_{\ell m} = \left[e^{-i(\varphi \check{\mathcal{Z}} \hat{\sigma}_z + \theta \check{\mathcal{X}} \hat{\sigma}_x)} \right]_{\ell m}. \tag{6.175}$$

The corresponding system Lindbladian can be written as

$$\begin{aligned} \mathcal{L}\hat{\rho} =& \Gamma \mathcal{D}[e^{-i\varphi\hat{\sigma}_z}\hat{a}_1 \cos\theta - i\hat{\sigma}_x e^{i\varphi\hat{\sigma}_z}\hat{a}_2 \sin\theta]\hat{\rho} \\ &+ \Gamma \mathcal{D}[e^{i\varphi\hat{\sigma}_z}\hat{a}_2 \cos\theta - i\hat{\sigma}_x e^{-i\varphi\hat{\sigma}_z}\hat{a}_1 \sin\theta]\hat{\rho}, \end{aligned} \tag{6.176}$$

which reproduces Eqs. (6.39) and (6.41) in the main text. It is interesting to note that if we were to ignore all $\hat{\sigma}_x$ operators in Eq. (6.176), the resulting Lindbladian would still be fully nonreciprocal, but now could be rewritten as $\Gamma \left(\mathcal{D}[e^{-i\varphi\hat{\sigma}_z}\hat{a}_1] + \mathcal{D}[e^{i\varphi\hat{\sigma}_z}\hat{a}_2] \right) \hat{\rho}$, which would be equivalent to sum of single unidirectional dissipators. The inclusion of $\hat{\sigma}_x$ in the jump operators would not affect local dynamics of system A; however, those $\hat{\sigma}_x$ operators matter for evolution of correlations between A and B subsystems. As discussed in Section 6.6, those correlations can be highly nonclassical and even result in entanglement generation between A and B.

Steady state of multi-dissipator unidirectional dynamics with bosonic lowering operators as $\hat{A}_\ell$

It is interesting to note that if subsystem A operators $\hat{A}_\ell$ are bosonic lowering operators of cavity modes a_ℓ, i.e. $\hat{A}_\ell = \hat{a}_\ell$, and if A is initialized in a Fock state where at most one cavity mode has nonzero photon(s), then we can further analytically derive the long-time limit of the quantum map generated by $\mathcal{L}_{\text{multi}}$. To see this, we first expand the master equation in Eq. (6.36) (i.e. Eq. (6.162)) and rewrite it as sum of quantum-jump, and no-jump contributions. Making use of the unitarity conditions in Eq. (6.38), the equation can

be simplified as

$$\mathcal{L}_{\text{multi}}\hat{\rho} = \Gamma \sum_{m,m'=1}^{N} \hat{A}_m \mathcal{E}_{mm'}(\hat{\rho}) \hat{A}_{m'}^{\dagger} - \frac{\Gamma}{2} \left\{ \sum_{n=1}^{N} \hat{A}_n^{\dagger} \hat{A}_n, \hat{\rho} \right\}, \tag{6.177}$$

$$\mathcal{E}_{mm'}(\hat{\rho}) = \sum_{j=1}^{N} \hat{u}_{jm} \hat{\rho} \hat{u}_{jm'}^{\dagger}. \tag{6.178}$$

If $\hat{A}_m = \hat{a}_m$, it is straightforward to show that

$$\lim_{t\to\infty} e^{\mathcal{L}_{\text{multi}} t} \left[(\hat{a}_m^{\dagger})^{\ell} |0\rangle\langle 0| \hat{a}_m^{\ell} \otimes \hat{\rho}_{B,\text{i}} \right] = (\mathcal{E}_{mm})^{\ell}(\hat{\rho}_{B,\text{i}}). \tag{6.179}$$

Thus, for general $\mathcal{L}_{\text{multi}}$ that cannot be rewritten as sum of single nonreciprocal dissipators, the long-time limit of dynamics within subsystem B generated by the unidirectional interaction will in general be dissipative, in contrast to the single-dissipator case in Eq. (6.16) (c.f. Section 6.4.3).

6.8.7 Gauge-symmetry-based nonreciprocity between two bosonic modes

As discussed in the main text, our recipe for building nonreciprocal QMEs is generally applicable to a broad range of systems. Here we consider an alternative type of system that host this physics; more specifically, we look at a nonreciprocal dissipator between two cavity modes a and b, as described by the following Lindblad master equation

$$\frac{d\hat{\rho}}{dt} = \mathcal{L}_{\text{bos}}\hat{\rho} = \Gamma \mathcal{D}[e^{-i\frac{\theta}{2}\hat{x}_b}\hat{a}]\hat{\rho}, \tag{6.180}$$

where $\hat{x}_b$ denotes the standard quadrature operator of the b mode

$$\hat{x}_b = \frac{1}{\sqrt{2}} \left(\hat{b} + \hat{b}^{\dagger} \right). \tag{6.181}$$

We can write out the corresponding Ito quantum stochastic differential equations [76] for a generic system operators $\hat{M}$ as

$$\begin{aligned}\frac{d\hat{M}}{dt} =& -\left[\hat{M}, e^{i\frac{\theta}{2}\hat{x}_b}\hat{a}^\dagger\right]\left[\frac{\Gamma}{2}e^{-i\frac{\theta}{2}\hat{x}_b}\hat{a} + \sqrt{\Gamma}\hat{a}_{\text{in}}\right] \\ &+ \left[\frac{\Gamma}{2}e^{i\frac{\theta}{2}\hat{x}_b}\hat{a}^\dagger + \sqrt{\Gamma}\hat{a}_{\text{in}}^\dagger\right]\left[\hat{M}, e^{-i\frac{\theta}{2}\hat{x}_b}\hat{a}\right]. \end{aligned} \tag{6.182}$$

Eq. (6.180) takes the general form of nonreciprocal master equations via gauge symmetry discussed in the main text (see Eq. (6.16)). It is thus straightforward to show that time evolution of expectation value of any local operator acting on the a cavity is closed within a mode, i.e. Eq. (6.180) describes an unidirectional coupling from mode a to b. The reverse is, as expected, not true: dynamics of the second cavity mode b in general depends on cavity mode a. For example, we can derive the equation of motion for the b mode momentum average $\langle\hat{p}_b\rangle$ as

$$\frac{d\langle\hat{p}_b\rangle}{dt} = -\gamma\frac{\theta}{2}\langle\hat{a}^\dagger\hat{a}\rangle. \tag{6.183}$$

This equation can be intuitively understood in terms of the measurement-and-feedforward picture (c.f. Section 6.4.5): the dissipator $\mathcal{D}[e^{-i\frac{\theta}{2}\hat{x}_b}\hat{a}]\hat{\rho}$ describes a process where the cavity mode a is weakly coupled to a photodetector, and every time a photon is detected, we apply a unitary transformation $e^{-i\frac{\theta}{2}\hat{x}_b}$ to mode b. Throughout time evolution, the quadrature operator $\hat{x}_b$ of mode b is conserved (i.e. generates a strong symmetry of the master equation). On the other hand, the unitary gates act as displacements on the conjugate quadrature $\hat{p}_b$. We can now understand system dynamics in terms of a stochastic unraveling via quantum trajectories: whenever a photon jump occurs in mode a, one would displace the quadrature $\hat{p}_b$ by a constant $-\theta/2$. Averaging over all stochastic trajectories thus gives rise to Eq. (6.183).

We also note that although the equations of motion for the expectation value of b mode quadratures are relatively simple, the dynamics is still highly non-Gaussian. To see this

explicitly, we first derive the EOMs of higher order moments of cavity quadrature as

$$\frac{d\langle\hat{p}_b^2\rangle}{dt} = -\gamma\theta\langle\hat{p}_b\hat{a}^\dagger\hat{a}\rangle + \gamma\frac{\theta^2}{4}\langle\hat{a}^\dagger\hat{a}\rangle, \tag{6.184}$$

$$\frac{d\langle\hat{p}_b^3\rangle}{dt} = -\gamma\frac{3\theta}{2}\langle\hat{p}_b^2\hat{a}^\dagger\hat{a}\rangle + \gamma\frac{3\theta^2}{4}\langle\hat{p}_b\hat{a}^\dagger\hat{a}\rangle - \gamma\frac{\theta^3}{8}\langle\hat{a}^\dagger\hat{a}\rangle, \tag{6.185}$$

so that we obtain the EOM of the third order cumulant $\langle\delta\hat{p}_b^3\rangle$ as

$$\begin{aligned}\frac{d\langle\delta\hat{p}_b^3\rangle}{dt} = &-\gamma\frac{3\theta}{2}\langle\delta\hat{p}_b^2\hat{a}^\dagger\hat{a}\rangle + \gamma\frac{3\theta}{2}\langle\delta\hat{p}_b^2\rangle\langle\hat{a}^\dagger\hat{a}\rangle \\ &+\gamma\frac{3\theta^2}{4}\langle\delta\hat{p}_b\hat{a}^\dagger\hat{a}\rangle - \gamma\frac{\theta^3}{8}\langle\hat{a}^\dagger\hat{a}\rangle.\end{aligned} \tag{6.186}$$

If the system starts in a product state between two cavity modes, all but the last term on the right hand side of Eq. (6.186) will vanish at initial time, leading to a nonzero third cumulant $\langle\delta\hat{p}_b^3(\delta t)\rangle$ at a positive infinitesimal time $\delta t > 0$ (as long as the cavity a has a nonzero photon number). Thus, the dynamics generated by Eq. (6.180) is in general non-Gaussian.

CHAPTER 7

SUMMARY AND OUTLOOK

In this thesis, we studied both the fundamental limits on quantum dynamics as imposed by physical constraints on quantum noise, and applications that utilize noise and fluctuation as a resource for quantum information processing. Those applications include characterization of noise properties in quantum systems, and recipes for engineering nontrivial classes of quantum dynamics such as nonreciprocal interactions without explicitly breaking time-reversal symmetry. Each chapter also contains a conclusion or summary and outlook section with a brief discussion on future directions. Here, we expand on those discussions, and comment on open problems connected to multiple chapters and other broadly related theoretical challenges with implications for quantum information processing.

Chapter 2 investigates what kind of purely dissipative dynamics can generate entanglement. A natural question to ask beyond our work is about the quantitative characterization of dissipatively generated entanglement dynamics in either the temporal or spatial dimension. Similar questions have attracted a lot of interest in the context of Hamiltonian dynamics [274, 275], in fermionic [276], spin [277, 278], as well as bosonic [279] systems, and those works show a rich interplay between entanglement and phase transitions, topology, etc. However, less is understood in the dissipative regime. As mentioned in Section 2.5, a technical challenge in the dissipative case is due to the existence of bound entanglement; even for entanglement that are detectable with the Peres-Horodecki criterion, quantification of mixed state entanglement dynamics is generally a nontrivial task. Recent progress on detecting mixed state entanglement [280] and computing negativity spectrum of random mixed states [281] provide promising avenues for solving this problem. Lastly, a tangentially related question is concerned with the mapping between purely dissipative dynamics and measurement-and-feedforward protocols discussed in Section 2.4.2; it will be interesting to explore if feedforward-based dynamics can be exploited as a resource for entanglement

generation, and even conversion from conditional to deterministic entanglement.

Chapter 3 presents approaches for realizing non-Hermitian Hamiltonian using fully unitary quantum dynamics. While we discussed a number of potential applications in Section 3.5, one remaining question is whether exceptional point sensor provides an advantage in terms of the sensitivity (signal-to-noise ratio, SNR) in the quantum regime. Indeed, Ref. [282] shows that an advantage in SNR in the quantum regime can be achieved using a harmonic oscillator chain with nonreciprocal Hamiltonian interactions, but it is unclear if a more general principle underlies those quantum sensors. Making connection with the discussion in above paragraph, a recurring question is about characterizing entanglement generation in those unitary non-Hermitian quantum systems; Ref. [279] categorizes the temporal entanglement growth via quadratic bosonic Hamiltonians, but the spatial structure is largely unexplored. In a different context, one could also consider the reverse problem, i.e., realizing Hermitian dynamical matrix via dissipative quantum dynamics. An interesting example of this is given in Ref. [283], where a dissipative bosonic coupling gives rise to a Hermitian contribution to the dynamical matrix, which in turn leads to emergence of curious dynamical instabilities. For this reverse problem, a general design principle remains unknown.

Chapters 4 and 5 are both related to method development for quantum sensing and quantum noise spectroscopy: Chapter 4 discusses a Keldysh-based approach for characterizing non-Gaussian quantum noise, and Chapter 5 presents a new quench-based sensing modality that gives access to the response properties of an unknown bath. While we primarily focus on using a single qubit sensor, one can naturally ask how these results generalize to the multiqubit setting. For the Keldysh-based noise characterization, introducing additional qubits could reveal new forms of nonclassical correlations in quantum bispectra. For the case of quench-based approach, having access to multiple qubit sensors could also enable the engineering and modulation of quench terms to enhance the sensing scheme. Recent work

has applied quantum noise spectroscopy to an effective two-level system formed by entangled states of qubits [284]; in this case, further measuring the quench phase shift would give us access to, e.g., the effective bath temperature. Another different and key question in the context of sensing applications is to theoretically predict the noise spectrum and response susceptibility function, especially for strongly interacting systems. Such knowledge can help us reconstruct the microscopic details of an unknown quantum environment — information that could be valuable for designing noise resilient quantum information processors. Last but not least, recent work has experimentally measured the quench phase shift for the case with non-interacting spin bath [285], and demonstrated its utility as a model-independent probe of spin bath polarization. It will be exciting to experimentally probe the quench phase shift in interacting spin baths, as well as explore the regime beyond the linear response approximation.

Chapter 6 proposes a general mechanism for realizing nonreciprocal quantum interactions that are distinct from the cascaded quantum systems. Our results motivate a broader question: can we come up with a general classification of all dynamics that are fully nonreciprocal? The answer to this question may further enlarge the dissipative toolbox for quantum information processing. Going back to the theme of dissipative entanglement creation, another open question is how to characterize the nature of entanglement generation via the multi-dissipator case of the nonreciprocal dynamics; in Section 6.6.3, we show that the nonreciprocal dynamics can generate transient entanglement, which eventually decays to zero, but it remains an open question whether this transient behavior could be a general consequence of the nonreciprocity. Shifting to potential applications, a version of the single nonreciprocal dissipator defined in Eq. (6.16) has been realized using superconducting qubits in the context of quantum-non-demolition detection [252, 253], and it will be interesting to explore if the general mechanism for realizing nonreciprocity discussed in Chapter 6 could provide an advantage in sensing and metrology.

BIBLIOGRAPHY

[1] A. Einstein, B. Podolsky, and N. Rosen, Phys. Rev. **47**, 777 (1935).

[2] J. S. Bell, Phys. Phys. Fiz. **1**, 195 (1964).

[3] W. K. Wootters and W. H. Zurek, Nature **299**, 802 (1982).

[4] S. L. Braunstein and C. M. Caves, Phys. Rev. Lett. **72**, 3439 (1994).

[5] R. P. Feynman, Int. J. Theor. Phys. **21**, 467 (1982).

[6] C. H. Bennett and G. Brassard, in *IEEE International Conference on Computers, Systems and Signal Processing*, Bangalore (IEEE, New York, 1984).

[7] C. H. Bennett, G. Brassard, C. Crépeau, R. Jozsa, A. Peres, and W. K. Wootters, Phys. Rev. Lett. **70**, 1895 (1993).

[8] P. Shor, in *Proceedings 35th Annual Symposium on Foundations of Computer Science* (IEEE, Santa Fe, 1994) pp. 124–134.

[9] V. Giovannetti, S. Lloyd, and L. Maccone, Phys. Rev. Lett. **96**, 010401 (2006).

[10] E. Altman, K. R. Brown, G. Carleo, L. D. Carr, E. Demler, C. Chin, B. DeMarco, S. E. Economou, M. A. Eriksson, K.-M. C. Fu, M. Greiner, K. R. Hazzard, R. G. Hulet, A. J. Kollár, B. L. Lev, M. D. Lukin, R. Ma, X. Mi, S. Misra, C. Monroe, K. Murch, Z. Nazario, K.-K. Ni, A. C. Potter, P. Roushan, M. Saffman, M. Schleier-Smith, I. Siddiqi, R. Simmonds, M. Singh, I. Spielman, K. Temme, D. S. Weiss, J. Vučković, V. Vuletić, J. Ye, and M. Zwierlein, PRX Quantum **2**, 017003 (2021).

[11] Google Quantum AI, Nature **614**, 676 (2023).

[12] V. V. Sivak, A. Eickbusch, B. Royer, S. Singh, I. Tsioutsios, S. Ganjam, A. Miano, B. L. Brock, A. Z. Ding, L. Frunzio, S. M. Girvin, R. J. Schoelkopf, and M. H. Devoret, Nature **616**, 50 (2023).

[13] Z. Ni, S. Li, X. Deng, Y. Cai, L. Zhang, W. Wang, Z.-B. Yang, H. Yu, F. Yan, S. Liu, C.-L. Zou, L. Sun, S.-B. Zheng, Y. Xu, and D. Yu, Nature **616**, 56 (2023).

[14] J. Preskill, Quantum **2**, 79 (2018).

[15] C. D. Bruzewicz, J. Chiaverini, R. McConnell, and J. M. Sage, Appl. Phys. Rev. **6**, 021314 (2019).

[16] L. Henriet, L. Beguin, A. Signoles, T. Lahaye, A. Browaeys, G.-O. Reymond, and C. Jurczak, Quantum **4**, 327 (2020).

[17] M. Kjaergaard, M. E. Schwartz, J. Braumüller, P. Krantz, J. I.-J. Wang, S. Gustavsson, and W. D. Oliver, Annu. Rev. Condens. Matter Phys. **11**, 369 (2020).

[18] A. Blais, A. L. Grimsmo, S. M. Girvin, and A. Wallraff, Rev. Mod. Phys. **93**, 025005 (2021).

[19] A. Seif, Y.-X. Wang, and A. A. Clerk, Phys. Rev. Lett. **128**, 070402 (2022).

[20] H.-P. Breuer and F. Petruccione, *The theory of open quantum systems* (Oxford University Press, Oxford, 2002).

[21] G. Lindblad, Commun. Math. Phys. **48**, 119 (1976).

[22] M. A. Nielsen and I. L. Chuang, *Quantum Computation and Quantum Information* (Cambridge University Press, Cambridge, 2010).

[23] A. A. Clerk, M. H. Devoret, S. M. Girvin, F. Marquardt, and R. J. Schoelkopf, Rev. Mod. Phys. **82**, 1155 (2010).

[24] H. Bruus and K. Flensberg, *Many-body quantum theory in condensed matter physics: an introduction* (Oxford University Press, Oxford, 2004).

[25] A. Peres, Phys. Rev. Lett. **77**, 1413 (1996).

[26] M. Horodecki, P. Horodecki, and R. Horodecki, Phys. Lett. A **283**, 1 (2001).

[27] H. M. Wiseman and G. J. Milburn, Phys. Rev. A **49**, 1350 (1994).

[28] M. Horodecki, P. Horodecki, and R. Horodecki, Phys. Rev. Lett. **80**, 5239 (1998).

[29] C. H. Bennett, D. P. DiVincenzo, T. Mor, P. W. Shor, J. A. Smolin, and B. M. Terhal, Phys. Rev. Lett. **82**, 5385 (1999).

[30] D. Bruß and A. Peres, Phys. Rev. A **61**, 030301(R) (2000).

[31] A. Metelmann and A. A. Clerk, Phys. Rev. A **95**, 013837 (2017).

[32] Y.-X. Wang and A. A. Clerk, Phys. Rev. A **99**, 063834 (2019).

[33] R. El-Ganainy, K. G. Makris, M. Khajavikhan, Z. H. Musslimani, S. Rotter, and D. N. Christodoulides, Nat. Phys. **14**, 11 (2018).

[34] R. Uzdin, A. Mailybaev, and N. Moiseyev, J. Phys. A: Math. Theor. **44**, 435302 (2011).

[35] M. V. Berry and R. Uzdin, J. Phys. A: Math. Theor. **44**, 435303 (2011).

[36] I. Gilary, A. A. Mailybaev, and N. Moiseyev, Phys. Rev. A **88**, 010102 (2013).

[37] A. Leclerc, G. Jolicard, and J. P. Killingbeck, J. Phys. B: At., Mol. Opt. Phys. **46**, 145503 (2013).

[38] E.-M. Graefe, A. A. Mailybaev, and N. Moiseyev, Phys. Rev. A **88**, 033842 (2013).

[39] D. Viennot, J. Phys. A: Math. Theor. **47**, 065302 (2014).

[40] T. J. Milburn, J. Doppler, C. A. Holmes, S. Portolan, S. Rotter, and P. Rabl, Phys. Rev. A **92**, 052124 (2015).

[41] H. Xu, D. Mason, L. Jiang, and J. G. E. Harris, Nature **537**, 80 (2016).

[42] J. Doppler, A. A. Mailybaev, J. Böhm, U. Kuhl, A. Girschik, F. Libisch, T. J. Milburn, P. Rabl, N. Moiseyev, and S. Rotter, Nature **537**, 76 (2016).

[43] K. V. Kepesidis, T. J. Milburn, J. Huber, K. G. Makris, S. Rotter, and P. Rabl, New J. Phys. **18**, 095003 (2016).

[44] X.-L. Zhang, S. Wang, B. Hou, and C. T. Chan, Phys. Rev. X **8**, 021066 (2018).

[45] J. Höller, N. Read, and J. G. E. Harris, Phys. Rev. A **102**, 032216 (2020).

[46] Z. Lin, H. Ramezani, T. Eichelkraut, T. Kottos, H. Cao, and D. N. Christodoulides, Phys. Rev. Lett. **106**, 213901 (2011).

[47] J. Wiersig, Phys. Rev. Lett. **112**, 203901 (2014).

[48] J. Wiersig, Phys. Rev. A **93**, 033809 (2016).

[49] W. Chen, Ş. Kaya Özdemir, G. Zhao, J. Wiersig, and L. Yang, Nature **548**, 192 (2017).

[50] H.-K. Lau and A. A. Clerk, Nat. Commun. **9**, 4320 (2018).

[51] M. Zhang, W. Sweeney, C. W. Hsu, L. Yang, A. D. Stone, and L. Jiang, Phys. Rev. Lett. **123**, 180501 (2019).

[52] S. Assawaworrarit, X. Yu, and S. Fan, Nature **546**, 387 (2017).

[53] Y. Ashida, S. Furukawa, and M. Ueda, Nat. Commun. **8**, 15791 (2017).

[54] M. Naghiloo, M. Abbasi, Y. N. Joglekar, and K. W. Murch, Nat. Phys. **15**, 1232 (2019).

[55] A. McDonald, T. Pereg-Barnea, and A. A. Clerk, Phys. Rev. X **8**, 041031 (2018).

[56] S. Lieu, Phys. Rev. B **98**, 115135 (2018).

[57] Z. Gong, Y. Ashida, K. Kawabata, K. Takasan, S. Higashikawa, and M. Ueda, Phys. Rev. X **8**, 031079 (2018).

[58] N. R. Bernier, L. D. Tóth, A. K. Feofanov, and T. J. Kippenberg, Phys. Rev. A **98**, 023841 (2018).

[59] Y.-K. Lu, P. Peng, Q.-T. Cao, D. Xu, J. Wiersig, Q. Gong, and Y.-F. Xiao, Sci. Bull. **63**, 1096 (2018).

[60] M. Aharonyan and E. G. D. Torre, Mol. Phys. **0**, 1 (2019).

[61] C. C. Gerry and P. L. Knight, *Introductory Quantum Optics* (Cambridge, Cambridge, UK, 2005).

[62] D. F. Walls and G. J. Milburn, *Quantum Optics* (Springer, Springer-Verlag, Berlin, 2008).

[63] A. Mostafazadeh, J. Math. Phys. **43**, 205 (2002).

[64] C. M. Bender, B. K. Berntson, D. Parker, and E. Samuel, Am. J. Phys. **81**, 173 (2013).

[65] M. Tsang and C. M. Caves, Phys. Rev. X **2**, 031016 (2012).

[66] M. J. Woolley and A. A. Clerk, Phys. Rev. A **87**, 063846 (2013).

[67] N. Didier, A. Kamal, W. D. Oliver, A. Blais, and A. A. Clerk, Phys. Rev. Lett. **115**, 093604 (2015).

[68] C. B. Møller, R. A. Thomas, G. Vasilakis, E. Zeuthen, Y. Tsaturyan, M. Balabas, K. Jensen, A. Schliesser, K. Hammerer, and E. S. Polzik, Nature **547**, 191 (2017).

[69] F. Y. Khalili and E. S. Polzik, Phys. Rev. Lett. **121**, 031101 (2018).

[70] S. Weimann, M. Kremer, Y. Plotnik, Y. Lumer, S. Nolte, K. G. Makris, M. Segev, M. C. Rechtsman, and A. Szameit, Nat. Mater. **16**, 433 (2017).

[71] R. Barnett, Phys. Rev. A **88**, 063631 (2013).

[72] S. Lieu, Phys. Rev. B **97**, 045106 (2018).

[73] W. P. Su, J. R. Schrieffer, and A. J. Heeger, Phys. Rev. Lett. **42**, 1698 (1979).

[74] H. Schomerus, Opt. Lett. **38**, 1912 (2013).

[75] A. Eddins, J. M. Kreikebaum, D. M. Toyli, E. M. Levenson-Falk, A. Dove, W. P. Livingston, B. A. Levitan, L. C. G. Govia, A. A. Clerk, and I. Siddiqi, Phys. Rev. X **9**, 011004 (2019).

[76] C. Gardiner and P. Zoller, *Quantum Noise: A Handbook of Markovian and Non-Markovian Quantum Stochastic Methods with Applications to Quantum Optics*, Springer Series in Synergetics (Springer, Berlin, 2004).

[77] S. L. Braunstein, Phys. Rev. A **71**, 055801 (2005).

[78] G. Vidal and R. F. Werner, Phys. Rev. A **65**, 032314 (2002).

[79] M. B. Plenio, Phys. Rev. Lett. **95**, 090503 (2005).

[80] T. E. Lee, Phys. Rev. Lett. **116**, 133903 (2016).

[81] S. Yao and Z. Wang, Phys. Rev. Lett. **121**, 086803 (2018).

[82] K. Kawabata, K. Shiozaki, M. Ueda, and M. Sato, Phys. Rev. X **9**, 041015 (2019).

[83] H. Zhou and J. Y. Lee, Phys. Rev. B **99**, 235112 (2019).

[84] H. Shen, B. Zhen, and L. Fu, Phys. Rev. Lett. **120**, 146402 (2018).

[85] R. Shindou, R. Matsumoto, S. Murakami, and J.-i. Ohe, Phys. Rev. B **87**, 174427 (2013).

[86] V. Peano, M. Houde, C. Brendel, F. Marquardt, and A. A. Clerk, Nat. Commun. **7**, 10779 (2016).

[87] H. Zhou, C. Peng, Y. Yoon, C. W. Hsu, K. A. Nelson, L. Fu, J. D. Joannopoulos, M. Soljačić, and B. Zhen, Science **359**, 1009 (2018).

[88] A. Mostafazadeh, J. Math. Phys. **43**, 2814 (2002).

[89] A. Mostafazadeh, J. Math. Phys. **43**, 3944 (2002).

[90] G. Demange and E.-M. Graefe, J. Phys. A: Math. Theor. **45**, 025303 (2011).

[91] Z. Lin, A. Pick, M. Lončar, and A. W. Rodriguez, Phys. Rev. Lett. **117**, 107402 (2016).

[92] H. Jing, Ş. K. Özdemir, H. Lü, and F. Nori, Sci. Rep. **7**, 3386 (2017).

[93] H. Hodaei, A. U. Hassan, S. Wittek, H. Garcia-Gracia, R. El-Ganainy, D. N. Christodoulides, and M. Khajavikhan, Nature **548**, 187 (2017).

[94] Y.-D. Wang and A. A. Clerk, Phys. Rev. Lett. **110**, 253601 (2013).

[95] L. Tian, Phys. Rev. Lett. **110**, 233602 (2013).

[96] Y.-D. Wang, S. Chesi, and A. A. Clerk, Phys. Rev. A **91**, 013807 (2015).

[97] C. Zhong, Z. Wang, C. Zou, M. Zhang, X. Han, W. Fu, M. Xu, S. Shankar, M. H. Devoret, H. X. Tang, and L. Jiang, Phys. Rev. Lett. **124**, 010511 (2020).

[98] S. L. Braunstein and P. v. Loock, Rev. Mod. Phys. **77**, 513 (2005).

[99] V. Peano, M. Houde, F. Marquardt, and A. A. Clerk, Phys. Rev. X **6**, 041026 (2016).

[100] Y.-X. Wang and A. A. Clerk, Phys. Rev. Research **2**, 033196 (2020).

[101] L. Cywiński, Phys. Rev. A **90**, 042307 (2014).

[102] G. A. Paz-Silva and L. Viola, Phys. Rev. Lett. **113**, 250501 (2014).

[103] L. M. Norris, G. A. Paz-Silva, and L. Viola, Phys. Rev. Lett. **116**, 150503 (2016).

[104] Y. Sung, F. Beaudoin, L. M. Norris, F. Yan, D. K. Kim, J. Y. Qiu, U. von Lüpke, J. L. Yoder, T. P. Orlando, S. Gustavsson, L. Viola, and W. D. Oliver, Nat. Commun. **10**, 3715 (2019).

[105] G. Ramon, Phys. Rev. B **100**, 161302 (R) (2019).

[106] T. Rao and M. Gabr, *An introduction to bispectral analysis and bilinear time series models*, Lecture notes in statistics (Springer, New York, 1984).

[107] N. Ubbelohde, C. Fricke, C. Flindt, F. Hohls, and R. J. Haug, Nat. Commun. **3**, 612 (2012).

[108] L. Levitov, H. Lee, and G. Lesovik, J. Math. Phys. **37**, 4845 (1996).

[109] Y. V. Nazarov and M. Kindermann, Eur. Phys. J. B **35**, 413 (2003).

[110] A. Bednorz and W. Belzig, Phys. Rev. Lett. **105**, 106803 (2010).

[111] A. A. Clerk, Phys. Rev. A **84**, 043824 (2011).

[112] P. P. Hofer, Quantum **1**, 32 (2017).

[113] P. Wang, C. Chen, X. Peng, J. Wrachtrup, and R.-B. Liu, Phys. Rev. Lett. **123**, 050603 (2019).

[114] J. Gambetta, A. Blais, D. I. Schuster, A. Wallraff, L. Frunzio, J. Majer, M. H. Devoret, S. M. Girvin, and R. J. Schoelkopf, Phys. Rev. A **74**, 042318 (2006).

[115] Z. Wang, S. Shankar, Z. K. Minev, P. Campagne-Ibarcq, A. Narla, and M. H. Devoret, Phys. Rev. Appl. **11**, 014031 (2019).

[116] P. P. Hofer and A. A. Clerk, Phys. Rev. Lett. **116**, 013603 (2016).

[117] K. Jacobs, *Stochastic Processes for Physicists* (Cambridge University Press, Cambridge, 2010).

[118] A. Kamenev, *Field Theory of Non-Equilibrium Systems* (Cambridge University Press, 2011).

[119] V. Chandran and S. Elgar, IEEE Trans. Signal Processing **42**, 229 (1994).

[120] J. Salo, F. W. J. Hekking, and J. P. Pekola, Phys. Rev. B **74**, 125427 (2006).

[121] A. A. Clerk, F. Marquardt, and J. G. E. Harris, Phys. Rev. Lett. **104**, 213603 (2010).

[122] A. A. Clerk and D. W. Utami, Phys. Rev. A **75**, 042302 (2007).

[123] G. Semerjian, L. F. Cugliandolo, and A. Montanari, J. Stat. Phys. **115**, 493 (2004).

[124] N. A. Sinitsyn and Y. V. Pershin, Rep. Prog. Phys. **79**, 106501 (2016).

[125] F. Li, A. Saxena, D. Smith, and N. A. Sinitsyn, New J. Phys. **15**, 113038 (2013).

[126] L. Onsager, Phys. Rev. **37**, 405 (1931).

[127] D. R. Brillinger and M. Rosenblatt, in *Spectral Analysis of Time Series*, edited by B. Harris (Wiley, New York, 1967) Chap. 10, pp. 189–232.

[128] R. Kubo, Rep. Prog. Phys. **29**, 255 (1966).

[129] G. S. Agarwal, Z. Phys. **258**, 409 (1973).

[130] H. J. Carmichael and D. F. Walls, Z. Phys. B **23**, 299 (1976).

[131] K. Tomita and H. Tomita, Phys. Lett. A **46**, 265 (1973).

[132] K. Tomita and H. Tomita, Prog. Theor. Phys. **51**, 1731 (1974).

[133] A. Denisov, H. M. Castro-Beltran, and H. J. Carmichael, Phys. Rev. Lett. **88**, 243601 (2002).

[134] I. Bialynicki-Birula, B. Mielnik, and J. Plebański, Ann. Phys. (N. Y.) **51**, 187 (1969).

[135] J. Gabelli and B. Reulet, Proc. SPIE **6600**, 66000T (2007).

[136] Y.-X. Wang and A. A. Clerk, Nat. Commun. **12**, 6528 (2021).

[137] C. L. Degen, F. Reinhard, and P. Cappellaro, Rev. Mod. Phys. **89**, 035002 (2017).

[138] A. G. Kofman and G. Kurizki, Phys. Rev. Lett. **93**, 130406 (2004).

[139] R. de Sousa, Electron spin as a spectrometer of nuclear-spin noise and other fluctuations, in *Electron Spin Resonance and Related Phenomena in Low-Dimensional Structures*, edited by M. Fanciulli (Springer Berlin Heidelberg, Berlin, Heidelberg, 2009) pp. 183–220.

[140] G. de Lange, Z. H. Wang, D. Ristè, V. V. Dobrovitski, and R. Hanson, Science **330**, 60 (2010).

[141] G. A. Álvarez and D. Suter, Phys. Rev. Lett. **107**, 230501 (2011).

[142] J. Bylander, S. Gustavsson, F. Yan, F. Yoshihara, K. Harrabi, G. Fitch, D. G. Cory, Y. Nakamura, J. S. Tsai, and W. D. Oliver, Nat. Phys. **7**, 565 (2011).

[143] O. E. Dial, M. D. Shulman, S. P. Harvey, H. Bluhm, V. Umansky, and A. Yacoby, Phys. Rev. Lett. **110**, 146804 (2013).

[144] Y. Romach, C. Müller, T. Unden, L. J. Rogers, T. Isoda, K. M. Itoh, M. Markham, A. Stacey, J. Meijer, S. Pezzagna, B. Naydenov, L. P. McGuinness, N. Bar-Gill, and F. Jelezko, Phys. Rev. Lett. **114**, 017601 (2015).

[145] V. M. Frey, S. Mavadia, L. M. Norris, W. de Ferranti, D. Lucarelli, L. Viola, and M. J. Biercuk, Nat. Commun. **8**, 2189 (2017).

[146] L. M. Norris, D. Lucarelli, V. M. Frey, S. Mavadia, M. J. Biercuk, and L. Viola, Phys. Rev. A **98**, 032315 (2018).

[147] K. W. Chan, W. Huang, C. H. Yang, J. C. C. Hwang, B. Hensen, T. Tanttu, F. E. Hudson, K. M. Itoh, A. Laucht, A. Morello, and A. S. Dzurak, Phys. Rev. Appl. **10**, 044017 (2018).

[148] C. Ferrie, C. Granade, G. Paz-Silva, and H. M. Wiseman, New J. Phys. **20**, 123005 (2018).

[149] P. Szańkowski, G. Ramon, J. Krzywda, D. Kwiatkowski, and Ł. Cywiński, J. Phys.: Cond. Matter **29**, 333001 (2017).

[150] F. Yan, D. Campbell, P. Krantz, M. Kjaergaard, D. Kim, J. L. Yoder, D. Hover, A. Sears, A. J. Kerman, T. P. Orlando, S. Gustavsson, and W. D. Oliver, Phys. Rev. Lett. **120**, 260504 (2018).

[151] U. von Lüpke, F. Beaudoin, L. M. Norris, Y. Sung, R. Winik, J. Y. Qiu, M. Kjaergaard, D. Kim, J. Yoder, S. Gustavsson, L. Viola, and W. D. Oliver, PRX Quantum **1**, 010305 (2020).

[152] Y. Sung, A. Vepsäläinen, J. Braumüller, F. Yan, J. I.-J. Wang, M. Kjaergaard, R. Winik, P. Krantz, A. Bengtsson, A. J. Melville, B. M. Niedzielski, M. E. Schwartz, D. K. Kim, J. L. Yoder, T. P. Orlando, S. Gustavsson, and W. D. Oliver, Nat. Commun. **12**, 967 (2021).

[153] N. Bar-Gill, L. Pham, C. Belthangady, D. L. Sage, P. Cappellaro, J. Maze, M. Lukin, A. Yacoby, and R. Walsworth, Nat. Commun. **3**, 858 (2012).

[154] X. Peng, H. Zhou, B.-B. Wei, J. Cui, J. Du, and R.-B. Liu, Phys. Rev. Lett. **114**, 010601 (2015).

[155] F. Casola, T. van der Sar, and A. Yacoby, Nat. Rev. Mater. **3**, 17088 (2018).

[156] B. Ye, F. Machado, C. D. White, R. S. K. Mong, and N. Y. Yao, Phys. Rev. Lett. **125**, 030601 (2020).

[157] E. J. Davis, B. Ye, F. Machado, S. A. Meynell, T. Mittiga, W. Schenken, M. Joos, B. Kobrin, Y. Lyu, D. Bluvstein, S. Choi, C. Zu, A. C. B. Jayich, and N. Y. Yao, Nat. Phys. 10.1038/s41567-023-01944-5 (2023).

[158] N. Zhao, Z.-Y. Wang, and R.-B. Liu, Phys. Rev. Lett. **106**, 217205 (2011).

[159] P. Huang, X. Kong, N. Zhao, F. Shi, P. Wang, X. Rong, R.-B. Liu, and J. Du, Nat. Commun. **2**, 570 (2011).

[160] W. Yang, W.-L. Ma, and R.-B. Liu, Rep. Prog. Phys. **80**, 016001 (2016).

[161] P. Szańkowski and Ł. Cywiński, Sci. Rep. **10**, 22189 (2020).

[162] R. J. Schoelkopf, A. A. Clerk, S. M. Girvin, K. W. Lehnert, and M. H. Devoret, Qubits as spectrometers of quantum noise, in *Quantum Noise in Mesoscopic Physics*, edited by Y. V. Nazarov (Springer, Dordrecht, 2003) pp. 175–203.

[163] G. A. Paz-Silva, S.-W. Lee, T. J. Green, and L. Viola, New J. Phys. **18**, 073020 (2016).

[164] G. A. Paz-Silva, L. M. Norris, and L. Viola, Phys. Rev. A **95**, 022121 (2017).

[165] D. Kwiatkowski, P. Szańkowski, and L. Cywiński, Phys. Rev. B **101**, 155412 (2020).

[166] A. Polkovnikov, K. Sengupta, A. Silva, and M. Vengalattore, Rev. Mod. Phys. **83**, 863 (2011).

[167] U. Weiss, *Quantum Dissipative Systems*, 4th ed. (World Scientific, Singapore, 2012).

[168] A. J. Leggett, S. Chakravarty, A. T. Dorsey, M. P. A. Fisher, A. Garg, and W. Zwerger, Rev. Mod. Phys. **59**, 1 (1987).

[169] E. Paladino, Y. M. Galperin, G. Falci, and B. L. Altshuler, Rev. Mod. Phys. **86**, 361 (2014).

[170] H. B. Callen and T. A. Welton, Phys. Rev. **83**, 34 (1951).

[171] F. Zamponi, F. Bonetto, L. F. Cugliandolo, and J. Kurchan, J. Stat. Mech. **2005**, P09013 (2005).

[172] L. F. Cugliandolo, J. Phys. A: Math. Theor. **44**, 483001 (2011).

[173] A. Shnirman, Y. Makhlin, and G. Schön, Phys. Scr. **T102**, 147 (2002).

[174] J. Schriefl, Y. Makhlin, A. Shnirman, and G. Schön, New J. Phys. **8**, 1 (2006).

[175] L. Cywiński, R. M. Lutchyn, C. P. Nave, and S. Das Sarma, Phys. Rev. B **77**, 174509 (2008).

[176] C. D. Wilen, S. Abdullah, N. A. Kurinsky, C. Stanford, L. Cardani, G. D'Imperio, C. Tomei, L. Faoro, L. B. Ioffe, C. H. Liu, A. Opremcak, B. G. Christensen, J. L. DuBois, and R. McDermott, Nature **594**, 369 (2021).

[177] X. You, A. A. Clerk, and J. Koch, Phys. Rev. Research **3**, 013045 (2021).

[178] J. Yoneda, K. Takeda, T. Otsuka, T. Nakajima, M. R. Delbecq, G. Allison, T. Honda, T. Kodera, S. Oda, Y. Hoshi, N. Usami, K. M. Itoh, and S. Tarucha, Nat. Nanotechnol. **13**, 102 (2017).

[179] J. Braumüller, L. Ding, A. P. Vepsäläinen, Y. Sung, M. Kjaergaard, T. Menke, R. Winik, D. Kim, B. M. Niedzielski, A. Melville, J. L. Yoder, C. F. Hirjibehedin, T. P. Orlando, S. Gustavsson, and W. D. Oliver, Phys. Rev. Appl. **13**, 054079 (2020).

[180] A. Gyenis, A. Di Paolo, J. Koch, A. Blais, A. A. Houck, and D. I. Schuster, PRX Quantum **2**, 030101 (2021).

[181] A. O. Caldeira and A. J. Leggett, Ann. Phys. **149**, 374 (1983).

[182] J. B. Johnson, Phys. Rev. **32**, 97 (1928).

[183] H. Nyquist, Phys. Rev. **32**, 110 (1928).

[184] M. H. Devoret, Quantum Fluctuations in Electrical Circuits, in *Quantum Fluctuations: Les Houches Session LXIII, June 27 to July 28 1995*, edited by S. Reynaud, E. Giacobino, and J. Zinn-Justin (Elsevier, Amsterdam, 1997) p. 351.

[185] B. Peropadre, D. Zueco, D. Porras, and J. J. García-Ripoll, Phys. Rev. Lett. **111**, 243602 (2013).

[186] F. Yan, S. Gustavsson, A. Kamal, J. Birenbaum, A. P. Sears, D. Hover, T. J. Gudmundsen, D. Rosenberg, G. Samach, S. Weber, J. L. Yoder, T. P. Orlando, J. Clarke, A. J. Kerman, and W. D. Oliver, Nat. Commun. **7**, 12964 (2016).

[187] P. Forn-Díaz, J. J. García-Ripoll, B. Peropadre, J.-L. Orgiazzi, M. A. Yurtalan, R. Belyansky, C. M. Wilson, and A. Lupascu, Nat. Phys. **13**, 39 (2017).

[188] J. F. Barry, J. M. Schloss, E. Bauch, M. J. Turner, C. A. Hart, L. M. Pham, and R. L. Walsworth, Rev. Mod. Phys. **92**, 015004 (2020).

[189] S. Kolkowitz, A. Safira, A. A. High, R. C. Devlin, S. Choi, Q. P. Unterreithmeier, D. Patterson, A. S. Zibrov, V. E. Manucharyan, H. Park, and M. D. Lukin, Science **347**, 1129 (2015).

[190] A. Ariyaratne, D. Bluvstein, B. A. Myers, and A. C. B. Jayich, Nat. Commun. **9** (2018).

[191] E. Bauch, C. A. Hart, J. M. Schloss, M. J. Turner, J. F. Barry, P. Kehayias, S. Singh, and R. L. Walsworth, Phys. Rev. X **8**, 031025 (2018).

[192] D. Bluvstein, Z. Zhang, C. A. McLellan, N. R. Williams, and A. C. B. Jayich, Phys. Rev. Lett. **123**, 146804 (2019).

[193] J. J. Sakurai and J. Napolitano, *Modern Quantum Mechanics*, 2nd ed. (Cambridge University Press, Cambridge, 2017).

[194] R. Kubo, J. Phys. Soc. Jpn. **17**, 1100 (1962).

[195] L. M. Sieberer, M. Buchhold, and S. Diehl, Rep. Prog. Phys. **79**, 096001 (2016).

[196] J. Gabelli and B. Reulet, Phys. Rev. Lett. **100**, 026601 (2008).

[197] R. L. Stratonovich, *Nonlinear nonequilibrium thermodynamics I* (Springer-Verlag, Berlin, 1994).

[198] A. Abragam, *The Principles of Nuclear Magnetism*, Comparative Pathobiology - Studies in the Postmodern Theory of Education (Clarendon Press, Oxford, 1961).

[199] L. Petit, J. M. Boter, H. G. J. Eenink, G. Droulers, M. L. V. Tagliaferri, R. Li, D. P. Franke, K. J. Singh, J. S. Clarke, R. N. Schouten, V. V. Dobrovitski, L. M. K. Vandersypen, and M. Veldhorst, Phys. Rev. Lett. **121**, 076801 (2018).

[200] T. Rosskopf, A. Dussaux, K. Ohashi, M. Loretz, R. Schirhagl, H. Watanabe, S. Shikata, K. M. Itoh, and C. L. Degen, Phys. Rev. Lett. **112**, 147602 (2014).

[201] E. J. Connors, J. Nelson, and J. M. Nichol, Nat. Commun. **13**, 940 (2022).

[202] C. M. Quintana, Y. Chen, D. Sank, A. G. Petukhov, T. C. White, D. Kafri, B. Chiaro, A. Megrant, R. Barends, B. Campbell, Z. Chen, A. Dunsworth, A. G. Fowler, R. Graff, E. Jeffrey, J. Kelly, E. Lucero, J. Y. Mutus, M. Neeley, C. Neill, P. J. J. O'Malley, P. Roushan, A. Shabani, V. N. Smelyanskiy, A. Vainsencher, J. Wenner, H. Neven, and J. M. Martinis, Phys. Rev. Lett. **118**, 057702 (2017).

[203] Y.-X. Wang, C. Wang, and A. A. Clerk, PRX Quantum **4**, 010306 (2023).

[204] M. J. Bowick, N. Fakhri, M. C. Marchetti, and S. Ramaswamy, Phys. Rev. X **12**, 010501 (2022).

[205] M. Fruchart, R. Hanai, P. B. Littlewood, and V. Vitelli, Nature **592**, 363 (2021).

[206] S. Shankar, A. Souslov, M. J. Bowick, M. C. Marchetti, and V. Vitelli, Nat. Rev. Phys. **4**, 380 (2022).

[207] K. Stannigel, P. Rabl, and P. Zoller, New J. Phys. **14**, 063014 (2012).

[208] H. Pichler, T. Ramos, A. J. Daley, and P. Zoller, Phys. Rev. A **91**, 042116 (2015).

[209] P. Lodahl, S. Mahmoodian, S. Stobbe, A. Rauschenbeutel, P. Schneeweiss, J. Volz, H. Pichler, and P. Zoller, Nature **541**, 473 (2017).

[210] K. Fang, Z. Yu, and S. Fan, Nat. Photon. **6**, 782 (2012).

[211] N. A. Estep, D. L. Sounas, J. Soric, and A. Alù, Nat. Phys. **10**, 923 (2014).

[212] H. Nassar, B. Yousefzadeh, R. Fleury, M. Ruzzene, A. Alù, C. Daraio, A. N. Norris, G. Huang, and M. R. Haberman, Nat. Rev. Mater. **5**, 667 (2020).

[213] A. Kamal, J. Clarke, and M. H. Devoret, Nat. Phys. **7**, 311 (2011).

[214] B. Abdo, K. Sliwa, S. Shankar, M. Hatridge, L. Frunzio, R. Schoelkopf, and M. Devoret, Phys. Rev. Lett. **112**, 167701 (2014).

[215] K. M. Sliwa, M. Hatridge, A. Narla, S. Shankar, L. Frunzio, R. J. Schoelkopf, and M. H. Devoret, Phys. Rev. X **5**, 041020 (2015).

[216] F. Ruesink, M.-A. Miri, A. Alù, and E. Verhagen, Nat. Commun. **7**, 13662 (2016).

[217] F. Lecocq, L. Ranzani, G. A. Peterson, K. Cicak, R. W. Simmonds, J. D. Teufel, and J. Aumentado, Phys. Rev. Appl. **7**, 024028 (2017).

[218] K. Fang, J. Luo, A. Metelmann, M. H. Matheny, F. Marquardt, A. A. Clerk, and O. Painter, Nat. Phys. **13**, 465 (2017).

[219] G. A. Peterson, F. Lecocq, K. Cicak, R. W. Simmonds, J. Aumentado, and J. D. Teufel, Phys. Rev. X **7**, 031001 (2017).

[220] N. R. Bernier, L. D. Tóth, A. Koottandavida, M. A. Ioannou, D. Malz, A. Nunnenkamp, A. K. Feofanov, and T. J. Kippenberg, Nat. Commun. **8**, 604 (2017).

[221] H. Xu, L. Jiang, A. A. Clerk, and J. G. E. Harris, Nature **568**, 65 (2019).

[222] D. Malz, L. D. Tóth, N. R. Bernier, A. K. Feofanov, T. J. Kippenberg, and A. Nunnenkamp, Phys. Rev. Lett. **120**, 023601 (2018).

[223] C. W. Gardiner, Phys. Rev. Lett. **70**, 2269 (1993).

[224] H. J. Carmichael, Phys. Rev. Lett. **70**, 2273 (1993).

[225] A. Metelmann and A. A. Clerk, Phys. Rev. X **5**, 021025 (2015).

[226] F. Verstraete, M. M. Wolf, and J. I. Cirac, Nat. Phys. **5**, 633 (2009).

[227] P. Zanardi and L. Campos Venuti, Phys. Rev. Lett. **113**, 240406 (2014).

[228] V. V. Albert, B. Bradlyn, M. Fraas, and L. Jiang, Phys. Rev. X **6**, 041031 (2016).

[229] C. Arenz and A. Metelmann, Phys. Rev. A **101**, 022101 (2020).

[230] B. Misra and E. C. G. Sudarshan, J. Math. Phys. **18**, 756 (1977).

[231] P. Facchi and S. Pascazio, Phys. Rev. Lett. **89**, 080401 (2002).

[232] P. Facchi and S. Pascazio, J. Phys. A **41**, 493001 (2008).

[233] D. Layden, E. Martín-Martínez, and A. Kempf, Phys. Rev. A **93**, 040301(R) (2016).

[234] Q. Xu, G. Zheng, Y.-X. Wang, P. Zoller, A. A. Clerk, and L. Jiang, arXiv preprint arXiv:2210.13406 (2022).

[235] J. Watrous, *The Theory of Quantum Information* (Cambridge University Press, 2018).

[236] A. Y. Kitaev, Russ. Math. Surv. **52**, 1191 (1997).

[237] This calculation amounts to computing the diamond norm between two unitary maps. An analytical derivation of diamond norm with such forms can be found in e.g. Sec. 3.3 of Ref. [235].

[238] H.-K. Lau and M. B. Plenio, Phys. Rev. Lett. **117**, 100501 (2016).

[239] B. Buča, J. Tindall, and D. Jaksch, Nat. Commun. **10**, 1730 (2019).

[240] B. Buca, C. Booker, and D. Jaksch, SciPost Phys. **12**, 97 (2022).

[241] M. Mirrahimi, Z. Leghtas, V. V. Albert, S. Touzard, R. J. Schoelkopf, L. Jiang, and M. H. Devoret, New J. Phys. **16**, 045014 (2014).

[242] R. Lescanne, M. Villiers, T. Peronnin, A. Sarlette, M. Delbecq, B. Huard, T. Kontos, M. Mirrahimi, and Z. Leghtas, Nat. Phys. **16**, 509 (2020).

[243] A. Grimm, N. E. Frattini, S. Puri, S. O. Mundhada, S. Touzard, M. Mirrahimi, S. M. Girvin, S. Shankar, and M. H. Devoret, Nature **584**, 205 (2020).

[244] J. M. Gertler, B. Baker, J. Li, S. Shirol, J. Koch, and C. Wang, Nature **590**, 243 (2021).

[245] J. Lebreuilly, K. Noh, C.-H. Wang, S. M. Girvin, and L. Jiang, arXiv preprint arXiv:2103.05007 .

[246] B. Kümmerer and H. Maassen, Commun. Math. Phys. **109**, 1 (1987).

[247] F. Fagnola, J. E. Gough, H. I. Nurdin, and L. Viola, J. Phys. A **52**, 385301 (2019).

[248] H. M. Wiseman, Phys. Rev. A **49**, 2133 (1994).

[249] Y. Castin, H. Wallis, and J. Dalibard, J. Opt. Soc. Am. B **6**, 2046 (1989).

[250] J. I. Cirac, R. Blatt, P. Zoller, and W. D. Phillips, Phys. Rev. A **46**, 2668 (1992).

[251] D. Leibfried, R. Blatt, C. Monroe, and D. Wineland, Rev. Mod. Phys. **75**, 281 (2003).

[252] S. Kono, K. Koshino, Y. Tabuchi, A. Noguchi, and Y. Nakamura, Nat. Phys. **14**, 546 (2018).

[253] J.-C. Besse, S. Gasparinetti, M. C. Collodo, T. Walter, P. Kurpiers, M. Pechal, C. Eichler, and A. Wallraff, Phys. Rev. X **8**, 021003 (2018).

[254] J.-C. Besse, S. Gasparinetti, M. C. Collodo, T. Walter, A. Remm, J. Krause, C. Eichler, and A. Wallraff, Phys. Rev. X **10**, 011046 (2020).

[255] Y. Shi, Z. Yu, and S. Fan, Nat. Photonics **9**, 388 (2015).

[256] D. L. Sounas and A. Alú, IEEE Antennas Wirel. Propag. Lett. **17**, 1958 (2018).

[257] F. Fratini, E. Mascarenhas, L. Safari, J.-P. Poizat, D. Valente, A. Auffèves, D. Gerace, and M. F. Santos, Phys. Rev. Lett. **113**, 243601 (2014).

[258] A. Rosario Hamann, C. Müller, M. Jerger, M. Zanner, J. Combes, M. Pletyukhov, M. Weides, T. M. Stace, and A. Fedorov, Phys. Rev. Lett. **121**, 123601 (2018).

[259] N. Nefedkin, M. Cotrufo, A. Krasnok, and A. Alú, Adv. Quantum Technol. , 2100112 (2022).

[260] M. A. Nielsen, Phys. Lett. A **303**, 249 (2002).

[261] We use script letters with overhead check mark to denote matrices acting on the complex linear space $\mathbb{C}^N$.

[262] F. Elste, S. M. Girvin, and A. A. Clerk, Phys. Rev. Lett. **102**, 207209 (2009).

[263] A. Sawadsky, H. Kaufer, R. M. Nia, S. P. Tarabrin, F. Y. Khalili, K. Hammerer, and R. Schnabel, Phys. Rev. Lett. **114**, 043601 (2015).

[264] H. Pichler, G. Zhu, A. Seif, P. Zoller, and M. Hafezi, Phys. Rev. X **6**, 041033 (2016).

[265] Y. Y. Gao, B. J. Lester, K. S. Chou, L. Frunzio, M. H. Devoret, L. Jiang, S. M. Girvin, and R. J. Schoelkopf, Nature **566**, 509 (2019).

[266] J. Dalibard, Y. Castin, and K. Mølmer, Phys. Rev. Lett. **68**, 580 (1992).

[267] S. Lieu, Y.-J. Liu, and A. V. Gorshkov, arXiv preprint arXiv:2205.09767 .

[268] G. H. Fredrickson and H. C. Andersen, Phys. Rev. Lett. **53**, 1244 (1984).

[269] E. Zohar, J. I. Cirac, and B. Reznik, Rep. Prog. Phys. **79**, 014401 (2015).

[270] L. Barbiero, C. Schweizer, M. Aidelsburger, E. Demler, N. Goldman, and F. Grusdt, Sci. Adv. **5**, eaav7444 (2019).

[271] V. Lienhard, P. Scholl, S. Weber, D. Barredo, S. de Léséleuc, R. Bai, N. Lang, M. Fleischhauer, H. P. Büchler, T. Lahaye, and A. Browaeys, Phys. Rev. X **10**, 021031 (2020).

[272] A. Celi, B. Vermersch, O. Viyuela, H. Pichler, M. D. Lukin, and P. Zoller, Phys. Rev. X **10**, 021057 (2020).

[273] N. Khaneja and S. J. Glaser, Chem. Phys. **267**, 11 (2001).

[274] V. Alba and P. Calabrese, SciPost Phys. **4**, 017 (2018).

[275] P. Calabrese, SciPost Phys. Lect. Notes , 20 (2020).

[276] M. Serbyn, Z. Papić, and D. A. Abanin, Phys. Rev. Lett. **110**, 260601 (2013).

[277] M. Žnidarič, T. c. v. Prosen, and P. Prelovšek, Phys. Rev. B **77**, 064426 (2008).

[278] J. H. Bardarson, F. Pollmann, and J. E. Moore, Phys. Rev. Lett. **109**, 017202 (2012).

[279] L. Hackl, E. Bianchi, R. Modak, and M. Rigol, Phys. Rev. A **97**, 032321 (2018).

[280] A. Elben, R. Kueng, H.-Y. R. Huang, R. van Bijnen, C. Kokail, M. Dalmonte, P. Calabrese, B. Kraus, J. Preskill, P. Zoller, and B. Vermersch, Phys. Rev. Lett. **125**, 200501 (2020).

[281] H. Shapourian, S. Liu, J. Kudler-Flam, and A. Vishwanath, PRX Quantum **2**, 030347 (2021).

[282] A. McDonald and A. A. Clerk, Nat. Commun. **11**, 5382 (2020).

[283] A. Pocklington, Y.-X. Wang, and A. A. Clerk, Phys. Rev. Lett. **130**, 123602 (2023).

[284] T. McCourt, C. Neill, K. Lee, C. Quintana, Y. Chen, J. Kelly, V. Smelyanskiy, M. Dykman, A. Korotkov, I. L. Chuang, and A. G. Petukhov, arXiv preprint arXiv:2201.11173 (2022).

[285] P. C. Jerger, Y.-X. Wang, M. Onizhuk, B. S. Soloway, M. T. Solomon, C. Egerstrom, F. J. Heremans, G. Galli, A. A. Clerk, and D. D. Awschalom, arXiv preprint arXiv:2303.02233 .